Pedro Mendes de Lacerda Peixoto de Magalhães

Mestre em Engenharia Electrotécnica e de Computadores

Study of pump control in residential grid-tied solar domestic hot water photovoltaic-thermal (PV-T) systems

Dissertação para obtenção do Grau de Doutor em
Engenharia Electrotécnica e de Computadores

Orientador: Doutor João Francisco Alves Martins,
Professor Auxiliar,
Universidade Nova de Lisboa
Co-orientador: Doutor António Luiz Moura Joyce,
Investigador Principal,
Laboratório Nacional de Energia e Geologia

Júri:

Presidente: Doutor Luís Manuel Camarinha de Matos
Arguente(s): Doutor António Manuel de Oliveira Gomes Martins
Doutor Duarte de Mesquita e Sousa

Vogais: Doutor Manuel Pedro Ivens Collares Pereira
Doutor Fernando José Almeida Vieira do Coito
Doutor João Francisco Alves Martins

FACULDADE DE CIÊNCIAS E TECNOLOGIA
UNIVERSIDADE NOVA DE LISBOA

Dezembro de 2017

Study of pump control in residential grid-tied solar domestic hot water photovoltaic-thermal (PV-T) systems

Copyright © Pedro Mendes de Lacerda Peixoto de Magalhães, Faculdade de Ciências e Tecnologia, Universidade Nova de Lisboa.

A Faculdade de Ciências e Tecnologia e a Universidade Nova de Lisboa têm o direito, perpétuo e sem limites geográficos, de arquivar e publicar esta dissertação através de exemplares impressos reproduzidos em papel ou de forma digital, ou por qualquer outro meio conhecido ou que venha a ser inventado, e de a divulgar através de repositórios científicos e de admitir a sua cópia e distribuição com objetivos educacionais ou de investigação, não comerciais, desde que seja dado crédito ao autor e editor.

"Energy is not a material commodity; it is an abstract concept invented by physical scientists in the 19th century to describe quantitatively a wide variety of natural phenomena."

David J. Rose,
Learning about Energy, 1986

Some come cripple and some come lame
Bear the burden in the heat of the day
Some come walking in Jesus name
Bear the burden in the heat of the day

Bear the Burden in the Heat of the Day
(traditional negro spiritual),
Paul Robeson and Alan Booth, 1955

Acknowledgments

While undertaking the activities described in this document, I was fortunate enough to benefit from the support, patience, advice, and humour of several individuals whom I would like to thank. Starting with close family and friends, in no particular order, I would like to thank my father, Hernani, my brother, Tiago, my maternal grandmother, Alice, aunts Rita, Belinha and Rosário, friends Ana, Sérgio, Daniel, and a special thank you to Natacha. I would be remiss not to mention the friendship and camaraderie of my colleagues Rui Lopes, José Lima, Francisco Ganhão, Pedro Ferreira, Slaviša Tomić, Pedro Pereira, and Vasco Gomes at the Faculdade de Ciências e Tecnologia, Universidade Nova de Lisboa (FCT-UNL). From other institutions, I am happy to recognise the contributions of Dr. Carlos Rodrigues, Dra. Maria João Carvalho, Dra. Susana Viana, Eng. David Loureiro, Mestre Nuno Mexa, and Mestre Ricardo Pereira, all at one point working at the Laboratório Nacional de Energia e Geologia (LNEG), and Nedzad Rudonja from the Faculty of Mechanical Engineering at the University of Belgrade. Similarly, I am deeply grateful to the staff at the FCT-UNL, LNEG, Laboratório Nacional de Engenharia Civil (LNEC), Instituto Superior Técnico (IST) and other institutions' libraries – foreign and domestic – for diligently providing me with the materials requested on numerous occasions. Their work proved invaluable to me, even in this day and age, as the publications consulted proved to be a significant catalyst in the work carried out and, though too numerous to enumerate here, I would find it ungrateful not to collectively acknowledge their authors, those that came before them and other influent authors not explictly acknowledged. I would also like to acknowledge the support and contributions from thesis supervisors Dr. João Martins and Dr. António Joyce, whom I can only thank for their patience over the years.

Another important contribution came from often anonymous software developers. Special thanks go out to the Debian GNU/Linux, Lyx, LaTeX, JabRef, LibreOffice, ConvertAll, and Kolourpaint contributors and development teams. I would also like to acknowledge numerous contributions from the MATLAB user community, including Jiro Doke (grabit), Timothy E. Holy (distinguishable_colors), Denis Gilbert (plotyyy), Peter Bodin (ploty4), Kelly Kearney (tick2text), Kyle J. Drerup (newton_n_dim), Mark Mikofski (newtonraphson), Brian Katz, David M. Kaplan, Brandon Levey and Ben Hinkle (applyhatch_pluscolor).

These efforts were made possible by a doctoral grant (SFRH/BD/76747/2011) issued by the Fundação para a Ciência e Tecnologia (FCT) but initially also benefitted from participation in the SOL3 project (QREN 2010/12516). The author would also like to thank LNEG, UNINOVA and FCT-UNL for the institutional support.

Abstract

A study of pump control focusing on active residential grid-connected solar domestic hot water (SDHW) photovoltaic-thermal (PV-T) systems was conducted. The main goal was to determine how the two main pump controls for this segment compare, namely the differential temperature static two-level hysteretic control (DTSTLHC) and the differential temperature static saturated hysteretic-proportional control (DTSSHPC), given the dual outputs of PV-T technology: heat and electricity. In order to do so, a dynamic PV-T collector model was developed for use in transient simulations and incorporated into a SDHW PV-T system model. A substantial number of annual simulations for each of the various locations selected were conducted to encompass the best performances using each control, with emphasis on multiple combinations of controller setpoints and mass flow rates. The results show PV-T systems using DTSSHPC and optimised for maximum auxiliary energy savings consistently outperforming those using DTSTLHC and optimised using the same criterion, though the opposite was true when seeking to optimise the electrical efficiency, with those using DTSTLHC performing best. However, the advantages at best correspond to single-digit percentages of the annual thermal energy demand, and less than 0.1% of the annual electrical efficiency. Similarly low performance advantages were reached from the standpoint of primary energy efficiency and load provision cost-effectiveness by using DTSSHPC, though not consistently due to the inability to reconcile electrical, thermal and parasitic performance advantages over DTSTLHC. Moreover, the advantages presented by DTSSHPC are low enough to be offset by one additional maintenance operation, which systems using this control are likelier to require first due to its complexity and higher switching frequencies. Finally, a study on setpoint selection for differential temperature controllers, namely DTSSHPC and DTSTLHC, for use in PV-T systems was also conducted using steady-state methods, which revealed marginal differences between setpoint selection for hybrid and non-hybrid systems.

Keywords: photovoltaic, thermal, pump, control, setpoint, proportional

Resumo

Levou-se a cabo um estudo sobre o controlo de bombas circuladoras em sistemas residenciais activos e ligados à rede, para aquecimento de águas sanitárias (AQS) com recurso a tecnologia fotovoltaico-térmica (PV-T). O objectivo principal visava comparar a utilização dos dois controladores de bombas circuladoras predominantes neste segmento de mercado, nomeadamente o controlo termostático diferencial de dois níveis (DTSTLHC) e o controlo termostático diferencial, proporcional e com saturação (DTSSHPC), em sistemas PV-T e em termos de desempenho térmico, eléctrico e global. Assim sendo, foi desenvolvido um modelo matemático de colector PV-T adequado para utilização em simulações dinâmicas de sistemas solar térmicos. Efectuaram-se várias simulações anuais para cada uma das localizações estudadas com vista à obtenção dos melhores desempenhos com um e outro controlador, tendo sido exploradas várias combinações de caudais mássicos e parâmetros dos controladores. Os resultados das simulações indicam que os sistemas controlados por DTSSHPC e optimizados para obter a maior fracção solar possível permitem obter sistematicamente uma maior fracção solar que os sistemas controlados por DTSTLHC e optimizados de acordo com o mesmo objectivo, embora se tenha verificado o oposto em termos de rendimento eléctrico. Contudo, o desempenho acrescido em ambos os casos revelou-se baixo e ainda mais em termos de eficiência energética primária e resultado financeiro. Em particular, as vantagens financeiras oferecidas pelo controlo DTSSHPC são baixas o suficiente para que uma operação de manutenção adicional as anule, o que é mais provável com este controlador devido à sua complexidade e frequência de comutação mais elevada. Abordou-se também a escolha de parâmetros de controladores termostáticos diferenciais – como o DTSTLHC e o DTSSHPC – em sistemas PV-T através de métodos baseados em regime permanente. No entanto, os métodos utilizados revelaram diferenças mínimas a este respeito entre sistemas híbridos PV-T e os não-híbridos.

Palavras-chave: fotovoltaico, térmico, bomba circuladora, controlo, parâmetro, proporcional

Contents

List of Figures

List of Tables

Nomenclature

Abbreviations

AC	Alternating current
AM	Air Mass
a-Si	Amorphous silicon
a-Si:H	Hydrogenated amorphous silicon
CCS	Carbon Capture and Storage
CdTe	Cadmium Telluride
CEN	European Committee for Standardization
CIS/CIGS	Copper indium (gallium) selenide
CPC	Compound parabolic concentrator/collector
CSP	Concentrated Solar Power
CTC	Cylindrical trough collector
DC	Direct current
DH	District heating
DHW	Domestic hot water
DNI	Direct normal irradiance
DTSSHPC	Differential temperature static saturated hysteretic-proportional control
DTSTLHC	Differential temperature static two-level hysteretic control
EC	European Commission
EEI	Energy Efficiency Index
ETC	Evacuated-tube collector

EVA	Ethylene-vinyl-acetate
FIT	Feed-in Tariff
FPC	Flat-plate collector
FS	Financial savings, €
GHG	Greenhouse Gas
HDI	Human Development Index
HFC	Heliostat field collector
HWB	Hottel-Whillier-Bliss (model)
IAM	Incidence angle modifier
ICC	Integral cycle control
IC	Incremental conductance
IEA	International Energy Agency
IEA-PVPS	IEA's Photovoltaic Power Systems Programme
IEA-SHC	IEA's Solar Heating and Cooling Programme
IEC	International Electrotechnical Commission
IPH	Industrial process heat
ISO	International Organization for Standardization
LEC	Low-emissivity coating
LFR	Linear Fresnel reflector
mc-Si	Monocrystalline silicon
MPP	Maximum power point
MTOE	Million Tonnes of Oil Equivalent
nc-Si	Nanocrystalline silicon
NOCT	Nominal operating cell temperature
NPV	Net present value, €
PAFC	Phase angle-firing control

P&O	Perturb and observe
pc-Si	Polycrystalline silicon
PDR	Parabolic dish reflector
PES	Primary energy savings, kWh
PH	Pool heating
PID	Proportional-Integral-Derivative
PPA	Power Purchase Agreement
PTC	Parabolic trough collector
PV	Photovoltaic
PV-T	Photovoltaic-thermal
PWM	Pulse width modulation
QDTM	Quasi-dynamic test method
RPS	Renewable Portfolio Standard
RTD	Resistance temperature detector
SC	Space cooling
SDHW	Solar domestic hot water
SH	Space heating
STC	Standard test conditions
ST	Solar thermal
TES	Thermal energy storage
TMY	Typical meteorological year
UV	Ultra-violet
VRE	Variable renewable energy

Greek Symbols

α	Absorptance
β	Electrical efficiency temperature coefficient, $^{\circ}C^{-1}$

δ	Thickness, m
$\Delta\Delta t_{pump}$	Pump running time difference, hour
Δf_{par}	Normalised parasitic energy consumption difference
Δf_{PES}	Normalised primary energy savings difference
Δf_{pv}	Normalised PV yield difference
Δf_{FS}	Normalised financial savings difference
Δp	Pressure difference, Pa
ΔT	Temperature difference, °C or K
Δt	Sampling time, s
Δt_{delay}	Minimum pump running time, s
$\Delta\hat{T}$	Temperature difference sensed by the controller, °C or K
ΔT_{off}	Differential temperature controller turn-off setpoint, °C or K
ΔT_{on}	Differential temperature controller turn-on setpoint, °C or K
ΔT_{sat}	Differential temperature controller saturation setpoint, °C or K
ΔT_{sky}	Effective sky temperature difference, °C or K
Δx	Segment length, m
ϵ	Heat exchanger effectiveness
η	Efficiency
η_0	Zero-reduced temperature thermal efficiency (QDTM)
γ_{pv}	Photovoltaic cell solar radiation coefficient
$\Lambda_{pv,off}$	Normalised PV conversion-induced variation of the minimum ΔT_{off} setpoint for cost-effective operation of PV-T systems
$\Lambda_{pv,on}$	Normalised PV conversion-induced variation of the minimum ΔT_{on} setpoint for stable operation of PV-T systems
ω	Angular speed, rad/s
ρ	Volumetric mass density, kg/m^3
ρ_{pv}	PV packing factor

σ	Stefan–Boltzmann constant, $W \cdot m^{-2} \cdot K^{-4}$
$(\tau\alpha)$	Transmittance-absorptance product
τ	Transmittance
θ	Incidence angle relative to the collector plane normal, rad
ε	Temperature measurement error, K or °C

Roman Symbols

A	Area, m^2
b_0	Beam radiation incidence angle modifier coefficient
c_1	Zero-reduced temperature heat loss coefficient for negligible wind conditions (QDTM), $W \cdot m^{-2} \cdot K^{-1}$
c_{13}	Zero-reduced temperature heat loss coefficient (QDTM), $W \cdot m^{-2} \cdot K^{-1}$
c_2	Temperature dependence of the heat loss coefficient (QDTM), $W \cdot m^{-2} \cdot K^{-2}$
c_3	Wind dependence of the heat loss coefficient (QDTM), $J \cdot m^{-3} \cdot K^{-1}$
c_4	Sky temperature dependence of the heat loss coefficient (QDTM)
c_5	Specific collector thermal capacity (QDTM), $J \cdot m^{-2} \cdot K^{-1}$
C_A	Specific collector thermal capacity, $J \cdot m^{-2} \cdot K^{-1}$
C_b	Bond conductance, $W \cdot m^{-1} \cdot K^{-1}$
C_E	Bandgap energy temperature coefficient, $°C^{-1}$
C_p	Specific heat, $J \cdot kg^{-1} \cdot K^{-1}$
$C_{t,he}$	Natural convection heat transfer coefficient for the storage tank heat exchanger
D	External diameter, m
d	Internal diameter, m
E	Energy, kWh
E_g	Bandgap energy, eV
E_L	Longwave thermal irradiance (QDTM), W/m^2
F	Fin efficiency

f_D	Darcy friction factor
F'	Collector efficiency factor
f_p	Primary energy factor
F_R	Collector heat removal factor
F'_R	Collector heat exchanger factor
$f_{sav,aux}$	Fractional (end use) energy savings
G	Irradiance, W/m^2
g_0	Zero-order coefficient (dynamic model fluid temperature equation), W/m^2
g_1	First-order coefficient (dynamic model fluid temperature equation), W $\cdot$ m^{-2} $\cdot$ K^{-1}
g_2	Second-order coefficient (dynamic model fluid temperature equation), W $\cdot$ m^{-2} $\cdot$ K^{-2}
g_3	Specific thermal capacity (dynamic model fluid temperature equation), J $\cdot$ m^{-2} $\cdot$ K^{-1}
g_4	Initial condition (dynamic model fluid temperature equation), °C
g_5	Composite coefficient (dynamic model fluid temperature equation), W $\cdot$ m^{-2} $\cdot$ K^{-1}
$G_{T,on}$	Minimum irradiance for useful heat collection, W/m^2
Gz	Graetz number
h	Heat transfer coefficient, W $\cdot$ m^{-2} $\cdot$ K^{-1}
h_0	Zero-order coefficient (dynamic model cell temperature equation), W/m^2
h_1	First-order coefficient (dynamic model cell temperature equation), W $\cdot$ m^{-2} $\cdot$ K^{-1}
h_2	Second-order coefficient (dynamic model cell temperature equation), W $\cdot$ m^{-2} $\cdot$ K^{-2}
H	Horizontal irradiation, kWh/m^2
H_T	Irradiation on the collector plane, kWh/m^2
H_t	Tank height, m

I	Current, A
i	Segment index
I_o	Dark saturation current due to recombination, A
$I_{o,1}$	Dark saturation current due to recombination in quasi-neutral regions, A
$I_{o,2}$	Dark saturation current due to recombination in the depletion region, A
j	Sample index
K	Incidence angle modifier
k	Thermal conductivity, $W \cdot m^{-1} \cdot K^{-1}$
k_B	Boltzmann constant, J/K
$(k\delta)$	Thermal conductivity-thickness product, W/K
K_I	Photovoltaic cell current temperature coefficient, A/°C
K_p	Pipeline coefficient, $W \cdot Kg^{-3} \cdot s^3$
$K_{par,aux}$	Parasitic to auxiliary energy price ratio
$K_{pv,el}$	PV to general-purpose electricity price ratio
K_V	Photovoltaic cell voltage temperature coefficient, V/°C
L	Length, m
m	HWB model auxiliary variable, m
$\dot{m}$	Mass flow rate, Kg/s
N	Quantity
n	Ideality factor
n_1	Ideality factor corresponding to $I_{o,1}$
n_2	Ideality factor corresponding to $I_{o,2}$
$n_{t,he}$	Natural convection heat transfer exponent for the storage tank heat exchanger
Nu	Nusselt number
o_0	Zero-order pump power polynomial coefficient, W

o_1	First-order pump power polynomial coefficient, $W \cdot Kg^{-1} \cdot s$
o_2	Second-order pump power polynomial coefficient, $W \cdot Kg^{-2} \cdot s^2$
o_3	Third-order pump power polynomial coefficient, $W \cdot Kg^{-3} \cdot s^3$
P	Power, W
p	Energy price, €/kWh
Pr	Prandtl number
$\dot{Q}$	Heat flow rate, W
Q	Volumetric flow rate, m^3/s
q	Electron charge, C
R	Electrical resistance, Ω
Ra	Rayleigh number
Re	Reynolds number
S	Solar radiation per unit area absorbed at the absorber plate, W/m^2
S_{pump}	Pump state
T	Temperature, °C or K
t	Time, s
T_R	Reduced temperature, $K \cdot m^2 \cdot W^{-1}$
T_{room}	Room temperature, °C
u_c	Differential temperature controller control signal
$U_{f,p}$	Thermal conductance between the absorber and the collector fluid, $W \cdot m^{-2} \cdot K^{-1}$
U_L	Overall collector heat loss coefficient, $W \cdot m^{-2} \cdot K^{-1}$
$U_{L,1}$	Zero-reduced temperature heat loss coefficient for negligible wind conditions, $W \cdot m^{-2} \cdot K^{-1}$
$U_{L,2}$	Temperature dependence of the heat loss coefficient, $W \cdot m^{-2} \cdot K^{-2}$
U_{sky}	Sky temperature dependence of the heat loss coefficient, $W \cdot m^{-2} \cdot K^{-1}$
U_t	Thermal storage tank heat loss coefficient, $W \cdot m^{-2} \cdot K^{-1}$

U_W	Wind dependence of the heat loss coefficient, $J \cdot m^{-3} \cdot K^{-1}$
u_W	Wind speed, m/s
V	Voltage, V
V_{load}	Daily load water volume, m^3
V_t	Tank volume, m^3
W	Riser tube spacing, m
x	Position, m

Subscripts

a	Ambient
aux	Auxiliary
avg	Time average
b	Beam irradiance
c	Collector
d	Diffuse irradiance
eff	Effective
el	Electrical, electricity
ext	External
f	Fluid
he	Heat exchanger
in	Inlet
ins	Insulation
int	Internal
m	Spatial mean
max	Maximum
min	Minimum
n	Normal to the collector plane

nom	Nominal
oc	Open-circuit
out	Outlet
p	Absorber plate
gas	Natural gas
par	Parasitic energy
bos	Balance of system
ph	Light-generated
pipe	Insulated pipe segment
pump	Circulation pump(s)
pv	Photovoltaic cell(s)
r	Reference
riser	Riser tube
s	Series
sc	Short-circuit
seg	Segment
sh	Shunt
stag	Stagnation
step	DTSSHP controller ramp step
T	Tilted collector plane
t	Thermal storage tank
th	Thermal
u	Utility
w	Thermal storage tank wall

Miscellaneous

X^*	Reference value for variable X fed to controller
$\hat{X}$	Measured value of X quantity
$\widetilde{X}$	Florschuetz model equivalent of X variable for the HWB model

1. Introduction

1.1. Motivation

Technologies capable of supplying heat and electricity sustainably are set to become increasingly important in the context of climate change, depletion of fossil-fuel reserves and energy deprivation among humans. Many technologies are already capable of doing so, directly or indirectly, yet solar thermal (ST) collectors and photovoltaic (PV) panels are mature and can be successfully deployed in most of Earth's regions and in a decentralised fashion. Similarly, hybrid photovoltaic-thermal (PV-T) collectors – which combine both technologies into a single design – can supply heat and electricity simultaneously while retaining a global and decentralised appeal.

Despite the apparent abundance of renewable energy resources, particularly solar energy, and the proliferation of renewable technologies, there is growing doubt about the potential of such technologies to supply Mankind's current and projected energy needs sustainably without major changes to the way human societies are organised. While by no means a panacea to such problems, PV-T technology has the advantage of potentially enabling a higher energy yield than separate side-by-side ST collectors and PV panels of equal combined area and effectively increase the useful energy density to maximise land use efficiency. At the same time, PV-T technology has not lived up to its potential, despite an already long maturation period, since some reliability issues still need to be addressed if it is to reach maturity.

The research efforts undertaken and summarised in this document concern knowledge gaps about the performance of solar domestic hot water (SDHW) PV-T systems with regard to the use of commonly available pump controllers. The following subsections lay out in greater detail the research activities conducted and the problems they seek to address, and prepare the reader to apprehend their significance and their potential application within the current context.

1.2. Context

1.2.1. Human development and sustainability

Energy access has been an important factor in human development, namely for historically significant activities such as heating, food preparation, agriculture and transportation (Smil, 2004). Energy access remains important for human development today, as demonstrated by correlations between the United Nations' Human

Development Index (HDI) for each country and the respective electricity consumption or other key energy consumption-based indicators (Pasternak, 2000; Martinez and Ebenhack, 2008; UNDP, 2011; Arto et al., 2016). However, more than 1 billion people worldwide – predominantly in Latin America, the Caribbean, Sub-Saharan Africa and South Asia – still lacked access to electricity in 2012, arguably the most versatile way to facilitate energy access today (Smil, 2004; UNDP, 2015).

On the other hand, the history of human development has been marred by, among other aspects, pollution, health hazards, loss of biodiversity and climate change, at least since the start of the Industrial Revolution (Crutzen and Stoermer, 2000; IEA, 2015b). Among these, climate change manifested through global average temperature increases, rising sea levels, retreating glaciers, permafrost thawing, among other trends, has arguably the most far-reaching implications and has been linked to anthropogenic emission of greenhouse gases (GHGs), particularly carbon dioxide (CO_2) (Hansen et al., 2008; Montzka et al., 2011). Furthermore, the responsibility for the bulk of cumulative GHGs emissions lies with developed countries and in recent years very high HDI countries – many of which are also among the highest cumulative GHG emitters – still emitted far more CO_2 per capita than low, medium and high HDI countries combined (UNDP, 2011; WRI, 2015; IEA, 2015a).

Several activities lead to GHG emissions but none more so than energy-related services, predominantly due to the combustion of fossil-fuels (IEA, 2015a; WRI, 2015). Despite its current role in human societies, the continued consumption of fossil fuels is bound to deplete reserves created over several hundred millions of years within a few decades or centuries at current production levels, while leading to catastrophic social, economic and environmental consequences in the process (Crutzen and Stoermer, 2000; IEA, 2013). In particular, climate scientists predict that the atmospheric concentration of CO_2 should be, at most, 350 parts per million (ppm) to safely prevent major changes to the Earth's climate and species via global average temperatures 1.7°C below pre-industrial levels (Hansen et al., 2008). However, by 2016 the global average temperature had reached 0.99°C above pre-industrial levels and CO_2 concentration levels reached 406 ppm in 2017, as seen Figure 1.1, increasing at an average rate of 2 ppm/year over the past decade, which projections indicate will continue being the trend unless action is taken (Hansen et al., 2008; Dlugokencky and Tans, 2017; NASA/GISS, 2017; IEA, 2015b,a). As such, the prevailing model for human development needs to be quickly revised.

In this respect, the Paris Agreement entered into force[1] in 2016 and commits 197 signatory countries to ensure the global average temperature remains "well below 2°C above pre-industrial levels" while pursuing efforts to "limit the temperature increase to 1.5°C" (UNFCCC, 2015). Notable for containing provisions to finance its implementation in developing countries by at least 100 billion USD per year – roughly 0.14% of gross world product in 2015 – the agreement has nevertheless

[1] At least 55 signatory countries, representing at least 55% of global GHG emissions, had to formally ratify the agreement for it to enter into force, a condition reached on the 5th of October 2016 which permitted its entry into force on the 4th of November 2016 (UN, 2016).

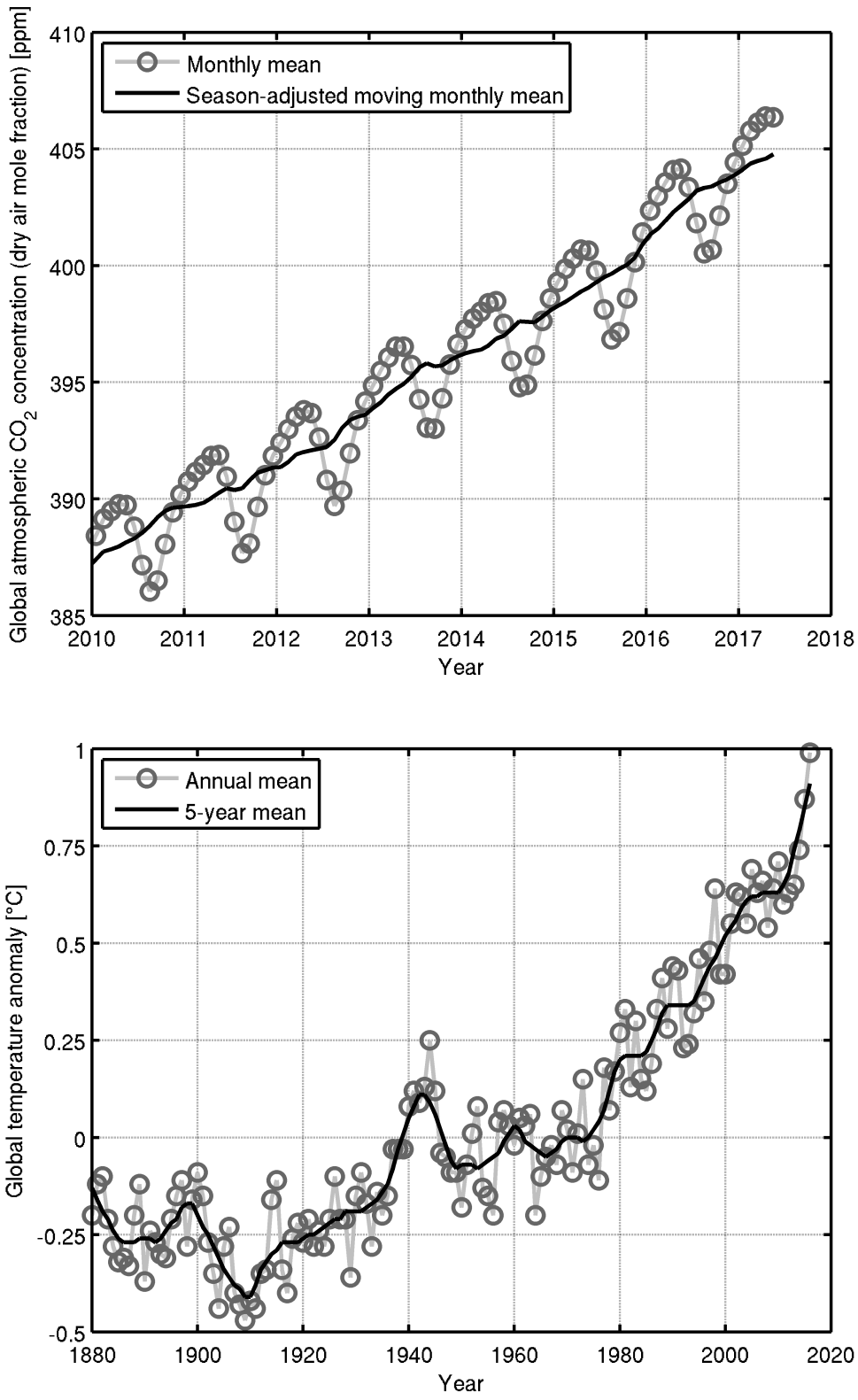

Figure 1.1.: Global atmospheric CO_2 concentration (first row plot) and global temperature anomaly (second row plot) (Source: NASA/GISS, 2017; Dlugokencky and Tans, 2017)

been criticised for encompassing private investment and financial instruments requiring repayment, such as loans with interest, in this financing goal (Orenstein, 2015; Buxton, 2016; OECD, 2015; World Bank, 2016). Several other criticisms have been levelled at the agreement including the exemption of international flights and shipping from GHG emissions' calculations, the over-reliance on inconsistent and experimental "negative emissions" technologies based on carbon capture and storage (CCS), the lack of enforceable mechanisms and the reliance on voluntary nationally determined pledges, revisable every 5 years (Milman, 2015a,b; Burt, 2015; Reyes, 2015). Regardless of intentions, the pledges for 2030 submitted up until late 2015 are projected to be insufficient to prevent global temperatures from exceeding 2°C above pre-industrial levels (IEA, 2015d; Peters et al., 2015; Rogelj et al., 2016). If confirmed, greater global political commitment is necessary for the agreement to conform with its purported aims and prevent "dangerous" climate change, namely by setting more ambitious targets and/or amending the agreement.

In addition to the absence of stronger international commitments on climate change mitigation, several challenges stand in the way of a timely transition towards sustainable human societies. In essence, these challenges concern the ability to supply the current and projected global energy needs, according to the prevailing supply reliability standards, with the existing renewable energy potential, its geographical distribution, the existing technologies, the limited raw materials and respective recycling processes, all in a cost-effective, environmentally sound and politically viable way. The uncertainty about the feasibility of such a bold and quick transformation has been fuelled by recent publications. For instance, recent studies reported that wind, solar and biofuel power densities may be significantly lower than previously estimated (de Castro et al., 2011, 2013, 2014; Jacobson and Archer, 2012; Adams and Keith, 2013; Moriarty and Honnery, 2016; García-Olivares, 2016). Moreover, promising technologies such as concentrated solar power (CSP) plants, PV panels and wind turbines are reported to have higher raw material requirements per unit generation than conventional technologies, which may pose supply problems due to limited reserves and competition with other uses if these technologies are to be scaled up to meet current consumption levels (Vidal et al., 2013; de Castro et al., 2013; Hertwich et al., 2015; Jeffries, 2015). Thus, improvements in mining, recycling and energy efficiency are desirable and likely necessary to smooth the transition towards sustainability, as is the determination of the most efficient technologies in terms of land use and other relevant criteria such as energy return on energy investment (Vidal et al., 2013; de Castro et al., 2014; García-Olivares, 2016).

1.2.2. Energy outlook

Mankind reached a record global primary energy demand of 568 EJ during the year 2013, which International Energy Agency (IEA) projections indicate will keep increasing at least until 2040, although at a slower pace (IEA, 2015d,c). In addi-

tion to this alarming scenario, the share of renewable energy sources[2] in the global primary energy demand is projected to increase from about 14% in 2013 to approximately 15%, 19% or 30% in 2040 for increasingly optimistic projections, the most optimistic of which ("450 Scenario") is only consistent with a 50% chance of limiting global average temperature increases to 2°C relative to pre-industrial levels (IEA, 2015d). Although inadequate to respond to the climate change challenge from an engineering standpoint, which prizes conservative design thresholds to ensure an outcome, the projected increase will be felt in electricity generation, heat use (except traditional biomass, which is expected to decline) and transport, whose shares of renewables in 2013 corresponded to 22%, 10% and 3%, respectively, and are expected to reach between 27-53%, 14-22% and 5-18% in 2040.

Despite these projections, the currently limited contribution of renewables for transport contrasts with the double-digit shares for heat use and electricity generation. Concretely, renewable electricity is still primarily provided by hydroelectric power plants (74% in 2013, down from 85% in 2008) and reached 16% of global electricity supply in 2013, whereas solar, wind and geothermal power accounted for less than 6%, despite notable capacity increases for wind and PV over the past decade – although behind hydropower, even in this regard (IEA, 2010, 2015d). Similarly, the vast majority (over 95%) of renewable heat is provided using bioenergy (including traditional biomass), accounting for around 25% of global heat in 2011, while ST and geothermal accounted for less than 1% of global heat and predominantly within the buildings sector (Eisentraut and Brown, 2014; IEA, 2015d). Thus, modern renewable technologies for heat and electricity – although outpacing those for transport – are yet to make a significant impact on the global energy supply and among renewable technologies themselves, despite great strides in recent years. Nonetheless, according to IEA projections, renewable heat technologies other than traditional biomass are set to deliver between 14% and 22% of the final demand for heat in 2040 while non-hydro renewable technologies are poised to deliver more than half of renewable electricity generation, the majority of which from variable renewable energy (VRE) sources such as the sun and the wind (IEA, 2015d).

1.2.2.1. Renewable electricity

While part of the increase in renewable electricity generation projected for this century can be accommodated without major changes to existing power grids, the integration of the projected high shares of VRE technologies raises questions about the feasibility, cost-effectiveness and sustainability of maintaining the level of supply reliability currently afforded by predominantly unsustainable yet dispatchable technologies (Steinke et al., 2013; Moriarty and Honnery, 2016; IEA, 2008, 2011,

[2]Renewable energy sources are generally defined as those which are continuously replenished by natural processes at rates compatible with their continued use, and are for practical purposes inexhaustible. These typically include direct solar energy (thermal, photochemical and photoelectric), indirect solar energy (wind, hydropower and photosynthetic), geothermal energy and tidal energy (Sorensen, 2004; Kaltschmitt, 2007; Ellabban et al., 2014).

2014). In essence, the fluctuating power output of VRE technologies may suddenly drop to a point that disrupts the supply of electricity – and increasingly so at higher penetrations of VREs such as in a 100% renewables scenario – unless compensated by dispatchable backup power generation and sufficient storage capacity, which current renewable technologies can't provide to the extent that non-renewables can. Among the dispatchable renewables, hydropower and CSP plants are compatible with gravitational and thermal energy storage, respectively, but their deployment (as well as that of geothermal power plants) is geographically sensitive due to terrain and insolation, respectively, while the global potential for the expansion of installed capacity is limited for all including biomass power plants – arguably the only dispatchable renewable technology not overly encumbered by geographical constraints (Field et al., 2008; WBGU, 2009; Steinke et al., 2013; Lako et al., 2003; Hamududu and Killingtveit, 2012; Fridleifsson et al., 2008).

So far, the countries with the highest shares of VREs (5-10%) in the respective energy mixes have not faced significant VRE grid integration challenges, which are only projected for shares above 25% (IEA, 2014). A recent example of the ability to handle current VRE power shortages occurred during the solar eclipse of March 20th 2015, which obscured the North Atlantic, Europe and North Africa for less than three hours. Estimates pointed to a maximum solar power reduction of close to 38% (34 GW) of the estimated installed capacity (90 GW) in the event of clear skies over Europe but the actual reduction only reached 19% and was handled by relying on alternative sources and demand reduction from the industrial sector (ENTSOE, 2015; Eckert, 2015). Future events, not limited to predictable and sporadic eclipses, are expected assume a greater importance as the share of VREs increases and in this sense the successful grid integration of VREs has been predicted to require enhanced energy storage capabilities, improved forecasting, better information and control of resources and loads, improved power system demand response, additional flexible capacity power systems and improved transmission networks (IEA, 2008, 2010, 2011, 2014; Steinke et al., 2013; Huber et al., 2014; Schaber et al., 2012).

1.2.2.2. Renewable heat

With regard to renewable heat use, its growth is projected to be more dynamic and diverse in the buildings sector, in which ST, biomass and other technologies are expected to contribute 17% of the total demand by 2040, up from 10% in 2013 (IEA, 2015d). In contrast, biomass is poised to remain the dominant source of renewable heat in industry for the foreseeable future as its share is projected to increase up to 12%, from 10% in 2014 (IEA, 2015d). Heat temperature and energy intensity requirements coupled with issues of resource availability and supply reliability constitute limiting factors for the deployment of most renewable heat technologies in this sector, particularly in the high temperature heat segment (>400°C). Nonetheless, a significant part – more than half in 2003 – of the industrial heat demand in European countries is required at low (<100°C) and medium (between 100°C and 400°C) temperatures which can be supplied using ST and geothermal in many

regions (POSHIP, 2001; ECOHEATCOOL, 2006). Concurrently, ST heat is a potential option in the high temperature segment for industries located in high direct normal irradiance (DNI) sunbelts, but whose deployment is set to remain limited until 2050, according to the IEA 2°C scenario (Eisentraut and Brown, 2014; IEA, 2015d). Nevertheless, industries will face increasing pressure to adjust to local renewable resources or relocate, in order to meet sustainability goals (Moriarty and Honnery, 2016). As such, the need to adjust industrial processes to existing renewable technologies, and vice-versa, to increase renewable heat use has been recognised and research efforts have been directed for this purpose (Frank et al., 2012).

1.2.2.3. Solar energy potential

Solar energy is presently an abundant renewable energy source on Earth and is expected to remain so for the foreseeable future[3] (Eicker, 2003; Schröder and Smith, 2008; IEA, 2010). Each year, about 5,500,000 EJ of incoming solar energy reaches the Earth's upper atmosphere, about 30% of which is reflected back to outer space, leaving a net contribution to the Earth's energy balance of roughly 3,850,000 EJ (Gustavson, 1979; Smil, 1999, 2003, 2008). In comparison, the global primary energy supply for the year 2013 amounted to 567 EJ, or roughly 0.01% of the annual net solar contribution (IEA, 2015c). At the same time, only part of the incoming solar radiation can be harnessed for stationary ground-level applications due to constraints such as geographical incidence, limited siting options, variable weather conditions and intermittency caused by syzygies and Earth's rotation on its axis. The influence of these factors leads to estimated geographic potentials of solar energy at least two orders of magnitude lower than the net solar contribution, whereas additional technical, economic or sustainability considerations further reduce its potential by up to three additional orders of magnitude, as summarised in Table 1.1. As such, covering mankind's current energy needs may not be possible only with direct solar energy but will likely require a diverse range of energy sources instead.

1.3. Review of selected solar energy technologies

The prospect of a limited role of solar energy in supplying mankind's energy needs makes developing and selecting the most land use and energy efficient solar energy technologies increasingly important. Solar energy technologies include – but are not limited to – ST collectors, CSP plants and PV panels which supply heat for final use, electricity from solar heat and electricity from photoelectric conversion, respectively. Photovoltaic-thermal (PV-T) technology, the focus of this study, is a hybrid variant of ST and PV technology – two of the most deployed solar energy technologies – capable of supplying heat and electricity simultaneously. As such, the states of PV and ST technologies are benchmarks for PV-T technology and

[3]The Sun's fusion reaction, responsible for its radiative power, is predicted to outlast life on Earth and possibly Earth itself (Eicker, 2003; Schröder and Smith, 2008; Duffie and Beckman, 2013).

Table 1.1.: Estimated global renewable energy potential by energy source and type of estimate, compiled from the following sources: Isaacs and Seymour (1973); Gustavson (1979); Barthel et al. (2000); Lako et al. (2003); Hoogwijk et al. (2004); Hermann (2006); Fridleifsson et al. (2008); Field et al. (2008); Trieb et al. (2009); Lu et al. (2009); Mork et al. (2010); Miller et al. (2011); de Castro et al. (2011, 2013); Gunn and Stock-Williams (2012); Schramski et al. (2015)

Source	Geographical	Technical	Economic/Sustainable	Unit
Hydropower	130-158	50-52	25-29	EJ/year
Geothermal	1,010-600,000	8-140	-	EJ/year
Wind	568-6,000	32-640	32-221	EJ/year
Solar	1,575-689,203	-	-	EJ/year
Solar (CSP)	-	10,605	-	EJ/year
Solar (PV)	-	726-15,463	65-130	EJ/year
Biomass	2,000-2,900	276-446	27-270	EJ/year
Tidal	79-85	-	-	EJ/year
Wave	65-117	3	-	EJ/year

relevant for a correct assessment of its merits and shortcomings, particularly for those unfamiliar with all of the above technologies. The following sections briefly review all three technologies, with emphasis on terrestrial, non-concentrating, low-temperature applications, particularly SDHW, where applicable.

1.3.1. Photovoltaics

1.3.1.1. Overview

Photovoltaic cells and modules are semiconductors optimised to generate electricity when exposed to solar radiation. Several semiconductor technologies can be used for PV conversion, each with its specific spectral sensitivity to electromagnetic radiation, which can be combined in tandem (multi-junction cell) to obtain a broader spectral response and higher efficiency, practical considerations notwithstanding. The respective theoretical efficiency limits were determined to be 34% for single junction cells at 25°C and under one sun (1000 W/m², AM1.5 spectrum) whereas for tandem solar cells with an infinite number of junctions the limits were determined to be 68% and 87% for one and multiple suns (i.e., concentrated light[4]), respectively (Shockley and Queisser, 1961; de Vos, 1980; Goswami, 2015).

As of 2017, maximum PV conversion efficiencies for non-concentrating technologies using single- and multi-junction cells are in the 9-29% and 13-39% ranges, respectively, and up to 46% for concentrator cells. However, maximum efficiencies for a given technology at a point in time are generally obtained using small labo-

[4]Light concentration refers to the practice of redirecting solar rays through reflection or refraction using areas larger than those used to absorb the radiation usefully. Alternatively, non-concentrating technologies use the same area to intercept and absorb solar radiation.

Table 1.2.: Maximum PV module efficiencies measured under the global AM1.5 spectrum (1000 W/m²) and cell temperatures of 25°C (IEC 60904-3: 2008, ASTM G-173-03 global), discriminated by technology (adapted from Green et al. (2017))

Photovoltaic Technology	Efficiency [%]	FF [%]	Area [m²]	Date
mc-Si (monocrystalline)	24.4 ± 0.5	80.1	1.32	09/2016
pc-Si (polycrystalline)	19.9 ± 0.4	79.5	1.51	10/2016
GaAs (thin film)	24.8 ± 0.5	84.7	0.09	11/2016
CdTe (thin film)	18.6 ± 0.6	74.2	0.70	04/2015
CIGS (Cd free)	19.2 ± 0.5	73.7	841	01/2017
CIGS (large)	15.7 ± 0.5	72.5	0.08	11/2010
a-Si/nc-Si (tandem)	12.3 ± 0.3	69.9	1.43	09/2014
Organic	8.7 ± 0.3	70.4	0.08	05/2014
InGaP/GaAs/InGas (tandem)	31.2 ± 1.2	83.6	0.10	02/2016

ratory cells rather than mass-produced non-concentrator multi-cell modules, which represent the bulk of installed capacity. Accordingly, peak efficiencies for technologies using single- and multi-junction non-concentrator modules are in the 9-24% and 13-31% ranges, respectively, as summarised in Table 1.2 (Green et al., 2017).

Solar cells do not inherently function at their peak electrical conversion efficiency but are rather conditioned by the incident radiation's intensity and spectral distribution, local weather and load matching. Naturally, incident solar radiation is essential for the conversion to occur and higher irradiance (G_T) levels enable a higher electrical power output, as illustrated on the right hand side of Figure 1.2. Concurrently, the absorption of solar radiation also heats up the cells and along with

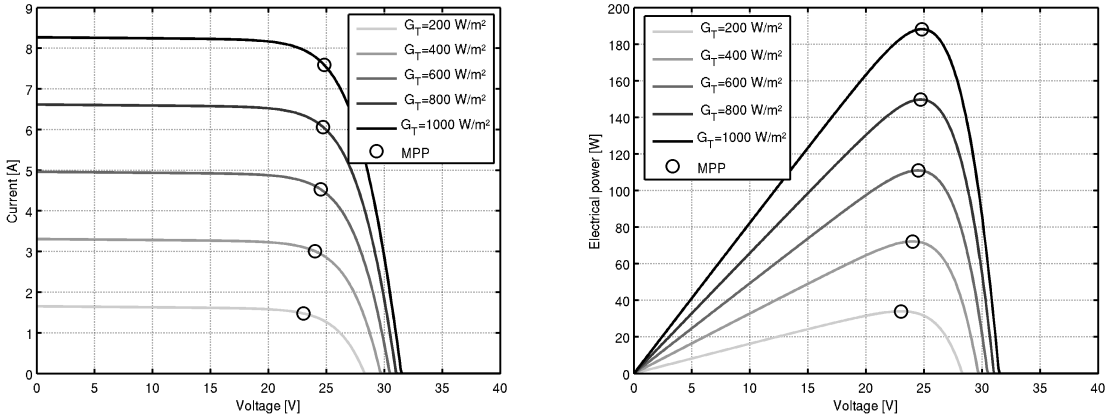

Figure 1.2.: Simulated effect of incident radiation (AM1.5 spectrum) on the current, voltage and power characteristics of a crystalline-silicon photovoltaic module at 45°C (using the model and parameters from Villalva et al., 2009)

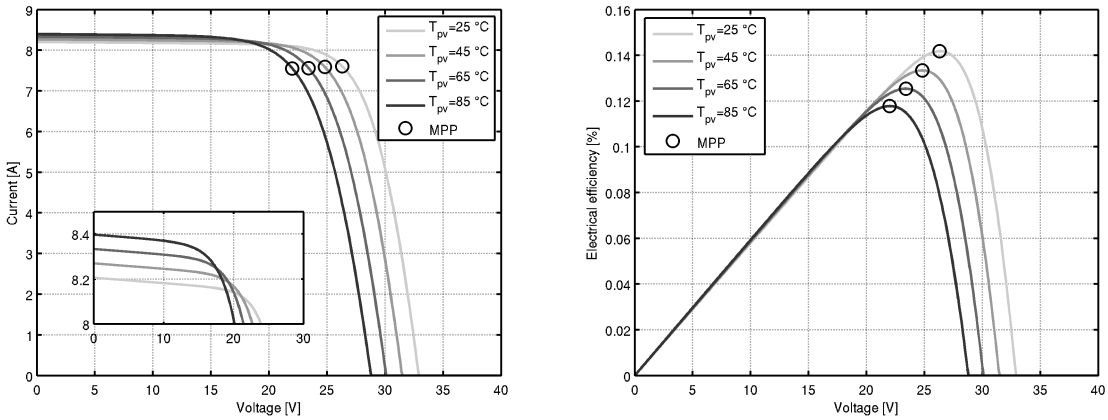

Figure 1.3.: Simulated effect of cell temperature on the current, voltage and efficiency curves of a crystalline-silicon photovoltaic module (under 1000 W/m², AM1.5 spectrum; using the model and parameters from Villalva et al., 2009)

other heat transfer mechanisms, such as longwave radiative heat transfer, natural and wind-based forced convective heat losses and thermal bridges, sets the operating cell temperature, whose influence on cell efficiency is generally negative as exemplified on the right hand side of Figure 1.3 (Skoplaki and Palyvos, 2009).

On the other hand, the load characteristics also influence the performance of solar cells. The effects of cell voltage (V), current (I), temperature (T_{pv}) and irradiance (G) are exemplified in the characteristic current-voltage (I-V) curves of Figures 1.2-1.3, which reveal a maximum power point (MPP) for each individual I-V curve, electrical output power levels rising with increasing irradiance levels as well as positive and negative temperature coefficients for the short-circuit current (I_{sc}) and open-circuit voltage (V_{oc}), respectively. The combined effect of open-circuit voltage and short-circuit current variations as temperatures increase adversely affects the efficiency (or power output) of most solar cells at the MPP, given how the former's temperature coefficient is higher and negative. Thus, the MPP efficiency of most PV cells exhibits a negative temperature coefficient (β_{pv}), often modelled as linear (Skoplaki and Palyvos, 2009). A known exception concerns hydrogenated amorphous silicon cells (a-Si:H), which can exhibit positive or negative temperature coefficients depending on the measurement period duration (Schiff et al., 2011). Table 1.3 lists the typical MPP cell efficiency temperature coefficients for several PV technologies.

Continuously tracking the MPP is of special interest to maximise PV electricity generation and can be achieved using several methods. Direct tracking methods include the perturb and observe (P&O) algorithm, the incremental conductance (IC) algorithm or periodic sampling of the I-V curve and other methods to determine the MPP dynamically, while indirect methods rely on limited measurements, empirical correlations or static assumptions to do so. For instance, a relatively reliable indirect method simply imposes a voltage equivalent to a seasonally-adjusted or constant fraction (e.g., 80%) of the periodically-measured open-circuit voltage,

Table 1.3.: Maximum power point (MPP) solar cell efficiency temperature coefficients and energy bandgap (at 300 K), by PV technology (adapted from Affolter et al., 2005; Skoplaki and Palyvos, 2009; Emery, 2011)

Photovoltaic Technology	MPP efficiency temperature coefficient [%/°C]	Energy Bandgap [eV]
0.53 eV GaInAs	-0.76 to -0.60	0.53
0.75 eV GaInAs	-0.72 to -0.50	0.75
CIGS ($CuIn_xGa_{1-x}Se_2$)	-0.65 to -0.24	1.04-1.68
pc-Si (polycrystalline)	-0.50 to -0.32	1.12
mc-Si (monocrystalline)	-0.52 to -0.29	1.12
InP	-0.41 to -0.16	1.27
GaInP/GaAs	-0.21 to -0.19	1.85/1.42
GaAs	-0.27 to -0.19	1.42
CdTe	-0.41 to -0.12	1.44
a-Si	-0.26 to -0.05	1.6-1.8
a-Si (tandem)	-0.23 to -0.00	1.6-1.8/1.1-1.7
1.7 eV AlGaAs	-0.17 to -0.10	1.7

given the approximately fixed relative proximities of the MPP voltage and current to the open-circuit voltage and the short-circuit current, respectively, which tend to hold even as the irradiance or cell temperatures change – see Figure 1.3 (Luque and Hegedus, 2011). Nevertheless, direct methods tend to perform best and are generally independent of the module type (Hohm and Ropp, 2000, 2003; de Brito et al., 2013; Bendib et al., 2015; Rezk and Eltamaly, 2015).

1.3.1.2. Applications

The electricity produced by PV modules, either at the MPP or not, can be stored, used locally or fed to local utility grids efficiently through the use of power converters. Grid-connected PV systems, which make up a majority of existing systems, typically inject electricity into local AC grids using MPP-tracking capable inverters or separate converters for each conversion stage (IEA-PVPS, 2016c). Similarly, autonomous PV systems rely on one or more power converters to charge electrochemical batteries and/or supply loads while performing MPP tracking or not. Moreover, MPP tracking in autonomous systems is possible as long as the loads and/or batteries can accommodate the respective power output, whereas grid-connected systems are generally prevented from supplying electricity during blackouts as a safeguard against the islanding phenomenon[5] (Bollen and Hassan, 2011; Karimi et al., 2016). Known autonomous applications include powering orbital satellites, spacecraft for inner Solar System exploration, water pumps, weather stations, communication equipment

[5]Islanding, in this case, refers to the system being disconnected from the grid and maintaining the voltage and frequency within the recommended limits (Smith et al., 2000).

in boats and other mobile equipment or other power uses at remote locations. Alternatively, grid-tied systems can function as distributed power generation units close to load centres or centralised systems whose power capacity is limited by land area occupied, land use efficiency and the PV technology (de Castro et al., 2013).

Accordingly, PV modules are modular, do not cause GHG emissions during use, have no moving parts (unless tracking is used) and can function as distributed or centralised power systems. At the same time, the technology's main operational disadvantages pertain to the variable nature of the solar resource for terrestrial applications, the slowly decreasing effective power rating (<1%/year) over a 20+ year useful lifespan, and debilitating though apparently uncommon reliability issues (Pern, 1996; Kato, 2012; Luque and Hegedus, 2011; Shioda, 2013).

1.3.1.3. Lifetime and reliability issues

PV modules are usually expected to have a useful lifespan of 20-30 years due to generous performance warranties (80% of nominal performance after said period). However, the technology also has reliability issues whose consequences range from permanent or temporary performance degradation to catastrophic module failure and fire hazards, stemming from inadequate installation and maintenance, harsh weather conditions and manufacturing defects (Vázquez and Rey-Stolle, 2008; Falvo and Capparella, 2015; Manzini et al., 2015; Hegedus and Luque, 2011; Tobías et al., 2011). The most pressing reliability issues include: PV encapsulant delamination and coloration due to high cell temperatures and UV exposure (Pern, 1996; Shioda, 2013); broken cell connections due to corrosion and thermal stress (Kato, 2012); hot spots due to partial shading and subsequent bypass diode failure due to overheating (Kato, 2012); and, potential induced degradation of cells due to series connection of PV modules, though most noticeably in utility-scale PV farms (Luo et al., 2017). Despite these issues, field failure rates for PV modules are reportedly low and often attributed to their compliance with demanding reliability tests such as those defined in IEC 61215 and IEC 61646 standards for crystalline-silicon and thin-film PV modules, respectively (Hegedus and Luque, 2011; Tobías et al., 2011).

1.3.1.4. Trends

The adoption of PV technology has been proceeding at increasing rates, as record global annual capacity increases have been reported nearly every year (IEA, 2015d; IEA-PVPS, 2016a). The cumulative global capacity of PV systems has also been increasing, along with the respective electricity generation. The former reached 228 GW by the end of 2015 while the latter amounted to roughly 139 TWh in 2013 ([6]), up from 12 TWh just 5 years prior, and is projected to reach up to 285 TWh in

[6]The cumulative installed PV capacity by the end of 2013 was at least 137 GW, which for a total generation of 139 TWh corresponds to a maximum global average capacity factor of 12%, the lowest among mainstream power system technologies (>100 GW) and indicative of the variable nature of the solar resource for terrestrial applications (IEA, 2015d).

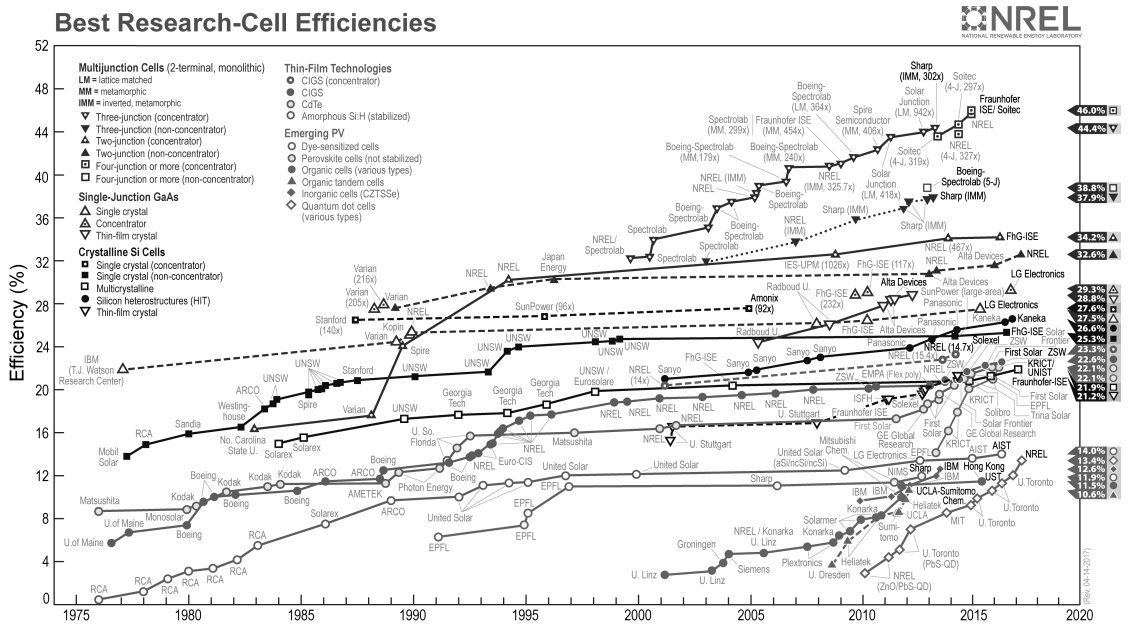

Figure 1.4.: Highest confirmed PV cell efficiencies since 1976, by technology (This plot is courtesy of the National Renewable Energy Laboratory, Golden, CO.)

2015 (IEA, 2010, 2015d; IEA-PVPS, 2014a). According to the IEA's Photovoltaic Power Systems Programme (IEA-PVPS), at least 86% of the total installed capacity by 2015 was in the grid-connected segment and in recent years increasingly in the form of comparatively cost-competitive utility-scale projects (IEA-PVPS, 2016c; SPE, 2016). Dramatic module cost reductions (down to roughly 0.4 USD/W, for some countries) and notable cell and module efficiency increases over the years – compare Figure 1.4 and Table 1.2 with the approximately 6% efficiency obtained with the first practical solar cell as detailed in Chapin et al. (1954) – have accompanied and benefited the PV industry's rapid growth but, on a negative note, may have contributed to an excessive PV manufacturing capacity and consequent under utilisation of manufacturing facilities, which resulted in consolidation, downsizing and bankruptcy of several companies (EIA, 2016; SPE, 2016; IEA-PVPS, 2016c).

Despite the turmoil, crystalline silicon (c-Si) technologies continue to dominate the PV market, accounting for an estimated 93% of all PV modules shipped in 2015, which breaks down to 69% and 24% for poly- (pc-Si) and mono-crystalline (mc-Si) modules, respectively (SPE, 2016; FISE, 2016). In contrast, thin film technologies were responsible for approximately 7% of shipments, primarily Cadmium Telluride (CdTe) and Copper Indium (Gallium) (Di-)Selenide ($CuIn_xGa_{1-x}Se_2$, collectively known as CIGS). Among thin films, only CdTe was produced by (one of) the top 10 PV manufacturers by capacity in 2014 and its rise in prominence has been accompanied by the relative demise of amorphous-silicon (a-Si) technologies (IEA, 2015d; FISE, 2016). Efficiency gains (see Table 1.2) and cost reductions have fuelled the success of CdTe technology but its potential for future expansion of in-

stalled capacity into the TW range has been questioned due to limited Tellurium (Te) reserves (Green, 2009, 2011). Similarly, current c-Si and CIGS technologies may also face difficulties in expanding to the TW range due to limited silver (Ag) and indium (In) reserves, respectively, although Ag may be replaced in future c-Si modules (Andersson, 2000; Feltrin and Freundlich, 2008; Luque and Hegedus, 2011; Candelise et al., 2012; de Castro et al., 2013; García-Olivares, 2015). As such, several PV technologies will likely be required for the installed capacity to reach the TW range, particularly since the technologies not overly encumbered by limited material reserves such as a-Si have comparatively low efficiencies at present – see Table 1.2 – and thus demand more land area for the same capacity.

1.3.1.5. Policies

The widespread deployment of PV systems over the years has occurred amid lower fossil-fuel energy prices, although so-called grid-parity may now be a reality in some locations. Government subsidies and other policies have been crucial in overcoming this disadvantage and in contributing to the adoption, research and development of PV technology (Pillai, 2015). Examples include tax credits and exemptions, preferential interest rates and loan programmes, direct incentives, building code mandates, power purchase agreements (PPA), feed-in tariffs (FiT), renewable portfolio standards (RPS), net metering, interconnection standards and pilot projects (Byrne and Kurdgelashvili, 2011; IEA-PVPS, 2010). Feed-in tariffs, in particular, are often credited with the PV boom since the early 2000s and remain the most used incentive mechanism for PV, according to IEA-PVPS data for 2015 (SPE, 2016).

The FiT mechanism, originally introduced in Germany, typically offers energy producers grid access privileges for long periods and guaranteed energy prices reflective of technology-specific generation costs. Nevertheless, German feed-in tariffs were initially generous and intended to decline over time to encourage or accompany cost reductions within the industry but have also been curtailed to contain the program's costs due to its widespread success (Wirth, 2016). Accordingly, PV support policies have increasingly focused on alternative mechanisms such as net metering or self-consumption (Campoccia et al., 2014; Dusonchet and Telaretti, 2015).

1.3.2. Solar thermal (ST) technology

1.3.2.1. Overview

Solar thermal heat technologies convert the Sun's electromagnetic radiation into useful heat through technology-specific devices collectively known as solar collectors. Solar collectors contain at least (but also generally) one contiguous high absorptance surface, commonly designated as the absorber, simultaneously designed to facilitate heat transfer with a fluid, known as the heat carrier, along a designated flow path from the collector's inlet to its outlet. When incident solar radiation reaches the absorber, its temperature increases and, although it leads to higher heat losses

Table 1.4.: Useful temperature range, concentration ratio and tracking requirements of relevant solar collector technologies (adapted from Kalogirou, 2009)

Motion	Collector Type	Concentration ratio	Temperature Range [°C]
Stationary	Flat-plate collector (FPC)	1	30–80
	Evacuated-tube collector (ETC)	1	50–200
	Compound parabolic collector (CPC)	1–5	60–240
		5–15	60–300
Single-axis tracking	Linear Fresnel reflector (LFR)	10–40	60–250
	Cylindrical trough collector (CTC)	15–50	60–300
	Parabolic trough collector (PTC)	10–85	60–400
Two-axis tracking	Parabolic dish reflector (PDR)	600–2000	100–1500
	Heliostat field collector (HFC)	300–1500	150–2000

to the surroundings, potentiates a higher heat transfer rate with a comparatively cold heat carrier, which can remove heat from the collector through circulation. Accordingly, gathering solar radiation, absorbing it, reducing absorber heat losses to the surroundings, and removing heat from the collector are the main subtasks for solar collectors, and how each is tackled determines the collector's performance, cost, longevity and potential application, generally defined by a temperature range.

Several of the collector designs proposed over the years reached maturity. These are typically categorised according to their most prominent features, namely geometry (i.e., shape of the absorber, reflector or the collector itself), solar tracking requirements, heat carrier (phase) and heat loss mitigation techniques (e.g., glass cover(s), selective absorber or vacuum). Additional differentiating factors include the type of materials used (e.g., polymeric), the fluid mover (pumps or blowers for active or forced circulation collectors; gravity for thermosyphon collectors), among others. Table 1.4 lists several prominent collector types and respective solar tracking requirements, concentration ratios and temperature ranges. Among these, two low- to medium-temperature collector types are among the most deployed and pertinent for the purposes of the current study, and can be briefly described as follows:

- Flat-plate collectors (FPC) are modular units employing flat or quasi-flat (e.g., roll-bonded, corrugated, extruded, soldered) surfaces to absorb radiation, less commonly in conjunction with the heat carrier itself (e.g., trickle down collectors). FPCs commonly house the absorber inside slim thermally-insulated boxes with one or more top-facing high-transmissivity glass covers. Alternatively, unglazed FPCs (e.g., pool heaters) also lack the thermally-insulated box, and are typically manufactured using light, inexpensive and often flexible plastic materials. In either case, heat is removed from the collector through circulation using heat exchangers in contact or embedded in the absorber;

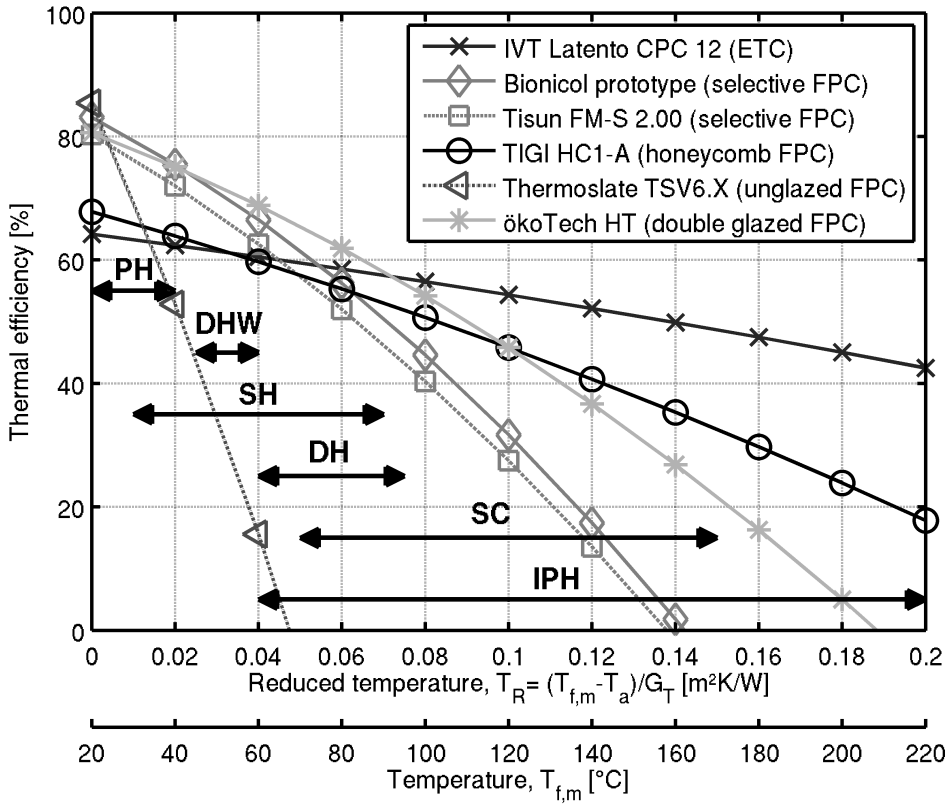

Figure 1.5.: Thermal efficiency curves (T_a=20°C, G_T=1000 W/m^2) for representative ST collectors (compiled using data from: Hermann, 2011; Solar Keymark, 2017) and temperature ranges for several applications listed in Table 1.5: pool heating (PH); domestic hot water (DHW); space heating (SH); district heating (DH); space cooling (SC); industrial process heat (IPH).

- Evacuated or vacuum tube collectors (ETC) employ very low pressures inside sealed modular glass tubes to greatly reduce heat losses to the surroundings from flat or tubular absorbers located inside. Some designs expose the absorber to vacuum using a single glass tube while others use two concentric glass tubes with a vacuum gap between them. ETCs typically feature several long and slender glass tube units arranged in parallel and whose top end connects to a narrow manifold, or a storage tank for some thermosyphon systems. Heat is removed from the absorbers through circulation along finned tubes, tubular absorbers, or using heat pipes[7] in conjunction with circulation in the header pipe or convection inside storage tanks. Finally, low concentration ratios can be achieved with these collectors by placing reflectors inside the tubes or externally, namely compound parabolic mirrors (Goswami, 2015).

[7]Heat pipes are heat transfer devices using gravity-assisted phase-changing loops inside sealed hollow pipes to achieve high heat transfer rates. Some ETC designs use slender single-fluid heat pipes finned to absorbers to transfer heat to a manifold or storage tank.

The suitability of a collector for a given application is in part limited by its temperature range, summarised in Table 1.4 for mature collector technologies. The temperature range can be determined from thermal efficiency curves assembled from performance tests (such as those described in standards EN 12975:2-2006 or ISO 9806:2013) conducted under mostly stable conditions, high insolation levels and for several collector inlet temperatures (CEN, 2006; ISO, 2013). These curves are often presented as a function of the reduced temperature ($T_{R,m}$), defined in (1.1) as the difference between the mean collector fluid temperature[8] ($T_{f,m}$) and the ambient temperature (T_a), divided by the global irradiance on the collector plane (G_T), which is useful for ST collector performance analysis. Thermal efficiency curves for technologically-representative low- and medium-temperature ST collectors are given in Figure 1.5 along with indicative temperature ranges for selected applications.

$$T_{R,m} = \frac{T_{f,m} - T_a}{G_T} \tag{1.1}$$

The curves have at least two noteworthy points, namely the curve's y- and x-intercepts. The former is the zero-reduced temperature thermal efficiency, since convective heat losses are negligible ($T_{f,m}$=T_a), and the latter corresponds to the stagnation temperature, the maximum collector temperature for useful heat generation[9]. In essence, this stagnation temperature must exceed an application's temperature requirements by a sizeable margin for the collector to be able to supply its heat requirements at reasonable efficiencies during at least part of the year.

1.3.2.2. Applications

Solar thermal technologies are compatible with space heating and cooling, domestic water heating, pool heating, desalination, district heating, electricity generation (CSP or thermoelectric) and industrial process heating. According to Kalogirou (2003), the most relevant industrial processes requiring heat include sterilising, pasteurising, drying, hydrolysing, distillation and evaporation, washing and cleaning, and polymerisation. FPCs, ETCs and CPCs are suitable for most low-temperature (<100°C) applications, as illustrated in Figure 1.5, and some medium temperature (<250°C) applications generally up to 150°C (Kalogirou, 2009; Goswami, 2015; Hess, 2016). A summary of temperatures required for several of the aforementioned applications is given in Table 1.5. More detailed information about industrial process heat applications can be found in Kalogirou (2003) and Lauterbach et al. (2012).

[8] The reduced temperature is also commonly given as a function of the collector inlet fluid temperature instead of the mean collector fluid temperature used in (1.1) (Zondag et al., 2002).

[9] Some ST collectors with very low heat losses can't reach their stagnation temperatures without physically damaging the collector itself in the process (Frank et al., 2015).

Table 1.5.: Design temperatures for selected ST-compatible low (<100°C) and medium (<250°C) temperature applications (compiled from: Eicker, 2003, 2009; Kalogirou, 2003; Kaltschmitt et al., 2007; Weiss et al., 2003; GES, 2010; Lauterbach et al., 2012; Chow et al., 2012; Duffie and Beckman, 2013; Davis, 2015)

Application	Temperature [°C]	Comments
Pool heating	-	
- swimming pool	18-28	Water temperature
- jacuzzi	33-40	
Space heating	-	
- radiator/convector	50-90	Delivery temperature
- underfloor	30-45	
Space cooling	-	
- adsorption	70	Supply temperature
- absorption, single effect	70-90	
- absorption, double effect	150-170	
Domestic water heating	45-60	Delivery temperature
District heating	60-95	DHW and SH
Industrial process heat	60-220	Various processes

1.3.2.3. Supply reliability

Many applications can require heat when ST systems are technically incapable of supplying it. This can occur due to a mismatch between the solar resource's availability and the heat demand (e.g., at night) or, more generally, the inability to meet the application's temperature specifications continuously (e.g., following a period of low insolation). For these reasons, many ST systems feature backup heaters and thermal storage to ensure a satisfying level of supply reliability.

Thermal energy storage

Thermal energy storage (TES) contributes to a decoupled supply and demand by storing thermal energy when it is not needed and allowing loads to be supplied at a later point in time. While not necessary for all applications[10], such a feature is essential for supply reliability in many, including domestic hot water (DHW).

Active SDHW systems typically employ thermally insulated water tanks as TES, cost and simplicity being among their main advantages. Loads are commonly supplied by withdrawing hot water from the top and replacing it with cold tap water at the bottom although internal heat exchangers can also be used for this purpose (Kaltschmitt et al., 2007). A mixing valve is also commonly used to mix hot tank water with cold tap water in the demand loop to meet the desired temperatures or simply to prevent scalding. In turn, the tank charging process can be

[10]Examples of solar heating systems without dedicated storage units include some pool heating systems and (wood, fruit or other) solar drying systems (Kaltschmitt et al., 2007; Hess, 2016).

direct[11] through double (inlet and outlet) ports or indirect via internal immersed coil, mantle[12] or external heat exchangers in combination with double ports. Figure 1.6 displays the basic diagrams for two of the most common types of active solar heating systems using immersed coil- and external heat exchangers.

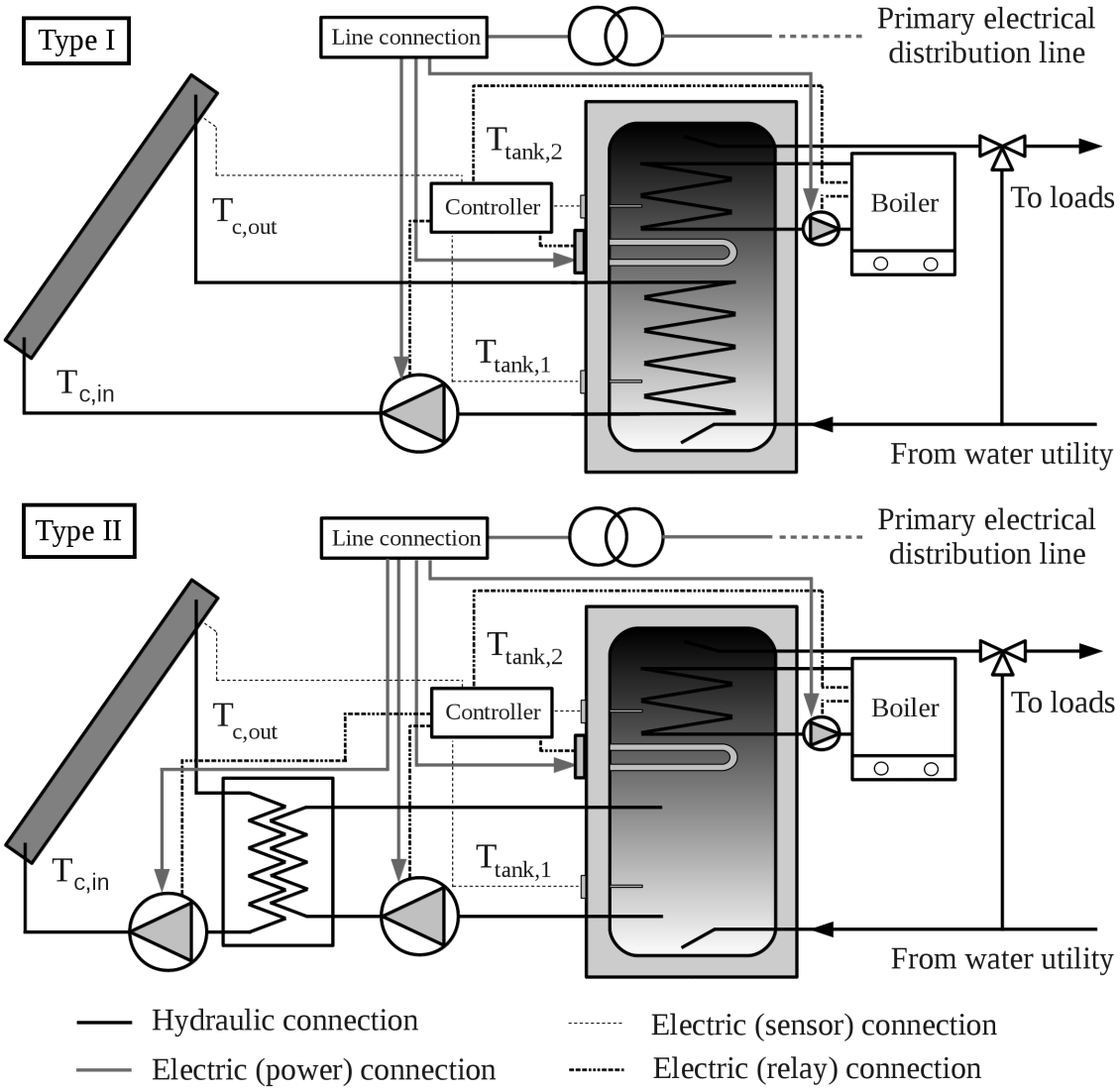

Figure 1.6.: Grid-connected forced circulation solar heating systems employing tank charging methods reliant on: I) internal heat exchangers (top diagram); II) external heat exchangers and direct double ports (bottom diagram)

Each of the aforementioned charging methods has a distinct influence on thermal

[11] According to Kalogirou (2009), a direct (circulation) system heats the fluid supplied to the loads by allowing it to circulate through the collectors, i.e., without heat exchangers in between.

[12] Mantle heat exchangers are embedded in double-walled storage tanks, tend to have a large heat transfer area compared to alternatives and are commonly (but not exclusively) used in thermosiphon systems (Kaltschmitt et al., 2007; Cruickshank and Baldwin, 2016).

stratification, that is, the existence of horizontal fluid layers of different densities, with light and hot layers at the top and cold heavy layers at the bottom, which can improve the collector and storage efficiencies (Han et al., 2009). In essence, the methods with mantle and external heat exchangers are known to preserve or enhance thermal stratification, namely at conventionally low specific mass flow rates, whereas using internal heat exchangers tends to mix the different fluid layers. Moreover, tanks featuring internal heat exchangers are commonly used in so-called "high-flow" systems featuring parallel-connected collectors and observing specific (relative to the collector area) mass flow rates in the range of 0.01-0.02 Kg/m²s for maximum temperature rises across the collector between 8 and 12 K (GES, 2010). In contrast, "low-flow" systems are optimised for thermal stratification by using direct double ports and external heat exchangers, and achieving higher temperature rises (up to 40-50 K) through combinations of lower specific mass flow rates (between 0.002 and 0.004 Kg/m²s) and series-connected collectors (Weiss et al., 2003; Kaltschmitt et al., 2007; Kalogirou, 2009; Goswami, 2015). Nevertheless, thermal stratification can also be improved by incorporating internal vertical distribution manifolds or baffle plates into the tank design, the latter to prevent incoming streams – either from the collector loop or from the water utility line – from mixing different fluid layers (Streicher and Bales, 2005; Cruickshank and Baldwin, 2016; Streicher, 2016).

Thermal stratification can only do so much in the absence of an adequate tank size. For SDHW systems, tanks are commonly sized to store thermal energy for periods ranging from days to months (i.e., seasonal storage). Small systems (< 10 m²) generally employ tanks sized for one or more days of storage which typically correspond to specific storage volumes relative to the total collector area between 35 and 70 L/m². In turn, large forced circulation systems (> 100 m²) have specific volumes in the range of 50-100 L/m², or at least 10 times higher for district heating (DH) systems with seasonal storage (Eicker, 2003; Weiss et al., 2003).

Auxiliary heaters

Systems with seasonal storage are among those that can dispense with auxiliary heaters, while many others require them for supply reliability. SDHW systems are traditionally among the latter group since they are sized for the Summer months and hence require additional energy during the Winter. Electrical heating elements, heat pumps, fossil-fuel or biomass-fired boilers can all be used for this purpose.

The auxiliary heaters can be further differentiated by their interactions with the storage tank. Some heaters, refered to as "instantaneous" or various other names[13], are designed to be placed in the same circuit as the loads whereas others are designed to charge storage vessels (Kaltschmitt et al., 2007; GES, 2010). The former group leads to lower stand-still heat losses, has the advantage of not interfering with the solar collection efficiency – unlike the latter whose use contributes to higher collector temperatures – and according to a couple of studies presents less health risks with

[13]Alternative names given to this type of heater include "tankless", "inline", "instantaneous", "on-demand", among others (Mathys et al., 2008; GES, 2010; Brazeau and Edwards, 2011).

regard to legionella[14] (Martinelli et al., 2000; Mathys et al., 2008; Brazeau and Edwards, 2011). However, instantaneous heaters tend to cycle more, commonly have higher power ratings than storage heaters, which is particularly troubling for electrical heaters given their consumption of peak time electricity, and can't be used if the energy supply is interrupted (e.g., a power blackout). In turn, storage heaters allow for independent control of boilers' outlet temperatures and mass flow rates relative to the loads (Streicher, 2012). Figure 1.6 shows diagrams for SDHW systems equipped with the two types of storage heaters emphasised in this study: tank-immersed electrical heating elements and boilers.

1.3.2.4. Flow control

Active closed-loop ST systems with storage require controllers to determine when to start, adjust and end heat carrier circulation in the supply-loop. Accordingly, their main objective is to collect and store heat efficiently although commonly in line with other practical concerns such as low parasitic energy and costs as well as controller output stability and overheating protection (Hirsch, 1985; Winn, 1993; Peuser et al., 2002). While irradiance- and pressure-induced controls have also been proposed, most low-temperature ST systems with storage tanks such as those exemplified in Figure 1.6 employ differential temperature controls, which are conceptually based on the fact that a positive temperature difference between the hottest point in the collectors and the coldest point susceptible to charging within the tank is a necessary condition for useful heat transfer between the two (Close, 1967; Peuser et al., 2002; Kaltschmitt et al., 2007). As such, their output is commonly governed by the temperature difference (ΔT) between the collector absorber or fluid near the outlet and the fluid near the bottom of the tank or slightly below the internal heat exchanger inlet port, as long as the heat carrier temperature is low enough – typically up to around 95°C for low-temperature systems – to rule out heat carrier boiling and damage to temperature-sensitive components (Beckman et al., 1994; Kaltschmitt et al., 2007; Kalogirou, 2009). The most common of these controllers simply initiates and ends fluid circulation once the aforementioned ΔT exceeds or falls below preset turn-on (ΔT_{on}) and turn-off (ΔT_{off}) setpoints, respectively, whereas more complex variants also adjust the collector flow rate dynamically.

Implementation

Implementation of these controls typically relies on actuation of electrical centrifugal pumps[15], particularly in the domestic low-temperature segment (Kutscher et al., 1982; Winn, 1993). As such, the flow rate is mainly manipulated either by electronic

[14] Legionella are bacteria commonly found in water sources and can cause Legionnaires' disease, an often fatal ailment. The bacteria tend to grow in water temperatures above 20°C, can't survive above 60°C and are typically transmitted through aerosols (EWGLI and EWGLINET, 2005).

[15] The term "pump" used throughout this document refers to the pump unit encompassing the pump, prime mover and the electronic speed drive (if any), unless otherwise stated.

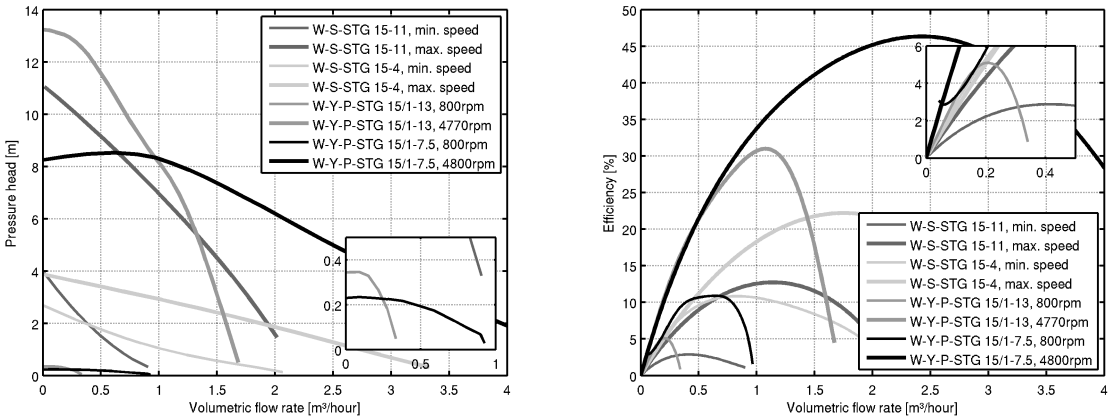

Figure 1.7.: Pressure-flow (left-hand side) and efficiency-flow (right-hand side) curves for currently available pumps suitable for low-temperature ST systems

speed control or simply by actuating a relay for variable-flow or two-state control, respectively, whereas throttling is reserved for sporadic manual flow adjustments. Manually-selectable multi-speed stage pumps are also commonly used alleviate the need for throttling in small two-state controlled systems whereas cost and superfluity imperatives determine that more flexible and typically larger high-efficiency speed-controlled pumps not be used in those systems (GES, 2010).

Pump selection

A comprehensive range of pumps are available today for use in low-temperature ST systems of virtually all common sizes, although this was not always the case. For example, domestic heating pumps were commonly used for small SDHW systems in Europe up until the last 15 years for lack of a better option despite being clearly oversized (Peuser et al., 2002; Eicker, 2003; GES, 2010). As a result, suboptimal pump efficiencies in the range of 2-7% were common due to the need to substantially curtail flow rates, namely via throttling – which is simpler and more affordable than dynamic speed control although widely understood to be less energy efficient (Volk, 2005; Stoffel, 2015). Over time, some pump designs have been reportedly optimised for ST systems in terms of temperature ratings, pressure-flow characteristics and efficiency (Peuser et al., 2002; GES, 2010). Figure 1.7 compares the performances of a few currently available centrifugal pumps for low-temperature ST systems.

Securing a high operating pump efficiency is highly desirable in ST systems since it generally contributes to a prolonged pump life and a reduced parasitic consumption (Peuser et al., 2002). Notably, the supply-loop parasitic consumption can account for as much as 15% and 10% of the energy collected as the result of its use in SDHW and solar combi-systems, respectively, unless high efficiency pumps are used (Eicker, 2003; Weiss et al., 2003). A few efforts have promoted the use of high

efficiency pumps, namely standardisation and the enactment of pump efficiency regulations. For example, the now withdrawn EN 12977:2001 standard suggests the pump power rating for small heating systems should not exceed 50 W or 2% of the system's nominal heat capacity, whichever highest, or 1% for large systems due to the higher efficiencies of larger pumps (Streicher, 2012). Furthermore, recent European Commission (EC) regulations mandating minimum pump efficiency standards – whose jurisdiction currently affects many of the world's leading pump manufacturers – have preceded and arguably led to the phased introduction of cost-effective high efficiency circulation pumps including some for ST systems (EC, 2009, 2012).

1.3.2.5. Trends

Solar thermal heat technologies have been deployed on a global scale. According to the International Energy Agency's Solar Heating and Cooling (IEA-SHC) Programme, the total installed capacity of solar thermal collectors reached a record high 410 GW-equivalent[16] by the end of 2014, due to an estimated 101 million systems in operation with a collector area of approximately 586 million square meters. As a result, solar heating systems generated at least 335 TWh in over 60 countries during 2014 and displaced 116 million tonnes of CO_2 worldwide, although predominantly from industrialised nations and economic blocs. In particular, the geographical distribution of installed capacity is very uneven with about 71% located in China, followed by Europe and North America with approximately 12% and 4%, respectively. Application-wise, about 91% of systems installed are used for DHW in mostly small (63%) but also large (28%) plants, about 6% for pool heating, 2% for combi-systems (i.e., systems providing DHW and space heating) and only 1% for other applications, which means an overwhelming majority of ST systems are used for low temperature applications (Mauthner et al., 2016).

On the other hand, the global market contracted by approximately 15% in 2014 relative to 2013. Despite an increase in total installed capacity of roughly 47 GW-equivalent, 2014 was the first year with a reported market reduction, followed decreasing growth rates in the two previous years and coincided with a period during which oil prices fell noticeably, albeit only during the last few months of 2014 (IEA, 2015d). Nevertheless, regional growth was reported in North America (1%), Latin America (8%) and Asia excluding China (3%) (Mauthner et al., 2016).

Regional markets have also revealed noticeable differences over the years. For instance, pool heating systems outnumber all other systems in North America, Australia, New Zealand and Sub-Saharan Africa while DHW systems represent the majority in all other regions including Asia and Europe. In terms of collector technology, ETCs lead all other technologies by installed collector area in China and the world (71%), whereas glazed and unglazed FPCs are the most representative collectors in Europe and North America, respectively, and the second (22%) and

[16]Solar thermal experts agreed to use a constant power density of 0.7 kW/m² to derive the nominal capacity of solar thermal systems from the respective collector area, for the purpose of comparing it with other energy sources (Mauthner et al., 2016).

third (6%) most deployed technologies globally. Similarly, about 78% of systems are passive (i.e., thermosiphon), particularly in North and Sub-Saharan Africa, Asia and Latin America, whereas active (i.e., forced circulation) systems are more common in North America and Europe (Mauthner et al., 2016). The aforementioned regional differences are related with several factors including the prevailing regional heat uses, climate, collector performance, cost, energy prices, policy and the existence of local manufacturers since, according to one survey, most manufacturers are medium-sized companies focused on local markets (Hudon, 2014; Epp and Banse, 2015). As such, these trends are indicative of a diverse global market.

Despite the progress made with ST heat technologies, some challenges remain. Among them, the ability to replace other sources of heat completely has proved limited (IEA, 2010). Seasonal storage is seen as part of the solution to this problem but is inherently large and typically expensive, although recent developments in thermal energy storage, such as large vacuum insulated tanks and thermochemical storage, are promising (Schmidt et al., 2003; Reuss and Melzer, 2013; Aydin et al., 2015). Another challenge concerns PV technology, whose cost decreases have outpaced those of ST technologies and have already rendered PV heating systems cost-competitive in some regions and segments, with the added advantage of being more exergy efficient, versatile and uniform – in stark contrast to the system complexity and diversity observed in the low temperature ST segment alone (Affolter et al., 2005; Drück, 2011; Drück and Sommer, 2013; Norton, 2014; Meyers et al., 2015; Streicher, 2016). Nevertheless, the projected limited potential for the expansion of PV capacity into the TW range and the need for larger areas may counter this trend and help secure a future for ST technology in the long run.

1.3.3. Hybrid photovoltaic-thermal (PV-T) technology

1.3.3.1. Overview

Photovoltaic-thermal (PV-T) collectors combine solar thermal and photovoltaic technology in a single collector capable of converting solar radiation into heat and electrical power simultaneously and otherwise. In other words, PV-T technology allows for uniform aesthetics while providing both energy forms but its key advantage is arguably the fact that it has been shown to outperform side-by-side PV and non-hybrid ST systems of equivalent combined area in several respects, namely energy density. According to simulations conducted by Dupeyrat et al. (2010), Dupeyrat et al. (2011a) and Fortuin et al. (2014), SDHW and combi- PV-T systems can lead to higher combined energy yields than side-by-side PV and ST systems, each with half the PV-T collector aperture area or, one or the other with the same aperture area as the PV-T collector array. Similarly, Dupeyrat et al. (2014) determined through simulations that PV and SDHW PV-T systems combined made better use of a 25 m^2 roof in terms of exergy output and primary energy savings than PV and ST systems. Thus, PV-T collectors potentiate shorter payback times and are well suited for densely populated urban areas or more generally sites with limited

available area for PV panels and ST collectors. Moreover, PV-T technology also has potential cost advantages in manufacturing, installation and maintenance due to shared facilities, savings in raw materials and labour, and lower collector areas although all of these have arguably failed to materialise in any meaningful way thus far (Zondag et al., 2003; Leenders et al., 2000; Affolter et al., 2005).

1.3.3.2. Concept, design and performance

While PV-T technology may appear new or unfamiliar to many, its concept is generally credited to a 1976 study about a solar combined heat and power system relying on flat-plate collectors with photovoltaic arrays as absorbers (Wolf, 1976). The concept takes advantage of the high absorptance of PV arrays – reportedly in the range of 85-93% for common types of cells – to act as or at least partially replace standard absorbers but is penalised by their typically high emittance of around 90% and by electricity generation (Vries, 1998; Rockendorf et al., 1999; Santbergen et al., 2010; Eicker and Dalibard, 2011; Dupeyrat et al., 2011b). The latter decreases the effective absorptance of a PV-T collector by a measure equivalent to the PV array's conversion efficiency. In contrast, non-hybrid ST collectors do not produce electricity and employ spectrally selective absorbers (e.g., black copper) to reach absorptance and emittance values as high as 98% and as low as 2%, respectively, and tend to have a lower specific heat capacity and lower thermal resistance between the absorber and heat carrier than equivalent PV-T collectors due to the latter's PV laminate (Florschuetz, 1979; Vries, 1998; Zondag et al., 2002; Goswami, 2015). Thus, the thermal performance of PV-T collectors tends to be inferior to that of state-of-the-art non-hybrid ST collectors for the same collector designs and has been likened to that of collectors without selective absorbers (Rockendorf et al., 1999; Dupeyrat et al., 2011b). Figure 1.8 compares the standardised (i.e., based on EN 12975-2:2006 or ISO 9806:2013) thermal efficiency curves of representative non-hybrid collectors and selected flat-plate PV-T collectors, whose collector design category is singled out in this document for reasons of scope and succinctness.

On the other hand, the electrical performance of flat-plate PV-T collectors can exceed or fall below that of standard PV modules using the same cell array. Concretely, comparatively higher electrical efficiencies are possible if cooling takes place (e.g., through fluid circulation or enhanced heat losses triggered by overheating prevention mechanisms) in PV-T collectors featuring PV cells whose efficiency is adversely affected by cell temperatures. However, this effect can be offset by thermal performance enhancing features namely back thermal insulation, glass covers and low-emissivity coatings (LEC) which either reduce heat losses, the optical efficiency or both relative to a standard PV module (Tripanagnostopoulos et al., 2002; Tripanagnostopoulos, 2007; Santbergen et al., 2010; Lämmle et al., 2016a,b). As a result, the design of PV-T collectors implies a limited trade-off between the thermal and electrical performances, which can to some extent be optimised to suit specific applications[17], though a thermal and electrical yield mismatch is largely unavoidable

[17]The trade-off originating from design choices can be adjusted dynamically in favour of the

and should thus be accomodated in system design (Andrews, 1981).

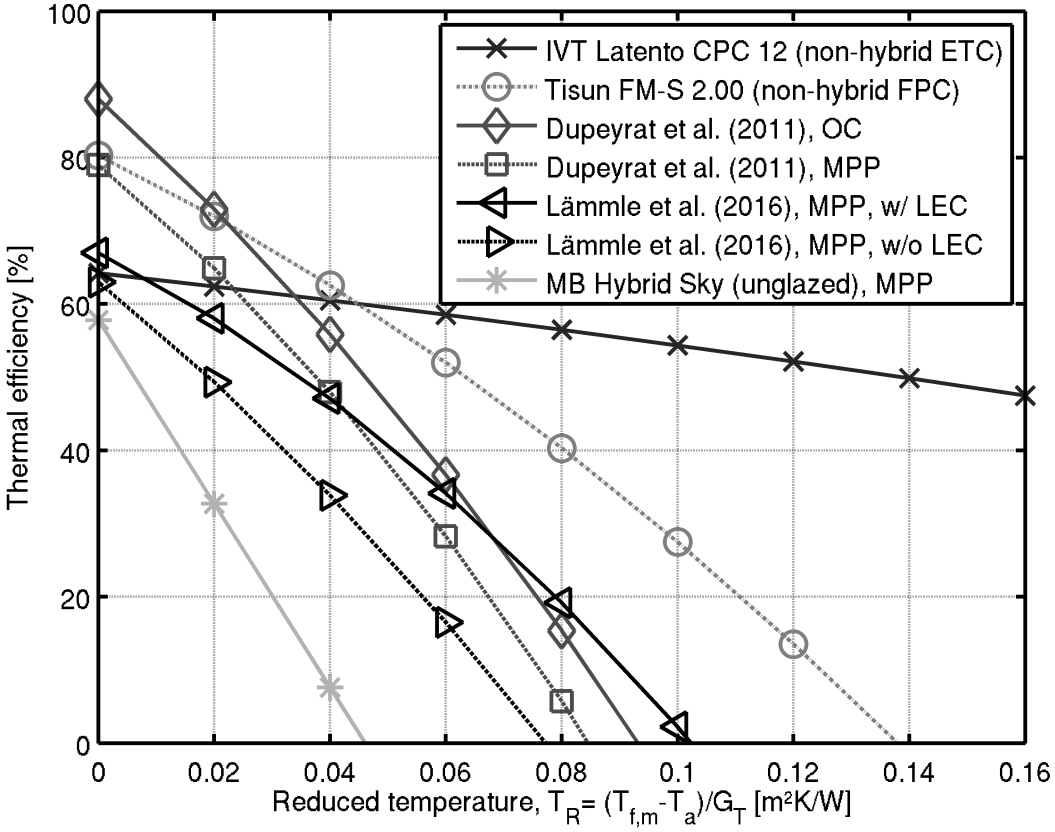

Figure 1.8.: Thermal efficiency curves (according to standards EN 12975-2:2006 or ISO 9806:2013) for state-of-the-art flat-plate PV-T collectors and representative non-hybrid ST collectors (compiled from: Hermann, 2011; Dupeyrat et al., 2011b; Lämmle et al., 2016a; Solar Keymark, 2017). Glazed and unglazed PV-T collectors are represented, the former type also with and without low-emissivity coatings (LEC) and in maximum power point (MPP) and open-circuit (OC) modes.

Flat-plate PV-T collectors are arguably the most common design type and feature solar cells in flat surfaces and in contact with or embedded in a posterior heat exchanger. Unglazed versions typically have the appearance of standard PV modules with back thermal insulation whereas glazed versions resemble glazed FPCs with the exception of the additional PV array connectors protruding from the insulated box. In the latter type of collector, the solar cell array is usually only covering part of the available surface and placed in the centre, away from the edges, to avoid shadows and optimise solar cell use. In either case, the solar cell array is electrically insulated

thermal output by curtailing the electrical power output, which proportionally increases the effective absorptance of PV modules and PV-T collectors (Santbergen et al., 2010).

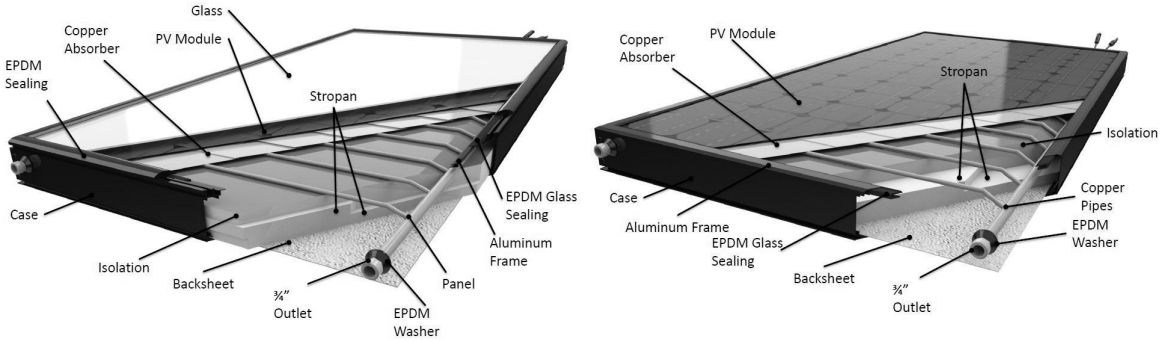

Figure 1.9.: Cutaway views of glazed (left-hand side) and unglazed (right-hand side) flat-plate PV-T collectors (courtesy of Solimpeks Solar Energy Corp.).

from the collector and commonly either glued to the absorber or laminated together with it to reach high heat transfer coefficients between the cells and heat carrier (Vries, 1998; Zondag, 2008; Dupeyrat et al., 2011b; Lämmle et al., 2016a). Figure 1.9 presents cutaway views of glazed and unglazed flat-plate PV-T collectors.

1.3.3.3. Deployment, markets and applications

Despite its advantages, PV-T technology has not yet had a discernible commercial impact although detailed figures about its deployment are not available from industry surveys and reports[18] (Epp and Banse, 2015; SPE, 2016; IEA-PVPS, 2016b; Mauthner et al., 2016). Nevertheless, the lack of detailed data from industry experts, the lack of public awareness, the limited number of manufacturers and intermittent production suggest its installed capacity is currently negligible relative to that of PV modules and ST collectors (Affolter et al., 2005; Zondag, 2008).

PV-T technology's lack of widespread acceptance in recent years also coincided with a steadily increasing presence of non-hybrid ST and PV systems, which tended to target the same markets (Mauthner et al., 2016; IEA-PVPS, 2016c). Indeed, the main market for PV-T collectors was believed to be in the residential segment, on the grounds that it comprised large shares of the ST and PV markets and was often characterised by limited collector or roof area particularly in multi-family buildings, in which PV-T collectors could excel against competitors (Affolter et al., 2005). Several niche markets for PV-T technology were also identified and included collective water heating, pool heating, space heating, solar cooling, autonomous systems, desalination and low temperature industrial applications such as clothes

[18]Kramer and Helmers (2013) provide a figure for the newly installed capacity of PV-T collectors in 2010 as 0.02% of newly added collector area in the same period, although the document cited for this purpose does not corroborate this statement and the corresponding author did not reply to an email requesting clarification for this discrepancy (Weiss and Mauthner, 2012).

washing, processing of agricultural products, solar drying and greenhouse heating.

However, the potential application of PV-T technology is limited by its reduced temperature range and temperature sensitive PV conversion. For instance, flat-plate PV-T collectors are generally regarded as inadequate for absorption cooling due to the former reason (Affolter et al., 2005; Mittelman et al., 2007). More generally, temperature ranges for non-concentrating PV-T collectors pale in comparison with that of other technologies namely ETC, which accounts for the majority of ST systems and new installations and had no PV-T counterpart until recently[19] (Affolter et al., 2005; Kalogirou and Tripanagnostopoulos, 2007; Mittelman et al., 2007; Mauthner et al., 2016). At the same time, high temperature operation of PV-T systems (e.g., through series-connected collector strings or low flow rates) contributes to higher collector heat losses and lower electricity yields since the conversion efficiency for most PV cell types is adversely affected by cell temperatures. Therefore, the comparative advantage of PV-T technology lies mostly in the low temperature segment.

The limited deployment of PV-T collectors has also been attributed to bureaucratic problems, marketing and reliability issues (Affolter et al., 2005). The bureaucratic issues mainly refer to the lack of adequate (performance and reliability) certification and legal status which undermined consumer confidence and access to incentives, respectively. Understandably, legal status can vary between nations, since it is also a political issue. Conversely, certification issues have been largely solved (Hofmann et al., 2010; Kramer and Helmers, 2013). On the marketing side, lack of awareness constitutes a problem since few people outside research and development circles are aware of PV-T technology (Affolter et al., 2005). Finally, reliability issues from prolonged exposure to high temperatures have been regarded as capable of impairing the lifetime of PV-T collectors relative to standard PV modules and ST collectors, which significantly compromises the technology's appeal (Zondag and van Helden, 2002; Dupeyrat et al., 2011b; Lämmle et al., 2016b).

1.3.3.4. Reliability issues

The appeal of PV-T technology is hindered by a range of reliability issues stemming from prolonged or repeated collector exposure to high temperatures (Affolter et al., 2005). Accordingly, these issues mostly concern concentrating or glazed flat-plate PV-T collectors due to their ability to reach high temperatures when exposed to solar radiation, notably during stagnation. In this regard, glazed and unglazed flat-plate PV-T collectors in open-circuit mode[20] can reach stagnation temperatures of approximately 150°C and 95°C, respectively, and a few degrees less in MPP mode,

[19] Vacuum tube PV-T collectors were at one point deemed unworkable by Affolter et al. (2005) but have since become available commercially (Naked Energy, 2012). Nevertheless, the technology's relative complexity, inherently low optical efficiencies and propensity for high absorber temperatures, namely during stagnation, constitute undesirable attributes for PV-T collectors.

[20] Open-circuit mode leads to worst-case scenario stagnation temperatures as far as the PV array status is concerned. In contrast, MPP mode leads to slightly lower stagnation temperatures due to the reduced effective absorptance (Rockendorf et al., 1999; Dupeyrat et al., 2011b).

whereas concentrating PV-T collectors can be expected to exceed 120°C (Mittelman et al., 2007; Kramer and Helmers, 2013; Lämmle et al., 2016a,b).

The issues themselves can also be found in non-hybrid ST systems and PV systems but are generally mitigated or enhanced by specific attributes of PV-T technology, respectively (Andrews, 1981; Harrison and Cruickshank, 2012; IEA-PVPS, 2014b). As such, other than the generic accelerated ageing of components also occurring in ST systems the most significant reliability issues are those affecting the electrical subsystem and its components. Among them is the PV encapsulant, particularly those made from ethylene-vinyl-acetate (EVA), which lose their mechanical properties at 130-140°C and as a result can delaminate or develop (brown or yellow) coloration under ultraviolet (UV) radiation. The former can lead to module failure and the latter to performance degradation due to reduced light transmission to the cells (Pern, 1996; Affolter et al., 1997, 2000; Zondag, 2008; IEA-PVPS, 2014b). In comparison, solar cells can reportedly withstand temperatures up to 220°C although cell interconnections can be severed over time due to thermal cycling, strain, accelerated corrosion, manufacturing defects and hot spots (Affolter et al., 2005; Kato, 2012; IEA-PVPS, 2014b). High collector temperatures also contribute to the overheating of bypass diodes in PV-T collectors – particularly given the additional back insulation relative to standard PV modules – which could result in their premature failure and render the array susceptible to hot spots by shading, cause delamination and even electric arc-generated fires (IEA-PVPS, 2014b). On a more general note, PV-T collectors suffer from enhanced vulnerability to manufacturing defects and hot spots by shading relative to comparable PV modules, and thus carry additional safety risks. Moreover, the PV laminates used in PV-T collectors are generally manufactured to the same specifications as regular terrestrial PV modules, which are only certified to operate safely up to 85°C in accordance with standards IEC 61215 and IEC 61646 for crystalline-silicon and thin-film modules, respectively, and no quantitative study of their reliability above 85°C is know to exist (Dupeyrat et al., 2011b; Fortuin et al., 2014; Lämmle et al., 2016a,b). Thus, continued operation at higher temperatures is prone to premature system failure and unless handled, these shortcomings contribute to a reduced lifetime of PV-T collectors compared to PV modules and ST collectors and ultimately compromise their appeal.

1.4. Research activities

Three main research activities were conducted, all of which pertaining to the study of PV-T systems. The first concerns a comparison between PV-T systems using different but common differential temperature pump controllers, an investigation yet to be found in the literature. The second activity preceded the first and concerns the development of a partially-novel dynamic PV-T collector model suitable for the first activity as well as other purposes. The third and final activity focuses on the study of steady-state setpoint selection methods for PV-T systems using common differential temperature pump controllers such as those compared in the first activity.

1.4.1. Comparison of supply-loop differential temperature controls for SDHW PV-T systems

1.4.1.1. Problem statement

Flow controllers are used to regulate the energy collection and storage processes in active SDHW systems. Several different types of control have been proposed over the years but in practice two dominate: differential temperature static two-level hysteretic control (DTSTLHC), which implements a simple two-state (on/off) control and is widely recognised to be the most used one; and, differential temperature static saturated hysteretic-proportional control (DTSSHPC), which shares some features of the DTSTLHC but adds variable flow control. The latter's use in PV-T systems has not been reported in the surveyed literature and neither has it been compared with the former for use in PV-T systems nor using the latest generation of circulation pumps. Nevertheless, its use in non-hybrid SDHW systems is reported to increase energy yields and the cumulative pump running time relative to the use of DTSTLHC, particularly during periods of intermittent or low insolation (Lewis and Carr, 1978b; Schiller et al., 1980; Naumann and Wolfson, 1984). Since both effects are to some extent opposed in terms of energy efficiency once the pump power is factored in, a quantitative analysis is necessary to determine which control performs best, by how much and under which circumstances.

Three main sets of factors can be predicted to influence this comparison: controller-independent factors, such as the local climate and energy prices; each controller's configuration, namely in terms of setpoints and flow rates; and the steps required to implement the controls, particularly with regard to flow adjustment and pump selection. Among these, the controllers' configuration can constitute bias unless it can bring about performances representative of the controls which, despite similarities, may imply different nominal flow rates and setpoints. Accordingly, systems using these controls may also benefit, from the standpoint of parasitic performance, from different pumps and flow control valve adjustments. In this respect, both standard and so-called high-efficiency pumps are compatible with both controls, though usually using different techniques. Moreover, previous comparisons focusing on non-hybrid systems and broad enough to encompass the parasitic performance relied on standard pumps, and thus focusing on higher efficiency pumps may lead to different conclusions (Schiller et al., 1980; Naumann and Wolfson, 1984).

The same principles hold for PV-T systems, although in those cases the effect on the PV yield must also be considered when comparing the systems' primary energy efficiency and other relevant composite functions of the PV yield. The load provision cost is arguably one of those, particularly for this comparison, but also depends on the prevailing energy prices, which can be expected to change over time and between jurisdictions (Naumann and Wolfson, 1984). Moreover, feed-in tariffs and other subsidies also need to be taken into account to differentiate between local subsidised renewable electricity generation and general purpose electricity consumption, although they are expected to be phased out eventually.

1.4.1.2. Research question

The following research question guided the research activities conducted on the comparison between PV-T systems using different pump controllers:

> Under which conditions, if any, and by how much does DTSSHPC enable SDHW PV-T systems to perform better than those using DTSTLHC in terms of primary energy efficiency and load provision cost?

1.4.1.3. Hypothesis

The hypothesis adopted for the activities conducted is the following:

> If the site experiences frequent bouts of intermittent and cloudy weather, the auxiliary and parasitic energy primary energy factors are equal, and the controllers are required to use the same speed-controlled pump unit and immutable hydraulic circuit, then using DTSSHPC in SDHW PV-T systems enables marginally better performances in terms of primary energy efficiency than in those using DTSTLHC. If in addition to the aforementioned conditions, except the one on primary energy factors, the parasitic energy price equals the auxiliary energy price, then the same is true in terms of load provision cost.

1.4.1.4. Approach

The hypothesis was tested through annual dynamic simulations of SDHW PV-T systems using either type of control. The simulations conducted for this purpose relied on typical meteorological year (TMY) or measured data, covered representative systems, multiple locations and included parametric analyses on relevant controller configuration variables such as the nominal and minimum mass flow rates and the controller setpoints. Moreover, the same variable-speed pump unit was reproduced for each controller although multiple flow control valve adjustments were evaluated to represent a diverse range of situations that may understandably occur in practice.

1.4.2. Dynamic photovoltaic-thermal collector model

1.4.2.1. Problem statement

Several PV-T collector models of varying complexity have been proposed over the years, ranging from steady-state to generally more accurate dynamic multi-dimensional models. Complexity, however, can also enhance computation times, parameter cross-correlation, numerical instability and does not guarantee accuracy in every situation despite some positive correlation with it (Schnieders, 1997; Haurant et al., 2015b). For these reasons, compromises can be made for practicality while retaining some measure of accuracy, namely for parameter identification or tasks requiring numerous simulations. One such example is the case of dynamic

single-node fluid temperature-based collector models widely used in solar collector thermal performance testing, particularly in the ISO 9806:2013 standard's quasi-dynamic test method, which is also compatible with PV-T collectors. However, this model does not estimate the electrical power output and consequently has no provision for dynamic plate temperature estimation that PV-T collector models typically require for electrical efficiency calculations, unlike higher order models. Alternatively, expressions for the mean plate temperature derived from the steady-state collector models can be used but these carry several limiting assumptions, including strictly linear collector heat losses, and can reproduce unrealistic behaviours during transients (Amrizal et al., 2013). Similarly, the single-node model can also behave unrealistically unless discretised into multiple segments along the flow direction (Haller et al., 2014). Hence, overcoming said limitations using a single-node PV-T collector model would arguably be a positive development for performance testing of PV-T collectors and for dynamic simulations of PV-T systems.

1.4.2.2. Research question

The following research question motivated the efforts undertaken on this topic:

> Is it possible to reconcile a dynamic single-node fluid temperature-based approach to PV-T collector modelling with accurate and realistic thermal and electrical power predictions during transients?

1.4.2.3. Hypothesis

The working hypothesis for the aforementioned research question is as follows:

> If the collector efficiency factor construct – which relates fluid with plate temperatures – used in steady-state models can be extended to transients, then a dynamic single-node PV-T collector model can predict both the thermal and electrical outputs of PV-T collectors.

1.4.2.4. Approach

The hypothesis was tested by validating a newly developed PV-T collector model. The model developed can be considered an extension of the dynamic single-node Perers (1993) model for PV-T collectors according to the steady-state modelling approach adopted by Florschuetz (1979), but avoiding the shortcomings of the solution proposed by Amrizal et al. (2013). In turn, the validation process did not rely on experiments but entailed two sets of comparisons with published and validated results: comparisons of the collector model response during non-hybrid operation against published results for various models and experimental data; and, comparisons with a well-known steady-state mean plate temperature correlation.

1.4.3. Selection of differential temperature controller setpoints for PV-T systems

1.4.3.1. Problem statement

Cost-effectiveness and limited pump cycling are often invoked as the criteria upon which the selection of the turn-on and turn-off differential temperature controller setpoints for non-hybrid ST systems should be based on. The same should hold for hybrid PV-T systems, which employ the same pump controllers as non-hybrid ST systems by default. However, faithfully applying the same criteria to PV-T systems implies taking into account the effect on PV generation: fluid circulation can cool the collector and enhance PV electricity generation whereas stagnation tends to have the opposite effect. Moreover, the effective absorptance decreases if the PV conversion efficiency increases and vice-versa. So far, the influence of PV generation on the selection of controller setpoints for PV-T systems has not been discussed in the literature, and while the main trends can be safely predicted, the magnitude of the changes introduced relative to non-hybrid systems is unclear.

1.4.3.2. Research question

The following research question guided the research activities conducted on the topic of differential temperature controller setpoint selection for PV-T systems:

> How should the selection of the differential temperature controllers' turn-on and turn-off setpoints for PV-T solar heating systems, based on cost-effectiveness and limited pump cycling, differ from the selection for non-hybrid ST systems based on the same underlying criteria?

1.4.3.3. Hypothesis

The hypothesis adopted for the activities conducted is the following:

> The differential temperature controller setpoints for PV-T systems should be selected as they would for a non-hybrid system as long as fluid circulation begins and ends while no PV generation is taking place, otherwise the turn-on and turn-off setpoints for PV-T systems should comparatively increase and decrease, respectively, in accordance with the PV conversion efficiency and its temperature dependence.

1.4.3.4. Approach

The approach followed to test the hypothesis consisted of the analytical derivation and numerical simulation of the conditions for cost-effective and cycling-free operation in PV-T systems. In order to do so, an updated version of the Florschuetz steady-state PV-T collector and a numerical extension of the ISO 9806:2013 steady-state test method equation were used (Florschuetz, 1979; ISO, 2013). The models

were employed to conduct parametric analyses on the conditions and compare them with those for equivalent non-hybrid ST systems or simply non-hybrid operation.

1.5. Structure

The current dissertation is structured into six main chapters encompassing the introduction, literature review, the research activities conducted and their conclusions. Additionally, appendices containing complementary information relevant to the activities conducted, such as mathematical models used in the simulations, are also included. The main chapters can be summarised as follows:

- Introduction (Chapter 1) - The (present) introductory chapter describes the motivation, context and background information deemed relevant to the dissertation's subject matter and sheds light on the knowledge gaps, objectives and methodology behind the research efforts undertaken;
- Literature review (Chapter 2) - The literature review summarises previous research activities pertinent to the topics at hand and covers the relevant literature on DTSTLHC and DTSSHPC, setpoint selection for these controllers and a summary of hybrid and non-hybrid solar collector models;
- Dynamic PV-T collector model (Chapter 3) - The third chapter addresses the development and implementation of a new dynamic single-node multi-segment compatible PV-T collector model, as well as its validation through comparisons with published and validated results and alternative models;
- Differential temperature controller setpoints for PV-T systems (Chapter 4) - This chapter is dedicated to the study of the conditions for cost-effective and cycling-free operation of PV-T systems through controller setpoint selection according to steady-state analytical and numerical approaches;
- Comparison of PV-T systems using DTSSHPC and DTSTLHC (Chapter 5) - The fifth chapter describes a simulation-based comparison between the performances of SDHW PV-T systems using DTSTLHC and DTSSHPC for multiple locations, controller configurations and system characteristics;
- Conclusions, contributions and future work (Chapter 6) - The final chapter concerns the conclusions reached, summarises the author's main contributions in the field and makes recommendations for future work.

2. Literature review

The present chapter reviews the available literature on: DTSTLHC and DTSSHPC pump controllers for low-temperature ST systems; and, mathematical modelling of PV, ST and PV-T technologies. Considering the slightly different nature of each topic, the respective discussions take place in separate sections, introduced and summarised at the beginning and end of each to facilitate their comprehension.

2.1. PV module and ST collector models

Solar heating systems are inherently dynamic in nature and PV-T systems are no exception. In particular, the solar collectors are routinely exposed to transients including wind gusts, intermittent cloud cover, rain, pump cycling, flow rate variations, among others and being able to predict how collectors react to these events can be a challenge. Since PV-T collectors combine both PV and ST technologies, their simulation models usually replicate features of PV module and ST collector models. For this reason, the present section addresses the literature on the simulation models for PV modules, non-hybrid ST collectors and PV-T collectors.

2.1.1. PV module models

The electrical performance of PV modules is usually reproduced using either equivalent circuit models or linear empirical correlations between efficiency and cell temperature, both of which have also been used to simulate PV-T collectors.

2.1.1.1. Equivalent circuit models

A common approach to PV module modelling is the use of equivalent circuits. The most prominent examples are the two and single diode equivalent circuits, which can be traced back to physical phenomena (Gray, 2011). The two diode equivalent circuit model is the most detailed, is represented by the diagram in Figure 2.1 and obeys (2.1), where V is the cell voltage, I is the cell current, I_{ph} is the light-generated current, V_{th} is the thermal voltage, R_s is the series resistance, R_{sh} is the shunt resistance, I_{o1} is the dark (or reverse) saturation current due to recombination in quasi-neutral regions, I_{o2} is the dark saturation current due to recombination in the depletion (or space-charge) region, and n_1 and n_2 stand for the the ideality factors for each of these saturation currents, respectively, and usually assume the values

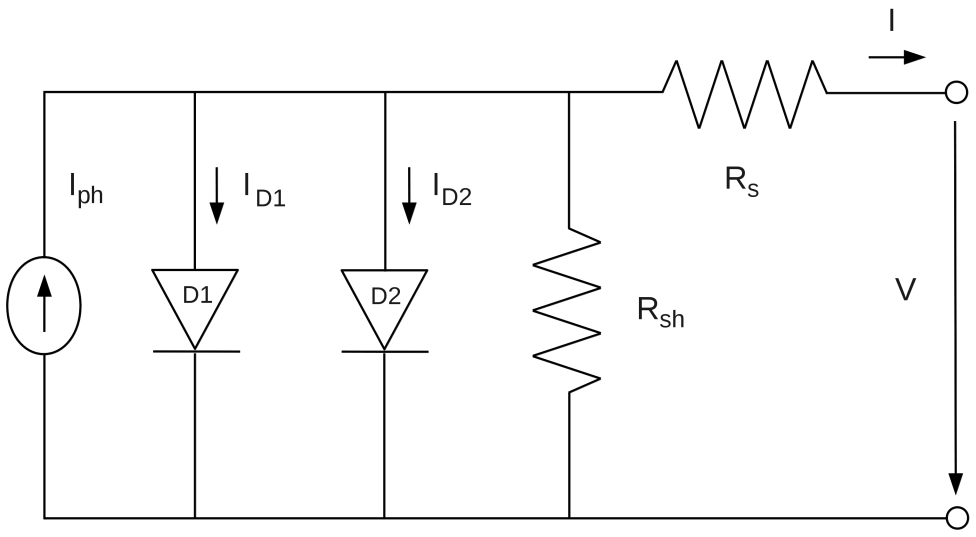

Figure 2.1.: Two diode equivalent circuit diagram for photovoltaic cells

1 and 2, also respectively (Gray, 2011; Ishaque et al., 2011). The effect of these saturation currents are modelled in the current terms for diodes D1 and D2.

$$I = I_{ph} - I_{o1}\left[\exp\left(\frac{V + I \cdot R_s}{n_1 V_{th}}\right) - 1\right] - I_{o2}\left[\exp\left(\frac{V + I \cdot R_s}{n_2 V_{th}}\right) - 1\right] - \frac{V + I \cdot R_s}{R_{sh}} \quad (2.1)$$

The equation's implicit nature and the number of parameters that need to be determined make (2.1) difficult to use. A common simplification neglects the dark saturation current in the depletion region by omitting the term and diode representing it in (2.1) and Figure 2.1, respectively, which leads to the single diode equivalent circuit model (Gray, 2011; Ishaque et al., 2011). A common version of this model is given by (2.2), where I_o and n represent the dark saturation current and the ideality factor ($1 < n < 2$), respectively, though iterative methods are still necessary (Villalva et al., 2009; Ghani and Duke, 2011). In turn, the thermal voltage for modules with $N_{pv,s}$ cells in series is given by (2.3), where T_{pv}, k_B and q represent the cells' temperature, the Boltzmann constant and the electron charge, respectively.

$$I = I_{ph} - I_o\left[\exp\left(\frac{V + I \cdot R_s}{n V_{th}}\right) - 1\right] - \frac{V + I \cdot R_s}{R_{sh}} \quad (2.2)$$

$$V_{th} = \frac{N_{pv,s} k_B T_{pv}}{q} \quad (2.3)$$

Another consideration is the temperature dependence of some parameters, particularly the light-generated current and dark saturation current. Many authors have modelled the latter according to (2.4), where $I_{o,r}$ stands for the dark saturation

current for reference conditions, $T_{pv,r}$ is the reference cell temperature, and E_g and $E_{g,r}$ represent the bandgap energy and the reference bandgap energy, respectively (Soto et al., 2006; Messenger and Ventre, 2005). According to Duffie and Beckman (2013), the temperature dependency of the bandgap energy can be given by (2.5), where C_E is the bandgap energy temperature coefficient, which equals 0.0002677 and 0.0003174 °C^{-1} for silicon and gallium arsenide, respectively.

$$I_o = I_{o,r} \left(\frac{T_{pv}}{T_{pv,r}} \right)^3 \exp \left[\frac{q}{n \cdot k} \cdot \left(\frac{E_{g,r}}{T_{pv,r}} - \frac{E_g}{T_{pv}} \right) \right] \tag{2.4}$$

$$\frac{E_g}{E_{g,r}} = 1 - C_E \cdot (T_{pv} - T_{pv,r}) \tag{2.5}$$

Alternatively, Villalva et al. (2009) proposed a correlation for I_o based on the constant open-circuit voltage and short-circuit current temperature coefficients, K_V and K_I, respectively. These are typically provided by manufacturers and allow the dark saturation current to be accurately determined over a wide range of temperatures according to (2.6), where $I_{sc,r}$ and $V_{oc,r}$ represent the reference short-circuit current and open-circuit voltage, respectively (Villalva et al., 2009).

$$I_o = \frac{I_{sc,r} + K_I \left(T_{pv} - T_{pv,r} \right)}{\exp \left[\left(V_{oc,r} + K_V \left\{ T_{pv} - T_{pv,r} \right\} \right) / (n V_{th}) \right] - 1} \tag{2.6}$$

The light-generated current is also temperature sensitive and often assumed to be equal to the short-circuit current, which is also proportional to the normalised irradiance according to (2.7), where G_T and $G_{T,r}$ represent the actual and reference irradiance on the (tilted) collector plane, respectively. A more accurate definition based on the equivalent circuit can be accommodated in combination with (2.8) but is ultimately more computationally demanding to use (Villalva et al., 2009).

$$I_{ph} = \frac{G_T}{G_{T,r}} \left[I_{ph,r} + K_I \left(T_{pv} - T_{pv,r} \right) \right] \tag{2.7}$$

$$I_{ph,r} = \frac{R_s + R_{sh}}{R_{sh}} I_{sc,r} \tag{2.8}$$

The cell temperature can also be difficult to calculate as it depends on various phenomena including electricity generation. For steady-state conditions, relatively simple correlations based on the nominal operating cell temperature (NOCT) test conditions[21] can be used, namely (2.9), where $T_{pv,NOCT}$ represents the cell temperature, $T_{a,NOCT}$ is the ambient temperature, $G_{T,NOCT}$ is the irradiance, and $U_{L,NOCT}$

[21] The NOCT test conditions for a PV module are defined as no-load operation ($\eta_{pv} = 0$ %), 800 W/m² normal to the module plane, AM1.5 spectrum, an ambient temperature of 20°C and a wind speed of less than 1 m/s (Messenger and Ventre, 2005; Duffie and Beckman, 2013).

is the overall heat loss coefficient, all of which for NOCT test conditions. In turn, T_{pv} represents the estimated cell temperature, U_L is the overall heat loss coefficient, η_{pv} is the electrical efficiency, and $(\tau\alpha)_{eff}$ is the effective transmittance-absorptance product. Since $\eta_{pv}/(\tau\alpha)_{eff} \ll 1$, (2.9) can be simplified into (2.10) with a minimal compromise in accuracy (Skoplaki and Palyvos, 2009; Duffie and Beckman, 2013).

$$T_{pv} = T_a + (\frac{G_T}{G_{T,NOCT}})(\frac{U_{L,NOCT}}{U_L})(T_{pv,NOCT} - T_{a,NOCT})[1 - \frac{\eta_{pv}}{(\tau\alpha)_{eff}}] \tag{2.9}$$

$$T_{pv} = T_a + (\frac{G_T}{G_{T,NOCT}})(\frac{U_{L,NOCT}}{U_L})(T_{pv,NOCT} - T_{a,NOCT}) \tag{2.10}$$

The alternative to steady-state cell temperature correlations, such as those given above, are dynamic energy balances. These allow for a more thorough assessment of the PV modules' thermal behaviour and respective effect on electrical performance, possibly including the effect of cell mismatch. The models can range from relatively simple one-dimensional ones to complex and hard to parametrise finite-element ones. One relatively complex example is the work by Siddiqui et al. (2012) on a three-dimensional thermal model coupled with a single diode equivalent circuit model, intended to study a PV module's performance in dynamic situations.

In essence, the equivalent circuit models are generally accurate but can be regarded as relatively computationally intensive, requiring iterative methods and numerous module-specific and load parameters, as well as the cell temperature (Soto et al., 2006; Villalva et al., 2009; Ghani and Duke, 2011; Ishaque et al., 2011).

2.1.1.2. Linear empirical models

A much simpler approach to PV module modelling is the use of empirical correlations assuming a linear influence of cell temperature on electrical efficiency under maximum power point (MPP) tracking. The most generic of these is given by (2.11), where η_{pv} stands for the cell efficiency at the MPP, $\eta_{pv,r}$ is the reference (e.g., at NOCT or STC[22] conditions) cell efficiency at the MPP, β_{pv} is the MPP cell efficiency temperature coefficient, and γ_{pv} is the solar radiation coefficient (≈0.12 for c-Si modules) (Evans, 1981; Skoplaki and Palyvos, 2009).

$$\eta_{pv} = \eta_{pv,r}\,[1 + \beta_{pv}\,(T_{pv} - T_{pv,r}) + \gamma_{pv}\log_{10} G_T] \tag{2.11}$$

A common simplification is to assume the solar radiation coefficient in (2.11) is zero, effectively making it independent of G_T except through the influence on the cell temperature (Evans, 1981; Skoplaki and Palyvos, 2009). By doing so, the

[22]Standard test conditions (STC) are defined as 1000 W/m² normal to the module plane, AM1.5 spectrum (as per IEC 60904-3) and cell temperatures at 25°C (IEC, 2005).

MPP cell efficiency can be estimated using data commonly supplied by PV module manufacturers, namely the cell efficiency or power temperature coefficient (β_{pv}) and the NOCT temperature ($T_{pv,NOCT}$) for use in (2.12) and (2.10), respectively.

$$\eta_{pv} = \eta_{pv,r} \left[1 + \beta_{pv} \left(T_{pv} - T_{pv,r}\right)\right] \tag{2.12}$$

2.1.2. Non-hybrid ST collector models

Several non-hybrid ST collector models have been proposed over the years and of varying complexity and purpose. The most prominent applications are parameter identification for performance estimation and reproduction of collector behaviour during transients. The former has been generally shown not to require a high model complexity, though the same can't be said of the latter and while complexity allows for higher accuracy, it has drawbacks. For instance, Schnieders (1997) identified three main problems with increasing model complexity: increased parameter intercorrelation; higher computational loads; and, worse numerical stability. Complexity is also one of the possible factors contributing to the limited modelling efforts focusing on the behaviour during stagnation, the other being its non-essential nature for the purposes of performance estimation. For these reasons, there is a high incentive to seek simple models. With the exception of finite-element approaches, the most pertinent non-hybrid collector models are briefly described in the following sections.

2.1.2.1. Hottel-Whillier-Bliss model

The Hottel-Whillier-Bliss (HWB) model is an analytical steady-state solar collector model whose main advantage is that it greatly simplifies predicting the useful heat generated by solar collectors compatible with its underlying assumptions[23] (Hottel and Whillier, 1955; Bliss, 1959). Consider the case of non-hybrid solar thermal collectors under steady-state conditions delivering useful heat at a rate $\dot{Q}$ through fluid circulation in accordance with (2.13), where $T_{f,out}$ is the collector fluid outlet temperature, $T_{f,in}$ is the collector fluid inlet temperature, $\dot{m}_c$ is the collector mass flow rate and $C_{p,c}$ stands for the collector fluid specific heat.

$$\dot{Q} = \dot{m}_c C_{p,c} \left(T_{f,out} - T_{f,in}\right) \tag{2.13}$$

[23] These are numerous and include steady-state operation, harp-type collector hydraulics, uniform flow distribution among the riser tubes, negligible header size relative to the collector, one-dimensional heat transfer through the back insulation, uniform ambient temperature surrounding the collector, infrared heat losses to the sky consistent with an equivalent blackbody sky temperature, temperature independent properties of materials, negligible dust effects on the cover, no shading of the absorber, one-dimensional heat transfer through the cover(s), negligible temperature drop across the cover(s), infrared radiation-opaque cover(s), negligible effect of the temperature of the cover(s) on collector heat losses, independent temperature gradients in the flow direction and between the parallel riser tubes, negligible temperature gradient in the flow direction, negligible temperature gradient around the tubes and negligible temperature gradient across the absorber plate (Kalogirou, 2009; Duffie and Beckman, 2013).

The useful heat flow rate enabled by the collectors can also be expressed as the difference between the absorbed solar radiation and the absorber plate heat losses according to (2.14) and (2.15), where A_c represents the collector area, S is the solar radiation per unit area absorbed at the absorber plate, U_L is the overall heat loss coefficient, $T_{p,m}$ is the mean plate temperature, T_a is the ambient temperature and $(\tau\alpha)_{eff}$ represents the effective transmittance-absorptance product.

$$\dot{Q} = A_c \left[S - U_L \left(T_{p,m} - T_a \right) \right] \tag{2.14}$$

$$S = (\tau\alpha)_{eff} G_T \tag{2.15}$$

Neither (2.13) nor (2.14) are practical to use in predicting the useful heat generated: the former, since is not an explicit function of the weather conditions; the latter, since $T_{p,m}$ is an implicit function of the energy balance between the absorbed solar radiation, the plate heat losses and the useful heat generated. The key concept introduced in the HWB model is the collector efficiency factor (F'), representing the ratio between the existing collector useful heat flow rate and that the collector would deliver if its entire absorber surface was at the mean collector fluid temperature ($T_{f,m}$), which greatly simplifies the task of predicting yields. The factor can be calculated through (2.16), (2.17) and (2.18), where W represents the riser tube spacing, D_{riser} is the riser tube external diameter, $U_{f,p}$ is the thermal conductance between the absorber and the collector fluid, F is the fin efficiency, k_p is the absorber plate thermal conductivity and δ_p is the absorber plate thickness.

$$F' = \left[\frac{W}{(W - D_{riser})\, F + D_{riser}} + \frac{U_L}{U_{f,p}} \right]^{-1} \tag{2.16}$$

$$F = \frac{\tanh\left[\frac{m}{2} (W - D_{riser}) \right]}{\frac{m}{2} (W - D_{riser})} \tag{2.17}$$

$$m^2 = \frac{U_L}{k_p \delta_p} \tag{2.18}$$

By making use of the collector efficiency factor, the useful heat can be expressed as a function of S, U_L and T_a in more practical ways than allowed by (2.14). While (2.19) is one possibility, (2.20) is a more practical option since it does not require parameters dependent on the collector output (e.g., the collector fluid mean or outlet temperatures) but rather the collector fluid inlet temperature and the collector heat removal factor (F_R) defined in (2.21), which is itself a function of F'. The collector

heat removal factor is conceptually similar to F' but represents the ratio between the useful heat generated by the collector and the useful heat the collector would generate if the mean plate temperature was equal to the fluid inlet temperature.

$$\dot{Q} = A_c F' \left[S - U_L \left(T_{f,m} - T_a \right) \right] \tag{2.19}$$

$$\dot{Q} = A_c F_R \left[S - U_L \left(T_{f,in} - T_a \right) \right] \tag{2.20}$$

$$F_R = \frac{\dot{m}_c C_{p,c}}{A_c U_L} \left[1 - \exp\left(-\frac{F' A_c U_L}{\dot{m}_c C_{p,c}} \right) \right] \tag{2.21}$$

The HWB model also provides for a conveniently simple correlation for the collector thermal efficiency ($\eta_{th,c}$), (2.22), sometimes given as a function of the reduced temperature ($T_{R,in}$), (2.23). The respective thermal efficiency curve as a function of $T_{f,in}$ has two notable points connected by a negatively-sloped line, the zero-heat loss temperature ($T_{f,in} = T_a$) and the stagnation temperature ($T_{f,in} = T_a + (\tau\alpha)_{eff} G_T / U_L$), which represent the y- and x-axis intercepts, respectively.

$$\eta_{th,c} = F_R \left(\tau\alpha \right)_{eff} - F_R U_L \left(\frac{T_{f,in} - T_a}{G_T} \right) \tag{2.22}$$

$$T_{R,in} = \frac{T_{f,in} - T_a}{G_T} \tag{2.23}$$

The model can also be combined with the ε-NTU method to cover ST systems with external heat exchangers, illustrated in Figure 1.6-II (Duffie and Beckman, 2013). Using the ϵ-NTU method, the useful heat flow rate from such systems can be predicted through (2.24), where ϵ is the heat exchanger effectiveness, $(\dot{m}C_p)_{min}$ is the minimum capacitance rate among those used in the collector and tank loops, $T_{t,out}$ is the heat exchanger tank-side ("cold") inlet temperature and F'_R stands for the collector heat exchanger factor, which can be shown to be given by (2.25).

$$\dot{Q} = A_c F'_R \left[S - U_L \left(T_{t,out} - T_a \right) \right] \tag{2.24}$$

$$F'_R = F_R \left[1 + \frac{A_c F_R U_L}{\dot{m}_c C_{p,c}} \left(\frac{\dot{m}_c C_{p,c}}{\epsilon (\dot{m} C_p)_{min}} - 1 \right) \right]^{-1} \tag{2.25}$$

2.1.2.2. Klein et al. dynamic single-node model

Klein et al. (1974) investigated the effect of thermal capacity on the performance of solar collectors through three collector models: the HWB model; a dynamic single-node model; and, a dynamic two-node model. The dynamic single-node model is especially interesting because it builds on the HWB model and assumes the collector thermal capacitance is concentrated in the collector fluid. It originates as an approximate solution to (2.26), a differential equation[24] corresponding to the energy balance for a non-hybrid collector's differential tube element in the flow direction (x), where C_A, T_f and t represent the effective or lumped specific collector thermal capacity, the local fluid temperature and the time variable, respectively.

$$WC_A\frac{dT_f}{dt} = F'W[S - U_L(T_f - T_a)] - \dot{m}_c C_{p,c}\frac{dT_f}{dx} \tag{2.26}$$

The approximate solution proposed assumed a collector fluid temperature distribution along the flow path based on a temperature difference between local temperatures (T_f) and those indicated by the HWB model (T_f^{HWB}) proportional to the normalised position (x/L_c) within the flow path ($0 \leq x \leq L_c$), i.e., (2.27), where the superscript HWB refers to variables calculated using the HWB model.

$$T_f - T_f^{HWB} = \frac{x}{L_c}\left(T_{f,out} - T_{f,out}^{HWB}\right) \tag{2.27}$$

The model proposed is obtained by integration of (2.26) and (2.27) along the collector length ($0 \leq x \leq L_c$) and replacing the latter in the former, and can be given by (2.28), which also accounts for on/off pump control through a control variable (S_{pump}) which equals: 0, for stagnation; and 1, during fluid circulation. Moreover, the collector efficiency factor is assumed to be one during stagnation, implying the mean fluid ($T_{f,m}$) and mean plate temperatures become equal.

$$\begin{aligned} C_A\frac{dT_{f,m}}{dt} &= [1 + S_{pump}(F' - 1)]\,[S - U_L(T_{f,m} - T_a)] \\ &\quad - S_{pump}\frac{\dot{m}_c C_{p,c}}{A_c}\,(T_{f,out} - T_{f,in}) \end{aligned} \tag{2.28}$$

The solution found by Klein et al. differs from simpler alternatives such as the linear collector fluid temperature distribution between the inlet and outlet previously proposed by Close (1967) and used extensively since then:

$$T_{f,m} = \frac{T_{f,out} + T_{f,in}}{2} \tag{2.29}$$

[24] According to Schnieders (1997), (2.26) was first proposed by Gicquel (1979). However, it can also be found in Klein et al. (1974), which predates the work by Gicquel (the translation and the original) and explicitly uses the collector efficiency factor (F'), unlike the latter.

The authors' assessment was that the HWB model proved adequate compared to alternatives in its ability to predict a collector's transient performance if hourly meteorological data was used, crediting typical collector time constants on the order of a few minutes as too low to register when considering such low resolution data.

2.1.2.3. Schiller et al. multi-segment single-node model

Schiller et al. (1980) used a multi-segment single-node collector model inspired by the differential equation put forward by Klein et al. (1974), or (2.26). The model, however, comprises N_s segments along the flow direction as a solution to (2.30), where S_{pump} is the flow regime control variable also used in the Klein et al. model. As such, the model also encompasses the stagnation regime but, unlike the Klein et al. model, assumes the same collector efficiency factor (F') for both regimes.

$$C_A \frac{dT_f}{dt} = F'[S - U_L(T_f - T_a)] - S_{pump} \frac{\dot{m}_c C_{p,c}}{W} \frac{dT_f}{dx} \tag{2.30}$$

2.1.2.4. Huang and Lu model

Huang and Lu (1982) and Huang (1994) proposed a single-node collector model addressing some of the perceived limitations of the Klein et al. and Schiller et al. models as far as the stagnation regime is concerned. In particular, the model is defined as a piece-wise function of the flow regime where the sub-functions, though analytically similar among themselves, use different parameters for the time constant and solar gain coefficient (roughly equivalent to $C_A/F'U_L$ and $(\tau\alpha)_{eff}/U_L$, respectively) instead of a different collector efficiency factor as in the Klein et al. model. This model was validated experimentally by Huang and Lu (1982) using a non-selective collector at a low slope (15°) – favourable to a relatively uniform collector temperature during stagnation as assumed by the model itself – though no other study was found validating or contradicting its conclusions.

2.1.2.5. Kamminga's multi-node dynamic models

Kamminga (1985, 1986) proposed multi-node dynamic models for FPCs and ETCs implemented using Fourier transforms. The ETC model can be represented by energy balances for the glass envelope, the absorber, the (heat pipe) condenser and the fluid, and is thus a 4-node model. In turn, the FPC model has 3 nodes corresponding to energy balances for the glass cover, the plate and the fluid. Kamminga's FPC model was later compared by Schnieders (1997) with lower-order models including a 2-node version of the FPC model – oddly enough in a study focusing on vacuum tube collectors – and found to be the most accurate, though simultaneously the most computationally intensive and hardest to parametrise.

2.1.2.6. DSC multi-segment single-node model

Muschaweck and Spirkl (1993) developed a dynamic solar collector (DSC) model based on N_s discretised series-connected single-node collector segments, each with $1/N_{seg}$ of the total collector area and heat capacity, i.e., a constant specific heat capacity (Schnieders, 1997; Nayak et al., 2000). The model's governing equation for the segment i ($1 \leq i \leq N_{seg}$) is given by (2.31), where $T_{f,m}[i]$ and $T_{f,m}[i-1]$ represent the average fluid temperatures for the segment i and $i-1$, respectively. Accordingly, the model's boundary conditions are given by (2.32) and (2.33).

$$\frac{A_c}{N_{seg}} C_A \frac{dT_{f,m}[i]}{dt} = \frac{A_c}{N_{seg}} F'[S - U_L(T_{f,m}[i] - T_a)] - \dot{m}_c C_{p,c} \left(T_{f,m}[i] - T_{f,m}[i-1]\right) \quad (2.31)$$

$$T_{f,m}[0] = T_{f,in} \quad (2.32)$$

$$T_{f,m}[N_s] = T_{f,out} \quad (2.33)$$

As noted by the original authors, the model can reveal significant errors if N_{seg} equals one, since each segment's outlet temperature corresponds to the average fluid temperature, and thus a large N_{seg} is desirable for accuracy. At the same time, Schnieders (1997) described the model's behaviour as similar to a two-node (plate and fluid) model though less computationally intensive and easier to parametrise.

2.1.2.7. Perers model

Perers (1993) introduced a dynamic single-node model intended for parameter identification via performance testing. While significantly indebted to the HWB and the single-node Klein et al. models, the model developed explicitly accounts for temperature and wind dependence of the heat loss coefficient, longwave radiative heat losses, handles the beam and diffuse solar radiation components separately, and relies on (2.29) to approximate the mean collector fluid temperature ($T_{f,m}$). A simplified version[25] of the model is given by (2.34) and (2.35), where G_b is the beam irradiance on the collector plane, G_d is the diffuse irradiance on the collector plane, K_b is the beam incidence angle modifier (IAM), b_0 is the beam IAM coefficient, θ is the incidence angle, K_d is the diffuse IAM, $(\tau\alpha)_n$ is the effective transmittance-absorptance product at an angle normal to the collector plane, $F'U_{L,1}$ is the zero-reduced temperature heat loss coefficient, $F'U_W$ is the wind dependence of the heat loss coefficient, u_W is the wind speed near the collector, $F'U_{L,2}$ is the temperature dependence of the heat loss coefficient, $F'U_{sky}$ is the sky temperature dependence of the heat loss coefficient and ΔT_{sky} is the effective sky temperature difference.

[25]The original version also models piping heat losses, whereas subsequent versions model the wind dependence of the zero-loss efficiency and condensation heat gains (Perers, 1997, 2010).

$$\begin{aligned}\frac{\dot{Q}}{A_c} =& F'\left(\tau\alpha\right)_n \left(G_b K_b + G_d K_d\right) - F'U_{L,1}(T_{f,m} - T_a) - F'U_{L,2}(T_{f,m} - T_a)^2 \\ & - F'U_W u_W (T_{f,m} - T_a) - F'U_{sky}\Delta T_{sky} - C_A \frac{dT_{f,m}}{dt}\end{aligned} \tag{2.34}$$

$$K_b = 1 - b_0 \left(\frac{1}{\cos\theta} - 1\right) \tag{2.35}$$

Perhaps the main advantage of the Perers model is its compatibility with parameter identification, namely through multilinear regression. This may have facilitated its adoption for thermal performance test methods, specifically the quasi-dynamic test method (QDTM) found in the EN 12975-2:2006 and ISO 9806:2013 standards, which also define the conditions necessary to accurately reproduce a collector's performance (Fischer et al., 2004; ISO, 2013). In addition to b_0 and K_d, the identifiable parameters in (2.34) and (2.35) include $F'\left(\tau\alpha\right)_n$, $F'U_{L,1}$, $F'U_{L,2}$, $F'U_W$ and C_A which correspond to η_0, c_1, c_2, c_3 and c_5, respectively, in the QDTM nomenclature convention – used in (2.36). Moreover, F' is not determined independently of other parameters. The parameter identification process also requires, among other conditions, data obtained during mostly stable conditions and continuous fluid circulation and thus it may not be accurate for stagnation (Perers, 1993).

$$\begin{aligned}\frac{\dot{Q}}{A_c} =& \eta_0 \left(G_b K_b + G_d K_d\right) - c_1(T_{f,m} - T_a) - c_2(T_{f,m} - T_a)^2 \\ & - c_3 u_W (T_{f,m} - T_a) + c_4 \left(E_L - \sigma T_a^4\right) - c_5 \frac{dT_{f,m}}{dt}\end{aligned} \tag{2.36}$$

While originally introduced at least as far back as 1993, the model has been updated more than once and implemented for use with the TRNSYS software package as type 832 – and previously as types 132 and 232. In this implementation, a multi-segment instantiation is also possible, which seeks to address unrealistic transients observed when using the single-segment version (Haller et al., 2014). Using a single-segment version, the linear collector fluid temperature profile assumed between inlet and outlet forces unrealistic outlet temperatures during transitions from stagnation to circulation and vice-versa. A multi-segment instantiation mitigates this problem by limiting the linear profile to each segment and more so as the segment count increases. A higher segment count also improves the model's computational stability according to (2.37) – which is the stability condition instantiations should comply with – where N_{seg} and Δt represent the number of segments and the sampling time.

$$\frac{\dot{m}_c C_{p,c} N_{seg} \Delta t}{A_c C_A} \geq 0.5 \tag{2.37}$$

2.1.2.8. Notes on stagnation modelling

A very select number of modelling efforts have focused on the collector behaviour during stagnation. This can be explained by the fact that modelling stagnation rigorously is not necessary to reproduce the thermal performance of ST collectors, and by the relative complexity and the difficult-to-generalise nature of the phenomenon, which prevents simple and accurate models. In this respect, Schnieders (1997) compared steady-state, single- and multi-node dynamic collector models and found none was able to properly reproduce the stagnation behaviour of the collectors tested, and added that test data measured during stagnation revealed slower fluid temperature increases than suggested by the models, which is consistent with a reduced pipe-fluid heat transfer coefficient – or collector efficiency factor – during stagnation. More specifically, the author suggested 100-fold heat transfer coefficient decreases as in the realm of possibility and recommended modelling this heat transfer as a function of the mass flow rate, which many models fail to do in a meaningful sense.

In turn, none of the collector models described earlier or those compared by Schnieders (1997) explicitly account for fluid boiling, which is likely to occur with most glazed collectors during stagnation. Chen et al. (2010, 2015) did study the behaviour of collectors during stagnation, with emphasis on fluid boiling, and developed a numerical model suitable for expansion vessel sizing. Though limited to steady-state conditions and solar loops with a good collector emptying behaviour, the model predicts the mass of fluid pushed into the expansion vessel from equilibrium equations for the solar loop, the boiling zone at the bottom of the collectors and the superheated vapour zone at the top. Numerical correlations for heat transfer coefficients are used to predict the amount of condensation in the pipes. Nevertheless, it is unclear whether this model remains reasonably valid during transients.

2.1.3. Hybrid PV-T collector models

The thermal and electrical performance of PV-T collectors can be reproduced using the same modelling techniques also used in non-hybrid ST collector and PV module models. The main difference with PV-T collector models is that, for coherence, both thermal and electrical submodels have to interact due to the reduced absorption caused by PV conversion and the effect it has on cell temperatures. This has been shown not to be a problem in steady-state or dynamic multi-node models, though these have other shortcomings. In contrast, dynamic single-node models based on fluid temperatures have not yet been shown to be capable of predicting cell temperatures without additional assumptions or simplifications.

Compatibility with standard performance tests is another desirable attribute for PV-T collector models, as is the ability to accurately reproduce stagnation behaviour. As it stands, PV-T collector models suffer from the same predicaments as non-hybrid collector models in terms of stagnation modelling, but it arguably assumes a greater importance for the former since PV conversion is temperature-sensitive and does not stop during stagnation. The following sections focus on

prominent PV-T collector models with emphasis on the aforementioned issues.

2.1.3.1. Florschuetz model

The Florschuetz model extends the HWB model to encompass PV-T collectors and shares its underlying assumptions (Florschuetz, 1979; Vries, 1998; Kalogirou, 2009; Duffie and Beckman, 2013). Since its introduction, the Florschuetz model has also been updated to reflect the additional heat transfer perpendicular to the flow direction through the PV laminate, the additional thermal resistance between the PV cells and the standard "absorber" plate, and the effect of the PV packing factor (ρ_{pv}) on performance (Vries, 1998; Dupeyrat et al., 2011b). Accordingly, the useful heat output from a PV-T collector can be given by (2.38), where $\widetilde{F}_R$ is the modified collector heat removal factor, $\widetilde{S}$ is the modified solar radiation per unit area absorbed at the absorber plate and $\widetilde{U}_L$ is the modified overall heat loss coefficient.

$$\dot{Q} = A_c \widetilde{F}_R \left[\widetilde{S} - \widetilde{U}_L \left(T_{f,in} - T_a\right)\right] \tag{2.38}$$

The preceding equation is essentially the same as its HWB model counterpart, except that S, U_L and F_R have been replaced by $\widetilde{S}$, $\widetilde{U}_L$ and $\widetilde{F}_R$, respectively. The new variables take into account the effect of PV generation while retaining the same basic meaning and are given by (2.39), (2.40) and (2.41), where α is the the combined cell and plate absorptance, τ is the glass cover transmittance, $(\tau\alpha)_{eff}$ is the effective transmittance-absorptance product, β_{pv} is the (generally negative) cell efficiency temperature coefficient, whereas $\eta_{pv,a}$ and $\eta_{pv,r}$ stand for the PV conversion efficiency at ambient and reference (e.g., STC) cell temperatures, respectively.

$$\widetilde{S} = S\left[1 - \frac{\rho_{pv}\eta_{pv,a}}{\alpha}\right] \tag{2.39}$$

$$\widetilde{U}_L = U_L + \tau\eta_{pv,r}\rho_{pv}\beta_{pv}G_T \tag{2.40}$$

$$\widetilde{F}_R = \frac{\dot{m}_c C_{p,c}}{A_c \widetilde{U}_L}\left[1 - \exp\left(-\frac{\widetilde{F}' A_c \widetilde{U}_L}{\dot{m}_c C_{p,c}}\right)\right] \tag{2.41}$$

Similarly, the classic HWB model variables such as the collector efficiency factor (F') and the fin efficiency (F) also have their counterparts in the Florschuetz model since they are ultimately functions of the modified overall heat loss coefficient ($\widetilde{U}_L$). Thus, the modified variables $\widetilde{F}'$, $\widetilde{F}$ and $\widetilde{m}$ are functions of $\eta_{pv,r}$ through $\widetilde{U}_L$ in accordance with (2.42), (2.43) and (2.44), where $U_{f,p}$ is the thermal conductance between

the absorber and the collector fluid, $(k\delta)_{p,eff}$ is the effective thermal conductance-thickness product for the plate and the various PV laminate layers, D_{riser} is the riser tube external diameter and W corresponds to the tube spacing (Vries, 1998).

$$\widetilde{F}' = \left[\frac{W}{(W - D_{riser})\,\widetilde{F} + D_{riser}} + \frac{\widetilde{U}_L}{U_{f,p}} \right]^{-1} \tag{2.42}$$

$$\widetilde{F} = \frac{\tanh\left[\frac{\widetilde{m}}{2}(W - D_{riser})\right]}{\frac{\widetilde{m}}{2}(W - D_{riser})} \tag{2.43}$$

$$\widetilde{m}^2 = \frac{\widetilde{U}_L}{(k\delta)_{p,eff}} \tag{2.44}$$

In turn, the PV-T collector power output is given by (2.45) – though originally expressed in a different and arguably less intuitive form – where $T_{pv,r}$ and $T_{pv,m}$ correspond to the reference and mean cell temperatures, respectively. The latter can be written as (2.46), a piecewise function of the collector mass flow rate ($\dot{m}_c$), to differentiate between fluid circulation and stagnation.

$$P_{pv} = A_c \tau \eta_{pv,r} \rho_{pv} G_T \left[1 + \beta_{pv}\left(T_{pv,m} - T_{pv,r}\right)\right] \tag{2.45}$$

$$T_{pv,m} = \begin{cases} T_{f,in} + \left(T_a + \frac{\widetilde{S}}{\widetilde{U}_L} - T_{f,in}\right)\left(1 - \widetilde{F}_R\right) & , \ \dot{m}_c \neq 0 \\ T_a + \frac{\widetilde{S}}{\widetilde{U}_L} & , \ \dot{m}_c = 0 \end{cases} \tag{2.46}$$

2.1.3.2. Zondag et al. dynamic multi-dimensional multi-node models

Vries (1998) initially and later Zondag et al. (2002, 2003) developed and compared several PV-T collector models, ranging from steady-state HWB model-inspired to dynamic multi-dimensional multi-node models. The latter group included a 4-node quasi-3D model based on energy balances for the glass cover, the PV laminate, the absorber plate and the tube, as well as a 2D simplification of the quasi-3D model. The heat transfer mechanisms considered included solar radiative heat transfer to the glass cover and absorber, radiative heat losses from the glass cover to the sky, radiative heat transfer between the glass cover and the PV laminate, convective heat transfer from the glass cover to the surroundings, convective heat transfer across the insulating air layer, conductive heat transfer from the cells to the absorber and, convective heat transfer from the absorber to the heat carrier fluid. In turn, the

PV efficiency (η_{pv}) was modelled according to (2.12), and used to arrive at the net effective transmittance-absorptance product via (2.47). In any case, the comparison undertaken revealed one-dimensional models were satisfactory for the purposes of daily and annual, thermal and electrical yield estimations.

$$(\tau\alpha)_{eff,net} = (\tau\alpha)_{eff} - \tau\eta_{pv} \tag{2.47}$$

2.1.3.3. Chow's dynamic multi-node plug-flow model

Chow (2003) also proposed a dynamic multi-node PV-T collector model but one incorporating a fluid transport delay (or plug-flow) routine[26]. The model encompasses equations for 7 nodes including the glass cover, the collector back surface, the PV laminate, the absorber plate, the insulation, the tube bond, and the fluid in the tubes. The electrical efficiency was modelled as (inversely) proportional to the cell temperature in accordance with (2.12), and the electrical output power was defined as an explicit function of the PV packing factor (ρ_{pv}) in addition to the standard variables (G_T, η_{pv} and A_c). The model was not validated experimentally but was nevertheless deemed suitable for transient analysis of PV-T collector behaviour.

2.1.3.4. Amrizal et al. dynamic single-node model

Amrizal et al. (2013) proposed and validated a single-node dynamic PV-T collector based on the EN 12975 standard's QDTM equation, that is, the Perers model. The main novelty of the model is how it adjusts the equation (2.36) for use with PV-T collectors: by subtracting the electrical power generated per unit area ($P_{pv}A_c^{-1}$) to the effective irradiance ($G_bK_b + G_dK_d$) in accordance with (2.48).

$$\begin{aligned}\frac{\dot{Q}}{A_c} =& \eta_0 \left(G_bK_b + G_dK_d - P_{pv}A_c^{-1}\right) - c_1(T_{f,m} - T_a) - c_2(T_{f,m} - T_a)^2 \\ & - c_3u_W(T_{f,m} - T_a) + c_4\left(E_L - \sigma T_a^4\right) - c_5\frac{dT_{f,m}}{dt}\end{aligned} \tag{2.48}$$

The model also uses the single-diode equivalent circuit model to estimate the electrical power generated (P_{pv}), though a few other details are noteworthy. First, the model is cell temperature dependent but does not take into account the temperature dependence of the bandgap energy (E_g) and photogenerated (I_L) current. In turn, the mean cell temperature is empirically estimated using (2.49), an equation lacking solid theoretical foundations despite similarities with (2.50) and (2.51), both of which are mean plate temperature equations derived from the HWB model[27],

[26] Cristofari et al. (2009) proposed a very similar model but without the transport delay mechanism.

[27] The corresponding author for Amrizal et al. (2013) was reached for clarification concerning the origin of (2.49) and, wittingly or unwittingly, erroneously assumed it to be equivalent to a similar equation, (2.51) [Equation (6.9.4), page 267 in Duffie and Beckman (2013)].

and in any case requiring information the performance tests don't provide, at least independently, namely the collector efficiency factor (F') and the F'-independent zero-reduced temperature heat loss coefficient ($U_{L,1}$ or c_1/F'), respectively. Third, these expressions do not accurately reflect the effect of PV generation – as equivalent Florschuetz model correlations do – and assume a negligible heat loss coefficient temperature dependence (c_2 or $F'U_{L,2}$=0 W/m²K²) even though (2.48) doesn't. It should be noted, however, that the heat loss coefficient temperature dependence was omitted in the model's experimental validation, presumably since this process relied on an unglazed PV-T collector – a design often associated with a negligible heat loss coefficient temperature dependence – and thus this omission likely had no repercussion on the model's validation though it does limit its scope. Fourth, the model does not explictly address transients or stagnation conditions but if the mean cell temperature equation proposed is used for this purpose, it leads to abrupt cell temperature variations during transitions from circulation to stagnation. Finally, the electrical power for the calculation of the specific heat flow rate in (2.48) appears to be calculated without taking into account the presence of (F' through) η_0, which according to the equation's underlying logic (also found in the HWB and Florschuetz models) would have required the mean collector fluid temperature ($T_{f,m}$) to be used instead of the mean plate temperature ($T_{p,m}$). This, however, should not be confused with the cell temperature required to calculate the actual or output P_{pv}.

$$T_{p,m} = T_{f,in} + \frac{\dot{Q}}{A_c U_L F'} (1 - F') \tag{2.49}$$

$$T_{p,m} = T_{f,m} + \frac{\dot{Q}}{A_c U_L F'} (1 - F') \tag{2.50}$$

$$T_{p,m} = T_{f,in} + \frac{\dot{Q}}{A_c U_L F_R} (1 - F_R) \tag{2.51}$$

Despite these options, the model was validated experimentally using procedures closely following those of the EN 12975-2:2006 standard for the thermal performance and a different procedure for the electrical performance. The latter relied on maintaining stable conditions while keeping the collectors covered, quickly uncovering them and measuring a current-voltage curve, and covering them again. In doing so, the cell temperatures are relatively stable while the measurements are done and their effect can be decoupled. The thermal performance model validation also relied on covering and uncovering the collectors which is not an officially sanctioned procedure according to the above-named standard though other conditions were met. In fact, the EN 12975-2:2006 standard does not specifically address the case of PV-T collectors nor does it exclude them but was replaced in 2013 by the ISO 9806:2013 standard, which does make recommendations for thermal performance testing of PV-T collectors (CEN, 2006; Kramer and Helmers, 2013; ISO, 2013).

2.1.3.5. Haurant et al. dynamic multi-dimensional multi-node model

Haurant et al. (2015b) developed perhaps the most detailed and accurate PV-T collector model to date, a dynamic 3-D multi-node PV-T collector model integrating optical, hydraulic, thermal and electrical submodels. The model uses energy balances for at least 7 nodes including those corresponding to the glass cover, the insulating air layer, the EVA layer, the cells, the heat exchanger, the back insulation and the fluid temperature. The electrical performance was simulated using the single-diode equivalent circuit, reproduced for several series-connected cells to evaluate mismatch effects – which were revealed to be negligible as had been demonstrated in several previous studies (Vries, 1998; Zondag, 2008). These components were combined with a hydraulic mesh designed to reproduce the performance of a custom-made FracTherm heat exchanger whose geometry resembles blood vessels (Hermann, 2013). Given the model's complexity, sampling times on the order of 0.01-0.001 seconds were required. Nevertheless, the model was able to keep outlet temperature errors down to 0.2°C and 2°C during steady-state and dynamic sequences, respectively, only increasing above that threshold (up to 6-7°C) during abrupt flow rate variations not prescribed in standard performance tests.

The authors also noted discrepancies between the predicted stagnation behaviour and experiments, reportedly due to probe placement. Specifically, the outlet temperature was found to decrease – rather than increase – during stagnation and this incoherent behaviour was linked to the temperature being measured too far from the modules, in a downstream pipe. This was remedied by adding a pipe node, in order to reflect the local heat loss mechanisms during the absence of flow.

2.1.3.6. Lämmle et al. dynamic two-node model

The PV-T collector model proposed by Lämmle et al. (2015) relies heavily on the generic solar collector model known as TRNSYS type 832 – which in turn is based on the Perers model (Haller et al., 2014; Lämmle, 2016). The latter has a special two-node mode allowing the fluid and absorber temperatures to be differentiated, which Lämmle et al. used to assign the absorber temperature as the cell temperature for an external PV model. For this, the TRNSYS type 832 model requires the fluid specific heat capacity and the heat transfer rate between the fluid and the absorber to be specified, which can be determined from the fluid volume the collector can accommodate and the collector efficiency factor, respectively. By doing so, the thermal and electrical performance of PV-T collectors can be reproduced during fluid circulation and stagnation with minimal computational effort and a reduced number of parameters. At the same time, it is unclear if the parameters determined through ISO 9806 performance tests can be used reliably without adjustment.

2.1.4. Summary

The following points can be concluded from the literature review:

- Two main types of PV module models are commonly used: those based on equivalent circuits or those assuming a linear cell efficiency temperature dependence at the MPP. The latter is commonly used in studies where the modules can be expected to operate continuously at the MPP, whereas the former is mainly used in detailed studies or those where variable loads can be expected;

- Among the equivalent circuit PV models, the single diode one offers a reasonable compromise over the two diode one. In turn, the generally less detailed and accurate linear model is still fairly accurate and has been used and validated in numerous studies including those focusing on PV-T systems;

- ST collector models vary greatly in complexity. Simple models are generally used for performance estimation whereas transient analyses typically benefit from more complex ones due to the improved accuracy under dynamic conditions. Complexity, however, can increase parameter cross-correlation, computation times and deteriorate numerical stability, all of which are undesirable;

- Complexity has also not been a guarantee for accurate ST collector modelling during stagnation. Single-node dynamic models have often relied on unrealistic assumptions such as an isothermal collector during stagnation, whereas higher-order models have largely refrained from reproducing the prevailing heat transfer mechanisms. Moreover, the only model surveyed explicitly accounting for fluid boiling was a steady-state non-hybrid collector model;

- Stagnation modelling for PV-T collectors can be seen as more important than for non-hybrid ones since PV electricity generation is temperature sensitive and does not stop with stagnation. Cell temperature estimation is thus a priority for PV-T collector models, whereas non-hybrid collector models can simply focus on fluid temperatures, and it has been addressed through: correlations built on the assumption of steady-state operation and linear collector heat losses; or, dynamic models with cell and fluid temperature nodes;

- Parameter estimation is possible through standardised performance tests using some hybrid and non-hybrid collector models, namely steady-state and low-order dynamic models, such as the ones by Amrizal et al. and Perers, which are compatible with the tests featured in the ISO 9806:2013 standard. These tests require stable conditions and continuous fluid circulation and as a such the results may not be representative of transients or stagnation;

- At the same time, not even the most detailed collector models, such as the PV-T collector model by Haurant et al., are able to address all observed phenomena. Transients, in particular, generally lead to higher errors than during quasi-dynamic or steady-state conditions. Conversely, one-dimensional PV-T collector models have been determined to be accurate enough for thermal and electrical yield predictions, and can be seen as a suitable compromise;

- The two-node PV-T collector model by Lämmle et al. is a noteworthy effort due to the compromise between the simplicity afforded by low-order models and the accuracy of multi-node models, but it is bound to be less stable, more computationally intensive than a single-node model and may not be ideally suited for or compatible with parameter estimation via standardised performance tests such as those described in the ISO 9806:2013 standard.

2.2. Supply-loop differential temperature control for low-temperature systems

Supply-loop flow control is essential for active ST systems and is chiefly used to regulate the energy collection process, though other uses are known (e.g., preventing the heat carrier from freezing). With regard to low temperature systems, the controllers commonly used for this purpose are either two-state or variable-flow controllers. Two among these have become standard in this segment since the late 1970s, namely the differential temperature static two-level hysteretic (DTSTLHC) and differential temperature static saturated hysteretic-proportional (DTSSHPC) controls, while others including PID and optimal controls have seen limited field application in this segment. The following sections review the literature on DTSTLHC and DTSSHPC and their use or lack thereof in PV-T systems.

2.2.1. Differential temperature static two-level hysteretic control

Differential temperature static two-level hysteretic control (DTSTLHC)[28] has been used at least since the late 1960s and is generally acknowledged to be the most common supply-loop fluid flow controller for active ST systems in use today and in previous decades (Close, 1967; Duffie and Beckman, 1980, 2013; Winn, 1983, 1993; Badescu, 2008; Kaltschmitt et al., 2007). The controller's success can be attributed to its simplicity, reliability and cost since it merely actuates a relay (or relays) to turn the pump(s) on and off as a temperature difference (ΔT) – measured between the collector absorber or fluid near the outlet and the storage fluid near the bottom of the tank or slightly below the internal heat exchanger inlet port – exceeds or falls below preset turn-on (ΔT_{on}) and turn-off (ΔT_{off}) setpoints, respectively. Accordingly, the controller does not make fine adjustments to the mass flow rate – instead allowing it to deviate freely from the design value – and does not measure the temperature of the heat carrier reaching the tank, as conveyed by the block diagram of Figure 2.2. The control thus conceivably allows the storage tank to be discharged at positive – however small – ΔT values, particularly if the system has long or uninsulated pipes or a heat exchanger in the circuit. In such cases, using higher controller setpoints than otherwise necessary can compensate for this effect.

[28] This is the formal designation proposed by the author for this type of control. Alternative designations are commonly used in the literature and include bang-bang, slam-bang, on/off,

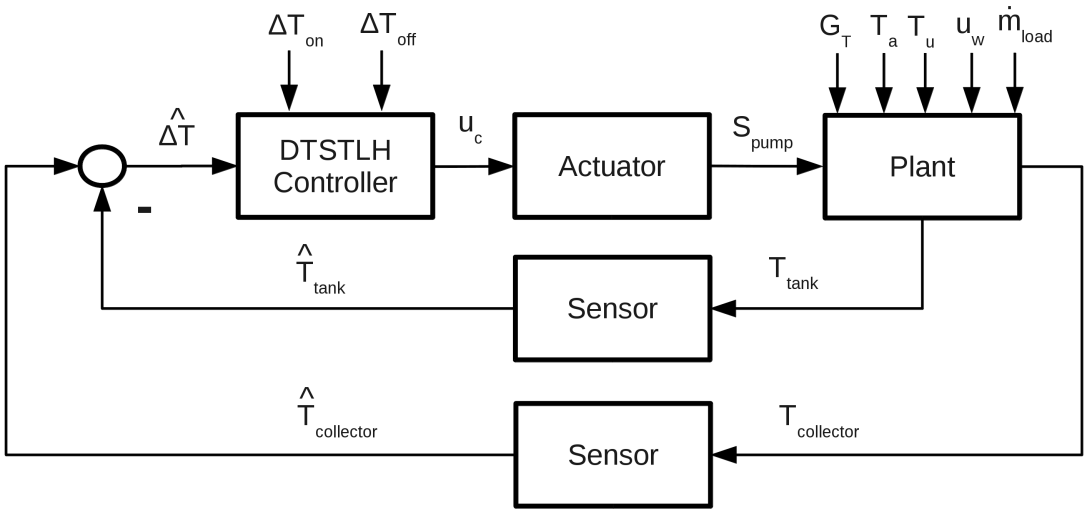

Figure 2.2.: Block diagram for differential temperature static two-level hysteretic control (DTSTLHC). The pump state (S_{pump}) is manipulated between on and off states in accordance with the controller output (u_c) while the mass flow rate is allowed to deviate freely from the nominal value without corrective action.

In any event, the turn-on setpoint is set higher than the turn-off setpoint to introduce hysteresis, as illustrated in Figure 2.3. The resulting deadband (ΔT_{on}-ΔT_{off}) can minimise unnecessary parasitic energy losses when only marginal heat gains are possible and, if sufficiently large, can also prevent instability in the form of excessive pump cycling[29], which controllers based on ΔT – as defined above – are prone to cause, particularly the DTSTLHC (Orbach et al., 1981).

2.2.1.1. Pump cycling

Pump cycling concerns the frequent switching of the supply-loop pump(s) between on and off states and occurs naturally in DTSTLHC-operated ST systems as ΔT increases and decreases in a relatively quick and successive manner. The phenomenon predominantly takes place during low or intermittent insolation, cold system starts or premature late afternoon shutdowns. Figure 2.4 shows a typical daily cycling pattern for ST systems using DTSTLHC, though without timer delays.

The phenomenon of pump cycling is known to arouse concern among system owners due to its unstable nature and has often been associated with accelerated equipment degradation (Conway, 1977; Herczfeld et al., 1978b; Lewis and Carr, 1978b; Kalogirou, 2009; Winn, 1983, 1993). However, no quantitative analysis of the latter was found in the literature although Winn (1983) assessed that limiting pump cycling to no more than 6 cycles per start-up or shutdown period would cause

on/off differential thermostat or simply differential temperature control.

[29] Also refered to as pump "hunting" or "short cycling" (Winn, 1993; Kalogirou, 2009).

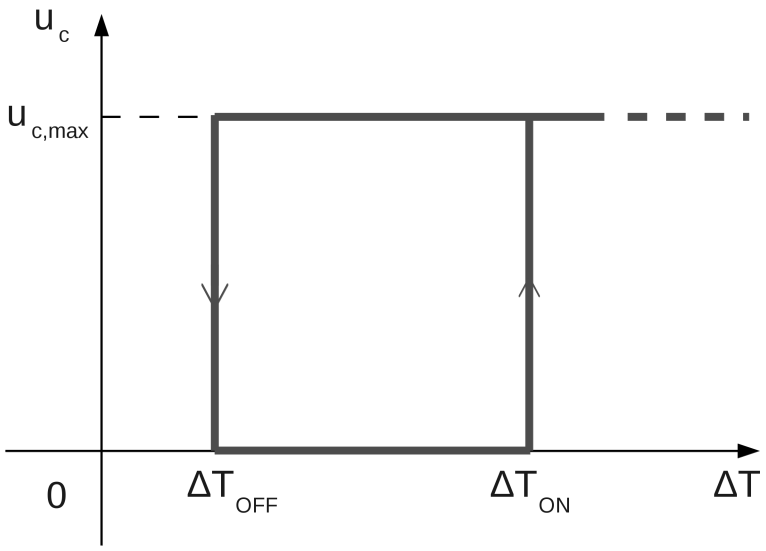

Figure 2.3.: Differential temperature static two-level hysteretic control function.

negligible enhanced degradation of windings, bearings and relays[30]. Moreover, pump cycling can enhance the collection of thermal energy, albeit not substantially, and thus completely avoiding it would imply a corresponding penalty (Kahwaji and Winn, 1986; Huang, 1994). Hence, moderate pump cycling is generally tolerated in ST systems using DTSTLHC as a compromise between the perceived equipment degradation and the potential performance penalty (Kalogirou, 2009).

Mitigating pump cycling in ST systems employing DTSTLHC is nevertheless possible through several means. Other than using larger deadbands, operating a system at lower flow rates can also lower the number of cycles but the downsides include higher average collector temperatures and heat losses (Herczfeld et al., 1978a,b; Winn, 1993). Alternatively, the controllers can force a minimum pump running time (also known as timer delays) to constrain cycling but in doing so can also keep the pump(s) on while no net heat gain is taking place (Schiller et al., 1980; Winn, 1993; Peuser et al., 2002). Peuser et al. (2002) reported typical minimum pump running times between 3 and 5 minutes whereas Schiller et al. (1980) had previously hinted at values in the range of 5-10 minutes. Efforts to reduce cycling also benefit from a collector sensor positioned near the end of the fluid flow path within the collector – the standard practice – as opposed to the start. Otherwise, the controller is more sensitive to the inrush of previously stagnant cold fluid from the collector loop, for the same controller setpoints, in addition to being slower to react during stagnation (Herczfeld et al., 1978b, 1980; Winn, 1993; Peuser et al., 2002).

[30]Winn (1993) revised down his assertion from a decade earlier concerning relay cycle ratings (from over 2 million to over 150,000) but maintained his original assessment (Winn, 1983).

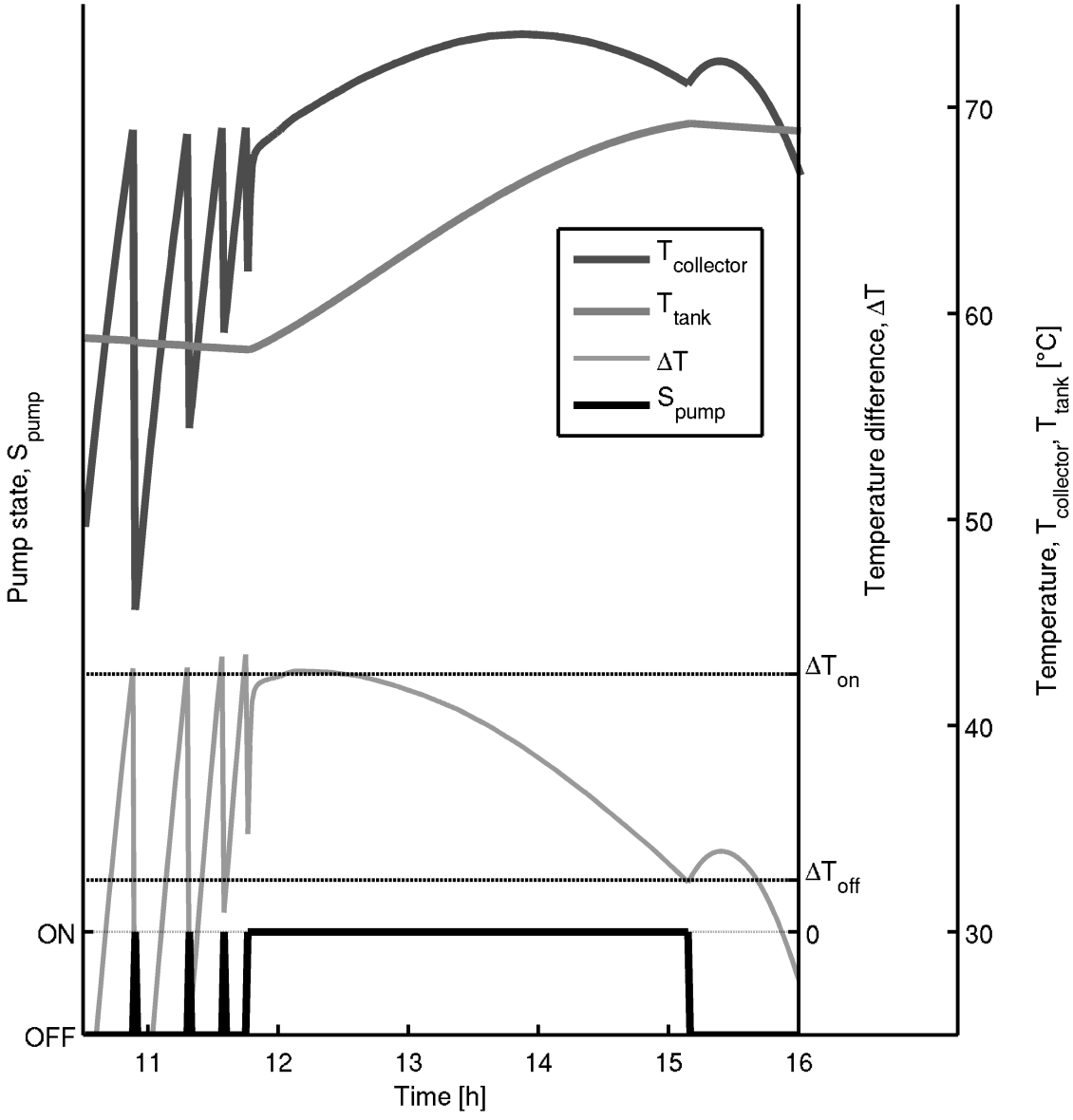

Figure 2.4.: Example of pump cycling in a low-temperature indirect DTSTLHC-operated ST system, using an internal heat exchanger as shown in Figure 1.6 (S_{pump}, pump state; ΔT, temperature difference sensed; $T_{collector}$, fluid temperature at the collector outlet; T_{tank}, tank water temperature at its bottom)

2.2.1.2. Effect of controller setpoints

The controller setpoints condition system operation and simultaneously influence the thermal efficiency, collection period and parasitic consumption in addition to pump cycling. As detailed earlier, the magnitude of pump cycling is correlated with the deadband's width. In turn, higher setpoints tend to reduce the pump running time since they cause fluid circulation to start later and stop earlier than it would otherwise, which tends to negatively influence the collection efficiency – although not necessarily in a monotonic way (Hirsch, 1985; Kahwaji and Winn, 1986; Muralidhar et al., 1989). As a result, setpoint selection implies a trade-off between many aspects but notably between the parasitic consumption and the ST energy yield.

The effect of controller setpoints on the parasitic consumption and thermal efficiency has received some attention in the literature, though mostly the latter and primarily through simulations. Schiller et al. (1980) simulated ST systems with a constant collector inlet temperature and found absolute daily collection efficiency increases between 0.5 and 3.4% by decreasing ΔT_{on} setpoints from 11.7 K to 5 K, which simultaneously led to relative collection period increases in the range of 3-69% and highest for low insolation or cloudy days. Kahwaji and Winn (1986) later conducted simulations for similar systems and found absolute daily collection efficiency increases up to 26% by allowing cycling through lower ΔT_{on} setpoints, and highest for low insolation days with correspondingly limited solar contributions (the highest increase corresponded to a day for which no energy collection was possible without some cycling). Huang (1994) subsequently reported absolute daily collection efficiency increases as high as 0.33% and 1.42% for systems with storage tanks under clear and cloudy sky days, respectively, by decreasing ΔT_{on} between 12 and 2 K. In other words, high ΔT_{on} setpoints reduce energy collection and this process is more sensitive to setpoints during low or intermittent insolation days.

On the other hand, the ΔT_{off} setpoint has received far less attention. Muralidhar et al. (1989) carried out experiments in a ST system with storage and determined the thermal energy collection process to be more sensitive to ΔT_{off} than to ΔT_{on} whereas Hirsch (1985) had previously found higher ΔT_{off} setpoints decreased the solar fraction negligibly for typical ΔT_{off} setpoints around 1 K. In conclusion, there is little evidence to suggest more than a marginal heat gain can be had through careful setpoint selection, though less so during low or intermittent insolation days.

2.2.1.3. Setpoint selection

Determining which setpoints to select for DTSTLHC-operated systems can be a complex task due to the subjective nature of a compromise involving pump cycling and the dynamic processes and weather conditions. Short of conducting detailed simulations for each individual system, setpoint selection can be aided by analytical design rules derived using the HWB model, premised on cost-effective and cycling-free fluid circulation, and given by (2.52) and (2.53), respectively, where $P_{el,pump}$ is the parasitic electrical power required by the pump(s), $\eta_{th,pump}$ is the (combined)

thermal efficiency of the pump(s) in relation to fluid heating, $K_{par,aux}$ is the ratio between the parasitic (p_{el}) and auxiliary (p_{aux}) energy prices, and ε is the effective ΔT measurement error. According to Dikkers et al. (1984) and Rabl (1985)[31], their derivation was originally the work of Davis (1975), corrected and enhanced by Alcone and Herman (1981), namely to consider the effect of sensor errors, and later expanded by Beckman et al. (1994) to cover systems with heat exchangers.

$$\Delta T_{off} > \frac{(K_{par,aux} - \eta_{th,pump})\, P_{el,pump}}{\epsilon(\dot{m}C_p)_{min}} + \varepsilon \tag{2.52}$$

$$\Delta T_{on} > \frac{\epsilon(\dot{m}C_p)_{min}}{A_c F'_R U_L} (\Delta T_{off} - \varepsilon) + \varepsilon \tag{2.53}$$

$$K_{par,aux} = \frac{p_{el}}{p_{aux}} \tag{2.54}$$

The first design rule (2.52) is used to arrive at the minimum economically[32] advantageous ΔT_{off} setpoint, which for small high-flow SDHW systems tends to be roughly in the same range as the ΔT measurement errors than can occur with commonly used sensors such as thermistors (±3°C) and resistance temperature detectors (RTDs; at least ±0.6°C for IEC 751 Class B sensors) and thus the setpoints need to be correspondingly higher (Schiller et al., 1980; Hirsch, 1985; Peuser et al., 2002; Kaltschmitt et al., 2007; Wilson et al., 2008). The second design rule (2.53) amounts to an upper limit on ΔT_{on}, for a given ΔT_{off}, since some cycling is tolerable and the condition is understood to be conservative (Winn, 1993). Conversely, it can be seen as unreliable because it does not account for collector heat capacity or the cold stagnated fluid in the connecting pipes, the latter being arguably the main cause of early morning cycling (Schiller et al., 1980; Winn, 1993; Beckman et al., 1994).

Beckman et al. (1994) also proposed using the previous methods for ST systems whose collectors show non-linear heat losses. Though no rationale or validation was provided, the suggestion was to replace $F_R U_L$ in the standard design methods with the thermal efficiency curve slope's absolute value near an efficiency of zero (i.e., stagnation), though it only applies to the condition for stable operation, (2.53).

Setpoint selection can also be aided by two empirical methods, particularly to select ΔT_{on}. The first holds that a given ratio between ΔT_{on} and ΔT_{off} akin to (2.53) should exist for there to be stable operation in liquid heat carrier-type FPC-based systems. According to Winn (1993), the ratios range from 4 up 6 for ΔT_{off} setpoints between 1 and 2 K with the highest values typically applied when ΔT_{off}

[31] Rabl (1985) reproduced the analytical relations derived by Alcone and Herman (1981) but adopted a different (though nowadays standard) sign convention for the heat loss coefficient.

[32] The rationale behind design rule (2.52) can be used for other purposes, namely primary energy efficiency by replacing the energy prices with the respective primary energy factors.

assumes the lowest value. Similarly, Schiller et al. (1980) cite ratios between 2 and 7. The second method consists of largely undifferentiated empirical setpoint ranges for ΔT_{on} and ΔT_{off}, one exception being those for indirect systems which are predictably higher than those for direct systems (Beckman et al., 1994; Kalogirou, 2009). According to Kalogirou (2009), indirect systems are typically configured using ΔT_{on} and ΔT_{off} setpoints in the range of 8-15 K and 3-6 K, respectively. In turn, a literature-based setpoint compilation revealed the following ranges: 3-11 K, for ΔT_{on}; and, 0.2-5 K for ΔT_{off} (Winn, 1993; Prapas et al., 1995; Knudsen, 2002; Eicker, 2003; Kaltschmitt et al., 2007; Badescu, 2008; Kalogirou, 2009).

Regarding PV-T systems, a literature survey reveals that the setpoints selected for the test and simulation of these systems have been consistent with the ranges for non-hybrid systems: 5-10 K for ΔT_{on}; and 1-4 K for ΔT_{off} (Rockendorf et al., 1999; Huang et al., 1999, 2001; Chow et al., 2009; Dupeyrat et al., 2014; Haurant et al., 2014, 2015a). However, no formal reasoning behind the choice of controller setpoints for PV-T systems was put forward in the aforementioned studies.

2.2.2. Differential temperature static saturated hysteretic-proportional control

One alternative to DTSTLHC can be described as differential temperature static saturated hysteretic-proportional control (DTSSHPC), though it is often referred to as simply "proportional" control. It is in essence a form of variable flow control for ST systems available at least since the late 1970s (Schlesinger, 1977; Lewis and Carr, 1978b). The control itself bears some resemblance to DTSTLHC since its output is a function of a temperature difference (ΔT) measured in the same way and because it also commands the start and end of fluid circulation in accordance with static turn-on (ΔT_{on}) and turn-off (ΔT_{off}) setpoints, possibly separated by a deadband, although that was not the norm in the late 1970s (Herczfeld et al., 1978a; Lewis and Carr, 1978a; Swanson and Ollendorf, 1979). Notwithstanding the resemblances, DTSSHPC obeys a control function – illustrated in Figure 2.5 – with a distinctive low ΔT segment and whose output (u_c) is positively correlated with the flow rate. In essence, the controller adjusts the flow rate – and thus demands variable-flow capabilities – according to a monotonically increasing function of ΔT, if fluid circulation is on, ΔT is above ΔT_{off} and below ΔT_{sat} – the saturation setpoint – above which the flow rate saturates at its nominal value.

Several DTSSHPC implementations have been discussed in the literature, all of which relying on speed-controlled pumps – though the use of throttling valves is a possible alternative (Winn, 1993). Two main types of AC pump speed (ω_{pump}) control are commonly used for this purpose. The traditional one consists of constant frequency, variable voltage operation of standard single-phase induction motor pumps, either through integral-cycle control (ICC; also known as burst-fired control), phase angle-fired control (PAFC) or possibly a combination of both (ICC/PAFC), and implemented via power converters with anti-parallel thyristors or TRIACs (Lewis,

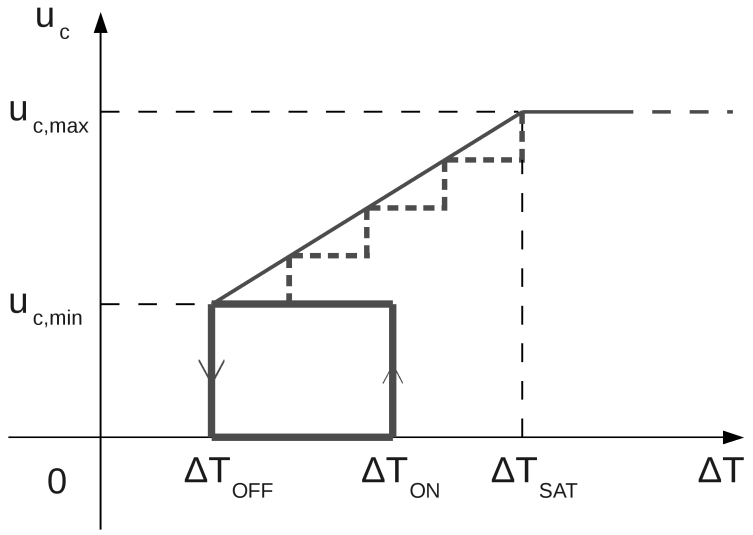

Figure 2.5.: Differential temperature static saturated hysteretic-proportional control (DTSSHPC) characteristic curves with a: a) stepless linear ramp (thick straight line); b) discretised linear ramp (thick dashed line).

1977; Lewis and Carr, 1978b; SEECI, 1981; Naumann and Wolfson, 1984; Winn, 1993; Asghar, 1999; Rashid, 2010). An alternative was made commercially available at least since the mid-1990s, namely pulse width modulation (PWM) control for high-efficiency pumps powered by dedicated frequency converters (Furbo and Shah, 1996; Grundfos, 2012; STECA, 2014; RESOL, 2015; Grundfos, 2016; Wilo, 2016). Hence, both types can be regarded as more individually expensive to implement than DTSTLHC, mainly due to additional power converter requirements (Swanson and Ollendorf, 1979; Naumann and Wolfson, 1984; Ntsaluba et al., 2016). At the same time, some low-end ST system control units are simultaneously compatible with DTSTLHC and DTSSHPC and thus opting for one over the other does not necessarily imply higher or noticeably higher initial costs, depending on whether or not such a control unit is purchased as part of a package deal, but also generally due to advances in electronics over the past 40 years that enabled greatly reduced costs (RESOL, 2015, 2016; Sonnenkraft, 2009). The traditional DTSSHPC methods are, however, simpler, more common and possibly cheaper though they are generally outperformed by the PWM variant in terms of power quality and speed control (Xu, 1992; Asghar, 1999; Rashid, 2010). In particular, ICC-based implementations can only provide discrete speed control capabilities, due to the need to keep the switching pattern duration below the motor's mechanical time constant to avoid severe torque ripple and speed variations, and often in open-loop since some implementations do not feature feedback signals – though the only in-depth experimental study of DTSSHPC reportedly relied on closed-loop ICC (Xu, 1992; Asghar, 1999; Naumann and Wolfson, 1984). As a result of these and other (e.g., stability) considerations, the DTSSHPC $\dot{m}$-ΔT characteristic curve differs depending on the

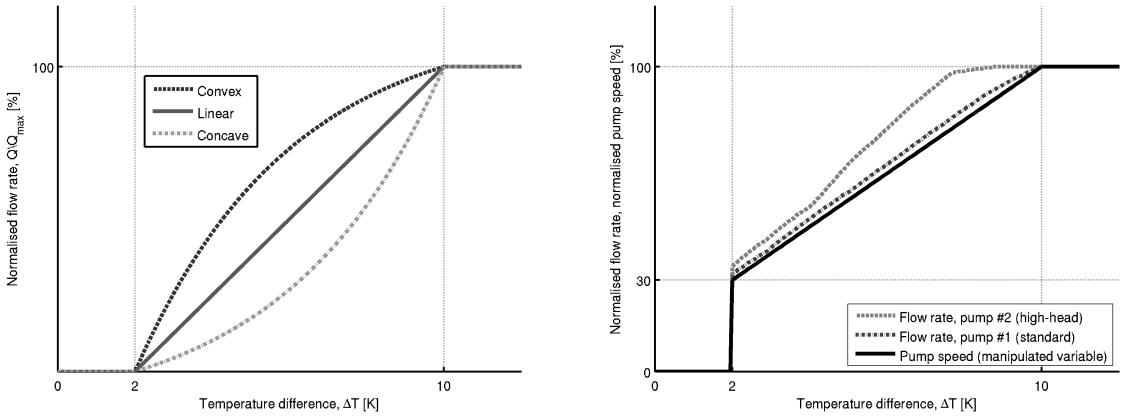

Figure 2.6.: Examples of DTSSHPC curves: left-hand side plot) convex, linear and concave functions defined by Swanson and Ollendorf (1979); right-hand side plot) linear function of the pump speed and resulting non-linear (convex) functions of the flow rate obtained through simulations for two different circulation pumps.

exact implementation, though the flow rate remains a monotonically increasing function of ΔT. Prominent examples include the linear $\dot{m}$-ΔT curves most commonly used in simulation studies, concave $\dot{m}$-ΔT curves resulting from open-loop PAFC and ICC implementations, and pseudo-convex $\dot{m}$-ΔT curves resulting from linear ω_{pump}-ΔT curves implemented via PWM speed control, as illustrated in Figure 2.6 (Lewis, 1977; Lewis and Carr, 1978b; Pejsa et al., 1978; Swanson and Ollendorf, 1979; Schiller et al., 1980; Naumann and Wolfson, 1984; STECA, 2014).

2.2.2.1. Operation

The differences between DTSSHPC and DTSTLHC are thus primarily felt at low temperature differences, which solar heating systems are more likely to face during the early morning hours, late in the afternoon or during periods of low or intermittent insolation. During the early morning of clear sky days, the flow rate is initially near the minimum and after a transient phase gradually increases as the collector heats up, possibly reaching the nominal value if ΔT reaches ΔT_{sat} or above, or alternatively peaking at a lower value around noon. The ability to reach the nominal flow rate early in the day generally prevents underperformance during clear sky days but this depends on the storage and weather conditions as well as the choice of setpoints and flow rate limits, and for these reasons, can be hard to guarantee without undermining system performance during poor weather days (Lewis and Carr, 1978b; Schlesinger, 1978; Schiller et al., 1980). As the day progresses, the flow rate gradually decreases in accordance with a decreasing ΔT – as the storage tank temperature increases and the collector cools down – from the nominal or a lower peak value until it reaches the minimum level and subsequently reaches zero once ΔT falls below ΔT_{off}. In turn, periods of intermittent insolation may lead to

multiple and significant flow rate variations in a DTSSHPC-operated system, though less pump cycling should occur compared to an equivalent DTSTLHC-operated system. DTSSHPC also allows for reduced pump cycling during the early morning start-up and the late-afternoon shutdown, since fluid circulation starts and ends at subnominal flow rates – often about 30% of the nominal value (Herczfeld et al., 1978a,b; Winn, 1993; Sonnenkraft, 2009; RESOL, 2015, 2016). Figure 2.7 exemplifies the behaviour of DTSSHPC-operated ST systems for different conditions.

The behaviour described and illustrated highlights an improved capability of DTSSHPC relative to DTSTLHC to adapt to low ΔT situations. Stability, however, remains a concern since the ΔT variations in the proportional region elicit a response opposed to the original perturbation and may cause oscillations (Kent and McGavin, 1978). For example, if ΔT is halfway between ΔT_{sat} and ΔT_{off} and drops due to external factors while circulation is taking place, the DTSSHPC response is to force a lower flow rate which, all other things being equal, eventually causes the collector(s) to heat up and ΔT to increase, in turn increasing the flow rate which will then cause ΔT to decrease, and so on until a stable regime is reached – see top right plot in Figure 2.7 for an illustration of this oscillatory behaviour. If the difference between ΔT_{sat} and ΔT_{off} happens to be small, the perturbations will result in higher controller output swings and thus more severe oscillations (Swanson and Ollendorf, 1979; Schiller et al., 1980). As a matter of fact, low and high ΔT_{sat} setpoints in relation to ΔT_{off} cause the control function to asymptotically approach that of DTSTLHC at the nominal and minimum output levels, respectively, though instability will be more prevalent in the former case. In any event, the control's intrinsic instability can be mitigated through setpoint selection.

2.2.2.2. Setpoint selection

The selection of DTSSHPC setpoints suffers from the same predicaments as that of DTSTLHC setpoints but is more complex, in part due to the additional setpoint. Setpoint selection can, nonetheless, benefit from the analytical design methods mainly developed for the DTSTLHC, as long as adjusted. Concretely, the method for the minimum ΔT_{off} setpoint (2.52) should assume the minimum as opposed to the nominal flow rate while the guideline for cycling-free operation (2.53) should consider the initialization flow rate enforced by the controller, which is known to vary between implementations (STECA, 2014; RESOL, 2015). Assuming the controller initially enforces the minimum flow rate, the method suggests a lower ΔT_{on} setpoint can be used to meet the stability criteria in DTSSHPC-operated systems than in a DTSTLHC-operated ones using the same ΔT_{off} setpoint and operating at the same nominal flow rate. It also means thermal energy collection can start earlier. In turn, a higher ΔT_{off} setpoint must be employed to ensure sparing of parasitic energy but this does not necessarily entail a shortened thermal energy collection period seeing as the lower flow rate allows for higher collector temperatures.

On the other hand, no analytical design methods exist to guide the saturation setpoint selection. Alternatively, the surveyed literature suggests ΔT_{sat} be selected

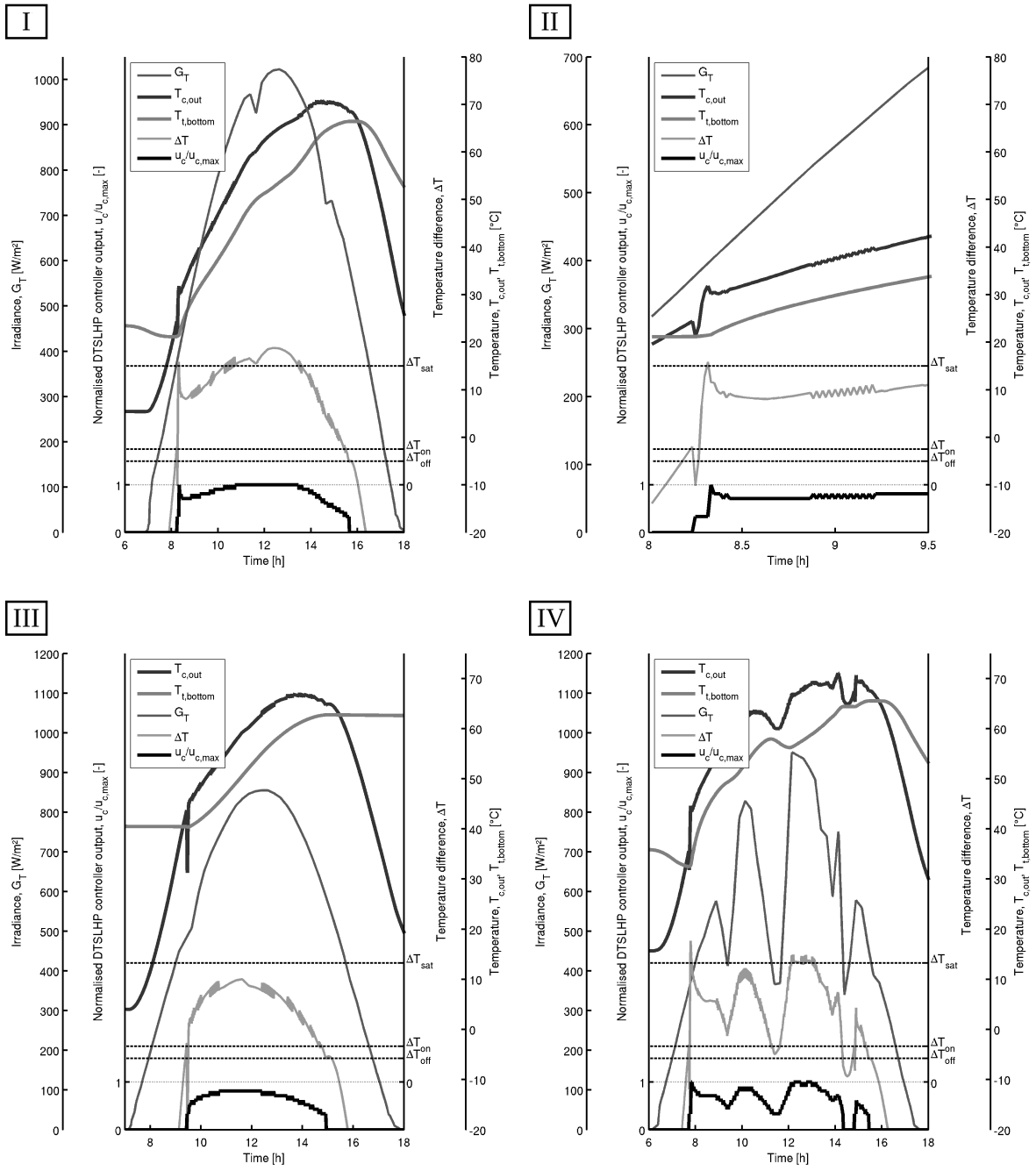

Figure 2.7.: Simulated dynamic behaviour of a DTSSHPC-operated PV-T system during: I) a sunny day with low initial storage temperature, during which the nominal flow rate is reached; II) close-up of top left plot, highlighting oscillations during flow rate (step) transitions; III) a sunny day with moderate initial storage temperature, during which the nominal flow rate is not reached; IV) intermittent insolation day, during which the flow rate varies significantly and cycling is avoided until late in the day. These simulations relied on the model defined in Appendix D whose DTSSHPC implementation obeys a discretised linear $\dot{m}$-ΔT curve.

in accordance with motor controllability and sensor accuracy in order to stave off instability, which implies it should be sufficiently higher than ΔT_{off} although this may reduce performance (Schlesinger, 1976; Herczfeld et al., 1978a; Swanson and Ollendorf, 1979; Schiller et al., 1980). At the same time, selecting a ΔT_{sat} setpoint higher than the predicted maximum ΔT at the maximum flow rate will limit the controller to the proportional region and prevent the system from operating at high flow rates and thus at high efficiencies. Conversely, high ΔT_{sat} setpoints could conceivably improve thermal stratification although the evidence is limited (Swanson and Ollendorf, 1979; Schiller et al., 1980; Naumann and Wolfson, 1984).

The aforementioned guidelines are largely in agreement with the setpoints cited for this controller in the relevant literature. Notably, the literature mainly focuses on ΔT_{off} and ΔT_{sat} setpoints whereas the ΔT_{on} setpoints are not explicitly mentioned nor figure in the control characteristics, though some publications regard ΔT_{on} as equal to ΔT_{off} (Herczfeld et al., 1978a; Pejsa, 1978; Naumann and Wolfson, 1984; Winn, 1993). As such, narrow deadbands are seen as the norm for these controllers. In turn, the ΔT_{off} and ΔT_{sat} setpoints cited are in the range of 1-2.5 K and 5-12 K (9-21°F), respectively, which are consistent with the ranges for ΔT_{off} and ΔT_{on} setpoints in high-flow DTSTLHC-operated ST systems, respectively (Swanson and Ollendorf, 1979; Schiller et al., 1980; Naumann and Wolfson, 1984). In fact, this apparent correspondence between the DTSSHPC and DTSTLHC setpoints can be found in many studies comparing these controls.

2.2.3. Comparisons between DTSTLHC- and DTSSHPC-operated solar heating systems

Direct comparisons between DTSTLHC- and DTSSHPC-operated ST systems have been few, limited in scope and date back to the late 1970s and early 1980s. Moreover, the studies surveyed focus exclusively on non-hybrid ST systems, are mostly based on sub-annual simulations using artificial or low resolution data, and in the latter case and in the case of experiments, have focused on locations with similar climates. Nevertheless, the main differences between the controls have been identified although only vague guidelines for the use of either – and DTSSHPC in particular since DTSTLHC is generally the first choice due to its simplicity, reliability and often comparable performance – have been put forward in spite of the fact that some low-end control units are compatible with both. Finally, the conclusions reached in these studies may not be up to date, particularly considering the developments in pump design and power electronics of recent decades.

2.2.3.1. Thermal performance

The surveyed literature is generally consistent with the view that DTSSHPC allows for qualified thermal performance enhancements compared to DTSTLHC. According to Winn (1993), Schlesinger (1977) determined through steady-state simulations that DTSSHPC enabled energy collection increases in the range of 6-8%

relative to high-ΔT_{on} DTSTLHC under cloudy and overcast weather conditions. Schlesinger (1978) later reported average daily increases in the range of 10-12%, depending on the insolation level, while conceding the annual thermal performance increase was more likely within 1-2%. Schlesinger (1978) also reported a 20% storage temperature advantage for a DTSSHPC-operated system in one side-by-side test during a clear sky medium insolation day (peak irradiance of 700 W/m² and daily irradiation of about 4.2 kWh/m²), although the DTSTLHC's turn-on setpoint (11.1 K) was somewhat higher than the DTSSHPC's saturation setpoint (6.7 K). In turn, Pejsa et al. (1978) conducted an annual dynamic simulation for a combi-system using Minneapolis, Minnesota (44°59´N, 93°16´W) weather data[33] and determined that a DTSSHPC-operated system (ΔT_{off}=ΔT_{on}=1.7 K) could outperform a DTSTLHC-operated equivalent (ΔT_{off}=1.7 K) by 3.8% while using a marginally higher saturation setpoint (ΔT_{sat}=6.7 K) than the latter's turn-on setpoint (ΔT_{on}=6.1 K).

Lewis and Carr (1978b) also acknowledged the energy collection-enhancing potential of DTSSHPC but noted the early morning gains enabled by a lower ΔT_{on} could be offset during the rest of the day unless ΔT quickly reached ΔT_{sat}. Such is the condition to attain the nominal flow rate and avoid higher collector temperatures and higher heat losses otherwise implicit with DTSSHPC (Schiller et al., 1979, 1980). The corollary with regard to PV-T systems is of course that lower electrical yields may result if DTSSHPC is used rather than DTSTLHC, although this hypothesis has not been proposed or tested in the surveyed literature.

Lewis and Carr (1978b) did not quantitatively compare the daily energy collection possible with DTSSHPC and DTSTLHC but linked its outcome to the insolation or more generally to factors predicted to influence one control more than the other, such as a high nominal flow rate and a high collector thermal capacity. According to the authors, the former and latter cause a DTSTLHC-operated system to comparatively underperform due to cycling and delayed start of circulation, respectively. The effect of the collector thermal capacity may have special relevance for the present study since PV-T collectors tend to have a higher thermal capacity than comparable non-hybrid designs and thus the DTSSHPC advantage over DTSTLHC may be comparatively higher in PV-T systems (Zondag et al., 2002). In any case, the comparison by Lewis and Carr focused more on weather conditions and reasoned that intermittent insolation days were the most favourable to DTSSHPC in contrast with clear sky days, generally viewed as favourable to DTSTLHC, while low insolation conditions were predicted to produce less consistent results (Lewis and Carr, 1978b; Swanson and Ollendorf, 1979; Schiller et al., 1979, 1980).

The effect of weather conditions on the comparison between the controls in relation to thermal performance was quantified in several independent studies which essentially corroborate the above-named claims. Pejsa et al. (1978) determined through dynamic simulations that a DTSSHPC-operated ST system in Minneapo-

[33]Minneapolis, Minnesota (U.S.A.) has a humid continental climate (Dfa in the Köppen-Geiger system), i.e., a snowy humid climate (minimum mean monthly temperature below -3°C) with hot summers (maximum mean monthly temperature over 22°C), and its annual average global horizontal irradiance (GHI) is about 1425 kWh/m²/year (Kottek et al., 2006; NREL, 2014).

lis could outperform a DTSTLHC-operated equivalent by 0.25% and 0.75% during clear sky and partly cloudy days, respectively. Similarly, Swanson and Ollendorf (1979) conducted extensive daily simulations using artificial data for clear skies whose results consistently revealed thermal performance advantages for DTSSHPC (ΔT_{off}=ΔT_{on}=1.7 K; ΔT_{sat}=5.6 K) over DTSTLHC (ΔT_{off}=1.1 K; ΔT_{on}=11.1 K), although limited to 3% and highest for low insolation and – to a lesser extent – low temperature conditions. The same study also presented monthly simulation results for different seasons using Washington, D.C. (38°54´17″N, 77°00´59″W) weather data[34] which revealed limited and inconsistent performance differences, including DTSSHPC underperforming during the Winter, attributed by the authors to the data resolution (one hour samples interpolated down to 36 s), stratification in the tank model and the simulations' accuracy. Schiller et al. (1979, 1980) also compared the controls' daily performance in dynamic simulations using artificial data for both clear and cloudy skies but only found clear advantages for DTSSHPC in terms of energy collection for cold and cloudy low insolation days, which led to relative thermal efficiency increases up to 81% – assuming the ΔT_{sat} setpoint matches the DTSTLHC's ΔT_{on} setpoint and the same nominal mass flow rate is used.

On the other hand, Naumann and Wolfson (1984) tested both controls experimentally in Middlebury, Vermont (44°0´7″N, 73°8´44″W)[35] and found DTSSHPC outperformed DTSTLHC during high (mostly clear sky) and low (cloudy) insolation days by as much as 2.5% and 50%, respectively. It can thus be established that DTSSHPC performs best relative to DTSTLHC during intermittent and low insolation conditions though in a highly-variable way since DTSTLHC-operated systems can perform almost as well or not even turn on – the best case from the point of view of DTSSHPC. At the same time, the energy collection enhancement enabled by DTSSHPC is low in an absolute sense even though it mostly takes place when it matters most (i.e., when the demand is harder to supply without auxiliary energy), namely during poor weather days or during the Winter (Schlesinger, 1978).

DTSSHPC has also been cited as potentially advantageous in terms of stratification relative to DTSTLHC, but the evidence to support such assertion is not conclusive (Schiller et al., 1980; Naumann and Wolfson, 1984). For instance, Schiller et al. (1980) suggested improved stratification as a potential advantage of DTSSHPC, given its propensity to enforce lower flow rates when comparable setpoints and nominal flow rates are used, while Naumann and Wolfson (1984) reported some evidence of improved stratification in experimental tests for those conditions, particularly during low insolation days, although the subject was recognised by the authors as

[34] Washington, D.C. (U.S.A.) has a humid subtropical climate (Cfa in the Köppen-Geiger system), i.e., a warm temperate climate (minimum mean monthly temperature over -3°C) with hot summers (maximum mean monthly temperature over 22°C), and its annual average global horizontal irradiance is about 1541 kWh/m²/year (Kottek et al., 2006; NREL, 2014).

[35] Middlebury, VT (U.S.A.) has a humid continental climate (Dfb in the Köppen-Geiger system), i.e., a snowy humid climate (minimum mean monthly temperature below -3°C) with warm summers (maximum mean monthly temperature below 22°C), and its annual average global horizontal irradiance is about 1342 kWh/m²/year (Kottek et al., 2006; NREL, 2014).

not being the main thrust of the study. Conversely, Swanson and Ollendorf (1979) determined the thermal energy gains attained by selecting DTSSHPC over DTSTLHC in daily simulation runs were reduced by considering stratification in the tank model. Furthermore, any advantage in terms of stratification will tend to be reduced by configuring DTSSHPC to use low ΔT_{sat} setpoints, which generally lead to the highest thermal energy yields, and thus it is doubtful DTSSHPC-enhanced stratification can have a significant impact (Schiller et al., 1979, 1980).

In turn, the effect of setpoints on the controller comparison was only specifically addressed in two studies and in a limited sense. Both determined higher ΔT_{sat} and ΔT_{on} setpoints decrease the thermal efficiency of DTSSHPC- and DTSTLHC-operated systems, respectively, but not to the same extent (Swanson and Ollendorf, 1979; Schiller et al., 1980). Concretely, Swanson and Ollendorf (1979) found the performance decreases (up to 1% for a 5.6 K setpoint variation) comparable yet mostly favourable to DTSTLHC in monthly dynamic simulations – about which the authors did not express full confidence in – while Schiller et al. (1979, 1980) reported higher decreases (up to 40% for a 6.7 K ΔT_{on} variation compared to up to 4% for an equivalent ΔT_{sat} variation) for DTSTLHC-operated systems, namely during cloudy and low gain clear sky days, although their simulations did not consider storage dynamics. As a result, it is not entirely clear from the literature how the choice of setpoints influences the comparison between DTSTLHC and DTSSHPC controls.

2.2.3.2. Parasitic performance

The differences between DTSTLHC and DTSSHPC also have repercussions in terms of parasitic performance. For example, the latter's enhanced energy collection during periods of low or intermittent insolation presupposes the pump is kept on for longer periods of time than under DTSTLHC but generally at subnominal flow rates which often imply a lower instantaneous pump power consumption, assuming both controls use the same pump and nominal flow rate. The balance between these two effects depends on several factors and has been investigated in a few studies, all of which assumed the same nominal flow rate for both controls and the DTSTLHC's turn-on setpoint to be comparable or equal to the DTSSHPC's saturation setpoint. Pejsa et al. (1978) conducted the first study and found DTSSHPC increased the annual pump energy consumption of a non-hybrid combi-system by slightly less than 6% while modelling the electrical pump power as a curve-fitted linear function of the normalised flow rate. In turn, Schiller et al. (1980) used a zero y-axis intercept linear pump power model and determined daily parasitic energy increases as high as 67% and 300% for low (5 K) and high (11.7 K) setpoints, respectively, but mainly highest for cold cloudy weather days. Similarly, Naumann and Wolfson (1984) measured 20% and 200% higher parasitic energy consumptions for DTSSHPC during good and poor weather days, respectively, in Middlebury, Vermont. Hence, there is evidence to suggest DTSSHPC implies a parasitic energy penalty relative to DTSTLHC for the systems represented in these studies, particularly during poor weather days.

2.2.3.3. Overall performance

A limited set of studies have considered the effect of the parasitic energy consumption on the performance comparisons between DTSTLHC- and DTSSHPC-operated ST systems and primarily in terms of final use – as opposed to primary – energy efficiency or load provision cost. The study by Pejsa et al. (1978) estimated a marginal load provision cost advantage (0.5% or $1.23 per year in 1977 U.S. dollars and equivalent to $4.94 per year in 2017 U.S. dollars, according to BLS, 2017) could be had by using DTSSHPC instead of DTSTLHC but, while noting modest extra implementation costs for the former ($15 in 1977, $60.3 in 2017), ultimately recommended the latter citing performance uncertainties with the former. The same study found an even higher load provision cost advantage (2% or $11.66 in 1977, $46.87 in 2017) could be had by opting for DTSSHPC over DTSTLHC in systems bound to use electrical heating elements for backup heat, although these were predicted to lead to higher annual load provision costs than the DTSTLHC- and DTSSHPC-operated gas-assisted alternative systems. In contrast, Swanson and Ollendorf (1979) did not factor in the parasitic energy consumption but reasoned the expenditures required to implement DTSSHPC, which according to the study required a large and expensive variable speed pump as opposed to a single-speed pump, were unjustified simply in light of the uncertain and at best limited thermal performance advantage – estimated at no more than 3% – over DTSTLHC.

Conversely, Schiller et al. (1979, 1980) accounted for the parasitic energy and found DTSTLHC and DTSSHPC ranked the same from the stand point of thermal efficiency and net energy efficiency by considering the most efficient (75 W) out of two pumps evaluated in daily simulations for multiple weather conditions. In turn, opting for the least efficient pump (373 W) improved DTSSHPC's net energy efficiency ranking for some clear sky conditions, illustrating its inability to quickly reach the nominal flow rate and the nominal pump power once circulation begins – as opposed to DTSTLHC. Also, the results generally show DTSTLHC and DTSSHPC performed best during clear and cloudy sky days, respectively, but the performances for each control differed in an absolute and relative sense by less than 1% and 11%, respectively, regardless of the circulation pump considered.

In turn, Naumann and Wolfson (1984) computed the net energy balance for single-day experiments which revealed higher net energy gains for the DTSSHPC-operated system. The gains were 1.1% and 38.5% higher than those observed for the DTSTLHC-operated system during good and poor weather days, respectively, although the authors acknowledged that a more realistic analysis would place a higher value on the parasitic energy (electricity), i.e., penalising its use. For instance, computing the net energy balance using the same data but assuming parasitic to auxiliary energy value ratios of 2 and 3 – instead of 1 – would lead to relative net energy gains for the DTSSHPC-operated system of 25% and 9.1% during poor weather days, respectively, and 0.6% and 2.6% relative net energy losses during good weather days. Anticipating this outcome, the authors recommended DTSSHPC for regions where low or intermittent insolation weather is common and where the parasitic

energy price does not significantly exceed that of auxiliary energy.

Although these recommendations were not quantified so as to guide a decision-making process, they are consistent with some of the surveyed literature, most noticeably the work by Pejsa et al. (1978). In it, choosing DTSSHPC over DTSTLHC in a ST system using electrical auxiliary heaters revealed higher load provision cost reductions than if the system used gas heaters, since in the former the parasitic energy price is not higher than but rather equal to the auxiliary energy price, and thus DTSSHPC is comparatively more advantageous in those systems. Similarly, switching from a low to high efficiency pump should comparatively favour DTSSHPC, at least during those days in which it excels thermal performance-wise, since it is equivalent to reducing the value of parasitic energy. However, the results of Schiller et al. (1979, 1980) add nuance to this view since DTSSHPC is shown to perform comparatively better during clear sky days if the low efficiency pump is selected, as discussed previously, meaning this depends on how fine-tuned DTSSHPC is to quickly reach the nominal flow rate and pump power after circulation begins.

Finally, the results found in the literature generally indicate DTSSHPC presents a small performance advantage over DTSTLHC. In an effort to explain these results, Naumann and Wolfson (1984) conceded the DTSSHPC's comparative advantage was likely limited since it was only manifest at low heat levels and required comparatively expensive electricity and equipment. This assessment relies on assumptions that are to a large extent are still true today but can be influenced by economic and technological developments and vary geographically, while the DTSSHPC's advantage at low heat levels can be said to be intrinsic to this control and thus limiting.

2.2.4. Summary

The following points can be summarised from the literature reviewed:

- DTSTLHC and DTSSHPC are differential temperature pump controls relying on a temperature difference (ΔT) measured in the same way, were introduced several decades ago, are the most widely used today for low-temperature ST systems and are both available even in some low-end control units;
- Notwithstanding the previous point, DTSTLHC is simpler to implement than any of the several DTSSHPC variants reported, including those using ICC, PAFC and PWM speed control, all of which manipulate the flow rate according to a monotonically-increasing function of the temperature difference between the turn-off (ΔT_{off}) and saturation (ΔT_{sat}) setpoints below and beyond which circulation stops and the flow rate saturates, respectively;
- DTSSHPC is known to be advantageous from the standpoint of stability relative to DTSTLHC but the literature, though itself limited, suggests only a qualified annual thermal performance advantage is to be had by opting for the former. The performance advantage is most noticeable during low or intermittent insolation days and consequently DTSSHP control may prove more

advantageous in locations experiencing such weather on a regular basis, as long as not to an extent that makes ST systems unappealing;

- The effect of system location and weather patterns on the comparison between DTSSHPC and DTSTLHC over long periods has not been systematically quantified and the limited set of studies focusing on uninterrupted multi-day periods have relied on low-resolution data for locations with similar weather;
- DTSSHPC can outperform DTSTLHC thermal performance-wise during low and intermittent insolation days due to longer collection periods at subnominal flow rates, which can also entail a higher parasitic consumption;
- Pump efficiency and (parasitic and auxiliary) energy prices have been predicted to influence the comparison between DTSSHPC and DTSTLHC but an in-depth study of these factors has not been carried out. According to the available literature, high auxiliary energy prices and higher pump efficiencies tend to favour DTSSHPC though less predictably in the latter case;
- DTSSHPC has not been studied for use in PV-T systems in comparison with DTSTLHC but preference for the former may lead to: lower PV yields due to lower flow rates and higher temperatures during clear sky days; higher thermal performance advantage due to the higher thermal capacity of PV-T collectors compared to equivalent non-hybrid collectors;
- The comparisons between DTSSHPC and DTSTLHC have relied on figures of merit that do not take primary energy efficiency into account or the specific attributes of PV-T systems, namely local electricity generation;
- The comparisons conducted so far have also focused on a limited set of controller setpoints and flow rates, which although typical for low-temperature ST systems, have not been optimised from a diverse pool of alternatives;
- Analytical design rules for the turn-off (ΔT_{off}) and turn-on (ΔT_{on}) setpoints, common to both DTSSHPC and DTSTLHC, have been developed based on cost-effective and cycling-free operation in non-hybrid ST systems, respectively, and taking into account the existence of measurement errors;
- The DTSSHPC's saturation setpoint (ΔT_{sat}), however, does not have a corresponding analytical design method though it is generally understood it should be selected in accordance with stability, motor controllability and sensor accuracy. Furthermore, it can be safely assumed ΔT_{sat} should be between ΔT_{off} and the maximum ΔT that can be expected at the nominal flow rate.

3. Dynamic PV-T collector model

Dynamic PV-T collector models are important tools to reproduce and study collector behaviour. Several dynamic PV-T collector models have been proposed but arguably none that accurately mimics the thermal and electrical performance during fluid circulation, stagnation and transients of PV-T collectors displaying a non-negligible collector heat loss temperature dependence, with minimal computational effort and easily configured according to publicly available performance data determined from standardised performance tests. The present chapter describes a dynamic single-node PV-T collector model designed to address this gap.

3.1. Description

3.1.1. Overview

The dynamic model proposed reproduces the thermal and electrical performance of PV-T collectors using a multi-segment compatible single-node approach, a zero-capacitance cell temperature estimator and a linear cell efficiency temperature dependence. Its development was undertaken to deliver a dynamic, accurate and computationally fast PV-T collector model compatible with parameter identification via the prevailing standardised performance tests (i.e., ISO 9806:2013) and suitable for thermal and electrical yield predictions as well as flow control studies. Accordingly, the model borrows heavily from numerous other ST collector models which, in one way or another, build on the HWB model, such as the Florschuetz (1979), Perers (1993), Muschaweck and Spirkl (1993) and Amrizal et al. (2013) models, but stops short of the two-node approach followed by Lämmle et al. (2015). In other words, the model attempts to reconcile a single-node approach to PV-T collector modelling – based on mean fluid temperatures – with accurate cell temperature estimation during fluid circulation, stagnation and transients, while taking into account the effect of electricity generation and a temperature dependent heat loss coefficient.

Cell temperatures can be estimated using various mean plate temperature equations based on the HWB or Florschuetz models – cf. Appendix C. However, for a non-negligible collector heat loss temperature dependence, these equations will be presumably inaccurate at higher temperatures. Alternatively, a single-node dynamic model can be made compatible with a temperature-sensitive heat loss coefficicent but then either the mean fluid or plate temperatures have to be estimated.

The approximate solution found to this predicament has not been proposed in the literature surveyed. Nevertheless, the single-node model developed by Amrizal et al.

(2013) is noteworthy due to its similarity to the one proposed. Amrizal et al. used the single-diode equivalent circuit model to reproduce the electrical power generated and, in turn, the specific heat flow rate while taking into account the PV generation-induced thermal performance reduction, and despite having validated their model experimentally, relied on an empirical mean plate temperature expression. Moreover, the expression does not account for the effect of electricity generation on cell temperatures and does not take the collector heat loss coefficient temperature dependence into account even though its thermal submodel – essentially based on the Perers model and common to the one being proposed here – does take this into account. The expression also depends on the heat flow rate and for this reason is bound to lead to steep variations during transients and a uniform collector temperature during stagnation if used as such, although there is no indication Amrizal et al. intended it to be used for these purposes. Finally, the interaction between the thermal and electrical performances appears to have been modelled in a way inconsistent with the underlying concept of F' – see Section 2.1.3.4. Conversely, the new model proposed estimates the mean cell temperature by taking the heat loss coefficient temperature dependence and electricity generation into account, during fluid circulation, stagnation and transients, and employs the linear cell efficiency temperature dependence (2.12) used and validated in multiple PV-T collector studies (Florschuetz, 1979; Zondag et al., 2002; Dupeyrat et al., 2011b).

3.1.2. Single segment model

3.1.2.1. Thermal submodel

The model proposed to reproduce the thermal performance of PV-T collectors extends the Perers (1993) model in a way not too dissimilar to the one proposed by Amrizal et al. (2013). In essence[36], a new term is added to (2.34), representing the specific thermal power output lost due to electricity generation, to arrive at (3.1). This term, however, is defined in accordance with the collector efficiency factor concept underpinning the original equation, meaning the term reflects the specific electrical power generated if the entire absorber plate (i.e., the cells) is at the mean fluid temperature, multiplied by the collector efficiency factor, to remain consistent with the other terms[37]. While possibly counter-intuitive, this approach can be traced back to the HWB steady-state collector model and the Florschuetz (1979) steady-state PV-T collector model previously reviewed in Sections 2.1.2.1 and 2.1.3.1, respectively. In a colloquial sense, the model proposed is to the Perers model what the Florschuetz model is to the HWB model.

[36]Longwave radiative heat losses have been neglected in (3.1) for convenience.

[37]Every term in (3.1) except $C_A dT_{f,m}/dt$ is based on the premise that the collector efficiency factor (F') is a valid construct, i.e., the useful heat flow rate can be predicted by multiplying the collector efficiency factor with the useful heat flow rate determined assuming the entire absorber, including the PV laminate, is at the mean fluid temperature.

$$\frac{\dot{Q}}{A_c} = F'\left(\tau\alpha\right)_n G_{T,eff} - F'U_{L,1}(T_{f,m} - T_a) - F'U_{L,2}(T_{f,m} - T_a)^2 - F'U_W u_W (T_{f,m} - T_a) - F'\left.\frac{P_{pv}}{A_c}\right|_{T_{pv,m}=T_{f,m}} - C_A\frac{dT_{f,m}}{dt} \tag{3.1}$$

$$G_{T,eff} = G_b K_b + G_d K_d \tag{3.2}$$

$$K_b = 1 - b_0\left(\frac{1}{\cos\theta} - 1\right) \tag{3.3}$$

Alternatively, Amrizal et al. (2013) proposed subtracting the specific electrical power generated (P_{pv}/A_c) to the effective irradiance on the collector plane ($G_{T,eff}$) in the term corresponding to the absorption of solar radiation, i.e., $F'\left(\tau\alpha\right)_n G_{T,eff}$. This alternative has been to some extent validated experimentally – see Section 2.1.3.4 – and can be shown to be comparable to one proposed here, namely by substituting (3.4) in (3.1) and rearranging until (3.5) is reached. Accordingly, the difference between them lies with how the PV generation-induced thermal performance reduction term is determined: the Amrizal et al. solution relies on the actual PV power generated, either estimated (at the mean cell temperature) or measured, whereas (3.5) relies on PV power generated assuming the cells are at the mean fluid temperature ($T_{f,m}$), which is incompatible with electrical power measurements.

$$P_{pv} = A_c \tau \rho_{pv} G_{T,eff} \eta_{pv} \tag{3.4}$$

$$\frac{\dot{Q}}{A_c} = F'\left(\tau\alpha\right)_n G_{T,eff}\left(1 - \frac{\tau}{\left(\tau\alpha\right)_n}\rho_{pv}\ \eta_{pv}|_{T_{pv,m}=T_{f,m}}\right) - F'U_{L,1}(T_{f,m} - T_a) - F'U_W u_W (T_{f,m} - T_a) - F'U_{L,2}(T_{f,m} - T_a)^2 - C_A\frac{dT_{f,m}}{dt} \tag{3.5}$$

Since the electrical efficiency is generally a weak function of cell temperature, and the mean plate and mean fluid temperatures are relatively close for typical liquid heat carrier collectors and respective flow rates, this discrepancy is likely not significant in practice. Nevertheless, the solution put forward in this Chapter suggests the thermal performance of a PV-T collector can be reproduced, when PV electricity is being generated or otherwise, using the typical measurements necessary for standardised thermal performance tests, namely those for the irradiance and mean fluid temperature. In other words, electrical power or cell temperature measurements are not strictly necessary for thermal performance tests of PV-T collectors.

3.1.2.2. Electrical submodel

The question then becomes: how to estimate the electrical power generated? The solution proposed assumes continuous operation at the MPP and relies on a linear cell efficiency temperature dependence, given by (3.6), which contrasts with the single-diode equivalent circuit model used by Amrizal et al. (2013). Accordingly, (3.5) can be rewritten as (3.7) and the PV electrical power output can be determined as long as the mean cell temperature ($T_{pv,m}$) can be estimated.

$$\eta_{pv} = \eta_{pv,r}\left[1 + \beta_{pv}\left(T_{pv,m} - T_{pv,r}\right)\right] \tag{3.6}$$

$$\begin{aligned}\frac{\dot{Q}}{A_c} =& F'\left(\tau\alpha\right)_n G_{T,eff} - F'\tau G_{T,eff}\rho_{pv}\eta_{pv,r}\left(1 + \beta_{pv}\left[T_{f,m} - T_{pv,r}\right]\right) \\ & - F'U_{L,1}(T_{f,m} - T_a) - F'U_W u_W (T_{f,m} - T_a) \\ & - F'U_{L,2}(T_{f,m} - T_a)^2 - C_A\frac{dT_{f,m}}{dt}\end{aligned} \tag{3.7}$$

The mean cell temperature estimator proposed rests on the assumption the collector efficiency factor construct is valid and can be extended to transients and stagnation. The idea is thus to determine the mean cell temperature from the independently determined mean fluid temperature. The procedure adopted is as follows:

1. Determine the mean fluid temperature ($T_{f,m}$) by solving (3.7);
2. Substitute the specific heat flow rate ($\dot{Q}/A_c$) in (3.7) with (3.8), its steady-state counterpart based on the mean cell temperature ($T_{pv,m}$);
3. Solve the new equation for $T_{pv,m}$ assuming steady-state conditions ($dT_{f,m}/dt = 0$) but using the dynamic $T_{f,m}$ solution to (3.7) determined in step 1.

$$\begin{aligned}\frac{\dot{Q}}{A_c} =& \left(\tau\alpha\right)_n G_{T,eff} - \tau G_{T,eff}\rho_{pv}\eta_{pv,r}\left(1 + \beta_{pv}\left[T_{pv,m} - T_{pv,r}\right]\right) \\ & - U_{L,1}(T_{pv,m} - T_a) - U_W u_W (T_{pv,m} - T_a) - U_{L,2}(T_{pv,m} - T_a)^2\end{aligned} \tag{3.8}$$

According to this model, the mean cell temperature is a function of the dynamic mean fluid temperature and is consistent with the standard usage of the collector efficiency factor though also extended to transients and stagnation. Implementing this estimator, however, requires additional parameters, namely the collector efficiency factor, the PV packing factor, the reference MPP PV efficiency, the cell efficiency temperature coefficient, the reference cell temperature and, if there are glass covers, their transmittance. Among these, the collector efficiency factor is arguably the most difficult to estimate since it can't be determined directly. It can, however, be

determined using the zero-heat loss efficiency (η_0) obtained in performance tests and the effective transmittance-absorptance product (Hermann, 2011).

Alternatively, Amrizal et al. (2013) proposed estimating the mean cell temperature using an expression for the mean plate temperature ostensibly derived from the HWB model – cf. Section 2.1.3.4. This approach also depends on the decoupled collector efficiency factor, is not fully adequate if the collector heat loss coefficient temperature dependence is non-negligible and/or if electricity generation is taking place, and can introduce steep variations of the mean cell temperature during transients if used during these events – though there is no indication Amrizal et al. intended it to be used for these flow regimes. For instance, a transition from fluid circulation to stagnation ($\dot{Q}$=0 W) would cause the mean cell temperature to instantly drop down to the inlet fluid temperature level, according to (2.49). Naturally, this behaviour is unrealistic and detrimental for studying different flow control strategies in PV-T systems as far as electricity generation is concerned, since stopping the pump(s) would then incorrectly entail a small PV yield increase in simulations.

Conversely, the model proposed tries to reproduce realistic cell temperature transients including between fluid circulation and stagnation. During stagnation, both the mean cell and mean fluid temperatures estimated gradually increase following the end of fluid circulation until both converge over time at the steady-state stagnation temperature, itself independent from the collector efficiency factor. However, this transition is modelled assuming a constant collector efficiency factor, as in the Schiller et al. (1980) model. In practice, this means the same heat transfer processes take place but, as Schnieders (1997) contended, this is generally not a rigorously valid assumption, as the heat transfer coefficient from the absorber plate to the fluid decreases substantially and thus the model can be predicted to overestimate fluid temperatures during stagnation, though ultimately converging in steady-state. Similarly, the mean plate temperature is bound to approach the stagnation temperature but it is not possible to determine if it is being overestimated or not during the transients without modelling the collector efficiency factor as a function of the mass flow rate. Hence, the cell temperature model approaches the correct steady-state values but is less rigorous concerning the heating and cooling times.

Another noteworthy shortcoming of the proposed cell temperature estimator is its direct dependence on the weather conditions rather than model outputs. This means the model can be too responsive to fast-changing conditions, most noticeably irradiance fluctuations, which can be arguably avoided if the weather conditions are reproduced at low resolutions (e.g., hourly data). The model also doesn't attempt to predict collector behaviour in the event of fluid boiling, as the Chen et al. (2015) model does. In any case, the solution found is meant to reproduce the basic dynamic behaviour of ST collectors in general and of PV-T collectors in particular.

3.1.3. Multi-segment model

The previously described collector model is essentially an extension of the Perers model to encompass PV-T collectors, and as a result, shares some of its short-

comings and faults. Other than the conditions for parameter identification, the Perers model is known to experience numerical convergence issues with high specific collector thermal capacitances and/or low sampling times, and assumes a linear temperature distribution from collector inlet to outlet during fluid circulation which, while generally a reasonable though not entirely accurate assumption, causes it to unrealistically predict outlet temperatures – in terms of response time and magnitude – following quick fluid inlet temperature variations (Schnieders, 1997; Nayak et al., 2000; Haller et al., 2014). These issues can be addressed by adopting a multi-segment approach to collector modelling, as done for the Perers model in the multi-segment instantiation of TRNSYS type 832 (Haller et al., 2014). According to this approach, one instantiation of the model described in the previous section only concerns $1/\mathrm{N_{seg}}$ of the collector flow path, area and heat capacity and thus $\mathrm{N_{seg}}$ instantiations of series-connected PV-T collector segments are necessary to model a whole PV-T collector[38]. Analytically, this corresponds to an approximate solution to (3.9), a differential equation reverse engineered from the PV-T model described in the previous section and from which the Florschuetz, Perers, Klein et al. and HWB models can be deduced, though originally inspired by the one put forward by Klein et al. (1974). Because the model proposed is for PV-T collectors, the discretisation also takes place at the plate (i.e., cell) temperature level in accordance with (3.10).

$$\begin{aligned} C_A \frac{\partial T_f}{\partial t} =& F' \left(\tau\alpha\right)_n G_{T,eff} - F' U_{L,1}(T_f - T_a) - F' U_W u_W (T_f - T_a) \\ & - F' \tau G_{T,eff} \rho_{pv} \eta_{pv,r} \left(1 + \beta_{pv} \left\{T_f - T_{pv,r}\right\}\right) \\ & - F' U_{L,2} (T_f - T_a)^2 - \frac{\dot{m}_c C_{p,c}}{W} \frac{\partial T_f}{\partial x} \end{aligned} \tag{3.9}$$

$$\begin{aligned} 0 =& \left(\tau\alpha\right)_n G_{T,eff} - U_{L,1}(T_{pv} - T_a) - U_W u_W (T_{pv} - T_a) \\ & - \tau G_{T,eff} \rho_{pv} \eta_{pv,r} \left(1 + \beta_{pv} \left\{T_{pv} - T_{pv,r}\right\}\right) \\ & - U_{L,2} (T_{pv} - T_a)^2 - \frac{\dot{m}_c C_{p,c}}{W} \frac{\partial T_f}{\partial x} \end{aligned} \tag{3.10}$$

The discretisation of (3.9) and (3.10) into multiple fluid and cell temperature segments, as opposed to just one of each, can also be advantageous from the point of view of PV performance accuracy with one main caveat. Despite the fact that the PV cell efficiency is not a strong function of temperature, a non-linear fluid temperature distribution along the collector flow path is more realistic, both during fluid circulation and during transitions from fluid circulation to steady-state stagnation, and is bound to have positive repercussions on cell temperature estimation. However, the linear cell efficiency temperature dependence equation (3.6) is generally

[38] This discretisation was originally inspired by the DSC model proposed by Muschaweck and Spirkl (1993), but the multi-segment version of TRNSYS type 832 is a more precise analogue.

used for modules or individual cells and may not be as accurate on an intra-cell or infinitesimal basis, though it was used as such in the Florschuetz model.

On a different note, the implications of the discretisation process with regard to parameter identification are unclear at this point and not the focus of this effort. Nonetheless, the DSC model – which is similar to the model proposed – has managed to reconcile a multi-segment approach with parameter identification and places fewer flow rate and inlet temperature restrictions on tests than the Perers model (Muschaweck and Spirkl, 1993; Schnieders, 1997; Nayak et al., 2000).

3.2. Implementation

The equations (3.9) and (3.10) are not directly usable as such for the intended purposes, such as simulation of flow control strategies. In order to rectify this, they first need to be discretised along the collector flow path ($0 \leq x \leq L_c$) into (3.11) and (3.12), respectively, where $T_{f,m}[i]$ and $T_{pv,m}[i]$ represent the mean fluid and cell temperatures for segment i – one out of $\mathrm{N_{seg}}$ segments whose lengths measure Δx – and $T_{f,out}[i]$ and $T_{f,in}[i]$ represent the segment's outlet and inlet temperatures.

$$\begin{aligned} C_A \frac{\partial T_{f,m}[i]}{\partial t} =& F' \left(\tau\alpha\right)_n G_{T,eff} - F' U_{L,1}(T_{f,m}[i] - T_a) - F' U_W u_W (T_{f,m}[i] - T_a) \\ & - F' \tau G_{T,eff} \rho_{pv} \eta_{pv,r} \left(1 + \beta_{pv} \left\{T_{f,m}[i] - T_{pv,r}\right\}\right) \\ & - F' U_{L,2} (T_{f,m}[i] - T_a)^2 - \dot{m}_c C_{p,c} \frac{T_{f,out}[i] - T_{f,in}[i]}{W \Delta x} \end{aligned} \tag{3.11}$$

$$\begin{aligned} 0 =& \left(\tau\alpha\right)_n G_{T,eff} - U_{L,1}(T_{pv,m}[i] - T_a) - U_W u_W (T_{pv,m}[i] - T_a) \\ & - \tau G_{T,eff} \rho_{pv} \eta_{pv,r} \left(1 + \beta_{pv} \left\{T_{pv,m}[i] - T_{pv,r}\right\}\right) \\ & - U_{L,2} (T_{pv,m}[i] - T_a)^2 - \dot{m}_c C_{p,c} \frac{T_{f,out}[i] - T_{f,in}[i]}{W \Delta x} \end{aligned} \tag{3.12}$$

The second step requires linearising the fluid temperature profile between inlet and outlet for each segment in accordance with (3.13), and taking into account that the segments are connected in series to form a whole collector as expressed by (3.14), i.e., each segment's inlet is the previous segment's outlet temperature.

$$T_{f,m}[i] = \frac{1}{2} \left(T_{f,out}[i] + T_{f,in}[i]\right) \tag{3.13}$$

$$T_{f,in}[i] = T_{f,out}[i-1] \tag{3.14}$$

Rearranging (3.13) for $T_{f,out}[i]$ and replacing it and (3.14) in (3.11) and (3.12) leads to (3.15) and (3.16).

$$\begin{aligned} C_A \frac{\partial T_{f,m}[i]}{\partial t} =& F' \left(\tau\alpha\right)_n G_{T,eff} - F' U_{L,1}(T_{f,m}[i] - T_a) - F' U_W u_W (T_{f,m}[i] - T_a) \\ & - F' \tau G_{T,eff} \rho_{pv} \eta_{pv,r} \left(1 + \beta_{pv} \left\{T_{f,m}[i] - T_{pv,r}\right\}\right) \\ & - F' U_{L,2} (T_{f,m}[i] - T_a)^2 - 2\dot{m}_c C_{p,c} \frac{T_{f,m}[i] - T_{f,out}[i-1]}{W \Delta x} \end{aligned} \tag{3.15}$$

$$\begin{aligned} 0 =& \left(\tau\alpha\right)_n G_{T,eff} - U_{L,1}(T_{pv,m}[i] - T_a) - U_W u_W (T_{pv,m}[i] - T_a) \\ & - \tau G_{T,eff} \rho_{pv} \eta_{pv,r} \left(1 + \beta_{pv} \left\{T_{pv,m}[i] - T_{pv,r}\right\}\right) \\ & - U_{L,2} (T_{pv,m}[i] - T_a)^2 - 2\dot{m}_c C_{p,c} \frac{T_{f,m}[i] - T_{f,out}[i-1]}{W \Delta x} \end{aligned} \tag{3.16}$$

The third step requires (3.15) be either discretised in the time-dimension or solved in closed-form for a single time interval (Δt). The former is a simple and intuitive way to address this issue and has been previously used, such as in the work of Amrizal et al. (2012), but the latter is more accurate though not always possible. However, if the problem is limited to a first order nonlinear ordinary differential equation in accordance with (3.17) and (3.22), a closed-form solution is possible.

$$g_3 \frac{\partial T_{f,m}[i]}{\partial t} = g_2 \cdot T_{f,m}^2[i] + g_1 \cdot T_{f,m}[i] + g_0 \tag{3.17}$$

$$\begin{aligned} g_0 =& F' \left(\tau\alpha\right)_n G_{T,eff} - F' \tau G_{T,eff} \rho_{pv} \eta_{pv,r} \left(1 - \beta_{pv} T_{pv,r}\right) - F' U_{L,2} T_a^2 \\ & + F' \left(U_{L,1} + U_W u_W\right) T_a + \frac{2\dot{m}_c C_{p,c}}{W \Delta x} T_{f,out}[i-1] \end{aligned} \tag{3.18}$$

$$\begin{aligned} g_1 =& - F' \left(U_{L,1} + U_W u_W\right) - F' \tau G_{T,eff} \rho_{pv} \eta_{pv,r} \beta_{pv} \\ & + 2F' U_{L,2} T_a - \frac{2\dot{m}_c C_{p,c}}{W \Delta x} \end{aligned} \tag{3.19}$$

$$g_2 = -F' U_{L,2} \tag{3.20}$$

$$g_3 = C_A \tag{3.21}$$

$$g_4 = T_{f,m}[i] \left(t = 0\,s\right) \tag{3.22}$$

Since (3.11) can be rewritten as (3.17) and an initial condition given by (3.22), the solution is given by (3.23), with (3.24) being used to keep the former readable.

$$T_{f,m}[i](t) = \begin{cases} \frac{g_5}{2g_2} \tan\left(\frac{g_5}{2} \cdot \left\{\frac{t}{g_3} + \frac{2}{g_5} \cdot \arctan\left[\frac{g_1+2\cdot g_2\cdot g_4}{g_5}\right]\right\}\right) - \frac{g_1}{2g_2} & , \ g_2 \neq 0 \\ \frac{g_0+g_1\cdot g_4}{g_1} \exp\left(\frac{g_1\cdot t}{g_3}\right) - \frac{g_0}{g_1} & , \ g_2 = 0 \end{cases} \tag{3.23}$$

$$g_5 = \sqrt{4 \cdot g_2 \cdot g_0 - g_1^2} \tag{3.24}$$

Alternatively, the solution to (3.17) becomes a quadratic equation for steady-state conditions or a negligible collector heat capacity (g_3=C_A=0 J/m²K). In turn, (3.16) can be rewritten as another quadratic equation, (3.25).

$$0 = h_2 \cdot T_{pv,m}^2[i] + h_1 \cdot T_{pv,m}[i] + h_0 \tag{3.25}$$

$$\begin{aligned} h_0 = &\left(\tau\alpha\right)_n G_{T,eff} - \tau G_{T,eff}\rho_{pv}\eta_{pv,r}\left(1 - \beta_{pv}T_{pv,r}\right) - U_{L,2}T_a^2 \\ &+ \left(U_{L,1} + U_W u_W\right) T_a + \frac{2\dot{m}_c C_{p,c}}{W\Delta x}\left(T_{f,m}[i] - T_{f,out}[i-1]\right) \end{aligned} \tag{3.26}$$

$$h_1 = -\left(U_{L,1} + U_W u_W\right) - \tau G_{T,eff}\rho_{pv}\eta_{pv,r}\beta_{pv} + 2U_{L,2}T_a \tag{3.27}$$

$$h_2 = -U_{L,2} \tag{3.28}$$

Thus, the mean fluid and cell temperatures for segment i ($\forall\, i \in \mathbb{N}$: $1 \leq i \leq N_{seg}$) and sample j ($\forall\, j \in \mathbb{N}$) according to a discrete-time implementation can be given by (3.29) and (3.30). The model is then completed by the boundary conditions (3.32) and (3.33), and by (3.31), which indicates the mean fluid temperature is taken as representative of outlet temperatures during stagnation ($\dot{m}_c = 0$).

$$T_{f,m}[i;j] = \begin{cases} \frac{g_5}{2g_2} \tan\left(\frac{g_5}{2} \cdot \left\{\frac{\Delta t}{g_3} + \frac{2}{g_5} \cdot \arctan\left[\frac{g_1+2\cdot g_2\cdot g_4}{g_5}\right]\right\}\right) - \frac{g_1}{2g_2} & , \ g_2 \neq 0 \\ \frac{g_0+g_1\cdot g_4}{g_1} \exp\left(\frac{g_1\cdot \Delta t}{g_3}\right) - \frac{g_0}{g_1} & , \ g_2 = 0 \end{cases} \tag{3.29}$$

$$T_{pv,m}[i;j] = \begin{cases} \frac{-h_1 \pm \sqrt{h_1^2 - 4\cdot h_2\cdot h_0}}{2\cdot h_2} & , \ h_2 \neq 0 \\ -\frac{h_0}{h_1} & , \ h_2 = 0 \end{cases} \tag{3.30}$$

$$T_{f,out}[i;j] = \begin{cases} 2T_{f,m}[i;j] - T_{f,out}[i-1;j] & , \ \dot{m}_c \neq 0 \\ \\ T_{f,m}[i;j] & , \ \dot{m}_c = 0 \end{cases} \tag{3.31}$$

$$T_{f,out}[0;j] = T_{f,in} \tag{3.32}$$

$$T_{f,out}[N_{seg};j] = T_{f,out} \tag{3.33}$$

The aforementioned equations reveal limited book-keeping is necessary to implement the N_{seg}-segment model. Essentially, a two-row N_{seg}-column array will suffice: one row for the mean fluid temperature and another for the oulet temperature, one column for each segment. This is possible since by solving the segments from collector inlet to outlet (i.e., increasing i), each segment's previous samples can be kept in the same cell until the next sample and then overwritten. The relevant variables can then be used to determine the thermal and electrical power output of the PV-T collector modelled according to (3.34) and (3.35), respectively.

$$\dot{Q}[j] = \dot{m}_c C_{p,c} \left(T_{f,out}[N_{seg};j] - T_{f,out}[0;j] \right) \tag{3.34}$$

$$P_{pv}[j] = \sum_{i=1}^{N_{seg}} \frac{A_c}{N_{seg}} \tau \rho_{pv} G_{T,eff} \eta_{pv,r} \left[1 + \beta_{pv} \left(T_{pv,m}[i;j] - T_{pv,r} \right) \right] \tag{3.35}$$

3.3. Validation

The model was validated for use in dynamic simulations through a combination of means other than physical experiments. The validation process thus comprised comparisons with other published results and other cell temperature models, and an assessment of the implications of assuming a constant collector efficiency factor.

3.3.1. Study of collector efficiency factor sensitivity

3.3.1.1. General comments

The PV-T collector model proposed is built on the assumption of a constant collector efficiency factor. This roughly translates as a constant ratio between the thermal resistances from the absorber plate to ambient air ($1/U_L$), and from the fluid to ambient air ($1/U_L$+$1/U_{f,p}$), as expressed by (3.36), which only differs from (2.16)

by assuming a uniform temperature distribution in the direction perpendicular to the flow direction and parallel to the absorber plate (Florschuetz, 1979).

$$F' = \frac{U_{f,p}}{U_L + U_{f,p}} \tag{3.36}$$

While not strictly constant in practice, the collector efficiency factor is generally regarded as a weak function of temperature and flow rate in textbooks (Kalogirou, 2009; Duffie and Beckman, 2013; Goswami, 2015). Though these textbooks don't quantify these variations in great detail, Wuestling et al. (1985) found only a 1% (absolute) F' reduction by lowering the flow rate from a conventional value (50 L/m²h) to a low one (10 L/m²h, or an 80% reduction) in a ST system with midrange flat-plate collectors, even though the convective heat transfer coefficient dropped by around 30%. The authors attributed this result to the magnitude of other thermal resistances such as the plate-tube bond, all of which are modelled into $U_{f,p}$.

On the other hand, the collector efficiency factor is usually expressed for steady-state fluid circulation, not transients or stagnation. In spite of it, several dynamic models assume a constant efficiency factor, including the Schiller et al. (1980), the DSC and the Perers model. This last model implicitly assumes a constant efficiency factor under continuous fluid circulation and modestly dynamic conditions, hence excluding some transients and stagnation. In contrast, the DSC model tolerates more abrupt variations though not stagnation. Indeed, if the collector efficiency factor can be regarded as the thermal resistance ratio described previously, then it should not be constant during stagnation, since $U_{f,p}$ can drop down to a single-digit percentage of its former value during stagnation and cause F' to decrease too. Hence, assuming a constant efficiency factor for all flow regimes, as many models do, namely the Schiller et al. (1980) model, means fluid temperatures are likely to be overestimated during stagnation, as Schnieders (1997) reported[39].

3.3.1.2. PV-T collectors

While the effect of flow rate and temperature on the collector efficiency factor of PV-T collectors should be no different than in non-hybrid collectors, a couple of exclusive influences can be highlighted. First, the additional thermal resistance found in PV-T collectors due to the PV laminate leads to a lower F' than would be possible in comparable non-hybrid designs and, can contribute to a reduced sensitivity to flow rate variations as Wuestling et al. (1985) suggested. On the other hand, PV conversion can be shown to increase $\tilde{F}'$ – rather than F' – through $\tilde{U}_L$, as expressed in (2.42), though the magnitude of this variation was predicted by Florschuetz (1979) to be limited to 1% for reasonable collector designs.

[39] Another plausible though less likely explanation for the discrepancy found by Schnieders (1997) is an inadequate experimental setup, namely if the outlet sensor is placed too far from the collector and is unable to measure representative fluid temperatures (Haurant et al., 2015b).

Nonetheless, an investigation into PV-T collector efficiency factor sensitivity to temperature, flow rate and irradiance was carried out and is detailed in Appendix B. Its results revealed a 22.2% decrease in $U_{f,p}$ and a 0.3-0.8% decrease in $\tilde{F}'$, for a flow rate decrease from 72 to 7.2 L/m²h (or a 90% reduction), fluid temperatures from 0°C up to 100°C and irradiance levels from 0 up to 1000 W/m². Thus, F' can be considered constant over a wide range of flow rate, temperature and irradiance conditions commonly found in ST systems, though not so for stagnation during which such an assumption has been shown to overestimate fluid temperatures.

3.3.2. Simulations

3.3.2.1. Comparison with published results

The reasoning behind this step is that a favourable comparison with validated non-hybrid collector models and respective results can attest for the accuracy of the proposed model, albeit in a limited sense. In this context, the detailed comparison by Schnieders (1997) of several collector models is specially relevant since results were published as well as the data necessary to reproduce them. However, rather than implementing each model, their responses were reconstructed by extracting data points from plots present in the original publication. Assuming the original plots' x- and y-axis are perfectly horizontal and vertical, respectively, the errors introduced by using this method should not exceed the combined thickness of the original line and axis, which is fairly low ($\ll$1°C). Because the accuracy of this process wasn't rigorously determined, the validation process is primarily visual rather than quantitative, though its accuracy is high enough for a confident assessment.

The relevant results published by Schnieders (1997) consist of step responses and experimental measurements. The former can be used to assess individual features of the model proposed under controlled circumstances, while the latter relied on an almost 30-minute long sequence of measurements of multiple variables displaying significant and concurrent variations, which can be useful to determine how accurate the model can be in practice. Naturally, these results can only be of use for validation as long as the proposed model can be correctly parametrised.

Schnieders (1997) compared more than one single-node model and provided the parameters used to configure them. Among these, the multi-segment DSC model is perhaps the most similar to the model being proposed and, for this reason, the same parameters chosen for the former were used to set up the latter. For the step responses, the parameters used were: $F'(\tau\alpha)_n$=0.7805; $F'U_{L,1}$=2.6635 W/m²K; $F'U_{L,2}$=0 W/m²K²; and, C_A=10000 J/m²K. For the test sequence, the parameters selected were: $F'(\tau\alpha)_n$=0.796; $F'U_{L,1}$=1.62 W/m²K; $F'U_{L,2}$=0 W/m²K²; and, C_A=10580 J/m²K. Additionally, PV generation was turned off in both instances since the results reproduced concern non-hybrid (evacuated tube) collectors, i.e., there was no need to define F' independently or any of the PV-related parameters.

Step responses

The model proposed was subjected to the irradiance, flow rate and inlet fluid temperature steps detailed by Schnieders (1997). These were set to start at t=100 s and consisted of an irradiance increase from 0 to 800 W/m^2, a capacitance rate decrease from 55.3 to 27.65 W/K and an inlet fluid temperature increase from 20°C to 70°C, whereas the reference values were an irradiance of 500 W/m^2 on the collector plane ($K_d = 1$; θ=0°), a capacitance rate of 55.3 W/K, and inlet fluid and ambient temperatures of 20°C. The responses revealed virtually no static errors compared to those for other models though the transient behaviour differed from model to model, as illustrated in Figures 3.1 and 3.2. In general, the proposed model's responses were similar to those of the multi-segment single-node DSC and single-node "1-point" models, and quicker to stabilise at the steady-state value than those of higher-order and reportedly more accurate models, such as a 3-node model.

The aforementioned pattern did not change for the capacitance rate and irradiance step responses as the model's number of segments was increased, a point illustrated in Figure 3.1. The same can't be said, however, of the collector inlet fluid temperature step responses, exemplified in Figure 3.2. These revealed a pattern of unrealistic behaviours for low numbers of segments, consistent with the known deficiencies of the Perers model discussed in Section 2.1.2.7, namely those stemming from the assumption of a linear temperature profile and convergence issues at low numbers of segments (Haller et al., 2014). In essence, a high-inlet temperature step can initially cause below average – and possibly negative – outlet temperatures, and a low-inlet temperature step can cause above average outlet temperatures, and ultimately lead to convergence issues, but increasingly less so as the number of segments increases.

The number of segments was also found to influence the dead time between the temperature step and the response, at least in the absence of convergence issues. As shown on the right-hand side of Figure 3.2, a higher number of segments was found to reduce the dead time beyond what the higher accuracy models (i.e., the 3-node model) predict but not as significantly as the 1-point model, which reacts instantly to the temperature step[40] and similarly to the single-segment model instantiation.

Experimental test sequence

The proposed collector model was compared with the experimental measurements featured in Schnieders (1997). In addition to the collector inlet and outlet temperatures, the measurements included the roughly constant ambient temperature, the capacitance rate – toggled between values mid-sequence – and the rapidly changing irradiance on the collector plane, which was reportedly manually adjusted to face the sun throughout the test sequence (θ=0°). The data points for these measurements were extracted in the same way as for the step responses but were subsequently inter-

[40]The original plots featuring the "1-point" model's temperature step response clearly show it reacting before t=100 s, thus preceding the step itself by a few seconds, presumably inadvertently (Schnieders, 1997). This discrepancy was corrected here by adding an appropriate delay.

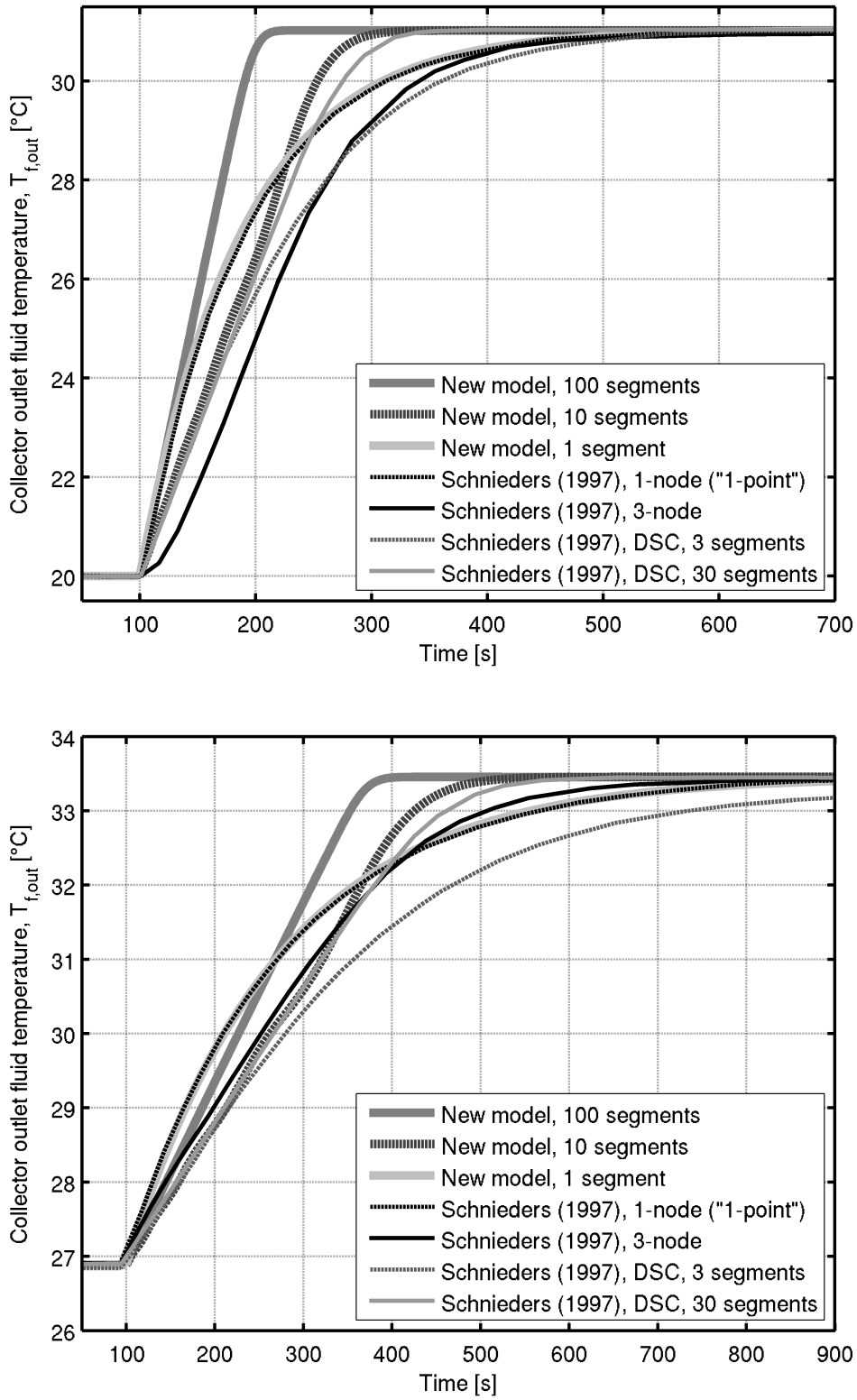

Figure 3.1.: Step responses of the model proposed and several others ("1-point"; 3 nodes; and DSC), reproduced from Schnieders (1997): first row) irradiance step from 0 to 800 W/m²; second row) capacitance rate step from 55.3 to 27.65 W/K.

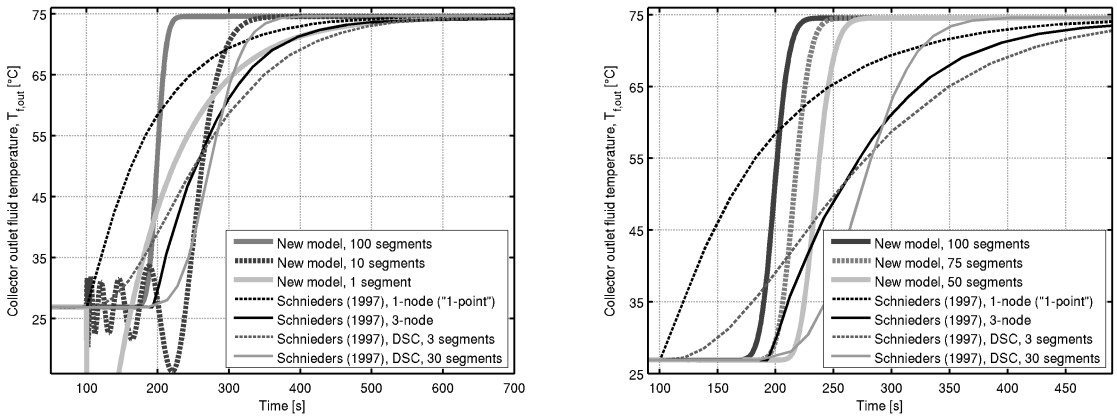

Figure 3.2.: Step responses of the model proposed and several others ("1-point"; 3 nodes; and DSC) reproduced from Schnieders (1997) to a collector inlet fluid temperature step from 20°C to 70°C. Note the new model's convergence and imposed linearity issues for a small number of segments on the left-hand side plot and, opposite it, the effect of the number of segments on the dead time.

polated at a sampling time of 1 s for synchronised use in discrete-time simulations. The input data and results of this comparison are displayed in Figure 3.3.

The comparison revealed the proposed model as being able to reproduce the measurements reported by Schnieders (1997) with some accuracy, though the transient performance is not always satisfactory. The best result was found for an instantiation with 3 segments, which led to errors below to 4°C. In contrast, higher (30 segments) and lower (1 segment) numbers of segments produced larger errors though the models still proved responsive to the inputs. It should be noted, however, that the parameters used in each of these cases were not optimised to fit the data with this model but were rather retrieved from Schnieders (1997), where they were reportedly used for the DSC model. Consequently, the possibility of better fits should not be excluded. In light of these findings and disclaimers, it can thus be concluded that the model developed is reasonably capable of reproducing the behaviour of ST collectors during steady-state conditions as well as transients, though in the latter case with additional limitations and subject to the quality of the parameter fit.

3.3.2.2. Comparison with steady-state cell temperature model

A single-segment instantiation of the model proposed is equivalent, in terms of thermal performance, to the model proposed by Amrizal et al. (2013) but, among other aspects, the mean cell temperature is estimated differently. Hence, a comparison between the two cell temperature models is in order. Since the mean plate temperature expression cited by Amrizal et al. has no solid theoretical basis and has other shortcomings, (2.50) was adopted as a reasonable alternative given its similarity, the fact it can be derived from the HWB model and that it can be used with key

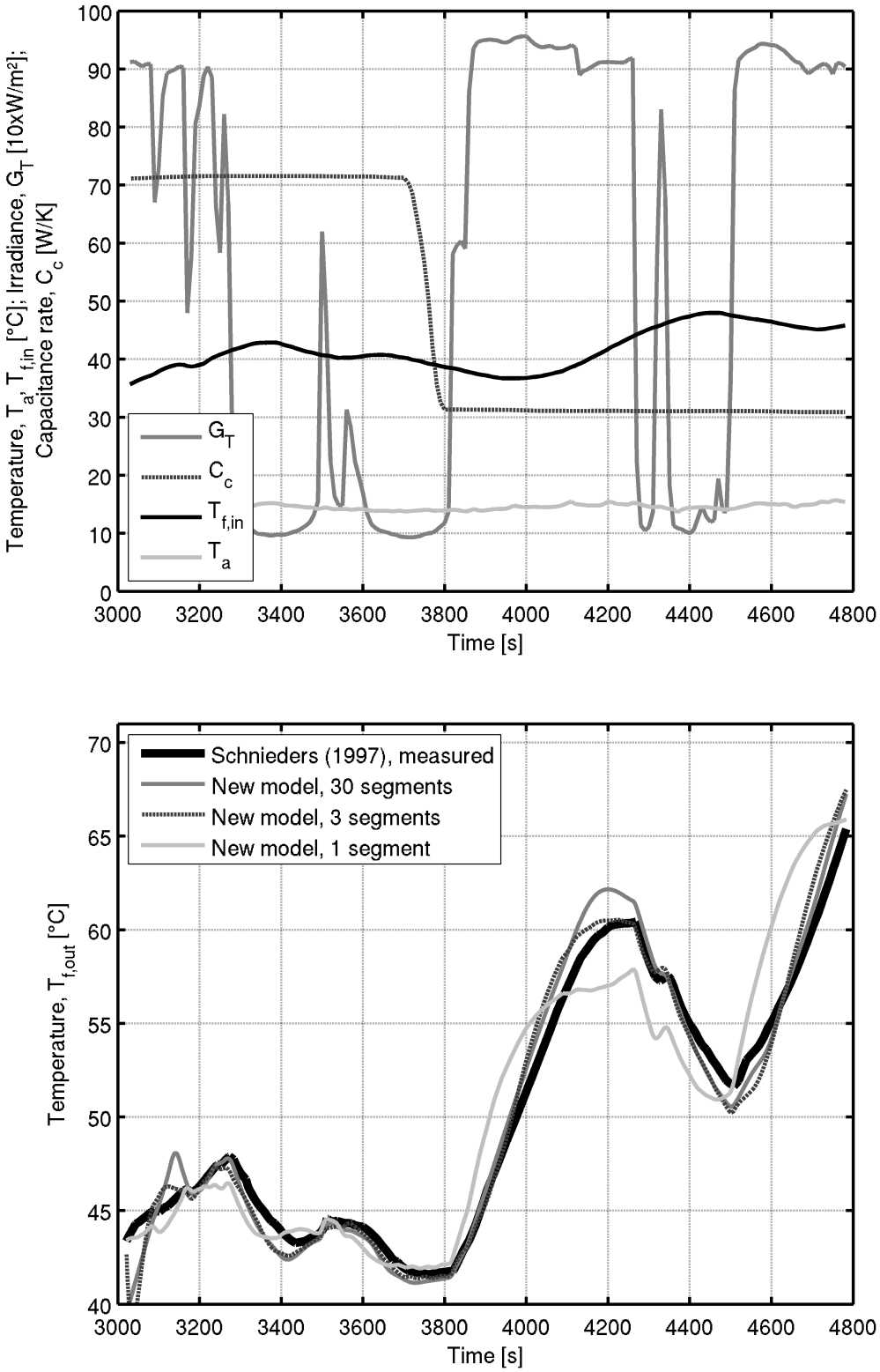

Figure 3.3.: Comparison between model responses (1, 3 and 30 segments) and measured collector outlet fluid temperatures (second row plot) for significantly variable conditions (first row plot), according to data in Schnieders (1997).

Amrizal et al. thermal submodel outputs, namely the specific heat flow rate and the mean fluid temperature, also returned by the model proposed. Furthermore, both models depend on the decoupled collector efficiency factor (F').

The comparison builds on the models' steady-state convergence if they comply with the most restrictive assumptions of the two. This generally means the HWB model assumptions, implying single-segment instantiation, negligible heat loss coefficient temperature dependence and no PV generation. Figure 3.4 documents the steady-state convergence of both models for simulated mass flow rate, collector inlet fluid temperature and irradiance step responses of the models, parametrised according to the reference PV-T collector for dynamic simulations described in Table D.2 of Appendix D except with regard to the heat loss coefficient temperature dependence ($F'U_{L,2}$=0 W/m²K²), PV generation ($\eta_{pv,r}$=0%) and the number of segments of the proposed model (N_s=1 or 100). The following analysis compares the model responses as the assumptions concerning negligible collector heat loss coefficient temperature dependence and lack of PV generation are lifted one at a time.

Step responses

The step responses of each model to mass flow rate, collector inlet fluid temperature and irradiance steps were compared. Despite converging under restrictive assumptions, the models generally revealed differences during transients but also during steady-state, particularly when hybrid operation and non-linear collector heat losses were considered. Focusing solely on steady-state conditions, the proposed model underestimated mean cell temperatures relative to the HWB model for a non-negligible heat loss coefficient temperature dependence ($F'U_{L,2} \neq$0 W/m²K²), either during hybrid or non-hybrid operation, but more so for the latter. In turn, the proposed model overestimated temperatures when a negligible heat loss coefficient temperature dependence ($F'U_{L,2}$=0 W/m²K²) and hybrid operation ($\eta_{pv,r} \neq 0\%$) were evaluated simultaneously. Table 3.1 summarises these results for the fastest-settling responses (100 segments). In essence, PV generation and the heat loss coefficient temperature dependence had opposite effects on the comparison, though in this particular analysis the latter proved strongest, ultimately leading the proposed cell temperature model to comparatively underestimate.

The other main difference between the models concerns the dynamic mean cell temperature behaviour. The HWB cell temperature model, in particular, leads to unrealistic though temporary mean cell temperature spikes and dips in the event of inlet temperature and flow rate steps. In both cases, the initial dynamic behaviour runs counter to the predictable effect (i.e., steady-state) the steps have: a flow rate step increase causes a sharp temperature increase and vice-versa, including during stagnation; a collector inlet fluid temperature step decrease brings about a sudden temperature increase and vice-versa. Both effects are thus generally undesirable, particularly since step-like flow rate and inlet temperature variations can be expected during normal ST system operation as the result of control actions, and can be predicted to influence flow control studies focusing on PV-T systems. The model

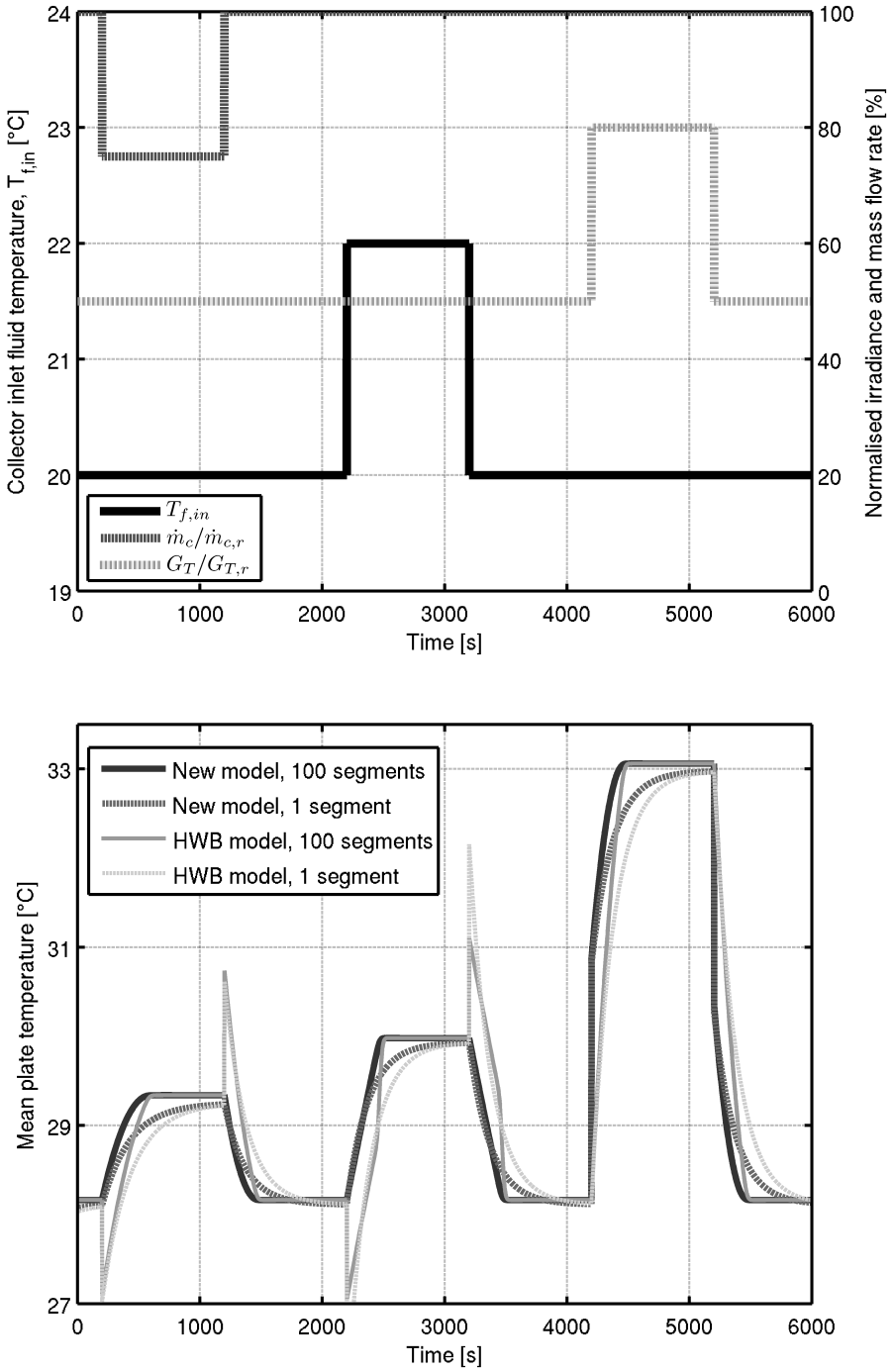

Figure 3.4.: Step responses of the proposed and HWB mean cell temperature models (second row plot) to mass flow rate, inlet temperature and irradiance steps (first row plot). The models were parametrised according to the reference PV-T collector except with regard to: $F'U_{L,2}$=0 W/m²K²; $\eta_{pv,r}$=0%; and, N_{seg}=1 or 100. The reference irradiance ($G_{T,r}$) and specific mass flow rate ($\dot{m}_{c,r}$) used to normalise the input variables were set to 1000 W/m² and 0.013 Kg/m²s, respectively.

Table 3.1.: Summary of mean plate temperature errors between the proposed ("new") and HWB model responses ($\Delta T_{pv} = T_{pv,new} - T_{pv,HWB}$) to the mass flow rate ($\dot{m}_c$), collector inlet fluid temperature ($T_{c,in}$) and irradiance (G_T) steps defined in Figure 3.4. The models were set up after the reference PV-T system, except concerning the number of segments (100 segments) and where noted.

			$\Delta T_{pv} = T_{pv,new} - T_{pv,HWB}$ [°C]		
Case #	$F'U_{L,2}$ [W/m²K²]	$\eta_{pv,r}$ [%]	$\dot{m}_c$ step	$T_{c,in}$ step	G_T step
1	0.000	0.00	0.00	0.00	0.00
2	0.026	0.00	-0.28	-0.32	-0.60
3	0.000	14.54	0.16	0.16	0.42
4	0.026	14.54	-0.10	-0.13	-0.15

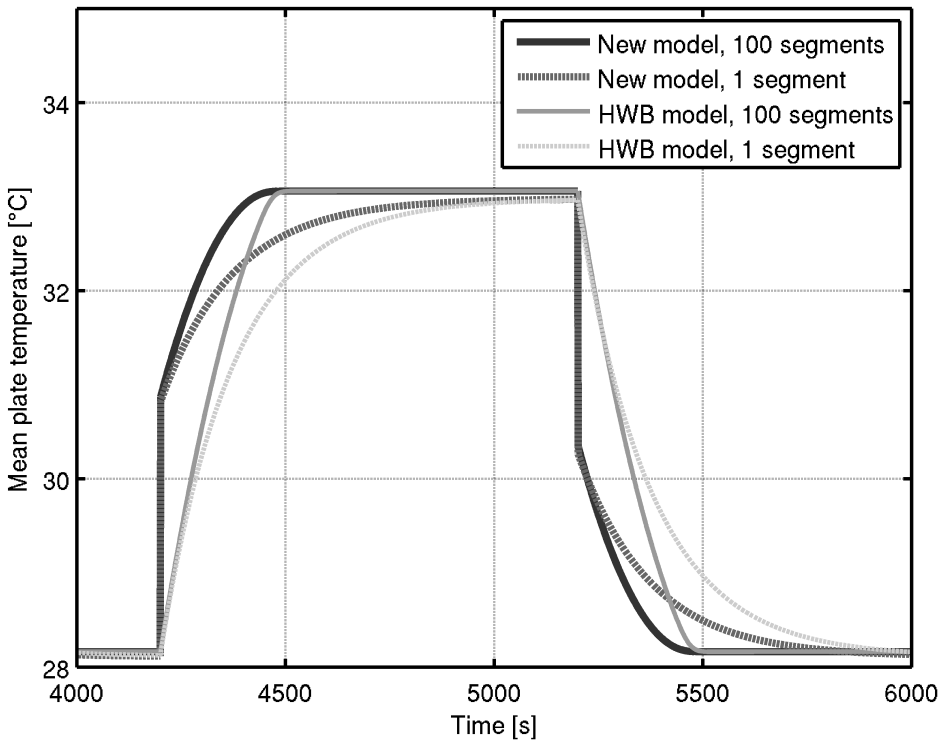

Figure 3.5.: Close-up of the irradiance step response of the proposed and HWB cell temperature models, previously shown in Figure 3.4.

proposed solves these issues but in doing so – at least partially because of these spikes and sags – comparatively overestimates and underestimates cell temperatures during heating and cooling transients, respectively, as shown in Figure 3.4.

In contrast, the model proposed does not respond as smoothly as the HWB model in the event of irradiance steps. In essence, the mean cell temperature estimated by the model proposed is a strong increasing function of the irradiance – since it is partially based on steady-state conditions – which becomes more noticeable during irradiance steps (e.g., intermittent insolation) whereas the HWB model expression is only indirectly sensitive to weather transients through $\dot{Q}$ and $T_{f,m}$. However, unlike the effect of mass flow rate and inlet temperature steps on the HWB model, irradiance steps cause the proposed cell temperature model to initially reproduce step-like spikes and dips that accurately mimic the predictable effect they would have in practice (i.e., a higher irradiance causes higher temperatures and vice-versa) and always short of the steady-state value, which is only reached when the smoothly-varying mean fluid temperature – an output of the underlying thermal submodel – reaches its respective steady-state value as well. Thus, the model proposed can still convey the effect of cell temperature on PV conversion during irradiance steps, though over- and underestimating cell temperatures during heating and cooling transients, respectively, relative to the HWB model. Figure 3.5 illustrates this effect.

Dynamic behaviour during SDHW system operation

In practice, ST collectors face changing conditions throughout the day, which only in a few specific instances resemble step-like inputs – notable examples include periods of intermittent insolation and sparse pump cycles. Hence, it is also important to compare the models during normal ST system operation. For this purpose, dynamic single-day and annual simulations of the reference grid-tied MPP-tracking SDHW PV-T system – whose model is described in Appendix D – using 15-minute resolution climate data for Almería, Spain (37°05'39"N, 2°21'35"W) were conducted using the proposed model and its primary results used to calculate the open-loop HWB model cell temperature response for comparison, as done for the step responses.

The simulations did not reveal significant differences between the two models, as summarised in Table 3.2. The highest absolute instantaneous mean cell temperature difference did not surpass 3°C and the maximum daily electrical efficiency variation was lower than 0.05% (absolute efficiency points) and, in all cases, higher for the model proposed. This reveals a general trend for lower temperatures when using the proposed model as opposed to the HWB model, though not in every situation: the former comparatively overestimated cell temperatures during stagnation heating periods, albeit quite modestly. In contrast, the model proposed comparatively underestimates during stagnation cooling and fluid circulation, particularly during the latter, which accounts for the correlation between higher magnitude differences and pump use evidenced in Table 3.2. The behaviour observed is thus largely consistent with the previous section's step responses, both during steady-state and during transients. Figures 3.6 and 3.7 illustrate these trends for a diverse selection (clear

Table 3.2.: Summary of the comparison between the HWB ("HWB") and the proposed multi-segment ("new") mean cell temperature models from single-day and annual simulations of the reference PV-T system using Almería, Spain climate data (H_T, global irradiation on the collector plane; Δt_{pump}, cumulative pump running time; $\Delta T_{pv} = T_{pv,new} - T_{pv,HWB}$; $\Delta \eta_{pv} = \eta_{pv,new} - \eta_{pv,HWB}$)

Day	Description	H_T [kWh/m²]	Δt_{pump} [hour]	$\Delta \eta_{pv}$ [%]	$(\Delta T_{pv})_{max}$ [°C]	$(\Delta T_{pv})_{min}$ [°C]
#1	Cloudy	3.4	1.4	0.00	1.0	-1.8
#2	Sunny, intermittent	5.3	2.6	0.01	0.8	-2.9
#3	Very cloudy	1.0	0.0	0.00	0.9	-0.4
#4	Sunny	7.7	7.0	0.05	0.8	-2.0
#5	Sunny, intermittent	5.1	3.6	0.02	1.1	-1.6
#6	Sunny, stagnation	7.6	2.6	0.02	2.4	-1.8
-	Annual	2136	1763	0.03	3.0	-2.5

and cloudy skies; pump use and stagnation) of single-day simulations.

Slightly different results were obtained for single-segment model instantiations, as indicated in Table 3.3. These revealed the HWB model as causing temperature spikes – similar to those shown in Figures 3.4 – as fluid circulation starts, which led to instantaneous cell temperature differences as high as 30°C, though only for a short period of time daily. As a result, their effect on the electrical efficiency was limited: the daily and annual electrical efficiencies differed by up to 0.04% and 0.03%, respectively, and the model proposed consistently led to the highest electrical electrical efficiencies – as was the case with multi-segment model instantiations.

The magnitudes of the aforementioned cell temperature and efficiency differences are quite low and arguably lower than the accuracies the proposed model can be

Table 3.3.: Summary of the comparison between the HWB ("HWB") and the proposed single-segment ("new") mean cell temperature models from single-day and annual simulations of the reference PV-T system using Almería, Spain climate data (H_T, global irradiation on the collector plane; Δt_{pump}, cumulative pump running time; $\Delta T_{pv} = T_{pv,new} - T_{pv,HWB}$; $\Delta \eta_{pv} = \eta_{pv,new} - \eta_{pv,HWB}$)

Day	Description	H_T [kWh/m²]	Δt_{pump} [hour]	$\Delta \eta_{pv}$ [%]	$(\Delta T_{pv})_{max}$ [°C]	$(\Delta T_{pv})_{min}$ [°C]
#1	Cloudy	3.4	0.8	0.00	2.9	-21.3
#2	Sunny, intermittent	5.3	2.5	0.01	2.0	-18.5
#3	Very cloudy	1.0	0.0	0.00	0.9	-0.4
#4	Sunny	7.7	6.8	0.04	2.1	-16.5
#5	Sunny, intermittent	5.1	3.2	0.02	3.0	-23.9
#6	Sunny, stagnation	7.6	2.5	0.01	3.3	-24.8
-	Annual	2136	1770	0.03	5.4	-30

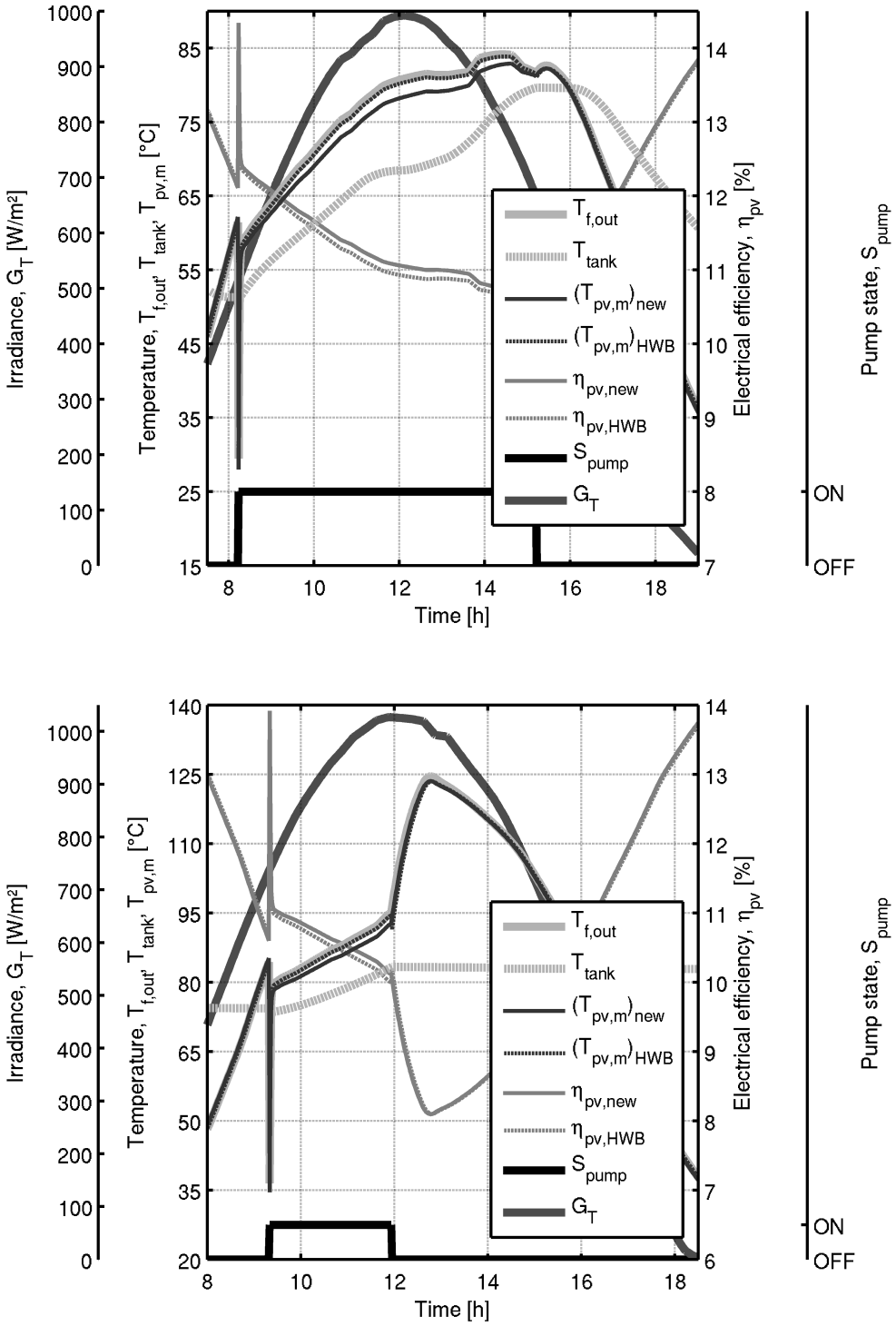

Figure 3.6.: Reference PV-T system single-day simulation results using the proposed ("new") and the Hottel-Whillier-Bliss ("HWB") cell temperature models: first row plot) normal sunny day (#4) with long collection period; second row plot) sunny day with low demand (#6), leading to hours of stagnation.

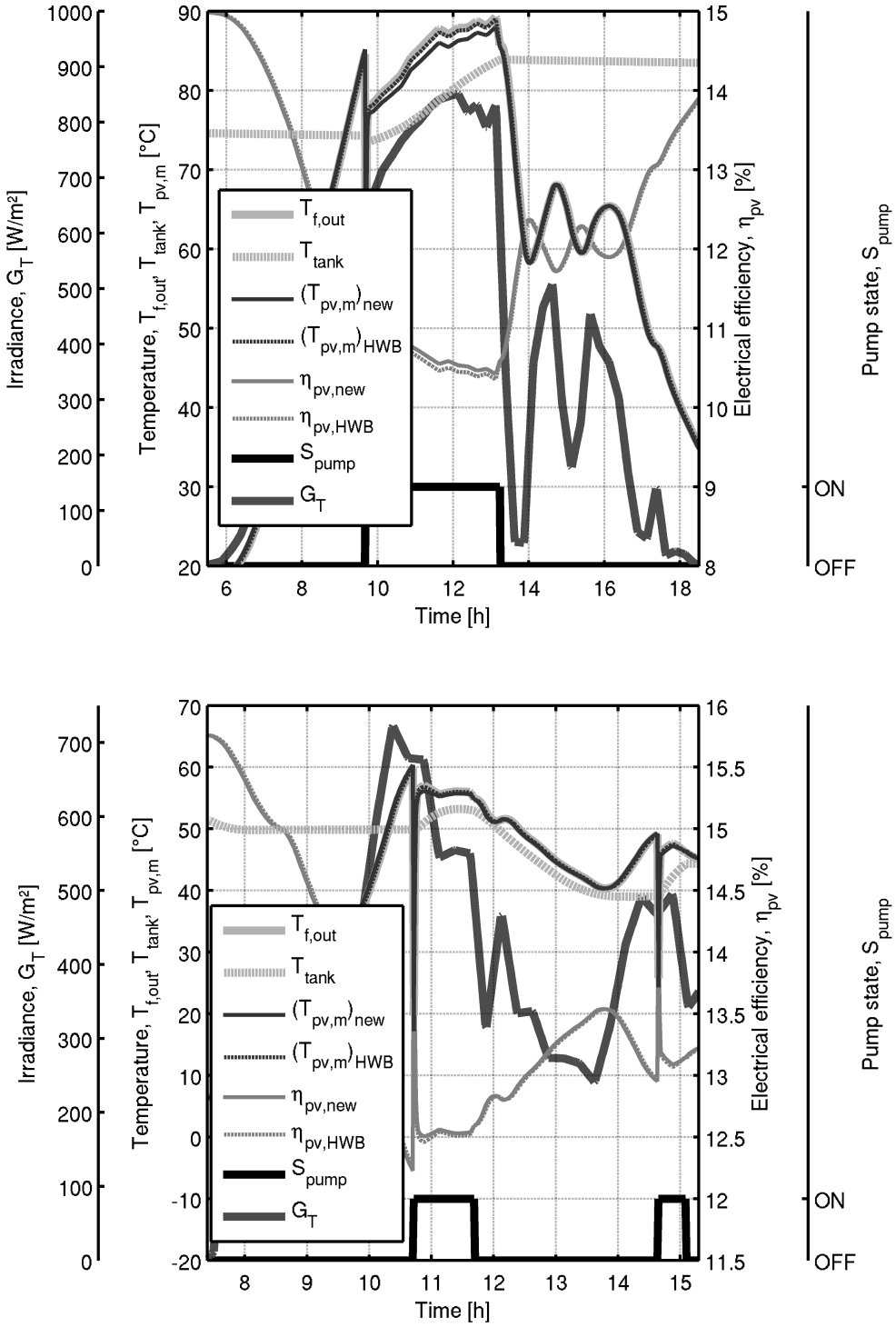

Figure 3.7.: Reference PV-T system single-day simulation results using the proposed ("new") and the Hottel-Whillier-Bliss ("HWB") cell temperature models: first row) Sunny day with some clouds and no demand (#5), prompting some stagnation; second row) Cloudy day (#1), leading to limited pump operation.

expected to deliver in relation to an existing installation. For instance, higher order and thus reportedly more accurate models can still present single-digit (centigrade) temperature and electrical power (W) errors (Haurant et al., 2015b). For these reasons, the cell temperature model proposed is essentially comparable to the HWB model equation but extends its use while addressing some of its shortcomings.

3.4. Discussion

3.4.1. Experimental validation

Experimental validation is an important step in the scientific process, and its absence for the model proposed is acknowledged. However, the model proposed does not represent a radical departure from comparable and validated hybrid or non-hybrid collector models, from which it borrows extensively. In essence, the proposed collector model extends the single-node Perers (1993) model to encompass PV-T collectors in a way consistent with the Florschuetz (1979) model, which relies on the classic HWB approach and the widely used linear cell efficiency expression (Skoplaki and Palyvos, 2009). Simultaneously, the model proposed addresses limitations found in comparable PV-T collector models, namely the Amrizal et al. (2013) model, whose shortcomings include a limited range of compatible flow regimes and cell temperature estimation for collectors generating electricity and reproducing a non-negligible collector heat loss temperature dependence. The proposed solution to this is a constant collector efficiency factor for all flow regimes, including stagnation, and a zero-capacitance cell temperature model based on this assumption.

The assumption of a constant collector efficiency factor for all flow regimes can be regarded as problematic during stagnation, whereas for other flow regimes this simplification is more common. As noted previously, the assumption can be predicted to lead to overestimated fluid temperatures during stagnation but it is harder to predict how it influences plate or cell temperatures. Despite this unknown, both mean fluid and mean plate temperatures converge during stagnation by design, since the steady-state stagnation temperature is independent of the collector efficiency factor, though likely at inaccurate paces. Hence, the assumption adopted mainly concerns the dynamic heating and cooling rates at which the correct steady-state values are reached, and not the reproduction of an unrealistic collector behaviour.

The other less consensual aspect of the cell temperature model is its dependence on weather variables, particularly the irradiance. In essence, the model can be unrealistically responsive to irradiance transients, limiting its accurate use to simulations using low resolution weather data. Nonetheless, the model's dependence on the dynamic mean fluid temperature mitigates this sensitivity to some extent, as illustrated in Figure 3.5. For these reasons, the lack of experimental validation is not seen as a significant shortcoming of the model validation process undertaken.

3.4.2. Predicted contribution to PV-T collector thermal performance testing

As mentioned earlier, the proposed model is an extension of the Perers model, which in turn is the basis of the ISO 9806:2013 standard's quasi-dynamic test method model. This test method is already compatible with PV-T collector thermal performance testing in MPP, open-circuit or short-circuit electrical operation modes but does not explicitly account for PV generation in the model. The model proposed addresses this apparent omission by introducing a term concerning the thermal efficiency reduction due to PV generation. Hence, the proposal described in this Chapter may constitute an improvement over the standard's current version if it can lead to a better fit and lower errors for PV-T collectors under MPP operation, particularly since it does not require additional measurements, though these might be necessary or desirable for other reasons. One possible obstacle to this is a deteriorated or a negligible improvement of the parameter identification process, since the added term's magnitude can be low compared to other terms and the term itself is a function of variables common to other terms though not all simultaneously, namely the zero-heat loss efficiency (η_0), the effective irradiance on the collector plane ($G_{T,eff}$) and the mean fluid temperature ($T_{f,m}$). Should this prove to be the case, the model can still be used for other purposes by determining relevant parameters from thermal performance tests for open-circuit or short-circuit electrical operation modes[41] and the PV parameters from electrical performance tests.

3.4.3. Compatibility with flow control studies

The primary intent behind this effort was to develop a PV-T collector model compatible with flow control studies. This essentially amounts to a realistic reproduction of dynamic collector behaviour to mass flow rate, collector inlet temperature and irradiance variations. Naturally, some higher order models are also compatible with this goal and can reproduce collector behaviour more realistically. Indeed, a two-node model would effectively improve cell temperature estimation over the model currently being proposed, particularly during transients, but such an approach would likely increase the required computational effort and complicate parameter identification through standardised performance tests as the result of increased complexity. For example, Schnieders (1997) noted strong cross-correlation between parameters in a plate and fluid two-node model, notably between the heat capacities of each node and reportedly due to the high heat transfer coefficient between the two. Moreover, high-order multi-dimensional PV-T collector models such as the one by Haurant et al. (2015b) still present significant temperature errors during transients (6-7°C) and otherwise (1-2°C), as well as during stagnation (Schnieders, 1997).

Conversely, steady-state PV-T collector models have been deemed sufficiently accurate to estimate energy yields, and previous flow control studies have relied on

[41] Hofmann et al. (2010) found indistinguishable results from EN 12975 standard thermal performance tests of PV-T collectors in open-circuit and short-circuit electrical operation modes.

comparable or simpler models, including recent efforts (Schiller et al., 1980; Orbach et al., 1981; Kahwaji and Winn, 1986; Zondag et al., 2002; Badescu, 2008; Nhut and Park, 2013; Ntsaluba et al., 2016). As such, the solution found arguably constitutes a just compromise between accuracy, computational effort and compatibility with parameter identification through standardised performance tests.

3.5. Summary

The following contributions can be highlighted from this chapter:

- A multi-segment single-node dynamic PV-T collector model was proposed to achieve compatibility with flow control studies, low computational loads, parameter identification and address some limitations of the Amrizal et al. (2013) model, namely by coherently extending dynamic cell temperature estimation to PV-T collectors generating electricity and/or displaying a non-negligible collector heat loss coefficient temperature dependence;
- An implementation of the aforementioned PV-T collector model was developed based on discretisation along the collector flow path and closed-form solutions to first-order linear or non-linear ordinary differential equations;
- Several efforts were made to validate the model proposed:
  - A study of PV-T collector efficiency factor sensitivity to temperature, flow rate and irradiance in order to determine the validity of a constant collector efficiency factor used in the model proposed, which found only a marginal variation (<1%) for a representative range of conditions;
  - Comparisons with published results for non-hybrid collectors, namely step responses and an experimental test sequence, which revealed the model as being able to reproduce collector dynamics for non-hybrid operation;
  - Comparisons between the proposed cell temperature submodel and a validated HWB model alternative for mass flow rate, collector inlet fluid temperature and irradiance steps, which led to convergence and more realistic transient responses for conditions compatible with both models, namely steady-state operation, a negligible collector heat loss coefficient temperature dependence and non-hybrid operation;
  - Annual and daily dynamic simulations of a SDHW PV-T system were conducted to compare the new and the validated HWB cell temperature models, revealing minimal but coherent differences between the two.

4. Differential temperature controller setpoints for PV-T systems

The classic design methods to aid the selection of differential temperature controller setpoints do not consider electricity generation, and thereby exclude hybrid operation of PV-T systems. The methods are based on the Hottel-Whillier-Bliss (HWB) collector model which was extended by Florschuetz (1979) to cover PV-T collectors. On the other hand, the HWB and Florschuetz models assume a negligible collector heat loss coefficient temperature dependence which is not a valid assumption in many cases. To overcome this limitation, the ISO 9806:2013 steady-state test method equation can be extended to reflect PV-T collectors by following the Florschuetz modelling approach. By applying the same design criteria to these PV-T collector models, the design methods can also be extended to PV-T systems.

4.1. PV-T collector models

4.1.1. Florschuetz model for PV-T systems with heat exchangers

The Florschuetz model can also be extended to consider heat exchangers in the supply loop by using the ϵ-NTU method previously used with the HWB model, as discussed in Section 2.1.2.1. Accordingly, the useful heat output from PV-T systems with heat exchangers can be expressed as (4.1), where $\widetilde{F}'_R$ stands for the collector heat exchanger factor for PV-T systems, in turn given by (4.2).

$$\dot{Q} = A_c \widetilde{F}'_R \left[\widetilde{S} - \widetilde{U}_L \left(T_{t,out} - T_a \right) \right] \tag{4.1}$$

$$\widetilde{F}'_R = \widetilde{F}_R \left[1 + \frac{A_c \widetilde{F}_R \widetilde{U}_L}{\dot{m}_c C_{p,c}} \left(\frac{\dot{m}_c C_{p,c}}{\epsilon (\dot{m} C_p)_{min}} - 1 \right) \right]^{-1} \tag{4.2}$$

The PV power output can still be expressed by (2.45) but the cell temperatures are influenced by the heat exchanger performance in accordance with (4.2) and (4.3).

$$T_{pv,m} = \begin{cases} T_{t,out} + \left(T_a + \frac{\widetilde{S}}{\widetilde{U}_L} - T_{t,out} \right) \left(1 - \widetilde{F}'_R \right) & , \ \dot{m}_c \neq 0 \\ T_a + \frac{\widetilde{S}}{\widetilde{U}_L} & , \ \dot{m}_c = 0 \end{cases} \tag{4.3}$$

4.1.2. Extended Perers model

ST collector performance tests can reveal a significant collector heat loss coefficient temperature dependence, which the Florschuetz model neglects. In turn, the Perers model extension proposed in Chapter 3 can overcome this limitation. Assuming steady-state operation, the model can be expressed as (4.4), (3.4), (3.6) and (3.8).

$$\frac{\dot{Q}}{A_c} = F' \left[(\tau\alpha)_{eff} G_T - U_{L,1} (T_{f,m} - T_a) - U_{L,2} (T_{f,m} - T_a)^2 \right] - F' \frac{P_{pv} (T_{pv,m} = T_{f,m})}{A_c} \tag{4.4}$$

This model was numerically extended to cover PV-T systems with external heat exchangers via the ϵ-NTU method in accordance with (4.5) where the collector inlet and outlet fluid temperatures and the heat flow rate are dependent variables determined iteratively using the Newton-Raphson method.

$$\begin{cases} T_{f,in} - T_{f,out} + \dot{Q} \left[\dot{m}_c C_{p,c} \right]^{-1} = 0 & , \ \dot{m}_c \neq 0 \\ T_{t,out} - T_{f,out} + \dot{Q} \left[\epsilon \left(\dot{m} C_p \right) \right]^{-1} = 0 & , \ \dot{m}_c = 0 \end{cases} \tag{4.5}$$

4.2. Design methods for PV-T systems

The previous models can be used to develop differential temperature controller setpoint design methods for PV-T systems following the steps of those for non-hybrid systems, namely those based on cost-effective and cycling-free operation.

4.2.1. Analytical method using the Florschuetz model

4.2.1.1. Condition for cost-effective fluid circulation

Consider closed-loop solar heating systems with storage, such as those illustrated in Figure 1.6. The storage tank can be charged using the collectors or an auxiliary heater, if and when necessary. However, it is wasteful to leave the supply-loop pump(s) on if the same outcome vis-à-vis useful heat costs less using the auxiliary heater. Hence, a reasonable cost-based condition to keep the pump(s) on can be represented by (4.6), where p_{el} stands for the general purpose electricity price, p_{aux} is the auxiliary energy price, $P_{el,pump}$ is the parasitic electrical power required by the pump(s), $\eta_{th,pump}$ is the (combined) thermal efficiency of the pump(s) in relation to fluid heating, and $\dot{Q}$ is the useful heat flow rate enabled by the solar collectors.

$$p_{el} P_{el,pump} < p_{aux} \left(P_{el,pump} \eta_{th,pump} + \dot{Q} \right) \tag{4.6}$$

According to this cost-based rationale, the pump(s) should be kept on if (4.6) holds true, since it would mean the parasitic costs ($p_{el}P_{el,pump}$) are lower than the cost of supplying the same heat flow rate ($P_{el,pump}\eta_{th,pump} + \dot{Q}$) at auxiliary energy prices. For PV-T systems, the PV revenue variation caused by stopping the pump(s) ($-p_{pv}\eta_{el,bos}\Delta P_{pv}$) should also be factored in. Thus, the pump(s) in a PV-T system should remain on as long as (4.7) is valid, where p_{pv} represents the PV electricity price, $\eta_{el,bos}$ is the balance of system (i.e., power conversion and transport) electrical efficiency and, ΔP_{pv} is the bulk PV power gain (that is, prior to transport and power conversion) due to a transition from stagnation to fluid circulation.

$$p_{el}P_{el,pump} - p_{pv}\eta_{el,bos}\Delta P_{pv} < p_{aux}\left(P_{el,pump}\eta_{th,pump} + \dot{Q}\right) \tag{4.7}$$

The bulk PV power gain can be given by (4.8) (see Appendix A for its derivation) while the PV electricity price (p_{pv}) can be modelled as proportional to the general purpose electricity price (p_{el}) according to (4.9), where $K_{pv,el}$ models the relative level of subsidies available for PV electricity generation in a PV-T system.

$$\Delta P_{pv} = \frac{U_L - \tilde{U_L}}{\tilde{U_L}}\dot{Q} \tag{4.8}$$

$$p_{pv} = p_{el}K_{pv,el} \tag{4.9}$$

Replacing (4.8) and (4.9) in (4.7) and rearranging for $\dot{Q}$ yields (4.10), the condition for cost-effective fluid circulation in PV-T systems, where $\Lambda_{pv,off}$ represents its PV conversion-induced normalised variation, given by (4.11), and $K_{par,aux}$ is the ratio between the parasitic and auxiliary energy prices, expressed as (4.12).

$$\dot{Q} > \left(K_{par,aux} - \eta_{th,pump}\right) P_{el,pump}\Lambda_{pv,off} \tag{4.10}$$

$$\Lambda_{pv,off} = \frac{\tilde{U_L}}{\tilde{U_L} + \left(U_L - \tilde{U_L}\right) K_{par,aux}K_{pv,el}\eta_{el,bos}} \tag{4.11}$$

$$K_{par,aux} = \frac{p_{el}}{p_{aux}} \tag{4.12}$$

The minimum heat flow rate requirement in (4.10) can be transformed into a temperature difference requirement between the collector and the tank (ΔT) using the ϵ-NTU method, yielding (4.13), with which ΔT_{off} should comply.

$$\Delta T > \frac{\left(K_{par,aux} - \eta_{th,pump}\right) P_{el,pump}}{\epsilon(\dot{m}C_p)_{min}}\Lambda_{pv,off} = \Delta T_{off,min} \tag{4.13}$$

4.2.1.2. Condition for cycling-free operation

Consider stagnated PV-T collectors generating electricity at a uniform and stable temperature (T_c), given by (4.14) in accordance with the Florschuetz model:

$$T_c = T_a + \frac{\widetilde{S}}{\widetilde{U}_L} \tag{4.14}$$

Immediately before the start of fluid circulation, the controller senses a temperature difference ΔT_{on} between the collector (T_c) and the tank ($T_{t,out}$):

$$\Delta T_{on} = T_a + \frac{\widetilde{S}}{\widetilde{U}_L} - T_{t,out} \tag{4.15}$$

The aforementioned formulation of ΔT_{on} has similarities with the useful heat output from PV-T collectors given by (4.16) after rearranging (4.1):

$$\dot{Q} = A_c \tilde{F}'_R \tilde{U}_L \left[T_a + \frac{\widetilde{S}}{\widetilde{U}_L} - T_{t,out} \right] \tag{4.16}$$

Thus, by replacing (4.15) in (4.16), the potential heat flow rate from PV-T collectors can be shown to be proportional to the measured temperature difference prior to fluid circulation, that is, the turn-on setpoint (ΔT_{on}).

$$\dot{Q} = A_c \tilde{F}'_R \tilde{U}_L \Delta T_{on} \tag{4.17}$$

For a PV-T system with negligible collector thermal capacity and piping heat losses, pump cycling can be avoided by selecting ΔT_{on} so that the useful heat according to (4.17) is superior to that implied by the choice of ΔT_{off} in accordance with the ϵ-NTU method. Otherwise, ΔT will necessarily drop below ΔT_{off} once fluid circulation begins, causing pump cycling in the process:

$$A_c \tilde{F}'_R \tilde{U}_L \Delta T_{on} > \epsilon (\dot{m} C_p)_{min} \Delta T_{off} \tag{4.18}$$

Thus, rearranging (4.18) yields the condition for cycling-free operation in PV-T systems, (4.19), otherwise known as stability criterion. The criterion is sensitive to the PV conversion efficiency through $\Lambda_{pv,on}$, given by (4.20), which equals one for non-hybrid operation or equivalent non-hybrid systems ($\Lambda_{pv,on} = 1$, if $\eta_{pv,r} = 0\%$).

$$\Delta T_{on} > \frac{\epsilon (\dot{m} C_p)_{min}}{A_c F'_R U_L} \Delta T_{off} \Lambda_{pv,on} \tag{4.19}$$

$$\Lambda_{pv,on} = \frac{F'_R U_L}{\tilde{F}'_R \tilde{U}_L} \tag{4.20}$$

4.2.1.3. Effect of temperature measurement errors

Alcone and Herman approach

The existence of temperature measurement errors can condition the successful application of (4.13) and (4.19). Alcone and Herman (1981) addressed this by anticipating the effect of measurement errors on the design rules for non-hybrid ST systems, which can be adapted for PV-T systems as well. Let us assume the temperature difference ($\hat{\Delta T}$) sensed by the controller has errors in accordance with (4.21), where ε and ΔT represent the combined measurement error of both sensors and the actual – as opposed to measured – temperature difference, respectively.

$$\hat{\Delta T} = \Delta T + \varepsilon \tag{4.21}$$

If ΔT is overestimated ($\varepsilon > 0$) and $\Delta T_{off} = \Delta T_{off,min}$ according to (4.13), the controller will turn the pump(s) off when $\hat{\Delta T} < \Delta T_{off}$ but this means ΔT is already below ΔT_{off} by at least ε, resulting in a measure of wasteful low-ΔT operation. If ΔT is underestimated ($\varepsilon < 0$), then the controller turns off the pump(s) before ΔT is below ΔT_{off}, meaning uneconomical use of the circulation pump(s) is prevented, albeit conservatively. Thus, cost-effective operation requires compliance with (4.22), which takes into account the effect of measurement errors on the selection of ΔT_{off}.

$$\Delta T_{off} > \frac{(K_{par,aux} - \eta_{th,pump})\, P_{el,pump}}{\epsilon(\dot{m}C_p)_{min}} \Lambda_{pv,off} + \varepsilon \tag{4.22}$$

Measurement errors can also influence the condition for cycling-free operation. If ΔT is overestimated ($\varepsilon > 0$) and ΔT_{on} equals the minimum ΔT_{on} compliant with (4.19) for a given ΔT_{off}, the start of fluid circulation will occur when $\hat{\Delta T}$ equals ΔT_{on} though ΔT is lower than ΔT_{on} by ε, which may cause pump cycling since the effective ΔT_{on} is lower than the minimum required. For the same ε, $\hat{\Delta T}$ will only reach ΔT_{off} in the ensuing ΔT drop when ΔT is already below ΔT_{off}, effectively mitigating pump cycling. Hence, overestimation errors can influence pump cycling in opposite ways, depending on the measurement errors for each situation. If ΔT is underestimated ($\varepsilon < 0$), the opposite will occur (higher effective ΔT_{on} and ΔT_{off} setpoints, reducing and enhancing pump cycling, respectively). In other words, (4.18) becomes (4.23) once measurement errors are considered, with which ΔT_{on} and ΔT_{off} should comply if pump cycling is to be prevented. Figure 4.1 illustrates the effect of measurement errors on controller behaviour vis-à-vis cost-effective and cycling-free fluid circulation which (4.22) and (4.24) seek to address.

$$A_c F'_R U_L \left(\Delta T_{on} - \varepsilon\right) > \epsilon(\dot{m}C_p)_{min} \Lambda_{pv,on} \left(\Delta T_{off} - \varepsilon\right) \tag{4.23}$$

$$\Delta T_{on} > \frac{\epsilon(\dot{m}C_p)_{min}}{A_c F'_R U_L} \Lambda_{pv,on} \left(\Delta T_{off} - \varepsilon\right) + \varepsilon \tag{4.24}$$

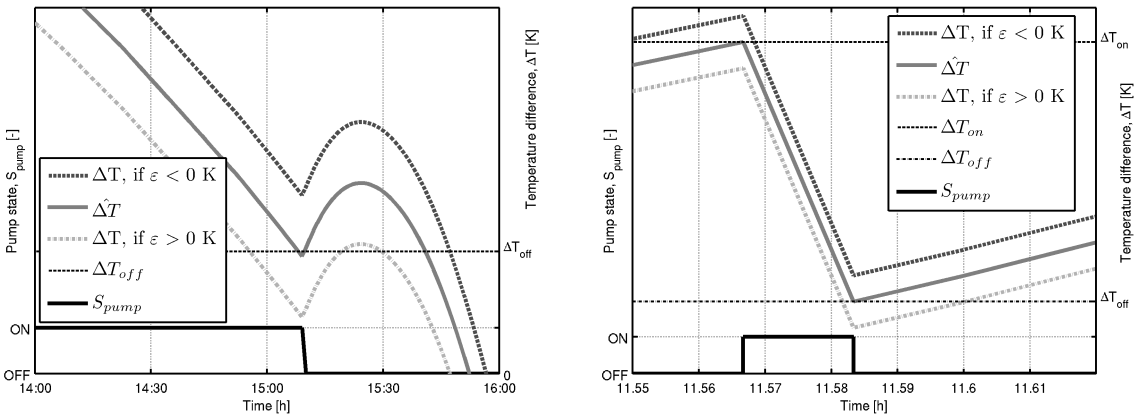

Figure 4.1.: Effect of measurement errors (ε) on controller behaviour and relation to the actual (ΔT) as opposed to measured temperature difference ($\hat{\Delta T} = \Delta T + \varepsilon$): left-hand side plot) overestimation errors ($\varepsilon > 0$) enable ΔT to go below ΔT_{off} during operation, whereas underestimation ($\varepsilon < 0$) errors prove conservative; right-hand side plot) errors can contribute to and mitigate pump cycling.

Conservative approach

The conditions given in (4.22) and (4.24) are only useful if the measurement errors are known. Since the errors are not known in practice, an alternative approach has to be devised for practical application. One approach is to adopt the polarity or polarities with the most conservative outcome and assume the error's magnitude to be equal to the measurement tolerance's absolute value ($|\varepsilon|$). Accordingly, ΔT_{off} setpoints compatible with cost-effective fluid circulation have to comply with (4.25).

$$\Delta T_{off} > \frac{(K_{par,aux} - \eta_{th,pump})\, P_{el,pump}}{\epsilon(\dot{m}C_p)_{min}} \Lambda_{pv,off} + |\varepsilon| \tag{4.25}$$

With regard to the condition for cycling-free operation, the polarities of two errors – i.e., those relative to ΔT_{on} and ΔT_{off} in (4.23) – have to be considered and thus four cases are possible. In order for the design rule to encompass all possible cases, albeit conservatively, the left- and right-hand sides of (4.23) have to minimised and maximised, respectively, which means assuming overestimation and underestimation errors for ΔT near ΔT_{on} and ΔT_{off}, as in (4.26).

$$A_c \tilde{F}'_R \tilde{U}_L \left(\Delta T_{on} - |\varepsilon|\right) > \epsilon(\dot{m}C_p)_{min} \left(\Delta T_{off} + |\varepsilon|\right) \tag{4.26}$$

Rearranging (4.26), yields (4.27), a conservative approach to the condition for cycling-free operation in the presence of measurement errors:

$$\Delta T_{on} > \frac{\epsilon(\dot{m}C_p)_{min}}{A_c F'_R U_L} \Lambda_{pv,on} \left(\Delta T_{off} + |\varepsilon|\right) + |\varepsilon| \tag{4.27}$$

4.2.2. Analytical method using the Beckman et al. (1994) approach for non-linear collector efficiency curves

The previous methods are meant for linear collector efficiency curves. Alternatively, Beckman et al. (1994) recommended using the thermal efficiency curve slope near an efficiency of zero to determine the relevant heat loss coefficient for the purposes of controller setpoint selection. The original recommendation was to determine the equivalent $F_R U_L$ from such a curve and use this value in the standard equations. In the following treatment, an equation dependent on the collector efficiency factor (F') is used instead of one using the collector heat removal factor (F_R), namely the steady-state PV-T collector model previously extended from the Perers model and given by (4.4). Using this model, the specific useful heat flow rate from a PV-T collector generating electricity can be given by (4.28).

$$\begin{aligned}\frac{\dot{Q}}{A_c} = {} & F' \left[(\tau\alpha)_{eff} G_T - U_{L,1} \left(T_{f,m} - T_a\right) - U_{L,2} \left(T_{f,m} - T_a\right)^2 \right] \\ & - F' \tau \rho_{pv} G_T \eta_{pv,r} \left[1 + \beta_{pv} \left(T_{f,m} - T_{pv,r}\right)\right]\end{aligned} \tag{4.28}$$

In turn, the respective thermal efficiency is given by (4.29), where $T_{R,m}$ represents the reduced temperature in turn given by (4.30).

$$\begin{aligned}\eta_{th,c} = {} & F' \left[(\tau\alpha)_{eff} - U_{L,1} T_{R,m} - U_{L,2} G_T T_{R,m}^2 \right] \\ & - F' \tau \rho_{pv} \eta_{pv,r} \left[1 + \beta_{pv} \left(T_{R,m} G_T + T_a - T_{pv,r}\right)\right]\end{aligned} \tag{4.29}$$

$$T_{R,m} = \frac{T_{f,m} - T_a}{G_T} \tag{4.30}$$

The thermal efficiency curve slope at an efficiency of zero is negative and its magnitude corresponds to an effective product between a collector efficiency factor and a heat loss coefficient, $(F'U_L)_{eff}$, which can be found by differentiating (4.29) with respect to $T_{R,m}$, as formulated in (4.31):

$$\left.\frac{d\eta_{th,c}}{dT_{R,m}}\right|_{\eta_{th}=0} = - \left(F'U_L\right)_{eff} \tag{4.31}$$

Differentiating (4.29) with respect to $T_{R,m}$, substituting $T_{R,m}$ with (4.30), replacing the result in (4.31), and rearranging for $(F'U_L)_{eff}$ yields (4.32), the slope magnitude as a function of the mean collector fluid temperature and the heat loss coefficients, namely (4.33), which is analogous to (2.40) from the Florschuetz model.

$$\left(F'U_L\right)_{eff} = F' \left[\tilde{U}_{L,1} + 2U_{L,2} \left(T_{f,m} - T_a\right) \right] \tag{4.32}$$

$$\tilde{U}_{L,1} = U_{L,1} + \tau\rho_{pv}\eta_{pv,r}\beta_{pv}G_T \tag{4.33}$$

In accordance with (4.29), a thermal efficiency of zero (i.e., stagnation) is reached at a collector fluid temperature given by (4.34), which is the relevant solution of $\eta_{th,c} = 0$ and where $\tilde{S}$ is given by (2.39) or $S(1 - \tau\rho_{pv}\eta_{pv,a}/(\tau\alpha)_{eff})$.

$$T_{f,m} = T_a - \frac{\tilde{U}_{L,1}}{2U_{L,2}} + \frac{\sqrt{\left(\tilde{U}_{L,1}\right)^2 + 4U_{L,2}\tilde{S}}}{2U_{L,2}} \tag{4.34}$$

Substituting (4.34) in (4.32), yields:

$$(F'U_L)_{eff} = F'\sqrt{\left(\tilde{U}_{L,1}\right)^2 + 4U_{L,2}\tilde{S}} \tag{4.35}$$

Assuming the collector efficiency factor is constant in relation to T_a, G_T, $T_{f,m}$ and electricity generation, the effective heat loss coefficient ($\tilde{U}_{L,eff}$) can be expressed as:

$$\tilde{U}_{L,eff} = \sqrt{\left(\tilde{U}_{L,1}\right)^2 + 4U_{L,2}\tilde{S}} \tag{4.36}$$

Thus, according to the suggestion by Beckman et al. (1994), originally for non-hybrid systems, the analytical setpoint selection method of Section 4.2.1 can also be used for PV-T systems generating PV electricity and exhibiting quadratic collector heat losses, by replacing $\tilde{U}_L$ with $\tilde{U}_{L,eff}$ in the various equations. Following this interpretation, this also applies to the condition for cost-effective fluid circulation since (4.13) also depends on $\tilde{U}_L$, unlike for non-hybrid ST systems.

4.2.3. Numerical method

Numerical solutions to the conditions for cost-effective and stable operation in PV-T systems can also be obtained using iterative methods (e.g., the Newton-Raphson method). The key advantage of this approach is that it simplifies the analysis of more complicated systems. For instance, those with non-negligible pipe heat losses and non-linear collector heat losses. The application of this method requires the above-named conditions to be generalised from the setpoint selection methods described in Section 4.2.1 to form equations and systems of equations, namely (4.37) and (4.38).

$$\Delta T_{off,min} - \frac{(K_{par,aux} - \eta_{th,pump})}{\epsilon\,(\dot{m}C_p)_{min}} P_{el,pump} + \frac{K_{pv,el}K_{par,aux}\eta_{el,bos}}{\epsilon\,(\dot{m}C_p)_{min}} \Delta P_{pv} = 0 \tag{4.37}$$

$$\begin{cases} \Delta T_{on,min} - (T_{c,stag} - T_{tank}) = 0 \\ \\ \frac{\dot{Q}}{\epsilon(\dot{m}C_p)_{min}} - \Delta T_{off} = 0 \end{cases} \tag{4.38}$$

Both equation (4.37) and the system of equations (4.38) are implicit in nature and rely on calls to PV-T system model functions. These functions are derived from the ϵ-NTU method and the model detailed in Section 4.1.2, whose most significant departures from the Florschuetz model include the assumption of a constant collector efficiency factor in relation to PV conversion, a linear collector heat loss coefficient temperature dependence, and the mean collector fluid temperature approximated as the arithmetic mean of the inlet and outlet temperatures during fluid circulation. The functions required include the collector outlet temperature during fluid circulation ($T_{f,out}$), the collector temperature during stagnation ($T_{c,stag}$), the bulk PV power gain (ΔP_{pv}) and the useful heat flow rate ($\dot{Q}$).

The condition for cost-effective fluid circulation, translated by (4.37), relies on calls to $T_{f,out}$ and ΔP_{pv}, both of which functions of the tank temperature (T_{tank}). This temperature is determined iteratively from the solutions to each equation, namely $\Delta T_{off,min}$ and $T_{f,out}$, and does not need to be specified: $T_{tank} = T_{c,out} - \Delta T_{off,min}$. As such, initial estimates are also required, which in this case were set to the explicit Florschuetz model solutions. The same was true for the condition for stable operation or (4.38), which relied on calls to $\dot{Q}$ and $T_{c,stag}$ to determine $\Delta T_{on,min}$ and T_{tank}, for a given ΔT_{off} setpoint. Unlike $T_{c,stag}$, $\dot{Q}$ is a function of T_{tank} which, in turn, is the link between both equations in (4.38).

Finally, due to the absence of explicit equations for $\Lambda_{pv,off}$ and $\Lambda_{pv,on}$, the effect of PV conversion on $\Delta T_{off,min}$ and $\Delta T_{on,min}$ has to be determined by solving the equations for PV-T systems under hybrid and non-hybrid operation. Hence, $\Lambda_{pv,off}$ and $\Lambda_{pv,on}$ can be numerically determined through (4.39) and (4.40).

$$\Lambda_{pv,off} = \frac{\Delta T_{off,min}\left(\eta_{pv,r} \neq 0\right)}{\Delta T_{off,min}\left(\eta_{pv,r} = 0\right)} \tag{4.39}$$

$$\Lambda_{pv,on} = \frac{\Delta T_{on,min}\left(\Delta T_{off}; \eta_{pv,r} \neq 0\right)}{\Delta T_{on,min}\left(\Delta T_{off}; \eta_{pv,r} = 0\right)} \tag{4.40}$$

4.3. Analysis and discussion

4.3.1. Analysis

The controller setpoint design methods described previously were analysed and compared for use in PV-T systems. The analysis was centred on a reference PV-T system, defined in Table 4.1, and focused on the analytical Florschuetz model

Table 4.1.: Parameter values for the reference PV-T system simulated

Parameter	Value	Unit	Parameter	Value	Unit
A_c	1.27	m^2	C_{bond}	10^6	W/mK
k_{plate}	237	W/mK	$h_{pv,p}$	700	W/m^{2}K
δ_{plate}	0.001	m	h_f	301	W/m^{2}K
k_{si}	148	W/mK	$\eta_{el,bos}$	95	%
δ_{si}	0.2	mm	$N_{strings}$	4	-
U_L	7	W/m^{2}K	$\dot{m}_c/A_c$	0.01	Kg/m^{2}s
$U_{L,2}$	0.03	W/m^{2}K^2	$(\dot{m}C_p)_{min}$	212	W/K
d_{riser}	0.008	m	UA_{he}	800	W/K
D_{riser}	0.01	m	$K_{pv,el}$	1	-
W	0.036	m	$K_{par,aux}$	2	-
α	94	%	T_a	20	°C
τ	94	%	$T_{pv,r}$	25	°C
$\eta_{pv,r}$	15	%	$G_{T,r}$	1000	W/m^2
β_{pv}	-0.45	%/°C	$P_{el,pump}$	50	W
ρ_{pv}	67	%	$\eta_{th,pump}$	0	%

method, the analytical Beckman et al. method and the numerical method. For simplicity, the three methods were configured to use the same collector efficiency factor for the same conditions, determined using the Florschuetz model, i.e., (2.42).

4.3.1.1. Analytical method using the Florschuetz model

As made clear through the way (4.13) and (4.19) are arranged, the conditions derived for cost-effective and cycling-free operation in PV-T systems bear resemblance to those for non-hybrid systems and their differences are modelled in the factors $\Lambda_{pv,off}$ and $\Lambda_{pv,on}$, respectively. The factors, given by (4.11) and (4.20) assuming the Florschuetz model conditions are valid, represent the normalised variation of the minimum ΔT_{off} setpoint and minimum setpoint ratio ($\Delta T_{on}/\Delta T_{off}$) for cost-effective and cycling-free operation in PV-T systems due to PV generation, respectively, and are sensitive to the irradiance level (G_T). Figure 4.2 illustrates the variation of $\Lambda_{pv,off}$ and $\Lambda_{pv,on}$ for PV-T systems based on the reference one defined in Table 4.1 unless otherwise stated, namely regarding the heat loss coefficient temperature dependence ($U_{L,2}$ = 0 W/m^{2}K^2). In essence, PV-T systems generating electricity can operate cost-effectively using lower ΔT_{off} setpoints ($\eta_{pv} \neq 0\%$; $\Lambda_{pv,off}<1$) than under non-hybrid operation ($\eta_{pv} = 0\%$; $\Lambda_{pv,off}=1$) since keeping the pump(s) running until later while ΔT is positive cools the cells and enhances revenue. In turn, higher ($\Delta T_{on}/\Delta T_{off}$) setpoint ratios are required to avoid cycling while electricity is being generated ($\eta_{pv} \neq 0\%$; $\Lambda_{pv,on}>1$) since the reduced effective absorptance caused by PV conversion leads to lower steady-state temperature differences (ΔT) following the start of fluid circulation for the same ΔT_{on} setpoint. Moreover, $\Lambda_{pv,off}$ and $\Lambda_{pv,on}$ decrease and increase with G_T, respectively, and more

so for higher PV conversion efficiencies and lower cell efficiency temperature coefficients, but less so for higher overall heat loss coefficients. In other words, the more thermally and electrically efficient the collectors are and temperature-sensitive the PV conversion's electrical efficiency is, the higher the difference between setpoint selection for hybrid and non-hybrid operation modes.

Quantitatively, the variations determined by $\Lambda_{pv,off}$ and $\Lambda_{pv,on}$ are not very significant, even at high G_T. For the reference system, the minimum ΔT_{off} setpoint ($\Delta T_{off,min}$) and minimum setpoint ratio decreased by as much as 10.9% and increased by up to 5.5%, respectively, whereas for the non-reference PV-T systems considered for Figure 4.2, the decrease and increased reached 22.7% and 13.1%.

In turn, factors such as the PV subsidy level ($K_{pv,el}$), the balance of system efficiency ($\eta_{el,bos}$), and the parasitic to auxiliary energy price ratio ($K_{par,aux}$) cause higher $\Lambda_{pv,off}$ reductions with G_T as they increase. Each of these factors exerts the same influence on $\Lambda_{pv,off}$ but only $K_{par,aux}$ can be reasonably expected to change significantly between systems and, unlike the others, also influences $\Delta T_{off,min}$ for non-hybrid operation. In the parametric analysis conducted based on the reference PV-T system defined in Table 4.1, $\Lambda_{pv,off}$ decreased by as much as roughly 70% (down to around 30%) at very high energy price ratios ($K_{par,aux}$=32) compared to roughly 10% for the reference energy price ratio ($K_{par,aux}$=2), while $\Delta T_{off,min}$ for non-hybrid operation (independent of G_T and equivalent to $\Lambda_{pv,off}$=1 or G_T=0 W/m²) increased up to 16-fold (1500% increase) relative to the reference value, as illustrated in Figure 4.3. Thus, the effect of $\Lambda_{pv,off}$ is also more significant in absolute terms at high $K_{par,aux}$, which does not occur with $K_{pv,el}$ or $\eta_{el,bos}$. The energy price relations are, however, more commonly in line with reference case and thus the absolute variations are not expected to be as pronounced in typical systems. In effect, the minimum cost-effective turn-off setpoint for PV-T systems should be modestly lower than for non-hybrid operation or equivalent non-hybrid systems, but the variation is only noticeable in an absolute sense if the setpoints for non-hybrid operation are already conventionally high, such as for low-flow gas-assisted systems.

4.3.1.2. Beckman et al. and numerical methods

Both the Beckman et al. (1994) and numerical methods for setpoint selection in PV-T systems were able to reproduce the results obtained using the traditional analytical method, as illustrated in Figure 4.4. However, by introducing a non-negligible collector heat loss coefficient temperature dependence ($U_{L,2} \neq 0$ W/m²K²), the Beckman et al. (1994) and numerical methods diverged in some respects though ultimately led to the same conclusions: cost-effective and stable operation of PV-T systems generating electricity is compatible with lower ΔT_{off} setpoints and requires higher ΔT_{on} setpoints (for the same ΔT_{off} setpoint), respectively, than for those not generating electricity or equivalent non-hybrid systems. Moreover, the factors $\Lambda_{pv,off}$ and $\Lambda_{pv,on}$ are of the same order of magnitude as those obtained using the analytical method, though other differences are worth highlighting.

The most noteworthy difference detected between the methods concerned the

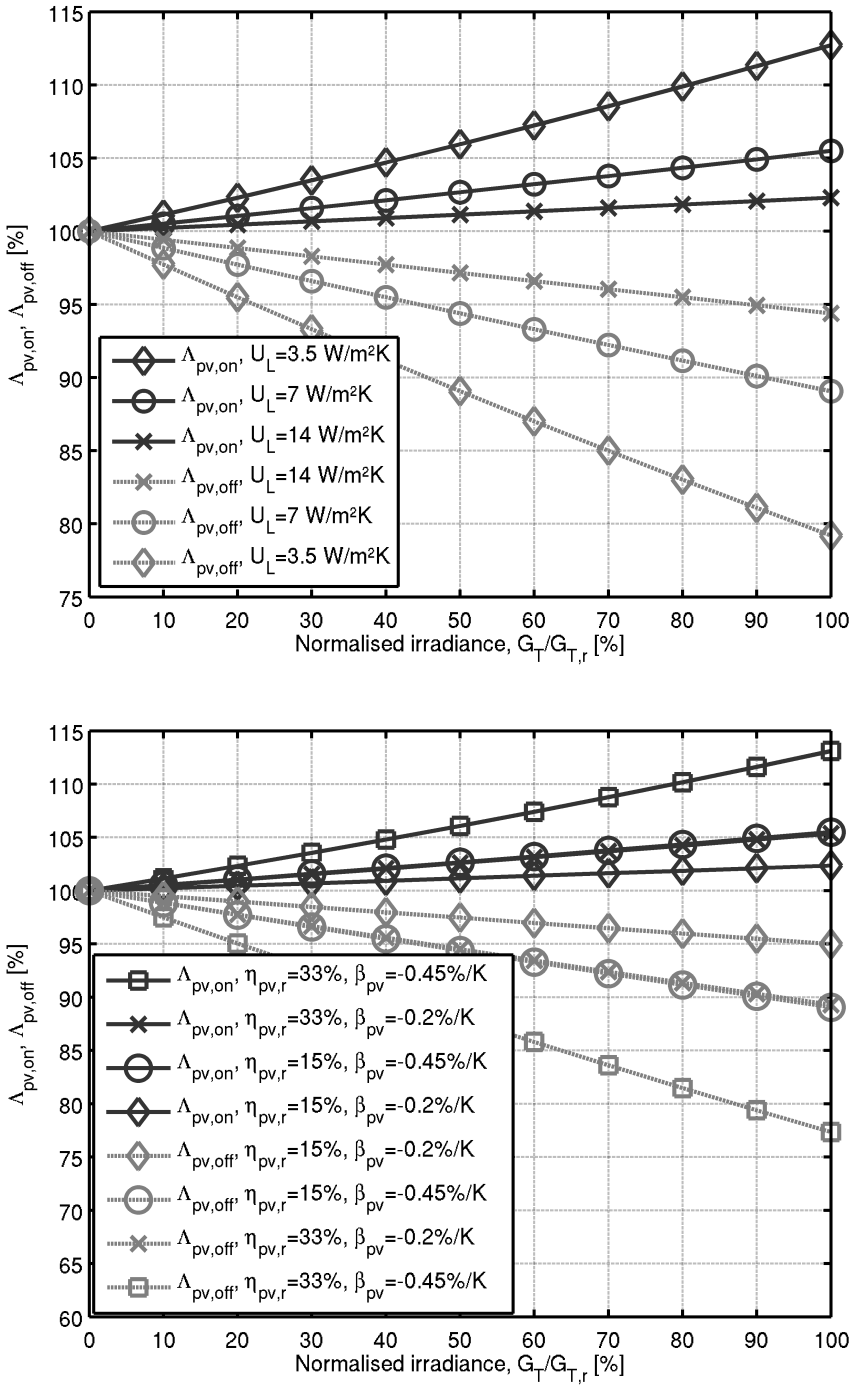

Figure 4.2.: Normalised PV generation-induced variation of $\Delta T_{off,min}$ and $(\Delta T_{on}/\Delta T_{off})_{min}$ for cost-effective ($\Lambda_{pv,off}$) and cycling-free ($\Lambda_{pv,on}$) operation, respectively, according to the analytical Florschuetz model approach, for reference PV-T system-based parametric analyses of the normalised irradiance ($G_T/G_{T,r}$) and: first row) the overall collector heat loss coefficient (U_L); second row) the reference cell efficiency ($\eta_{pv,r}$) and cell efficiency temperature coefficient (β_{pv}).

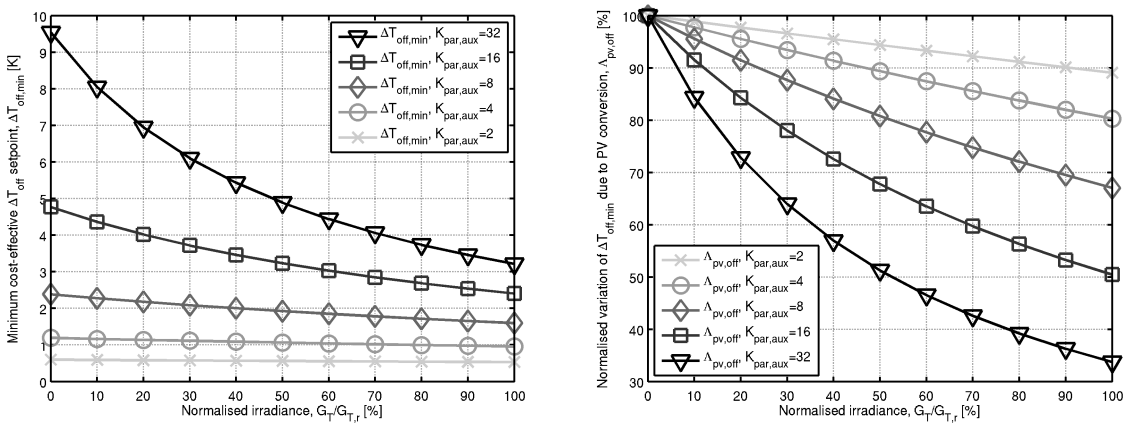

Figure 4.3.: Minimum ΔT_{off} setpoint for cost-effective operation (left-hand side plot) and its respective normalised variation due to PV generation (right-hand side plot), according to the analytical method, for parametric analyses on the irradiance (G_T) and parasitic to auxiliary energy price ratio ($K_{par,aux}$).

condition for cost-effective operation. According to the Beckman et al. approach, a higher heat loss coefficient temperature dependence can cause lower $\Lambda_{pv,off}$ values at low irradiances than would otherwise be possible, whereas the numerical method reveals the opposite trend and independently of the irradiance level. Hence, the numerical method results are consistent with those obtained using the traditional method in the sense that higher collector heat losses reduce the differences between hybrid and non-hybrid operation – cf. Figure 4.2. The above-named outcome can also be intuitively understood: higher collector heat losses essentially contribute to passive collector cooling, which benefits PV generation independently of fluid circulation, and for this reason, there are fewer incentives to prolong fluid circulation (i.e., $\Delta T_{off,min}$ increases as $U_{L,1}$ or $U_{L,2}$ increase). It is also worth noting that the Beckman et al. approach was not explicitly meant for PV-T systems and originally only applied to the stability criterion, since the condition for cost-effective operation in non-hybrid systems is independent of collector performance. For these reasons, the Beckman et al. method is presumably flawed as it relates to cost-effective operation of PV-T systems with non-negligible quadratic heat losses.

Conversely, the numerical and Beckman et al. methods produced distinctly similar results concerning stable operation of PV-T systems, as Figure 4.4 demonstrates. In essence, PV-T systems generating PV electricity require higher ΔT_{on} setpoints for stability than under non-hybrid operation, though if the heat loss coefficient temperature dependence is not negligible ($U_{L,2} \neq 0$ W/m²K²) the increase is not proportional to G_T, unlike previously determined using the traditional method. While this outcome is not intuitive, it coincides with decreasing ΔT_{on} setpoints with G_T for both hybrid and non-hybrid operation, as shown in Figure 4.5, unlike for systems with a negligible heat loss coefficient temperature dependence. Hence, the ΔT_{on} setpoint increase due to PV generation indicated by $\Lambda_{pv,on}$ proved insuffi-

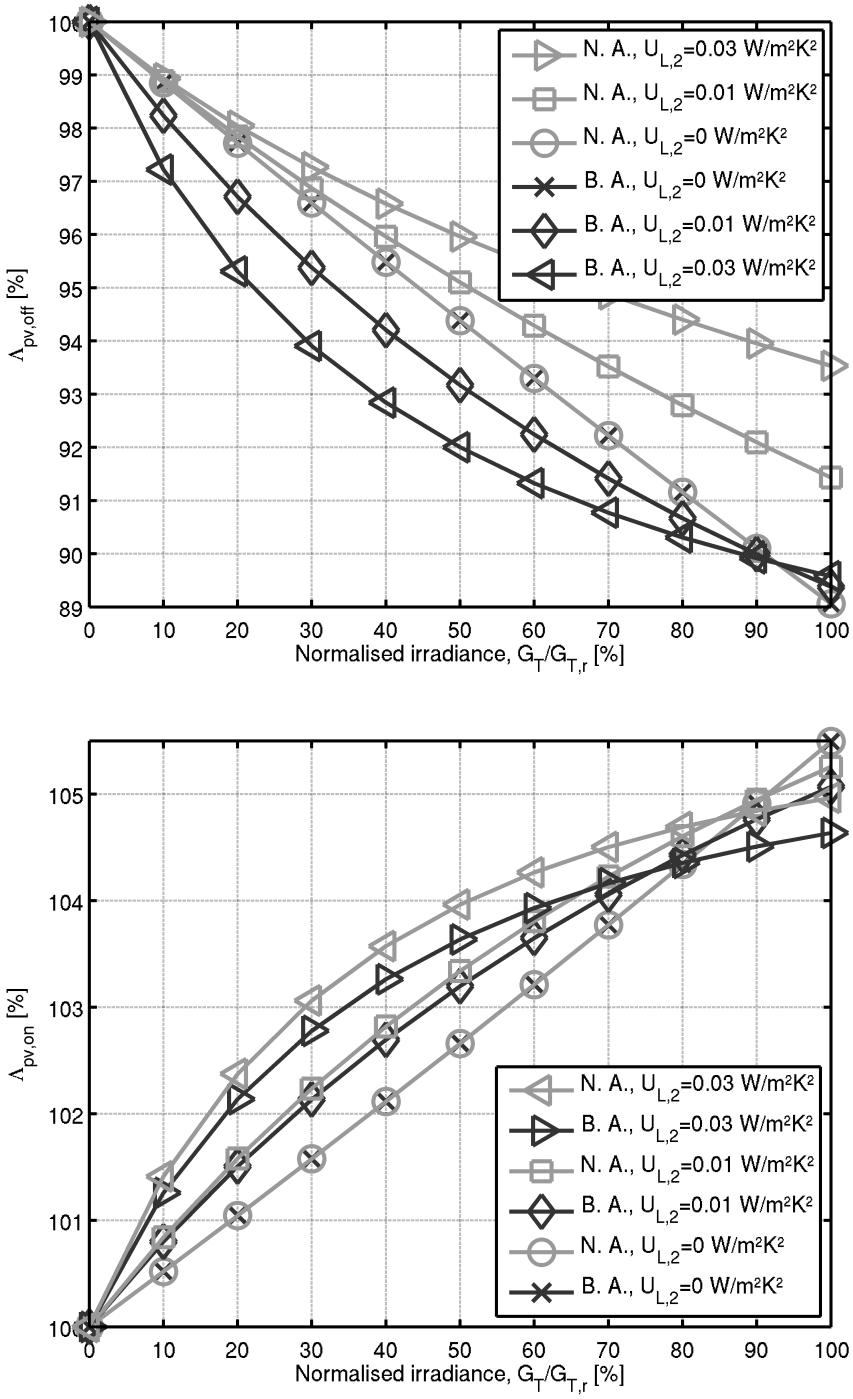

Figure 4.4.: Normalised PV generation-induced variations of the minimum ΔT_{off} and ΔT_{on} setpoints for cost-effective ($\Lambda_{pv,off}$; first row plot) and cycling-free ($\Lambda_{pv,on}$; second row plot) operation of PV-T systems, respectively, according to the numerical (N.A.; $\Delta T_{off} = 2$ K) and Beckman et al. (B.A) approaches, for reference PV-T system-based parametric analyses of the irradiance level (G_T) and the collector heat loss coefficient temperature dependence ($U_{L,2}$).

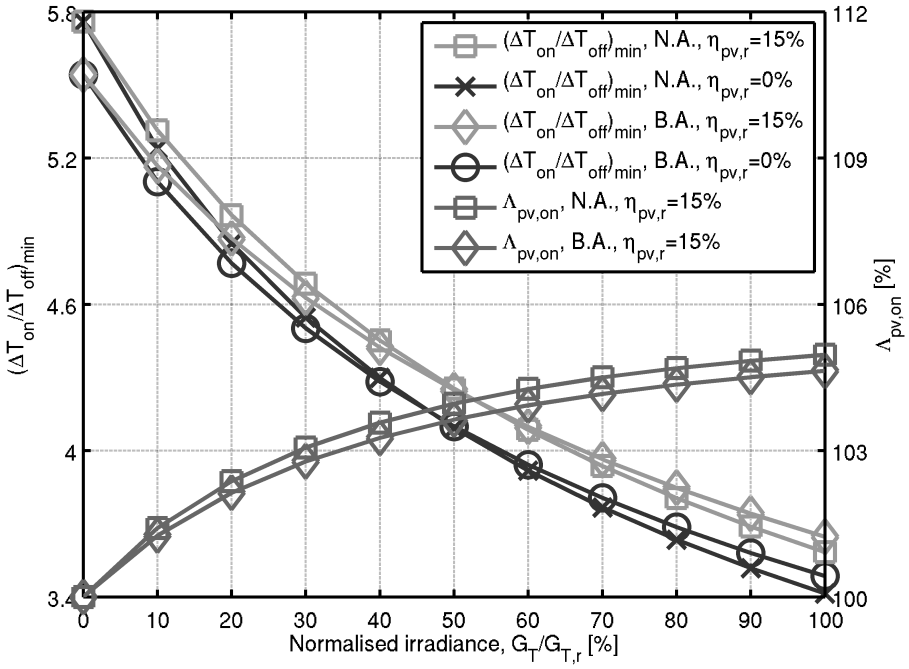

Figure 4.5.: Minimum setpoint ratio ($\Delta T_{on}/\Delta T_{off}$) for cycling-free operation and its normalised variation ($\Lambda_{pv,on}$) due to PV generation, according to the Beckman et al. (1994) (B.A.) and numerical (N.A.; ΔT_{off}=2 K) approaches, for parametric analyses on the irradiance level (G_T) and the reference cell efficiency ($\eta_{pv,r}$).

cient to counter the decrease with G_T, for the cases considered. In other words, the minimum setpoint ratio $(\Delta T_{on}/\Delta T_{off})_{min}$ for cycling-free hybrid operation of PV-T systems is slightly higher than for non-hybrid operation or equivalent non-hybrid systems but is nonetheless within the same order of magnitude and can decrease with G_T if the heat loss coefficient temperature dependence is not negligible. This was also found to be valid for various ΔT_{off} setpoints, as illustrated in Figure 4.6.

4.3.2. Practical considerations

The effect of PV conversion on the conditions for cost-effective and cycling-free operation of PV-T systems, determined using the analytical and numerical methods described, can be predicted to be conservative or lacking in practical relevance in some situations. In general, PV generation in PV-T systems almost certainly anticipates and continues beyond the start and end of fluid circulation, respectively, meaning it likely has repercussions for setpoint selection, however small. However, one reason why the repercussions are likely limited concerns the occurrence of the highest and lowest $\Lambda_{pv,on}$ and $\Lambda_{pv,off}$, respectively, at high irradiances ($\approx G_{T,r}$), which are not generally associated with the start and end of fluid circulation, except during low demand periods, and thus their significance on an annual basis is likely

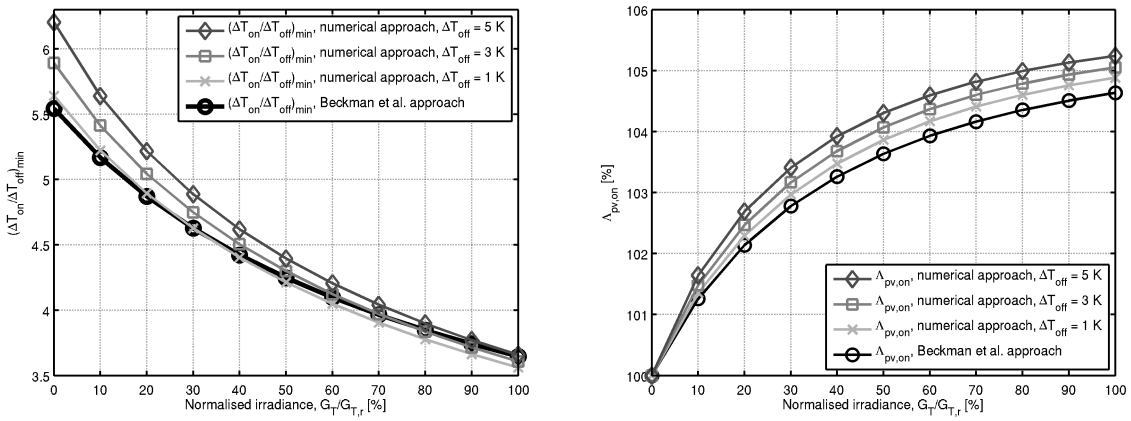

Figure 4.6.: Effect of ΔT_{off} on the minimum setpoint ratio (left-hand side plot) for cycling-free operation of the reference PV-T system and its normalised variation (right-hand side plot) according to the numerical method and comparison with the Beckman et al. (1994) method, versus the normalised irradiance ($G_T/G_{T,r}$).

low, although presumably less so for combi- or space-heating PV-T systems.

Similarly, the assumption of a negligible collector heat capacity implies swift PV conversion efficiency and respective revenue reductions following transitions from fluid circulation to stagnation and vice-versa. In practice, however, the repercussions from a transition from fluid circulation to stagnation are (as much as 30 minutes) slower to set in due to thermal inertia, and lower in magnitude if G_T is decreasing, as in a typical late afternoon shutdown (Zondag and van Helden, 2002).

Also, the $\Delta T_{off,min}$ reduction with G_T may not have practical significance in typical high-flow PV-T systems for which low ΔT_{off} setpoints ($\lesssim$2K) are theoretically cost-effective – according to (4.13) – since compliance is generally handled conservatively in light of model limitations and parameter uncertainty, the limited thermal performance sensitivity to low ΔT_{off} setpoints ($\approx$1K), and predictable temperature measurement errors (Hirsch, 1985; Winn, 1993; Peuser et al., 2002). In turn, the condition for cycling-free operation is generally regarded as merely indicative if not unreliable, hence accommodating the effect of PV conversion would be of little consequence (Schiller et al., 1980; Winn, 1993; Duffie and Beckman, 2013).

Among the aforementioned factors, measurement errors can limit the ability of controllers to take advantage of the predicted effect of PV conversion on the conditions for cost-effective and cycling-free operation, and reap potential rewards, however small. As noted above, this is arguably more important concerning the former since cycling-free operation is generally not a priority in practice. The basic idea is that a low effective ΔT measurement tolerance ($|\varepsilon_{\Delta T}|$) is desirable to take advantage of the lower ΔT_{off} setpoints – enabled by PV conversion – in the least conservative way possible, i.e., in accordance with (4.25). The same can be said about pump efficiency developments, which would ideally allow ST systems to operate cost-effectively for longer – due to lower $\Delta T_{off,min}$ enabled by a lower P_{pump} –

but, in practice, this is limited by the temperature measurement tolerance.

On the other hand, there is scant evidence to suggest anything more than marginal thermal and electrical performance enhancements would result in typical Summer-sized high-flow PV-T systems by taking into account the effect of PV conversion on setpoint selection. This assessment is based on the limited thermal performance sensitivity of non-hybrid systems to ΔT_{off} at low values as documented by Hirsch (1985) and others, the comparable thermal performance of hybrid and non-hybrid collectors of equivalent designs, the reduced $\Delta T_{off,min}$ variation in absolute terms predicted for PV-T systems generating electricity relative to non-hybrid systems, and the generally low cell efficiency temperature coefficients. Naturally, this assessment is likely less valid for some low-flow PV-T systems and/or for those bound to use comparatively expensive parasitic energy (high $K_{par,aux}$) since, for these, $\Delta T_{off,min}$ will drop more substantially in absolute and relative terms.

In conclusion, there are reasons to consider these findings as having a marginal effect on setpoint selection but they nevertheless indicate at least slightly different setpoints should be used for PV-T systems. Accordingly, setpoint selection based on cost-effective and stable operation of PV-T systems can be aided by analytical and numerical methods, though the former are best used for systems whose collectors display a negligible heat loss coefficient temperature dependence or otherwise solely to determine the condition for stable operation. Moreover, given the effect of the irradiance level on the results, this process should be conducted using a representative irradiance level for each situation, which should be at least as high as the minimum irradiance level for useful heat collection ($G_{T,on}$), given by (4.41).

$$G_{T,on} = \frac{U_{L,1}\left(T_{f,m} - T_a\right) + U_{L,2}\left(T_{f,m} - T_a\right)^2}{1 - \frac{\rho_{pv}\eta_{pv,r}}{\alpha}\left[1 + \beta_{pv}\left(T_{f,m} - T_{pv,r}\right)\right]} \tag{4.41}$$

4.4. Summary

The following contributions can he highlighted from the current chapter:

- Derivation of differential temperature controller setpoint design methods for cost-effective and cycling-free operation of PV-T systems, using the Florschuetz (1979) steady-state collector model, the ϵ-NTU method for systems with heat exchangers, and the Alcone and Herman (1981) approach to account for the effect of temperature measurement errors on the design methods;
- Development of a conservative approach to controller setpoint design methods taking into account the effect of temperature measurement errors on setpoint selection, based on the Alcone and Herman (1981) approach;
- Development of analytical methods for differential temperature controller setpoint selection based on cost-effective and cycling-free operation of PV-T systems, using the Beckman et al. (1994) approach, the extended Perers (1993) model, the ϵ-NTU method and the Florschuetz (1979) model;

- Development of numerical methods for differential temperature controller setpoint selection based on cost-effective and cycling-free operation of PV-T systems using the extended Perers (1993) model and the ϵ-NTU method;
- Validation of the numerical and analytical Beckman et al. methods for PV-T systems with collectors reproducing a negligible heat loss coefficient temperature dependence and critical assessment of the methods otherwise:
  - Cost-effective and cycling-free operation of PV-T systems generating electricity is possible using lower ΔT_{off} setpoints and requires higher ΔT_{on} setpoints, respectively, than for PV-T systems not generating electricity or equivalent non-hybrid ST systems, according to all methods tested;
  - The normalised controller setpoint variations due to PV conversion were limited to double-digits in the parametric analyses conducted;
  - For PV-T systems with collectors reproducing a negligible collector heat loss coefficient temperature dependence, lower cell efficiency temperature coefficients, lower collector heat loss coefficients and higher PV conversion efficiencies exacerbated the normalised controller setpoint variations;
  - The analytical method based on the Beckman et al. approach and the numerical method were found to diverge in relation to the condition for cost-effective operation of PV-T systems with collectors reproducing a non-negligible heat loss coefficient temperature dependence, and only the latter proved consistent with earlier findings: higher heat losses lead to less pronounced ΔT_{off} reductions due to PV conversion;
  - The minimum setpoint ratio required for stable operation in hybrid or non-hybrid ST systems with a non-negligible collector heat loss coefficient temperature dependence was shown to decrease with G_T;
  - The effect of PV conversion on differential temperature controller setpoint selection for PV-T systems was reasoned to be limited or lacking in practical relevance on account of the usual timing of fluid circulation in ST systems, the non-negligible heat capacity of ST collectors, model limitations and parameter uncertainty, the limited thermal performance sensitivity to controller setpoints and temperature measurement errors.

5. Comparison of PV-T systems using DTSSHPC and DTSTLHC

The present chapter details a comparison between SDHW PV-T systems employing DTSTLHC and DTSSHPC as pump control, arguably the two most common ones in this market segment. While the controllers are not new, comparisons between ST systems using them have been limited in scope and have exclusively focused on non-hybrid systems. The comparison described next was designed to study under which conditions each controller comparatively excels and by how much.

5.1. Methodology

5.1.1. Outline

The comparison undertaken relied on a comprehensive set of dynamic simulations of SDHW PV-T systems employing DTSTLHC and DTSSHPC. While intrinsically less realistic than physical experiments, simulations have the advantage of allowing for simpler, quicker and broader comparisons between different systems under the same exact conditions. Accordingly, the PV-T systems reproduced were equivalent except with regard to the controller and controller-dependent options, and representative of the single-family grid-connected residential SDHW segment, which is generally seen as the main market for PV-T technology (Affolter et al., 2005). In particular, the emphasis was on indirect systems where solar charging of thermal storage tanks takes place through internal coiled heat exchangers and small PV-T collector areas whose electrical output is in turn fed to the local utility grid.

5.1.2. Research vectors

The simulations focused on a set of factors predicted to influence a comparison between both controllers, some of which are independent of the controllers and others which are not. The most predictable of these factors are highlighted in the hypothesis proposed in Section 1.4.1.3 and include location- and controller-related attributes, all of which have been at least hinted at in previous studies though focusing on non-hybrid systems: the weather pattern; the auxiliary system and the relation between auxiliary and parasitic energy prices and primary energy factors; and the circulation pump. Conversely, the hypothesis implies PV generation is not predicted to have a decisive effect on the comparison, or at least not one likely to tilt the

comparison in favour of DTSSHPC, since a trend for higher collector temperatures has been reported in the literature and can also be inferred from its control function, assuming the same nominal (i.e., maximum) flow rate is used. Herein lies one important difference between previous comparisons and the current one: extensive parametric analyses on mass flow rates and controller setpoints were conducted for each controller. This allows for the comparison of optimised systems rather than just conventionally matched systems, which have been often characterised by configurations using the same nominal mass flow rate and ΔT_{off} setpoint, relying on equivalent ΔT_{on} and ΔT_{sat} setpoints for the DTSTLHC- and DTSSHPC-operated systems, respectively, and a low ΔT_{on} setpoint ($\Delta T_{on} \simeq \Delta T_{off}$) for the latter.

The use of optimisation is to address shortcomings associated with this tacit convention, namely how it does not represent all conceivable scenarios and may constitute bias. This is most evident in relation to the ΔT_{off} setpoints but a more general case can be made. Concerning setpoints, the convention makes some sense with regard to ΔT_{sat} and ΔT_{on} but comparisons limited to the same ΔT_{off} fail to take into account DTSSHPC operation at subnominal flow rates, particularly late in the afternoon. In turn, the general case is that a comparison between otherwise equivalent DTSSHPC- and DTSTLHC-operated systems may be biased depending on how they are configured (Schiller et al., 1980). In other words, if one controller is set to underperform, the other may comparatively excel, and vice-versa. Hence, optimisation can render representative differences between the controllers visible by bringing out their true potential, in a way the conventional comparison can only approach. In turn, extreme scenarios can complement the analysis.

Another noteworthy aspect not previously addressed, though hinted at by Swanson and Ollendorf (1979), is the effect of climate data resolution on the comparison between these controllers. Accordingly, simulations were conducted using 15- and 60-minute resolution data for the same location, with the latter set of data averaged from the former, which is based on measurements for an entire year. In turn, standard 60-minute resolution typical meteorological year (TMY) data was used to investigate the effect of location-related weather patterns on the comparison. In any event, both groups of simulations concerned a full year, which is arguably the minimum time-frame necessary to conduct a meaningful analysis of ST heating systems and is also compatible with intra-year analyses (e.g., on a monthly basis).

5.1.3. Evaluation criteria

The analysis undertaken is also defined by the evaluation criteria selected. In this regard, emphasis is given to load provision cost-effectiveness and primary energy efficiency, which are among the most relevant for public and private decision-making, though other standard criteria were also considered. The first group of criteria were also selected due to the need to encompass the thermal and electrical performance of PV-T systems and other system-level considerations (e.g., parasitic energy, user thermal comfort, etc.) for representative assessments. Previous comparisons between DTSTLHC and DTSSHPC have mainly focused on more limited though still

relevant criteria such as thermal collection efficiency, which fail to take into account the dual nature of PV-T collector performance and neglect some system level dynamics, whereas PV-T technology studies have generally relied on more suitable criteria including primary energy efficiency (Lämmle et al., 2015).

5.2. System description

5.2.1. Overview

The PV-T system represented in this study is a small active grid-connected residential solar thermal system for domestic water heating and AC grid injection of locally-generated electricity, as illustrated in Figure 5.1. It relies on an electrical circulation pump on the return line for indirect solar charging of the storage tank through an internal coiled heat exchanger stretching over more than half of the tank's vertical height starting at the bottom. The pressurised collector loop is completed by flow and return pipes partially exposed to outdoor and indoor temperatures.

The system's thermal storage tank is of the vertical cylindrical type commonly found in this segment and is compatible with on demand heating via one of two methods: an immersed electrical heating element placed above the solar heat exchanger; or, a gas-fired boiler in line with another coiled heat exchanger placed above the solar one. The two previous tank charging methods can be used to keep the load provision volume hot enough to meet load requirements (45°C) and prevent the

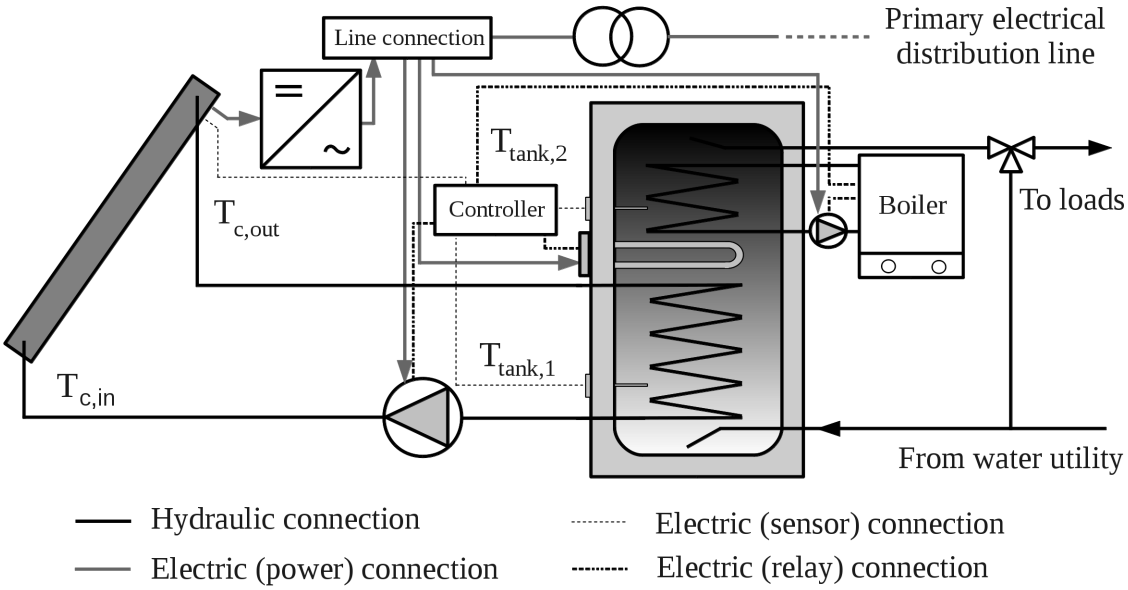

Figure 5.1.: Diagram for the active indirect grid-connected SDHW PV-T system reproduced in simulations for the purposes of the comparison between supply-loop differential temperature pump controls (DTSTLHC and DTSSHPC)

growth of *legionella* (60°C), the latter being the most demanding. Hence, a demand-loop mixing valve circuit complements the system by allowing tank and mains water to be mixed in order to prevent user scalding while meeting load specifications.

The PV-T system also generates electricity concurrently with DHW production, and via PV cells with negative MPP cell efficiency temperature coefficients. The electricity generated is fed to the local AC utility grid through a grid-tied MPP-tracking inverter, generating returns at a potentially subsidised rate. Consequently, the influence of user and control dynamics on electricity generation is limited to the cell temperature effect and, as such, does not extend to load matching as it would in autonomous systems. In this sense, continuous heat removal is generally desirable to lower cell temperatures and increase PV yields, whereas stagnation is not.

With regard to stagnation, the system is not equipped with measures to prevent collector overheating during such events. This is a deliberate option so the merits of each controller can be ascertained without undue interference. Nevertheless, the controllers are set to prevent fluid circulation if the collector loop becomes too hot (>95°C) and stagnation is assumed to be handled successfully according to the steam-back principle, and hence, no fluid release via the safety valve takes place in a way that would prevent system operation from resuming after a cool down period.

5.2.2. Supply-loop pump controllers

As stated earlier, the pump controllers under consideration are the DTSTLHC and DTSSHPC previously discussed in Chapter 2. In a nutshell, the former is a two-state (on/off) controller while the latter requires variable-flow capabilities and has a few variations, yet both controller types are governed by the same temperature difference. In the case of indirect systems with internal coiled heat exchangers in general, and in this one in particular, the temperature difference is measured between the collector plate or outlet fluid closest to the flow line and the water in the vicinity of the heat exchanger but not above or below (Streicher, 2012).

The focus of this study is on the standard DTSTLHC and one of the several DTSSHPC variants. Concretely, the DTSSHPC variant emphasised features a characteristic curve with a proportional region discretised over N_{step} steps – as seen in Figure 2.5 – and uses the pump speed as the control signal and the mass flow rate as the controlled variable. The implementation, represented by the block diagram of Figure 5.2, requires selecting the nominal and minimum mass flow rates in addition to other controller setpoints (ΔT_{on}, ΔT_{off}, ΔT_{sat} and N_{step}), and its correct use implies close agreement between the design flow rates and the system hydraulics, which are largely characterised by the pump and pipeline. In contrast, an implementation based on the pump speed as the controlled variable and control signal is easier to parametrise (since it can operate using normalised values in which case the nominal pump speed corresponds to 100% and thus there is one less parameter to consider), does not place special requirements on the hydraulics and as a result can work off-the-shelf (which is presumably why it is the more common version) but may lead to different $\dot{m}$-ΔT curves depending on the combination of circulation pump

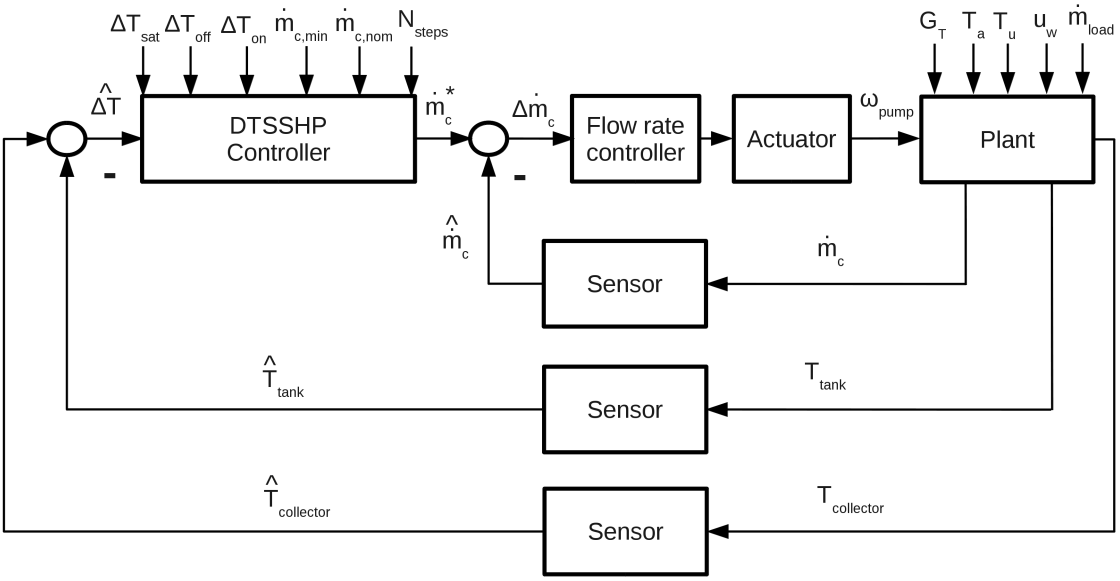

Figure 5.2.: Block diagram for the DTSSHPC variant studied: the pump speed is the manipulated variable; the mass flow rate is the controlled variable.

and system pipeline, as shown in Figure 2.6. Hence, the focus is on DTSSHPC with system invariant and easily reproducible $\dot{m}$-ΔT curves.

5.2.3. Hydraulics

The PV-T systems under consideration are hydraulically compatible with the range of flow rates commonly used in similar SDHW systems, which typically employ specific mass flow rates in the range of 0.005-0.02 Kg/m²s. The controls can enforce these flow rates via throttling and/or pump speed adjustments for a given pipeline, which then requires a flow control valve and dynamic pump speed control capabilities, respectively. Naturally, the latter is only required for DTSSHPC but, despite its higher initial cost, can also be used with DTSTLHC and may in some cases be advantageous in terms of parasitic performance via low speed operation. Hence, speed-controlled pumps are considered for both controls, though in the case of DTSTLHC these can also be seen as single-speed pumps of equivalent performance. Moreover, flow control valve adjustments are strictly preset to ensure compatibility between pump and pipeline at the design flow rate(s). Figure 5.3 exemplifies the use of throttling and pump speed adjustment for this purpose.

5.3. Simulations

A set of simulations were conducted for SDHW PV-T systems employing each controller in various locations. The simulations also reproduced different auxiliary

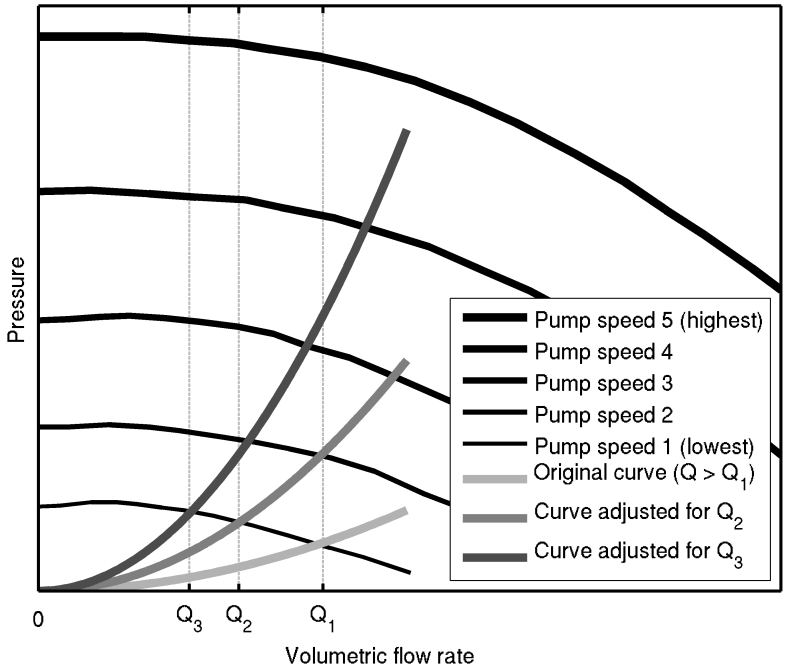

Figure 5.3.: Example of throttling and pump speed adjustment

systems, pumps and encompassed parametric analyses on the nominal and minimum mass flow rates, the controller setpoints, energy prices and the climate data resolution. A system model was developed to carry out this task and set up in accordance with the system characteristics outlined earlier. A set of appropriate figures of merit were defined to facilitate the comparison of simulation results.

5.3.1. System model

A system model was developed to carry out this comparison. The model assumes constant fluid properties and for that reason is divided into thermodynamic and hydraulic submodels: the controllers determine the flow rates in thermodynamic simulations, regardless of the hydraulic implications; and, *a posteriori*, the pump speed and flow control valve adjustments necessary to achieve a given (range of) flow rate(s) are determined, though strictly for the calculation of the parasitic consumption. This greatly simplifies the simulation process and allows for different pump and pipeline combinations to be tested without repeating simulations.

Nevertheless, the system model comprises several component models interacting dynamically with each other in accordance with the diagram of Figure 5.1. Most of these models are standard or simple and, as such, warrant little description, though more information is provided in Appendix D. The exceptions are the dynamic PV-T collector model, already described in Chapter 3, and the flow controllers being compared – particularly the DTSSHPC – which are described next.

5.3.1.1. DTSTLHC and DTSSHPC models

The DTSTLHC and DTSSHPC models reproduce the characteristic diagrams of Figures 2.3 and 2.5. In the implementations used, however, u_c represents the normalised mass flow rate ($\dot{m}_c = \dot{m}_{c,nom} \cdot u_c$, with $\dot{m}_{c,nom}$ being the nominal or maximum mass flow rate) since the thermodynamic and hydraulic components of the system model are decoupled. In other words, DTSTLHC and DTSSHPC are simulated as having no problems in quickly and consistently reaching the pre-established and reference mass flow rates, respectively. Nonetheless, a timer-based minimum pump running time and a collector-loop overheating shutdown were also modelled. The essential DTSTLHC and DTSSHPC model behaviours – i.e., neglecting the overheating protection feature – are described in the flowcharts of Figures 5.4 and 5.5, where the DTSSHPC's characteristic function, or $u_c(\Delta T)$, is given by (5.1), where *floor(x)* represents the rounding function returning the closest integer to x lower than or equal to x ($\forall x \in \mathbb{R}$), $u_{c,step}$ is the normalised flow rate step given by (5.2), and ΔT_{step} is the temperature difference step expressed by (5.3).

$$u_c(\Delta T) = \begin{cases} u_{c,min} + u_{c,step} \cdot floor\left[\frac{\Delta T - \Delta T_{off}}{\Delta T_{step}}\right] & , \quad \Delta T_{off} \leq \Delta T \leq \Delta T_{sat} \\ \\ u_{c,max} & , \quad \Delta T > \Delta T_{sat} \end{cases} \tag{5.1}$$

$$u_{c,step} = \frac{u_{c,max} - u_{c,min}}{N_{steps} - 1} \tag{5.2}$$

$$\Delta T_{step} = \frac{\Delta T_{sat} - \Delta T_{off}}{N_{steps} - 1} \tag{5.3}$$

5.3.1.2. Implementation

The system model was implemented in Mathworks' MATLAB environment and the simulations conducted made use of the SIMULINK and SYSTEMTEST tools. Each simulation relied on the built-in discrete solver in accordance with the discrete nature of the system model, and made use of Forward Euler integration method.

5.3.2. Setup

5.3.2.1. Climate data

The present study used climate data for several Central and Western European locations, namely Lisbon, Portugal (38°42'N, 9°8'W), Almería, Spain (37°5'N, 2°21'W), Freiburg, Germany (47°59'N, 7°51'E) and De Bilt, Netherlands (52°7'N, 5°12'E). Figure 5.6 illustrates some of the most pertinent differences between the

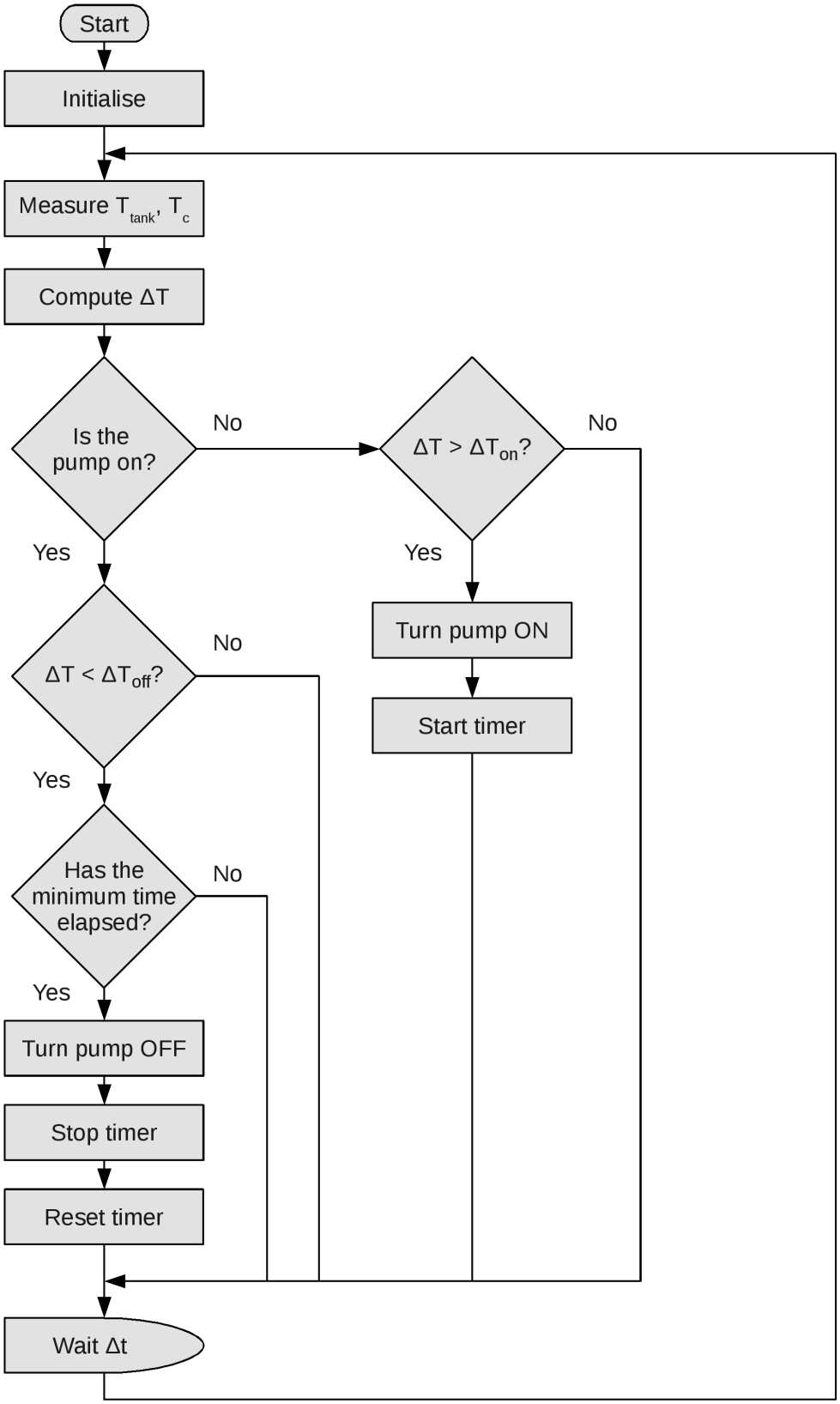

Figure 5.4.: Basic flowchart for the DTSTLHC model implemented

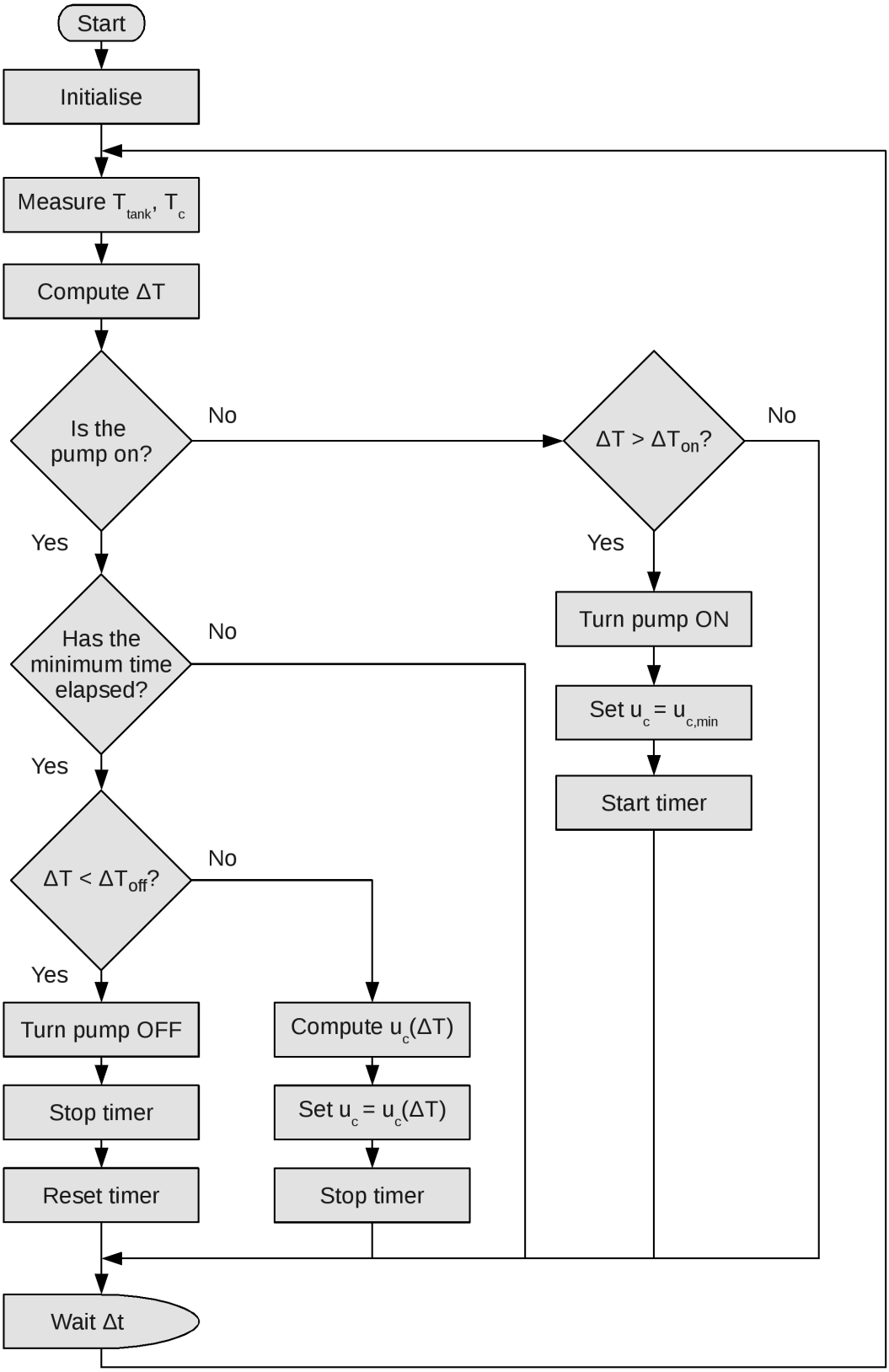

Figure 5.5.: Basic flowchart for the DTSSHPC model implemented

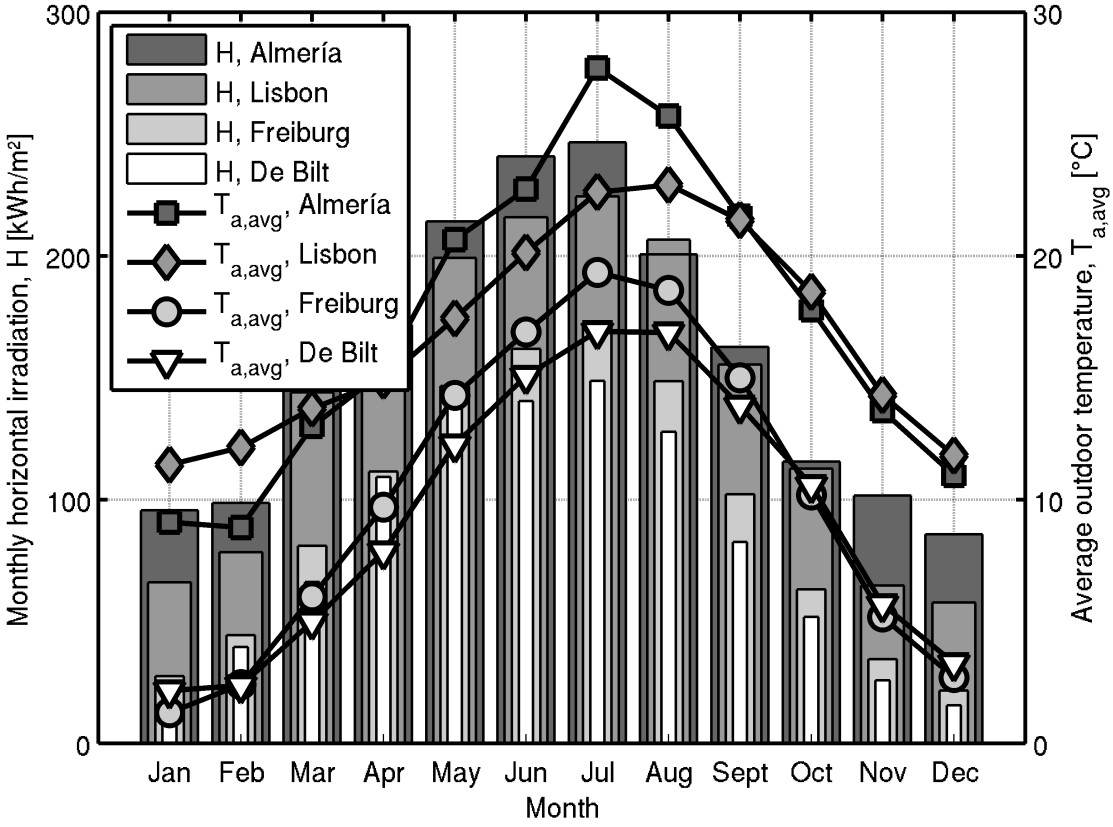

Figure 5.6.: Monthly horizontal irradiation (H) and average ambient temperature ($T_{a,avg}$), by source location: Almería, Spain; Lisbon, Portugal (TMY data); Freiburg, Germany (TMY data); De Bilt, Netherlands (TMY data).

data sets used, which were deemed sufficiently different from those used in previous studies[42]. Among these, all but those for Almería correspond to typical meteorological years with a 60-minute resolution. In turn, the data for Almería is based on measurements for a single year with a 15-minute resolution, which was also averaged to obtain an equivalent 60-minute resolution set for comparison (Solargis, 2017).

The data samples used were interpolated down to the simulation sampling time

[42]According to IVPH (2017), Lisbon has a warm temperate climate (Csa in the Köppen-Geiger system) with dry and hot summers (minimum mean monthly temperature over -3°C; maximum mean monthly temperature above 22°C), and its annual global horizontal irradiance is about 1683 kWh/m²/year according to the TMY data used (Kottek et al., 2006). In turn, the Almería region has an arid cold steppe climate (BSk in the Köppen-Geiger system) and its annual average global horizontal irradiance is about 1882 kWh/m²/year, according to the data used. Finally, both Freiburg and De Bilt have warm temperate climates (Cfb in the Köppen-Geiger system) with fully humid seasons and warm summers (maximum mean monthly temperature below 22°C), and their annual average global horizontal irradiance is about 1114 and 971 kWh/m²/year, respectively, according to the TMY data used (TRNSYS, 2009; Solargis, 2017).

but these were limited to the horizontal and diffuse global irradiation, the ambient temperature and the wind speed. Nonetheless, the irradiance on the collector plane was computed using the isotropic model while the collector incidence angle was determined using the horizontal coordinate system (Duffie and Beckman, 2013). Finally, the mains water temperature (T_u) was modelled as an annual triangular wave – inspired by Cristofari et al. (2009) and Dupeyrat et al. (2014) – whose extrema were made to occur on the same day as those of the outdoor temperature and adjusted tentatively for each location: for Lisbon and Almería, the annual average mains temperature was set to 15°C and the amplitude to 7°C (±3.5°C); for Freiburg and De Bilt, the average was set to 10°C and the amplitude to 7°C.

5.3.2.2. Load profile

The hot water demand simulated was based on the daily ISSO schedule, as described by Zondag et al. (2002). According to this load profile, hot water is withdrawn between the hours of: 7 and 8 am; 12 and 14 pm; 17 and 20 pm; and, 21 and 23 pm. The cumulative daily volume of hot water demand was set to 200 liter at 45°C – roughly equivalent to a 4-member family's demand – and tapped at no more than one eighth of the average daily flow rate. The daily profile was then used according an annual load profile alternating between 5-day and 7-day load weeks plus four one-week Summer vacations spread a month apart from June till September.

5.3.2.3. System model

The system model was set up to reproduce a SDHW system featuring a 300 L storage tank (U_t=0.15 W/m²K) and four (≈5 m² in total) PV-T collectors hydraulically-connected in parallel and feeding electricity to the grid at a balance-of-system (i.e., transport plus power conversion) electrical efficiency of 90%. The individual collector reproduced in this study is the glazed PV-T collector reported by Dupeyrat et al. (2011b), which used direct lamination of mono-crystalline silicon cells on a custom absorber. The performance data provided in the original publication was used to set up the dynamic PV-T collector model described in Chapter 3, namely the EN 12975-2:2006 thermal performance test results for open-circuit mode and the electrical performance during MPP mode, though while some performance parameters were used directly, others were adjusted and some estimated: the cells' electrical efficiency at STC ($\eta_{pv,r}$) was estimated at 14.54% using the optical and electrical performance data reported and assuming a cell efficiency temperature coefficient of -0.45%/K; the nominal heat loss coefficient (equivalent to $F'U_{L,1}$+$F'U_W u_w$) and the open-circuit stagnation temperature were used to arrive at the wind dependence of the heat loss coefficient ($F'U_W$) and the heat loss coefficient for negligible wind conditions ($F'U_{L,1}$) according to the method detailed in Appendix E; the collector efficiency factor was estimated at 95%, given the even higher values for non-hybrid collectors using the same channel technology (Hermann, 2011); the collector specific heat capacity was assumed to be 20 kJ/m²K, since PV-T collectors are expected to

have a higher one than equivalent non-hybrid designs (Zondag et al., 2002); and the beam IAM coefficient and diffuse IAM were estimated at 0.1 and 1, respectively.

Moreover, the collectors were simulated as facing south at a slope with the horizontal plane of 30° for Lisbon and Almería, and 45° for Freiburg and De Bilt, all benefiting from a 20% ground reflectance. In turn, water was selected as the heat carrier for Lisbon and Almería whereas water (60%) and propylene glycol (40%) solutions were assumed for Freiburg and De Bilt. The thermophysical properties of each heat carrier were assumed to be constant and evaluated at atmospheric pressure and 60°C, which was also used as the auxiliary system's reference tank temperature.

The auxiliary system model was set to keep the top tank node – roughly representative of the load provision volume – within 5°C of the reference temperature. The tank itself was modelled as four nodes in the vertical direction, the bottom three of which were simulated as encompassing the solar heat exchanger, and their heat losses calculated assuming a constant room temperature of 22°C. The same room temperature was used to compute the heat losses for the collector loop indoor pipe segment flow and return pair – 3 metres long each – whereas the ambient temperature was used for those of the outdoor segment pair – 2 metres long each.

The entire collector loop, encompassing all the aforementioned components and others not explicitly modelled, was assumed to have pressure losses consistent with a minimum K_p of 1000 W/Kg^3/s^3, a common assumption in similar studies using the model described in Appendix D (Saltiel and Sokolov, 1985; Nhut and Park, 2013). Nonetheless, the pressure losses associated with the individual components modelled (the pipes, the collectors and the heat exchanger) were found to be inferior to those implied by the previous assumption (for all components), and thus consistent.

A low head high efficiency (or low Energy Efficiency Index: EEI$\leq$0.23) speed-controlled circulation pump was reproduced. Compatibility between the pump, the base pipeline and the reference flow rates was ensured through virtual pump speed adjustments and throttling. For DTSSHPC, K_p was increased to reach lower minimum flow rates than would otherwise be possible at the minimum pump speed. For higher minimum flow rates than possible with the minimum K_p, higher preset pump speeds were selected. In turn, dynamic speed adjustments were simulated to reach higher than minimum flow rates, up to the nominal value, during operation. The same basic procedure was also adopted for DTSTLHC, except only for a single speed. Additional system model details are given in Appendix D.

5.3.2.4. System and controller configurations

A comprehensive set of flow rates and flow rate ranges were simulated. For DTSSHPC, the minimum ($\dot{m}_{c,min}/A_c$) and nominal ($\dot{m}_{c,nom}/A_c$) specific mass flow rates adopted were all valid combinations ($\dot{m}_{c,nom}>\dot{m}_{c,min}$) of the following values, also used as nominal values for DTSTLHC: 0.005 Kg/m^{2}s; 0.0075 Kg/m^{2}s; 0.01 Kg/m^{2}s; 0.0125 Kg/m^{2}s; 0.015 Kg/m^{2}s; and, 0.02 Kg/m^{2}s. All compatible combinations were encompassed by up to six values of K_p which, in addition to a single point for low speed operation at 0.02 Kg/m^{2}s, correspond to specific mass flow

rates within the following ranges: 0.005-0.02 Kg/m²s; 0.0075-0.02 Kg/m²s; 0.01-0.02 Kg/m²s; 0.0125-0.02 Kg/m²s; and, 0.015-0.02 Kg/m²s. Naturally, these ranges include redundancies and some may be generally undesirable but they are conceivable and were therefore considered for optimisation purposes.

The relevant temperature difference for the occurrence of fluid circulation in the collector loop was measured between the collector model's outlet temperature and the bottom tank node, for both controls. Moreover, a wide range of controller setpoint combinations were simulated for each controller. The emphasis was on the ΔT_{on} (5, 10, 15 and 20 K) and ΔT_{sat} (5, 6, 8, 10, 12, 14, 15, 16, 18 and 20 K) setpoints for DTSTLHC and DTSSHPC, respectively, and the ΔT_{off} setpoints for both (0, 1, 2, 3 and 4 K). Conversely, the role of the ΔT_{on} setpoints for DTSSHPC was downplayed and these were instead selected according to the conventional understanding, i.e., as low as possible while complying with the ΔT_{off} setpoints (3 K, for ΔT_{off}<3 K; 5 K, for 2 K <ΔT_{off}< 5 K). Finally, a four-minute minimum pump running time per cycle (or timer delay) was used with each controller to minimise pump cycling, and the maximum allowed loop temperature was set to 95°C which, once reached, disabled fluid circulation until the loop cooled down to 85°C.

5.3.3. Figures of merit

The primary simulation results were used to compute a set of figures of merit in line with the evaluation criteria previously discussed. These figures of merit include the primary energy savings (PES) and the financial savings (FS), given by (5.4) and (5.5), where $E_{aux,r}$ is the reference auxiliary system end use energy (equal to the thermal demand), E_{aux} is the auxiliary system end use energy, E_{par} is the parasitic energy consumption, E_{pv} is the PV electricity delivered to the grid, η_{aux} is the auxiliary system efficiency, $f_{p,aux}$ is the auxiliary system fuel primary energy factor, $f_{p,el}$ is the primary energy factor for electricity, p_{aux} is the auxiliary system energy price, p_{el} is the electricity price, and p_{pv} is the unit value of PV electricity.

$$PES = f_{p,aux}\left(\eta_{aux}\right)^{-1}\left(E_{aux,r} - E_{aux}\right) - f_{p,el}E_{par} + f_{p,el}E_{pv} \tag{5.4}$$

$$FS = p_{aux}\left(\eta_{aux}\right)^{-1}\left(E_{aux,r} - E_{aux}\right) - p_{el}E_{par} + p_{pv}E_{pv} \tag{5.5}$$

Both figures of merit are essentially given by the same function – adapted from Lämmle et al. (2015) to account for the parasitic consumption – but use different coefficients to reflect different priorities (primary energy efficiency and load provision cost-effectiveness). Among these coefficients, η_{aux}, $f_{p,aux}$ and p_{aux} vary depending on the type of auxiliary system: for electrical heaters, η_{aux} is assumed to be 100%, $f_{p,aux}$ is equal to $f_{p,el}$ and p_{aux} is equal to p_{el}; for natural gas-fired boilers, η_{aux} is assumed to be 90%, and $f_{p,aux}$ and p_{aux} are equal to the primary energy factor ($f_{p,gas}$) and energy price (p_{gas}) for natural gas, respectively. In turn, electricity generation

Table 5.1.: Reference primary energy factors and energy prices for each location

Country	p_{el}[€/kWh]	p_{gas}[€/kWh]	$f_{p,el}$[-]	$f_{p,gas}$[-]
Portugal	0.2324	0.0864	2.5	1.1
Spain	0.2234	0.0767		
Germany	0.2973	0.0651		
Netherlands	0.1606	0.0794		

was assumed to be valued at rates equivalent to the general purpose electricity (p_{pv} equals p_{el}). Table 5.1 lists the reference energy prices and primary energy factors used in the simulations. These correspond to the 2016 average energy prices for households according to Eurostat and the primary energy factors are taken from DIN V 18599-1 (DIN, 2011, 2013; Lämmle et al., 2015; Eurostat, 2017a).

The aforementioned figures of merit were used to compare the performance of DTSSHPC- and DTSTLHC-operated PV-T systems by way of the respective differences. In other words, subtracting a given figure of merit obtained with controller A to the one obtained with controller B for an otherwise equivalent system, including with regard to the backup heater. However, to make the comparisons more relatable and intuitive among themselves as location and other system details change, the key figures of merit were normalised, namely the end use auxiliary energy savings[43], primary energy savings and financial savings differences, which were normalised in relation to the respective system's end use thermal energy demand ($E_{aux,r}$), primary thermal energy demand ($f_{p,aux}E_{aux,r}/\eta_{aux}$) and load provision cost ($p_{aux}E_{aux,r}/\eta_{aux}$), respectively, in accordance with (5.6), (5.7) and (5.8). In turn, electricity generation can be compared through electrical efficiency differences since these reflect the local insolation but these hardly convey a sense of proportion in relation to the thermal energy demand. For this purpose, the PV yield differences were also normalised in relation to $E_{aux,r}$, as were the parasitic energy differences, in (5.9) and (5.10).

$$\Delta f_{sav,aux} = \frac{(E_{aux,r} - E_{aux,DTSSHPC}) - (E_{aux,r} - E_{aux,DTSTLHC})}{E_{aux,r}} \tag{5.6}$$

$$\Delta f_{PES} = \frac{PES_{DTSSHPC} - PES_{DTSTLHC}}{f_{p,aux}\,(\eta_{aux})^{-1}\,E_{aux,r}} \tag{5.7}$$

$$\Delta f_{FS} = \frac{FS_{DTSSHPC} - FS_{DTSTLHC}}{p_{aux}\,(\eta_{aux})^{-1}\,E_{aux,r}} \tag{5.8}$$

$$\Delta f_{pv} = \frac{E_{pv,DTSSHPC} - E_{pv,DTSTLHC}}{E_{aux,r}} \tag{5.9}$$

[43]The normalised or fractional end use auxiliary savings is equivalent to the solar fraction figure of merit often used in ST studies (Kalogirou, 2009; Duffie and Beckman, 2013).

$$\Delta f_{par} = \frac{E_{par,DTSSHPC} - E_{par,DTSTLHC}}{E_{aux,r}} \tag{5.10}$$

5.4. Results and analysis

5.4.1. Effects of flow rates and controller setpoints

The simulations conducted encompassed numerous combinations of setpoints and nominal flow rates for each control, whose effect on SDHW PV-T system performance could not be rigorously predicted. Based on these simulations, a brief study of their effect was conducted with emphasis on the pump running time, pump cycling, the auxiliary energy savings and the electrical energy efficiency.

5.4.1.1. DTSTLHC-operated PV-T systems

The variations caused by the DTSTLHC setpoints and the nominal flow rate on the pump running time and pump cycling proved consistent with the surveyed literature, as summarised in Section 2.2. Accordingly, narrow deadbands increased pump cycling and higher setpoints decreased the pump running time while higher flow rates contributed to pump cycling and shorter collection periods. In contrast, the effects on the auxiliary energy savings and electrical efficiency were comparatively less predictable, at least for some nominal flow rates, as Figures 5.7 and 5.8 document. In general, higher ΔT_{on} setpoints decreased the auxiliary energy savings, in turn a non-monotonic function of ΔT_{off} and distinctly influenced by the nominal flow rate: higher flow rates tended to decrease the ΔT_{off} setpoint leading to maximum auxiliary energy savings. However, the most curious result proved to be the effect on the electrical efficiency, which saw higher ΔT_{on} setpoints increase it at low flow rates, albeit marginally, whereas at conventionally high flow rates a strongly non-linear pattern emerged, though low setpoints generally led to the worst performances. Though perhaps counter-intuitive, this result can be attributed to increasing storage temperatures as the thermal energy collection improves, in combination with the timing of the first few morning cycles, whose cooling effect can be more advantageous later in the morning rather than early on.

5.4.1.2. DTSSHPC-operated PV-T systems

The effect of nominal flow rates, saturation and turn-off setpoints on DTSSHPC-operated SDHW PV-T systems was also studied. According to the simulations, the pump running time tended to increase with the saturation setpoint and decrease with the turn-off setpoint and nominal flow rate, whereas pump cycling was highest for small ΔT_{sat}-ΔT_{off} deadbands and high flow rates. More surprising results were found concerning the effect of setpoints and flow rates on the auxiliary energy savings, illustrated in Figure 5.9, which varied between locations particularly those

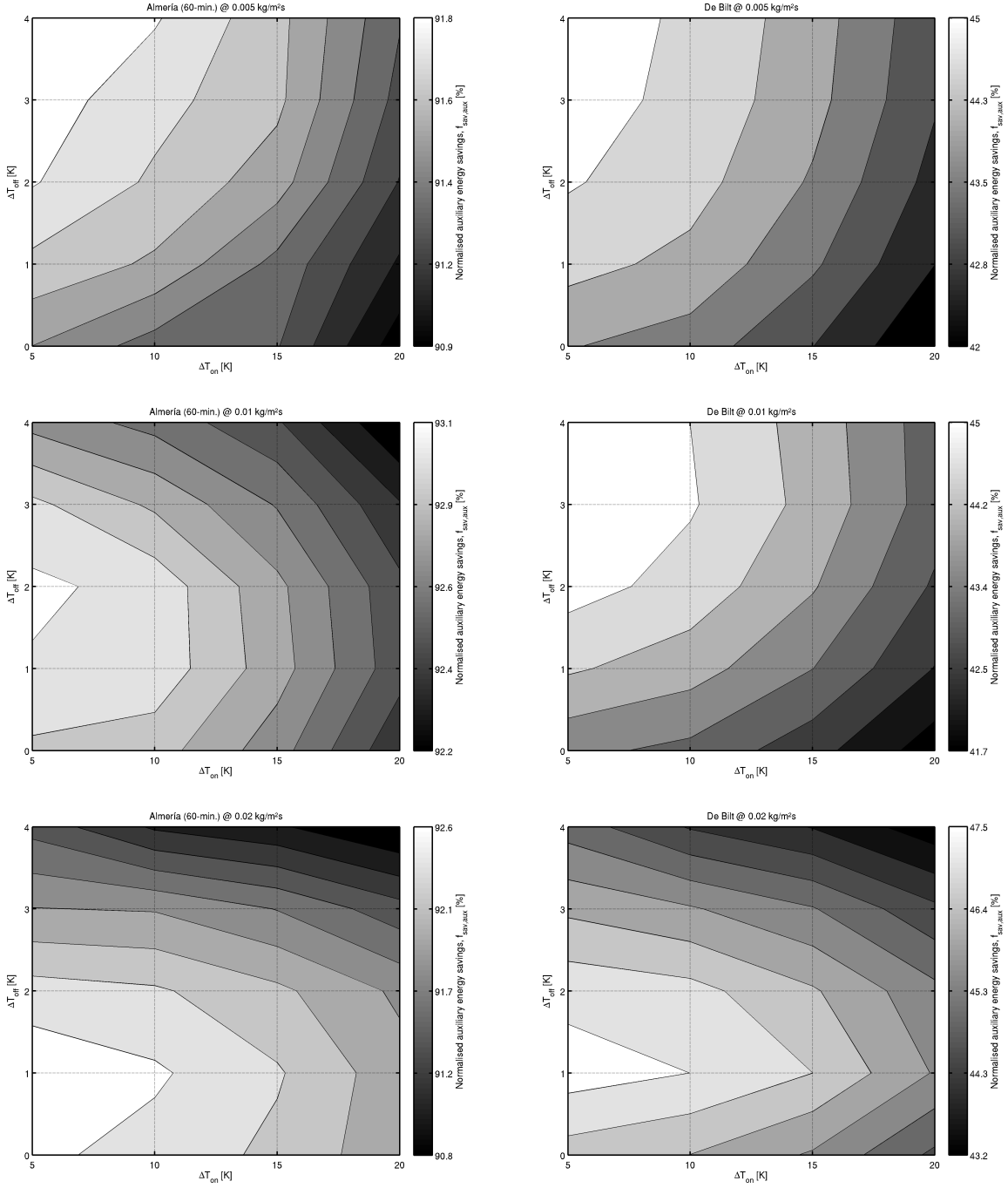

Figure 5.7.: Effect of ΔT_{on} and ΔT_{off} setpoints on the fractional energy savings ($f_{sav,aux}$) of SDHW PV-T systems using DTSTLHC, by nominal specific mass flow rate (0.005, 0.01 and 0.02 Kg/m²s) and location (Almería and De Bilt).

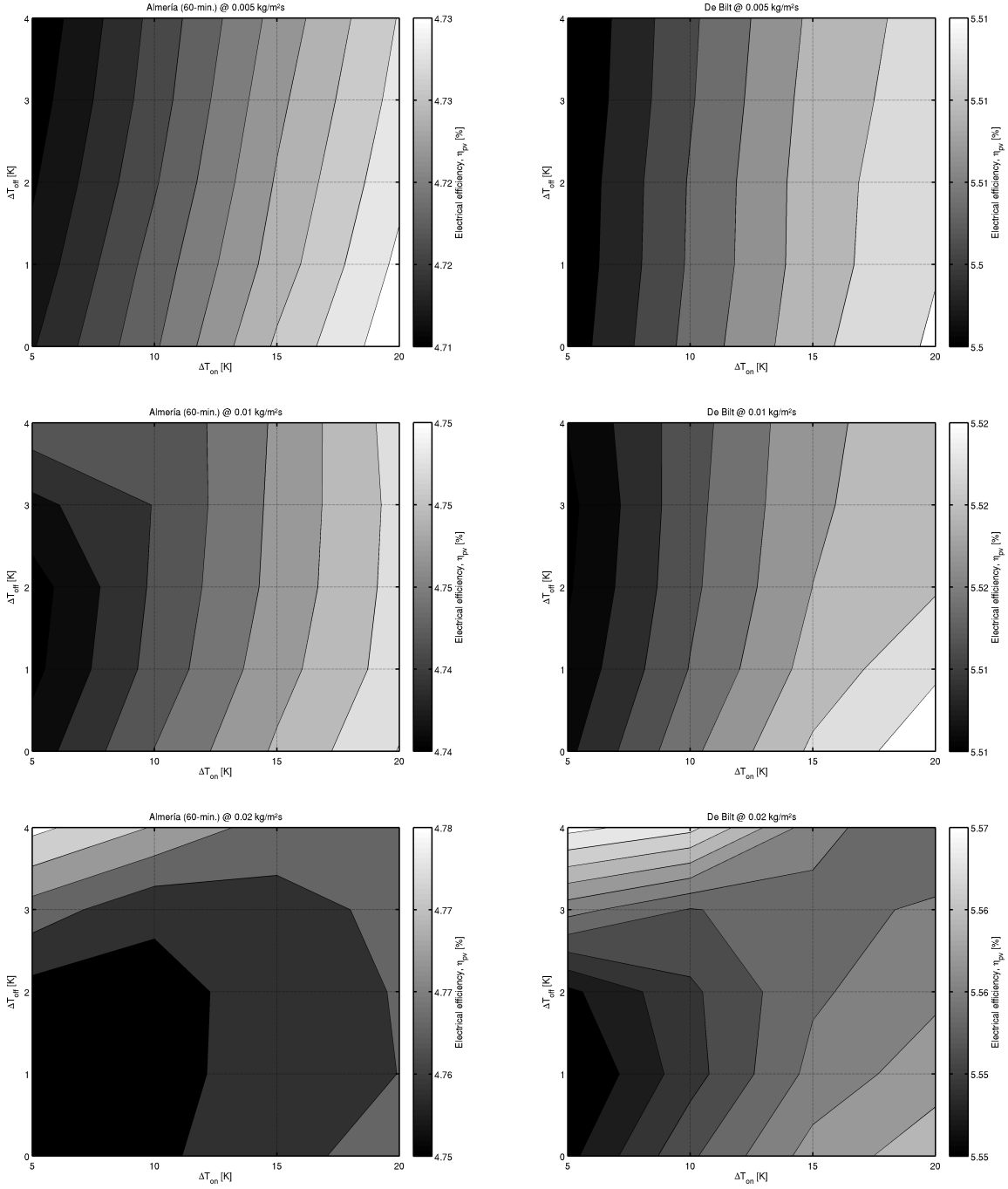

Figure 5.8.: Effect of ΔT_{on} and ΔT_{off} setpoints on the electrical efficiency ($\eta_{pv,el}$) of SDHW PV-T systems using DTSTLHC, by nominal specific mass flow rate (0.005, 0.01 and 0.02 Kg/m²s) and location (Almería and De Bilt).

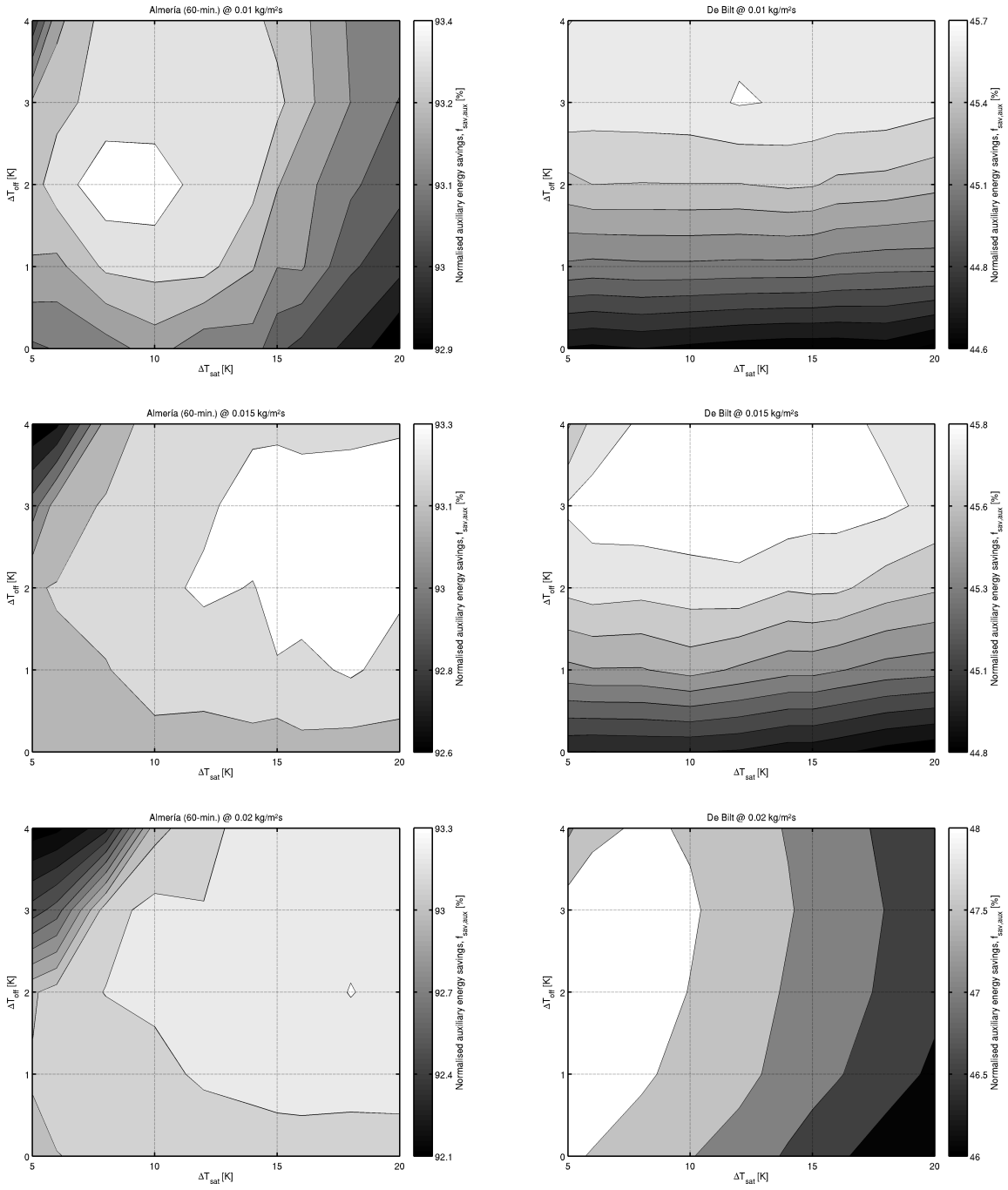

Figure 5.9.: Effect of ΔT_{sat} and ΔT_{off} setpoints on the fractional energy savings ($f_{sav,aux}$) of SDHW PV-T systems using DTSSHPC (0 K$\leq$ ΔT_{off} $\leq$2 K, ΔT_{on} = 3 K; 3 K$\leq$ ΔT_{off} $\leq$4 K, ΔT_{on} = 5 K; minimum specific mass flow rate, 0.005 Kg/m^{2}s), by nominal specific mass flow rate (0.01, 0.015 and 0.02 Kg/m^{2}s) and location (Almería and De Bilt).

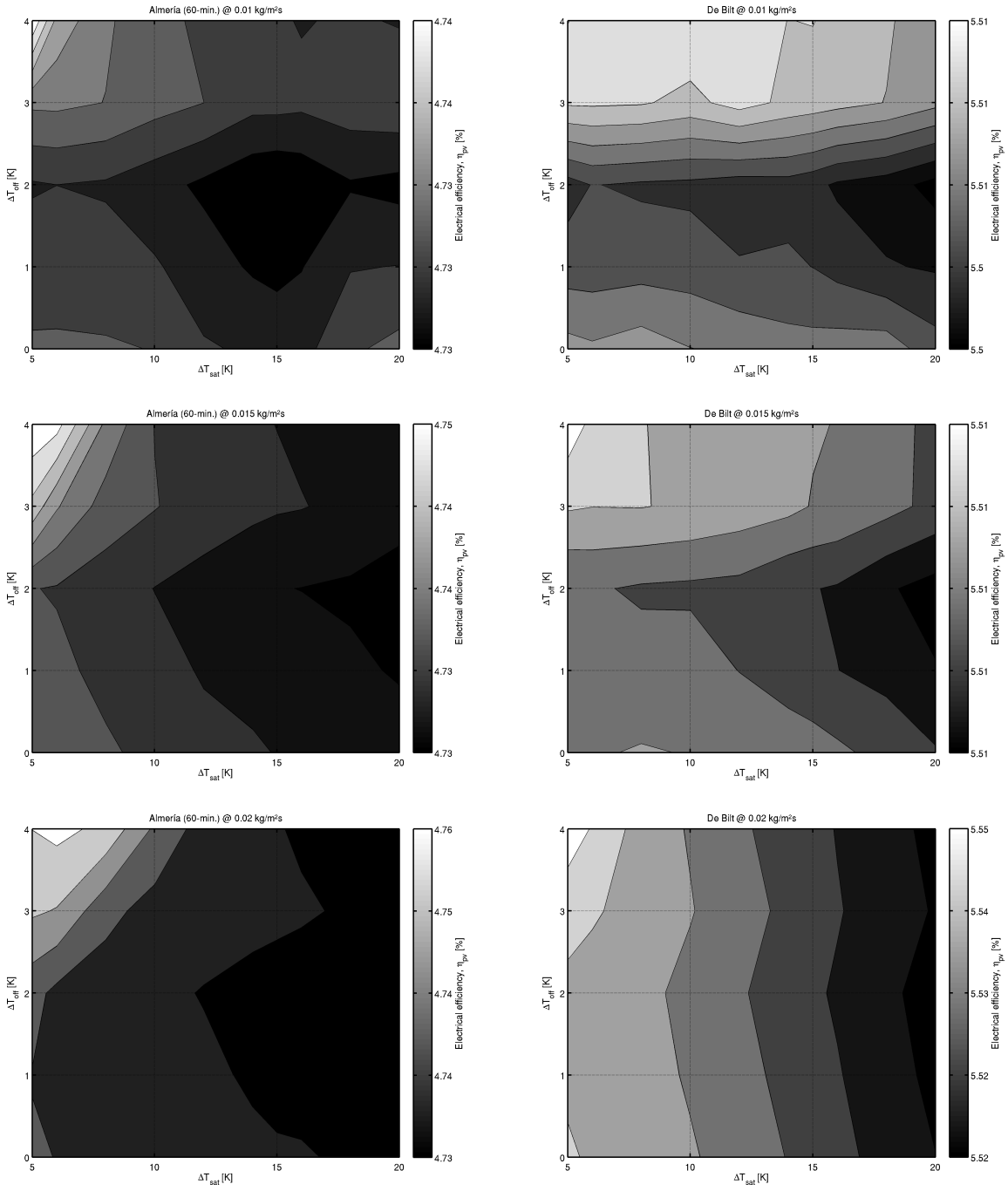

Figure 5.10.: Effect of ΔT_{sat} and ΔT_{off} setpoints on the electrical efficiency ($\eta_{pv,el}$) of SDHW PV-T systems using DTSSHPC (0 K $\leq \Delta T_{off} \leq$2 K, ΔT_{on} = 3 K; 3 K $\leq \Delta T_{off} \leq$4 K, ΔT_{on} = 5 K; minimum specific mass flow rate, 0.005 Kg/m²s), by nominal specific mass flow rate (0.01, 0.015 and 0.02 Kg/m²s) and location (Almería and De Bilt).

with distinctly different annual thermal performance levels, that is, the simulations for Lisbon and Almería produced similar results, as did those for Freiburg and De Bilt. Moreover, these results do not feature any obvious or consistent patterns. The same proved to be mostly true with regard to the electrical efficiency, shown in Figure 5.10, since no immediate pattern was detected, though a case can be made that higher ΔT_{sat} setpoints generally lead to underperformance in this regard, although marginally so (<0.1%). In conclusion, the effect of these variables on the auxiliary energy savings and electrical efficiency proved significantly more erratic and difficult to generalise than the effect of those evaluated concerning the DTSTLHC.

5.4.2. Comparison of systems using the same nominal flow rate and pipeline

A comparison between DTSSHPC- and DTSTLHC-operated SDHW PV-T systems using the same nominal flow rate and pipeline was initially undertaken. The analysis thus concerns simple, intuitive and arguably prevalent cases, namely standard systems where the option between DTSTLHC and DTSSHPC does not require additional equipment, since both can rely on the same pump and control unit, and limited knowledge or experience exists to fine-tune the nominal flow rate used by each control. In practice, this can represent standard DTSTLHC and ICC-based DTSSHPC implementations, achieving the nominal mass flow rate at full voltage (no off cycles), or more complex implementations. Nonetheless, the comparison was repeated for multiple nominal flow rates, and in each case, several controller setpoint combinations and compatible minimum mass flow rates were considered.

5.4.2.1. Thermal and electrical performance

Annual performance

The PV-T system performance comparison undertaken confirmed many of the same trends observed in previous studies focusing on non-hybrid systems but also adds more nuance: DTSSHPC enabled higher auxiliary energy savings than DTSTLHC, but not unconditionally in terms of minimum flow rates and controller settings for each location, and in many cases requiring significantly longer collection periods (in some instances reaching hundreds of hours annually) to do so. In particular, the advantage of DTSSHPC over DTSTLHC in terms of auxiliary energy savings was limited to 6.6% of the local $E_{aux,r}$ (or roughly 132 kWh), in an extreme scenario requiring the latter to be configured for the worst possible system performance. Conversely, DTSTLHC-operated systems could not outperform DTSSHPC-operated ones by more than 2.5% (or 55 kWh), even by assuming the latter is set to underperform. A more realistic assessment, based on the assumption that the controls are optimised for maximum auxiliary energy savings for each nominal flow rate, revealed the systems using DTSSHPC consistently outperforming those using DTSTLHC by up to 1.2% and by as little as less than 0.1%, and by

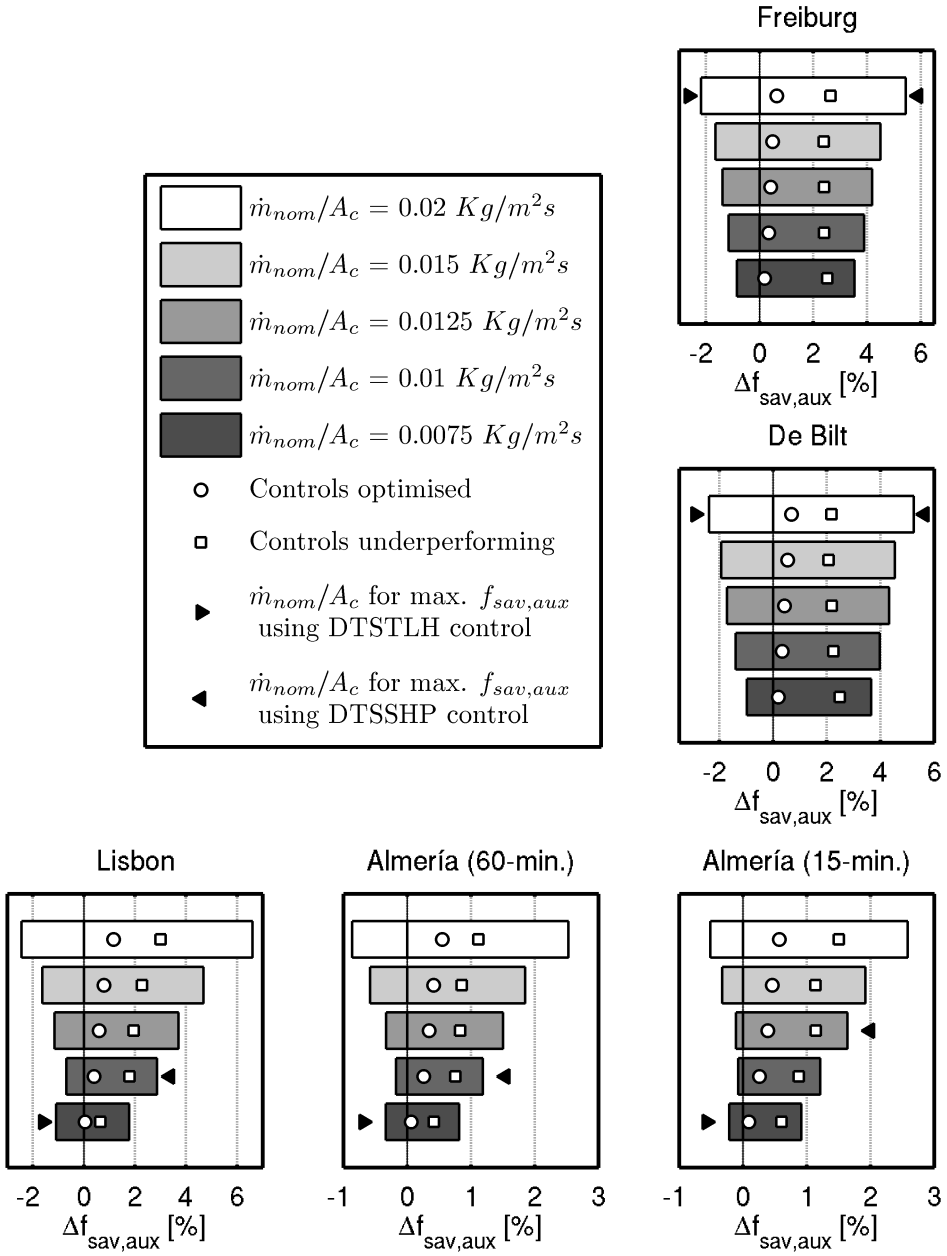

Figure 5.11.: Range of normalised auxiliary energy savings differences ($\Delta f_{sav,aux}$) between equivalent DTSSHP- and DTSTLH-controlled SDHW PV-T systems utilising the same nominal specific mass flow rate, by system location. The symbols ○ and □ denote the cases in which both controls are configured to perform at their best and worst, respectively, whereas ▶ and ◀ point to the absolute optimum nominal flow rates for DTSTLHC and DTSSHPC, also respectively.

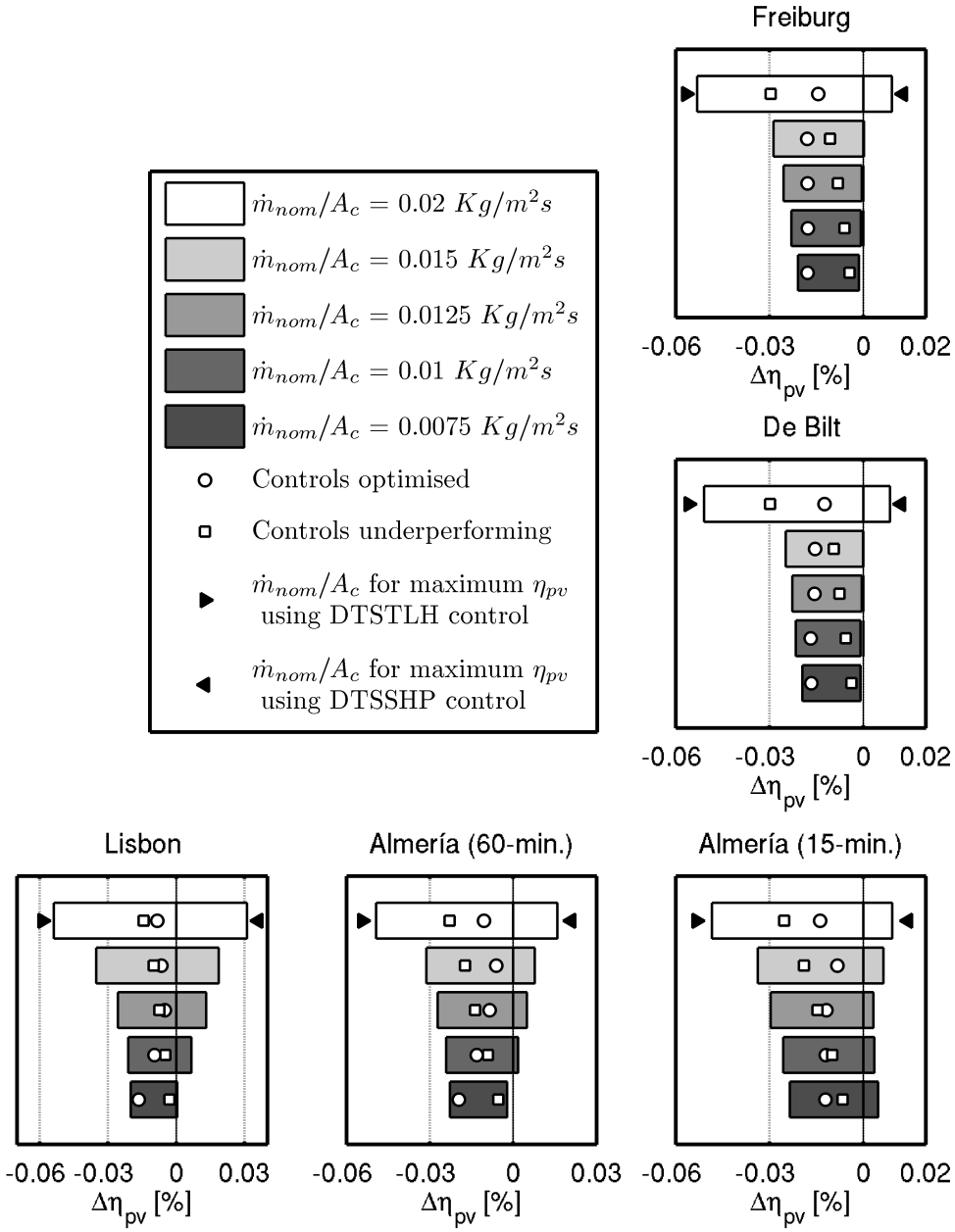

Figure 5.12.: Range of electrical energy efficiency differences ($\Delta\eta_{pv}$=$\eta_{pv,DTSSHP} - \eta_{pv,DTSTLH}$) between equivalent DTSSHP- and DTSTLH-controlled SDHW PV-T systems utilising the same nominal specific mass flow rate, by system location. The symbols ∘ and □ denote the cases in which both controls are configured to perform at their best and worst, respectively, whereas ▶ and ◀ indicate the absolute optimum nominal flow rates for DTSTLHC and DTSSHPC, respectively.

increasingly higher margins at higher nominal flow rates. Hence, the advantage of DTSSHPC – which arguably bears the burden of proof given its status, higher complexity and cost – concerning energy savings appears to be conditional and limited to single-digit percentages of the annual thermal load, as summarised in Figure 5.11.

The auxiliary energy savings advantage enabled by DTSSHPC over DTSTLHC contrasts with the effect on electricity generation, summarised in Figure 5.12. The simulation results show the electrical efficiency tends to be lower for DTSSHPC-operated SDHW PV-T systems using the same nominal mass flow rate as equivalent DTSTLHC-operated systems but only by less than 0.06% (absolute efficiency), or up to a numerical equivalent of 0.4% of the local $E_{aux,r}$. In comparison, the electrical efficiency advantage DTSSHPC was able to reach was only a little over 0.03% (or 0.2% of $E_{aux,r}$) and for an extremely biased comparison premised on the lowest-performing configuration of DTSTLHC, which was otherwise able to reach the best results for every system location and nominal mass flow rate.

Seasonal performance

The simulation results also show the fractional energy savings advantage of one controller over the other to vary throughout the year, as Figure 5.13 illustrates. In particular, the auxiliary energy savings advantage presented by DTSSHPC over DTSTLHC tended to peak during the Winter for Almería and Lisbon and drop markedly during the Summer, though not necessarily leading DTSTLHC to perform best during this period. Conversely, this proved not to be the case for the Freiburg and De Bilt systems simulated, the two northernmost and lowest-performing (in terms of auxiliary energy savings) ones, for which DTSSHPC was able to fare better in terms of energy savings during the Summer as opposed to the Winter, in apparent contradiction with the typical view that DTSSHPC excels in poor weather conditions. A suitable explanation for this apparent contradiction contends that oversizing leaves less room for improvement by opting for one control over the other, particularly during the stagnation-ridden Summer months, whereas undersized systems can more effectively take advantage of alternative controls all year round.

Concerning electrical efficiency differences, limited seasonal variations were observed in the simulations for SDHW PV-T systems configured for maximum electrical efficiency, which generally also found DTSTLHC performing best on a monthly basis. The exception proved to be the simulations for Almería using 15-minute resolution data, according to which DTSSHPC was able to outperform DTSTLHC during the Summer, in contrast with the results obtained using the same data at a 60-minute resolution, and underperforming even more during the Winter. This result reflects comparatively lower and higher average flow rates for DTSSHPC during the Winter and Summer months, respectively, which oversized ST systems can be predicted to experience due to increased stagnation in the Summer, though in this case prompted by the more unstable irradiance regime. At the same time, higher data resolution had a limited effect on the thermal performance seasonal variation but a more noticeable one on the electrical performance, as depicted in Figure 5.13.

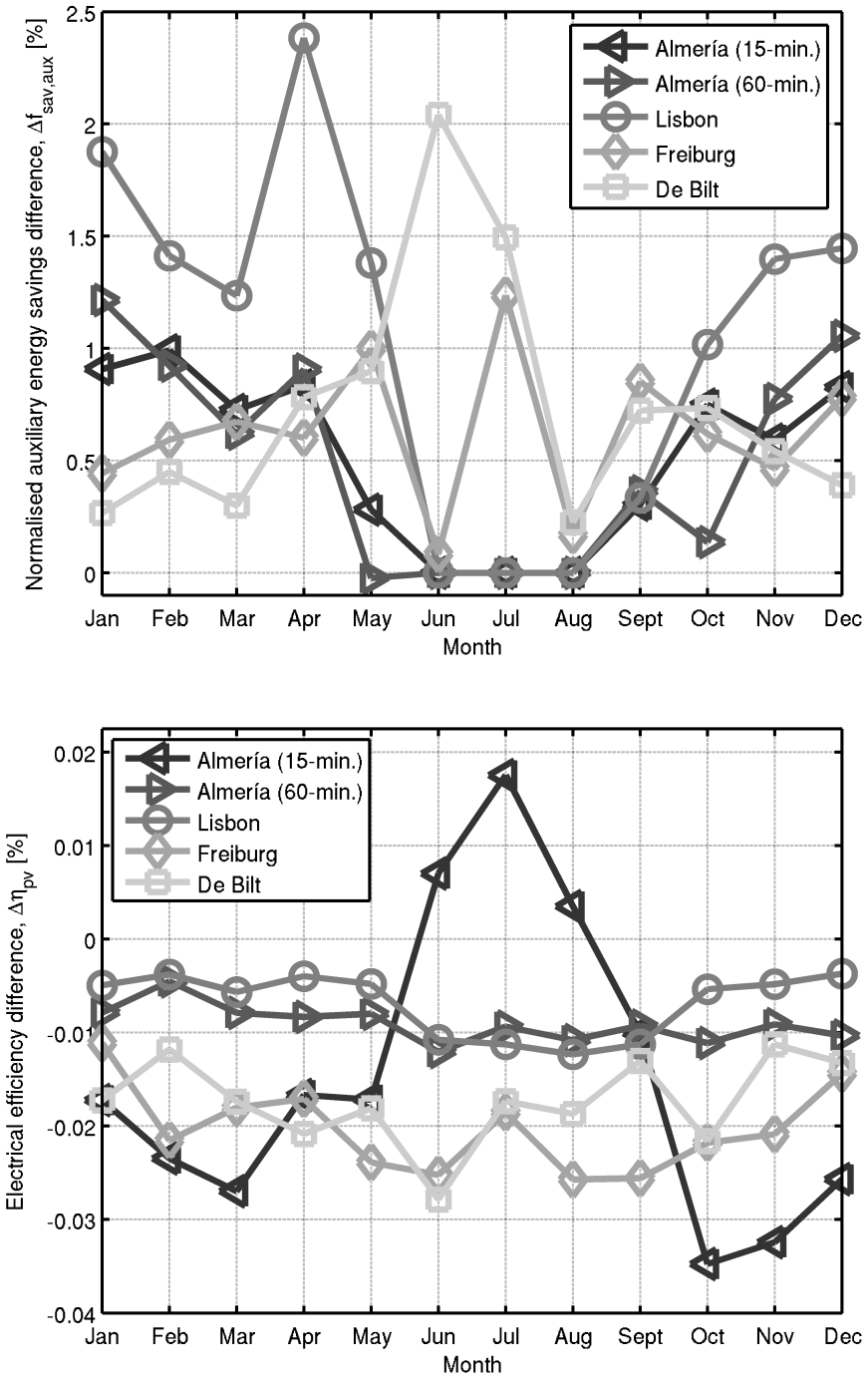

Figure 5.13.: Monthly normalised auxiliary energy savings (above) and electrical energy efficiency (below) differences between DTSSHPC- and DTSTLHC-operated SDHW PV-T systems using the same nominal flow rate (selected for the maximum annual $\Delta f_{sav,aux}$ and $\Delta\eta_{pv}$, respectively, to highlight the variations) and otherwise configured to reach the maximum auxiliary energy savings and electrical efficiency on an annual basis, respectively, for each location studied.

5.4.2.2. Parasitic performance

Maximising the auxiliary energy savings or the electrical efficiency in SDHW PV-T systems employing DTSSHPC and DTSTLHC revealed a propensity for longer collection periods with the former, as illustrated on the first row subplot of Figure 5.14. While not true for every location and nominal flow rate combination simulated, the pump running time increase reached up to hundreds of hours annually and also contributed to a higher parasitic energy consumption for many of the DTSSHPC-operated systems, assuming both controls rely on the same pump and pipeline (i.e., the pump power or pump efficiency function of the collector mass flow rate is the same), as depicted on the second row subplot of Figure 5.14. Moreover, the parasitic energy consumption increase for the DTSSHPC-operated systems reached up to approximately 0.1% of $E_{aux,r}$, if configured for maximum electrical efficiency, and up to 0.6%, if configured for maximum auxiliary energy savings, which for some cases proved to be sufficiently high to outweigh potential gains (up to 1.2% of $E_{aux,r}$) in an end use energy sense. As such, it may be necessary to configure DTSSHPC and DTSTLHC in PV-T systems so as to ensure the parasitic consumption difference doesn't outweigh the thermal or electrical performance advantage enabled.

5.4.2.3. Composite performance

The end result of the controls' simultaneous effects on the auxiliary energy savings, parasitic energy consumption and electrical efficiency of PV-T systems was studied in terms of primary energy efficiency and load provision cost-effectiveness. According to the simulations, summarised in Figures 5.15 and 5.16, DTSSHPC can still prove advantageous in relation to DTSTLHC in both regards but the opposite is also true: DTSSHPC-ooperated systems outperformed DTSTLHC-operated ones in terms of primary energy efficiency by as much as 6.4% of the reference primary energy demand, but also underperformed by up to 2.6%; similarly, the systems employing DTSSHPC exceeded the financial savings enabled by those using DTSTLHC by up to 6.4% (or around 35 €) of the reference load provision cost, but in other cases fell behind by up to 2.9% (or 15 €). More substantive results were revealed through optimisation: optimising both controls as far as setpoints and the minimum mass flow rate are concerned led to performance margins up to 1.5% and 0.2% of the reference primary energy demand for DTSSHPC over DTSTLHC and vice-versa, respectively, and likewise by 1.5% ($\backsimeq$6 €) and 0.2% ($<$ 1 €) of the reference load provision cost. Hence, the persistent advantage of DTSSHPC over DTSTLHC within the aforementioned constraints appears to be currently limited to no more than 2% of the reference primary energy demand and load provision cost.

On the other hand, the normalised FS and PES advantage presented by DTSSHPC over DTSTLHC also tended to increase with the nominal flow rate and surpassed the maximum normalised auxiliary energy savings advantage level determined previously (1.2%). This outcome mainly stems from the dominant role of the auxiliary energy savings differences – which also tended to increase with the nominal flow

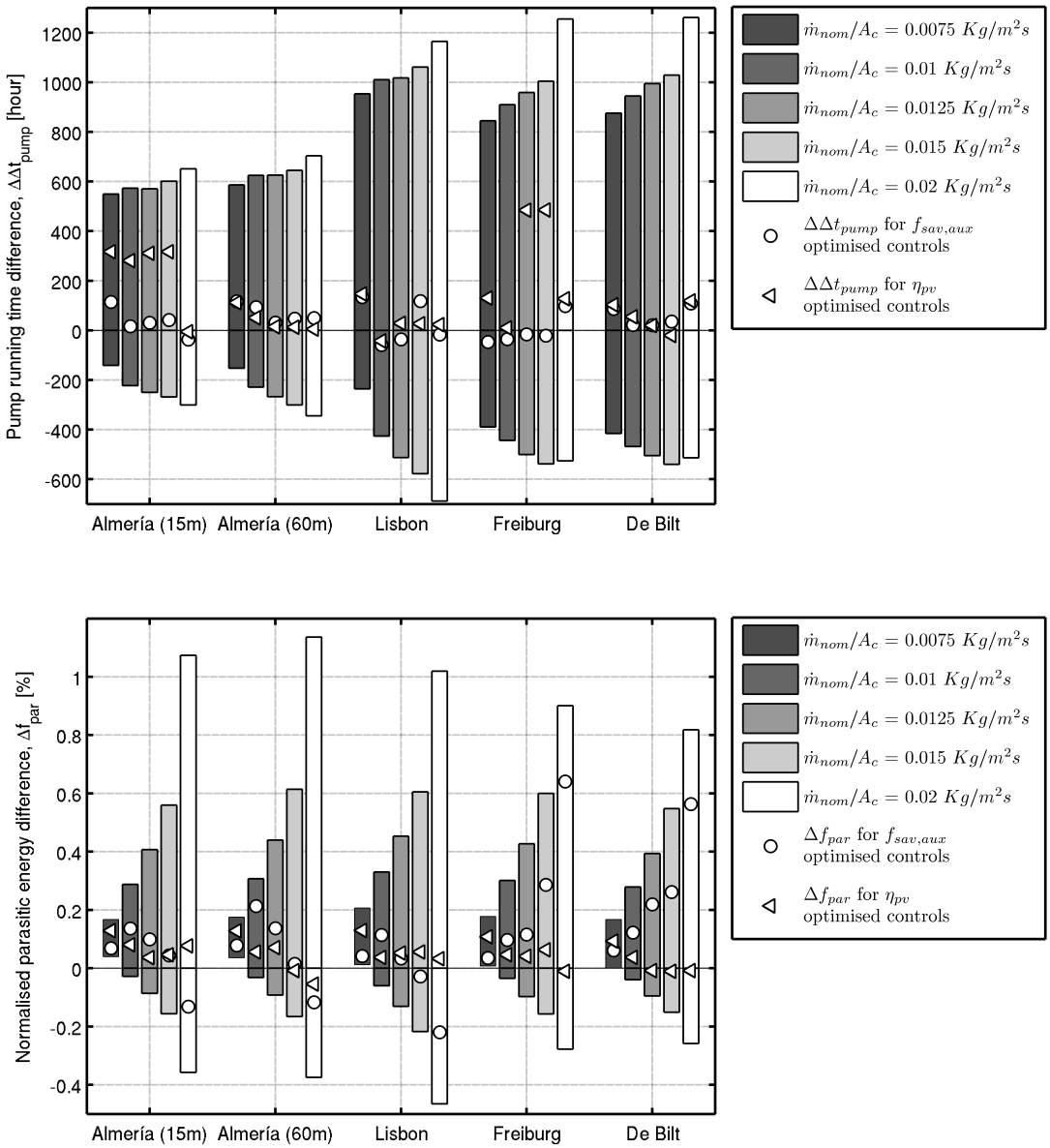

Figure 5.14.: Pump running time (first row plot; $\Delta\Delta t_{pump} = \Delta t_{pump,DTSSHPC} - \Delta t_{pump,DTSTLHC}$) and normalised parasitic energy (second row plot; $\Delta f_{par} = [E_{par,DTSSHPC} - E_{par,DTSTLHC}]/E_{aux,ref}$) differences between DTSSHPC- and DTSTLHC-operated SDHW PV-T systems configured to reach the maximum auxiliary energy savings (denoted by the symbol:○) and electrical energy efficiency (denoted by the symbol:◁), within the complete range of $\Delta\Delta t_{pump}$ and Δf_{par} (pipeline #1, cf. Table D.1) results obtained.

rate as depicted in Figure 5.7 – but also parasitic energy reductions, namely for the Almería and Lisbon systems. In these systems, DTSSHPC was also found to require less parasitic energy than DTSTLHC to reach the maximum auxiliary energy savings advantage – cf. Figure 5.14. Thus, the main advantage of DTSSHPC for use in PV-T systems appears to be its potential for increased auxiliary energy savings, which was found to exist at all but the lowest flow rates evaluated.

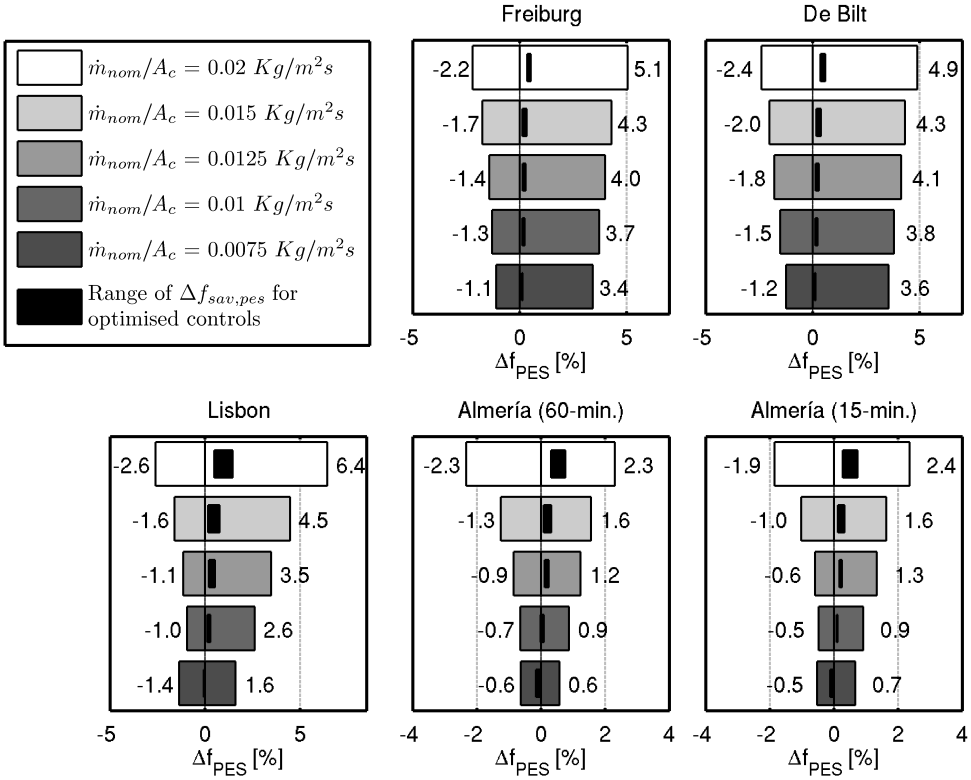

Figure 5.15.: Range of normalised primary energy savings differences (Δf_{PES}) between equivalent DTSSHPC- and DTSTLHC-operated SDHW PV-T systems utilising the same $\dot{m}_{nom}/A_c$. The narrow black band represents the Δf_{PES} range for gas- and electricity-assisted PV-T systems using PES-optimised controls.

5.4.3. Unconstrained comparison

The previous analysis was limited to DTSSHPC- and DTSTLHC-operated PV-T systems bound by the same nominal flow rate and pipeline. While this can intuitively demonstrate key differences between the controls, it excludes the lowest specific mass flow rate for DTSTLHC (0.005 Kg/m²s) from consideration and prevents global optimisation. The analysis presented next removes these constraints.

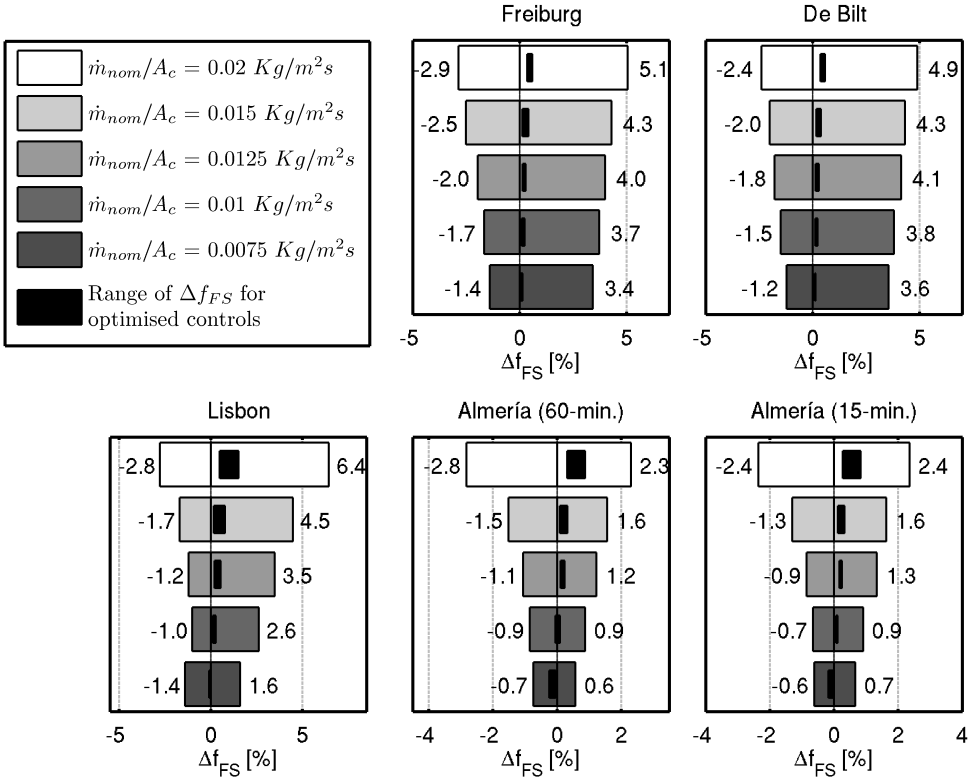

Figure 5.16.: Range of normalised financial savings differences (Δf_{FS}) between equivalent DTSSHPC- and DTSTLHC-operated SDHW PV-T systems utilising the same $\dot{m}_{nom}/A_c$. The narrow black band represents the Δf_{FS} range for gas- and electricity-assisted PV-T systems using FS-optimised controls.

Table 5.2.: Highest normalised auxiliary energy savings ($f_{sav,aux}$) obtained for SDHW PV-T systems using DTSSHPC and DTSTLHC and the corresponding nominal specific mass flow rate ($\dot{m}_{nom}/A_c$), for each location considered.

	DTSSHPC		DTSTLHC		
Location	$\dot{m}_{nom}/A_c$ [Kg/m²s]	$f_{sav,aux}$ [%]	$\dot{m}_{nom}/A_c$ [Kg/m²s]	$f_{sav,aux}$ [%]	$\Delta f_{sav,aux}$ [%]
Almería (15-min.)	0.0125	93.89	0.0075	93.69	0.19
Almería (60-min.)	0.0100	93.38	0.0075	93.19	0.19
Lisbon	0.0100	79.83	0.0075	79.60	0.23
Freiburg	0.0200	53.68	0.0200	53.05	0.63
De Bilt	0.0200	48.42	0.0200	47.74	0.69

5.4.3.1. Electrical performance

Easing the comparison's constraints did not alter the previous section's findings in terms of annual electrical efficiency-optimised controls, which had determined DTSTLHC to be marginally better. Unsurprisingly, DTSTLHC operation of SDHW PV-T systems at a lower flow rate did not improve their electrical efficiency and, since the highest efficiencies were consistently obtained at the highest nominal flow rate (0.02 Kg/m2s) for either controller as highlighted in Figure 5.12, systems using DTSTLHC maintained consistent electrical efficiency advantages over those using DTSSHPC in all locations when configured for maximum electrical efficiency. Moreover, DTSSHPC underperformed in this regard even though it tended to require comparatively longer collection periods (up to 128 hours per year and generally decreasing with insolation) for maximum electrical efficiency.

Magnitude-wise, the electrical efficiency advantage of DTSTLHC-operated PV-T systems was limited to 0.02% (absolute efficiency; roughly 2 kWh or 0.1% of the local $E_{aux,r}$) versus optimised DTSSHPC-operated systems, but more otherwise. In particular, DTSTLHC-operated systems were found to outperform DTSSHPC-operated ones by as much as roughly 0.07% (roughly 0.4% of $E_{aux,r}$), if the latter group was configured to perform at its worst, though the opposite case revealed advantages for DTSSHPC up to 0.06% (approximately 0.5% of $E_{aux,r}$), which is arguably a more extreme comparison. Hence, DTSSHPC does not appear to be a safe control option to enhance the electrical efficiency of PV-T systems.

5.4.3.2. Thermal performance

Global optimisation of each control in terms of auxiliary energy savings revealed consistent advantages of DTSSHPC over DTSTLHC but within a narrower magnitude range, as summarised in Table 5.2. According to the results obtained, DTSSHPC consistently outperformed DTSTLHC in terms of normalised auxiliary energy savings for all locations and by progressively higher margins for the systems with lower performance levels (Almería, Lisbon, Freiburg and De Bilt, in that order), requiring comparatively longer collection periods to do so (17-121 hours per year). However, the magnitude of these differences remained within 0.2-0.7% of $E_{aux,r}$, and thus the low and high ends of the range increased and decreased, respectively, relative to what was previously determined for nominal flow rate-constrained comparisons (<0.1% and 1.2%). Hence, the annual thermal performance advantage of DTSSHPC-operated SDHW PV-T systems over those using DTSTLHC remained consistent when both controls are optimised but is lower than previously determined and does not exceed 1% of the end use energy demand.

Notwithstanding these results, the maximum conceivable advantages of one control over the other – namely if one or the other is not configured for optimum performance – increased due to the loosened constraints. Based on the simulations conducted, DTSSHPC can conceivably outperform DTSTLHC by between 2-7% of $E_{aux,r}$, or underperform by 1-4%. Moreover, the magnitude of these differences

decreased with the performance level, as was also previously established for the contrained comparisons between optimised SDHW PV-T systems.

5.4.3.3. Composite performance

The global optimisation of each control in terms of load provision cost-effectiveness and primary energy efficiency did not provide for the same level of consistency previously obtained within the thermal and electrical performance comparisons. In particular, most of the PV-T systems simulated performed best using DTSSHPC but only consistently so with regard to both figures of merit and both auxiliary systems for Freiburg, De Bilt and Almería using 15-minute resolution data, as illustrated in Figure 5.17. The other salient detail from these comparisons is that the normalised primary energy and financial savings differences dropped up to 0.3% (absolute) relative to normalised auxiliary energy savings differences, which were previously determined to have favoured DTSSHPC but only by 0.7% of $E_{aux,r}$ and highest for low $f_{sav,aux}$ systems. In effect, this makes Freiburg and De Bilt arguably the only locations favourable to DTSSHPC in a meaningful sense from the standpoint of primary energy efficiency and load provision cost-effectiveness (>0.1%).

These results indicate the controller configurations required for optimum performance, according to each figure of merit, do not entail advantages for either controller on all three relevant performance components: parasitic, electrical and thermal. In other words, it was not possible to achieve increased auxiliary energy savings, electrical energy efficiency gains and lower parasitic energy consumptions simultaneously. Nevertheless, the clearest and most decisive trend leading to these FS and PES results proved to be improved auxiliary energy savings by using DTSSHPC instead of DTSTLHC, which was observed in all cases except one (and only by 0.002% of $E_{aux,r}$), and was the most significant magnitude-wise, reaching tenths of a percentage point of $E_{aux,r}$ in many cases. Figure 5.17 illustrates how the compromises required for optimum FS (and PES, as the results for this figure of merit were equivalent) in SDHW PV-T systems using DTSSHPC and DTSTLHC translate in terms of PV yield, parasitic energy and auxiliary energy savings differences.

Pump efficiency

Pump efficiencies for small SDHW systems have improved in recent years, as discussed in Chapter 1. Though the reference pump reproduced is among the latest generation of pumps, an attempt was made to simulate how the results shown in Figure 5.17 can be expected to change if the improvements continue. For this purpose, an extreme case was considered: a 100% efficiency pump, and otherwise equivalent to the main pump considered, namely in terms of range of operation. The results of this experiment are summarised in Figure 5.18 and show the DTSSHPC-operated PV-T systems consistently outperforming DTSTLHC-operated ones, though in some cases the margins favourable to DTSSHPC dropped slightly in relation to the results featured Figure 5.17, namely for gas-assisted systems in Freiburg and De Bilt.

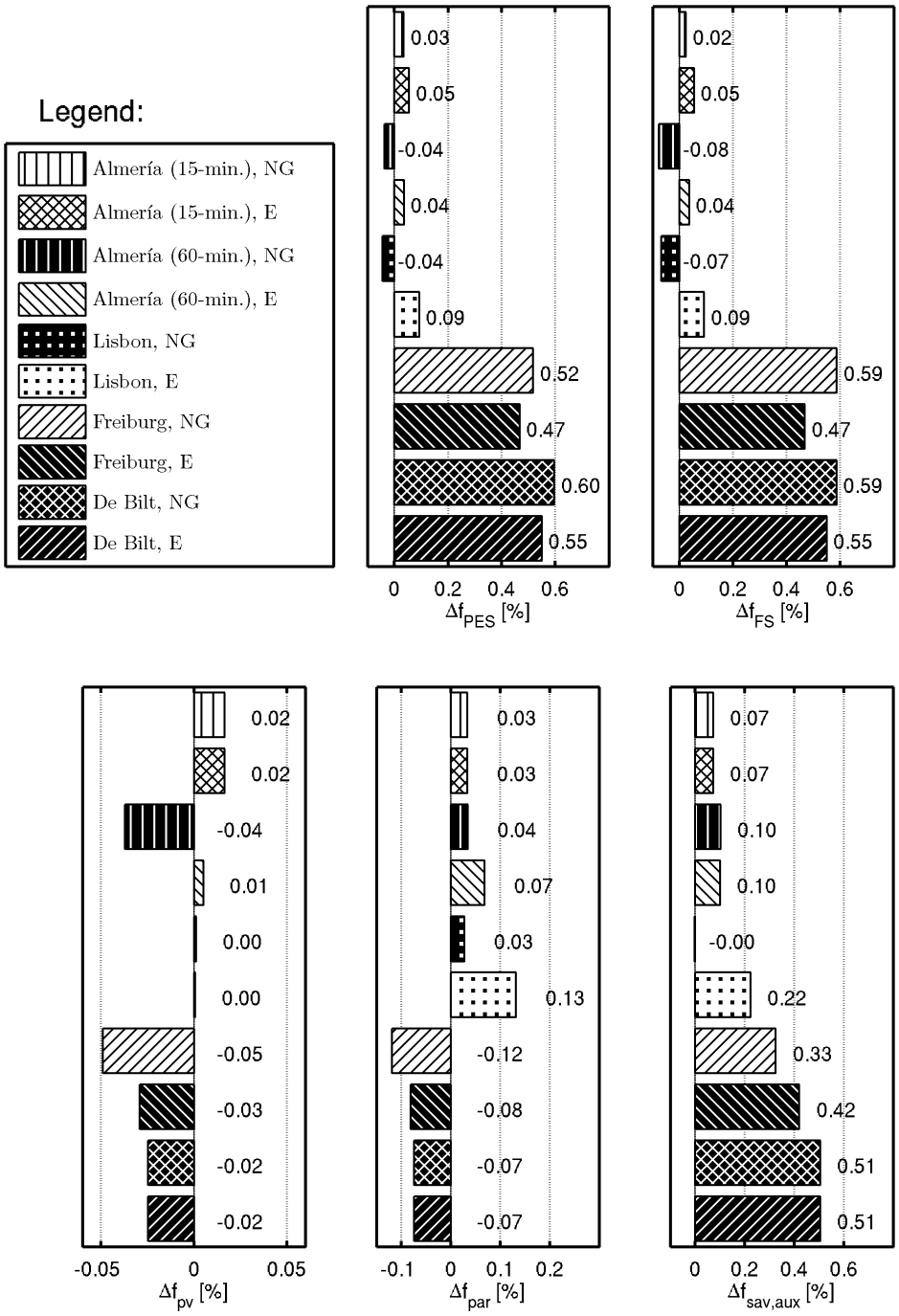

Figure 5.17.: Normalised primary energy (Δf_{PES}) and financial (Δf_{FS}) savings differences between DTSSHPC- and DTSTLHC-operated SDHW PV-T systems configured for maximum PES and FS, respectively (top row plots), and normalised PV yield (Δf_{pv}), parasitic energy (Δf_{par}) and auxiliary energy savings ($\Delta f_{sav,aux}$) differences due to FS-optimisation of each system (bottom row plots), by location and auxiliary heater (NG, natural gas-fired; E, electrical).

Despite this discrepancy, the overall results are more in line with the consistent normalised auxiliary energy savings potential of DTSSHPC identified earlier, which saw increasingly undersized systems benefit more from this control, and suggest higher pump efficiencies will tend to favour DTSSHPC but not decisively so.

Energy prices and financial viability

Energy prices are among the factors predicted to influence the controls' financial performance, namely the relation between parasitic and auxiliary energy prices (Naumann and Wolfson, 1984). The basic rationale behind this is that DTSSHPC requires more parasitic energy to enhance the thermal enery collection relative to DTSTLHC and displace auxiliary energy use, and thus comparatively low auxiliary energy prices make it uncompetitive. This was confirmed in a sensitivity analysis on natural gas prices, which saw higher natural gas prices make optimised gas-assisted SDHW PV-T systems using DTSSHPC increasingly more financially appealing than those using DTSTLHC. Nonetheless, the normalised financial savings differences illustrated in Figure 5.19 generally remained under the normalised auxiliary energy savings limit as the gas prices were varied. Moreover, doubling the reference natural gas prices was sufficient to lead all optimised gas-assisted DTSSHPC-operated systems simulated to outperform their DTSTLHC-operated counterparts, albeit marginally, whereas systems using electrical heaters were already found to do so at reference energy prices, as Figure 5.17 illustrates. In turn, higher electricity prices essentially shift both plots in Figure 5.19 further to the right, that is, requiring higher gas prices for a comparable effect on the financial savings difference.

Then, the question remaining is that of profitability and how energy prices, initial costs and other factors can influence it. Back in the late 1970s, the additional costs of ICC- or PAFC-based DTSSHPC suitable for standard pumps averaged around 15$ (60.3$ in 2017, or around 51.4 € using an exchange rate of 1 USD = 0.8526 €), according to one survey, but currently those and PWM-based variants of DTSSHPC can be found in low-end control units along with standard DTSTLHC implementations, and thus at virtually no additional cost (Pejsa et al., 1978). In that case, DTSSHPC can be predicted to be financially viable as long as the normalised financial savings advantage is positive – which proved not to be the case for some gas-assisted systems at reference energy prices – and the choice of controller does not entail extra maintenance. On the other hand, if additional costs are incurred by opting for DTSSHPC in the PV-T systems simulated, either initially or later on, the investment can be expected to be profitable in some cases at reference energy prices and if the initial costs or present value of future costs remain under approximately 32 €, according to net present value (NPV) calculations summarised in Table 5.3 and based on optimised controls, a discount rate of 0.25%, fixed annual payments equivalent to the annual FS over a ten year period of system operational lifetime. In contrast, biased comparisons predicated on poorly configured DTSTLHC-operated systems show investments up to 39-457 €, depending on the system, as being technically viable. It is important to stress, however, that these calculations concern the

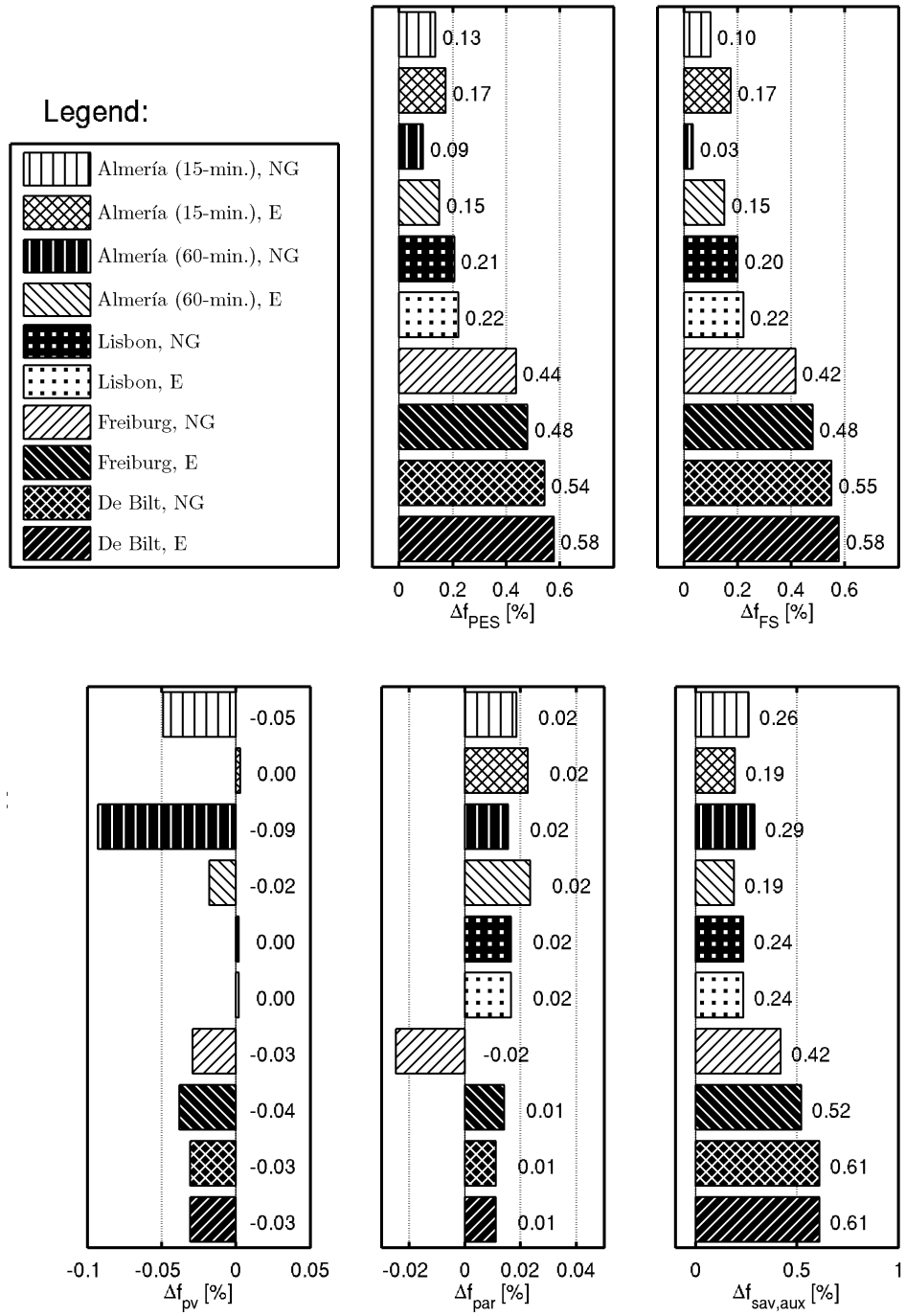

Figure 5.18.: Normalised primary energy (Δf_{PES}) and financial (Δf_{FS}) savings differences between DTSSHPC- and DTSTLHC-operated SDHW PV-T systems configured for maximum PES and FS, respectively (top row plots), and normalised PV yield (Δf_{pv}), parasitic energy (Δf_{par}) and auxiliary energy savings ($\Delta f_{sav,aux}$) differences due to FS-optimisation of each system (bottom row plots; from left to right, respectively), assuming a fictitious 100% efficiency circulation pump, by location and auxiliary heater (NG, natural gas-fired; E, electrical).

Table 5.3.: Normalised financial savings (Δf_{FS}) and net present value (NPV) difference incurred by opting for SDHW PV-T system using DTSSHPC instead of DTSTLHC, assuming reference energy prices, 0.25% discount rate, and fixed annual payments over a ten year period (NG stands for natural gas-fired backup heater, and E stands for electrical backup heater).

Location		Optimised controls		Best case for DTSSHPC	
	Backup system	Δf_{FS} [%]	NPV [€]	Δf_{FS} [%]	NPV [€]
Almería (15-min.)	NG	0.02	0.40	2.34	39.25
	E	0.05	2.39	2.44	107.19
Almería (60-min.)	NG	-0.08	-1.30	2.34	39.27
	E	0.04	1.58	2.44	107.33
Lisbon	NG	-0.07	-1.28	6.42	121.22
	E	0.09	4.22	6.56	299.78
Freiburg	NG	0.59	9.76	6.59	109.47
	E	0.47	31.89	6.70	457.19
De Bilt	NG	0.59	11.86	6.82	137.90
	E	0.55	20.25	6.86	252.75

financial viability of DTSSHPC relative to DTSTLHC in SDHW systems, and not the SDHW system itself, which was not addressed in this study.

5.5. Discussion

5.5.1. Practical considerations

The simulations suggest DTSSHPC-operated SDHW PV-T systems can outperform DTSTLHC-operated ones in terms of primary energy and financial savings, but the gains proved dependent on several factors including the system location and local energy prices, and overall were quite low. In particular, the performance advantage enabled by DTSSHPC appears to be currently limited to single-digit percentages of the reference primary energy demand and load provision cost at best, which is lower but consistent with the results reported for non-hybrid systems (the relative, as opposed to normalised, end use energy savings advantage presented by DTSSHPC over DTSTLHC in this study is in the range of 0.2-1.3%, whereas the literature for non-hybrid systems presents relative energy collection increases in the range of 1-4% and load provision cost decreases in the range of 0.5-2.0%), but arguably too low in relation to modelling errors to allow for confident decision-making (Pejsa et al., 1978; Pejsa, 1978; Schlesinger, 1978; Swanson and Ollendorf, 1979; Furbo and Shah, 1996). As a result, opting for DTSSHPC does not appear to be a conservative decision, particularly since this control is more complex, can introduce power quality issues, requires higher-frequency switching and is for that reason more likely to fail

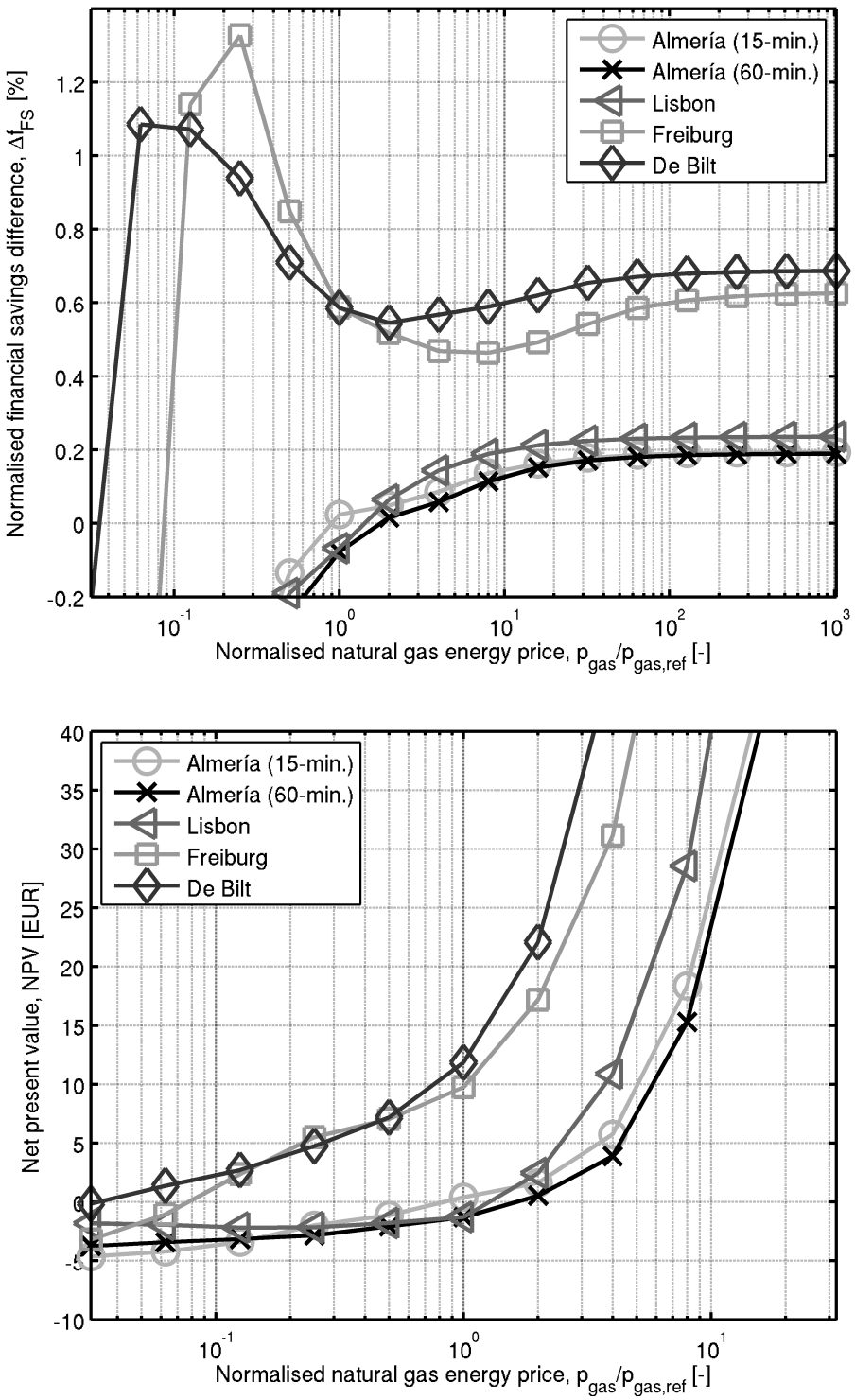

Figure 5.19.: Normalised financial savings (first row plot) and net present value (second row plot, in €) differences between SDHW PV-T systems using optimised DTSSHPC and DTSTLHC, as a function of the normalised natural gas price for each location (normalised in relation to each location's reference price) .

sooner, and by labour cost standards in several European countries (roughly 14-33€/hour in 2016 for the countries targeted, and by coincidence decreasing with the local insolation), one additional hour-long maintenance operation can be enough to offset the financial gains predicted assuming optimised controls (Eurostat, 2017b). Another concern is the need for optimised controls to certifiably reach a competitive performance, since this can be difficult to verify and correct in a practical way. In conclusion, DTSSHPC should be reserved for systems where it can certifiably produce substantial benefits over DTSTLHC, which currently does not appear to be the case for SDHW PV-T systems such as those simulated.

5.5.2. Limitations

The activities summarised here can be said to have limitations that can and should be addressed in future efforts. The most important are, in the writer's opinion, the relatively low resolution climate data used and the PV-T collector model accuracy. The first point limits the analysis to relatively stable irradiance regimes that may underestimate the potential of DTSSHPC to achieve higher auxiliary energy savings though possibly a higher parasitic energy consumption too. The two climate data sets for Almería (based on 15 and 60 minute samples) were able to translate this to some extent, since the higher resolution data set led to, for instance, higher normalised auxiliary energy savings and normalised financial savings, though the system analysed for this purpose was perhaps not the most conclusive one in light of the high insolation for Almería and the trends uncovered with respect to system sizing. Concerning the second point, the PV-T collector model used is a pragmatic solution that will likely not be able to accurately reproduce the collector behaviour for more unstable irradiance regimes and transients than those reproduced in this study. In particular, the cell temperature model is partly based on steady-state conditions and weather variables, and although the cell efficiency temperature coefficient is not high, the model is bound to introduce errors during transients. In this regard, a two-node PV-T collector model is a step in the right direction.

A less relevant point, in the writer's opinion, can be made about the pool of controller setpoints used. Concretely, DTSSHPC was simulated using lower ΔT_{on} setpoints than DTSTLHC, though the difference is not significant (2 K), and this can be understood to favour the former with regards to thermal energy collection. However, as Winn (1983) notes, DTSTLHC using a similarly low ΔT_{on} setpoint would also cause more pump cycling, which is one of the reasons why ΔT_{on} setpoints are higher for this control, the other being higher parasitic energy costs. Moreover, using timers to deal with cycling can facilitate low-ΔT_{on} DTSTLHC operation but can also increase parasitic energy costs. Hence, there are grounds to account for this limitation. Another point can be made about the number of setpoint combinations considered for each control, which was higher for DTSSHPC. This mainly stems from the more non-linear effect of ΔT_{sat} on DTSSHPC performance in comparison with the more predictable effect of ΔT_{on} on DTSTLHC performance, and should not constitute significant bias. In any case, both these limitations arguably reflect

positively on DTSTLHC, since if addressed higher performances could potentially be attained using this control, and thus reinforce the conclusions reached.

5.5.3. Outlook

This chapter describes the first known comparison between SDHW PV-T systems using DTSSHPC and DTSTLHC as supply-loop pump controllers. As it stands, the former shows limited and conditional benefits relative to the latter in many regards but most importantly, does not demonstrate a clear affinity with the specific attributes of PV-T technology, namely electricity generation. Thus, electricity generation is not expected to be the main reason to opt for DTSSHPC in PV-T systems, but in general, it was also not shown to produce tangible benefits over DTSTLHC.

5.6. Summary

The following points can be summarised from this chapter:

- A simulation-based comparison between SDHW PV-T systems using DTSTLHC and DTSSHPC was conducted. The analysis eschewed the conventional comparison and instead focused on optimised controls for a definitive assessment of their differences while also considering extreme scenarios, however unlikely;

- DTSSHPC was shown to be able to increase the auxiliary energy savings relative to DTSTLHC by up to 7% of the reference auxiliary energy consumption, in an extreme scenario predicated on the latter's underperformance, but also to decrease them by 5% in another extreme scenario based on DTSSHPC underperformance. In turn, global optimisation of both controls consistently led DTSSHPC-operated systems to auxiliary energy savings increases between 0.2% and 0.7% of the reference end use thermal energy demand;

- The normalised auxiliary energy savings advantage enabled by DTSSHPC over DTSTLHC was found to be negatively correlated with the auxiliary energy savings level, for the same system size, and the insolation level;

- The auxiliary energy savings advantage presented by DTSSHPC was also found to have a seasonal variation reflecting the system size: comparatively undersized systems tended to perform best during the Summer, unlike oversized systems which performed best during the Winter;

- DTSSHPC-operated PV-T systems configured for maximum electrical efficiency generally underperformed relative to equivalent DTSTLHC-operated systems. Nevertheless, the maximum difference amounted to less than 0.07% (absolute) or the equivalent to 0.4% of the reference end use energy demand;

- DTSSHPC was able to surpass DTSTLHC in terms of primary energy and financial savings, if configured for the respective optimum performance, in many of the systems simulated but not all, namely in oversized gas-assisted systems. In general, the advantage presented by DTSSHPC over DTSTLHC also tended to decrease with the fractional energy savings level;
- Lower parasitic and auxiliary energy price ratios were to some extent found to be beneficial to DTSSHPC in relation to DTSTLHC in terms of load provision cost-effectiveness, particularly by bringing out the former's auxiliary energy savings potential, whereas higher pump efficiencies also proved advantageous from the standpoint of primary energy efficiency;
- In conclusion, DTSSHPC is not predicted to produce tangible risk-free benefits in relation to DTSTLHC for use in SDHW PV-T systems, and as such the latter should be preferred as the more conservative of the two.

6. Conclusions, contributions and future work

6.1. Conclusions

The work described in this document allowed a set of conclusions to be drawn. These concern the research questions formulated, all three of which related with the study of PV-T technology and systems: the development of fast and accurate single-node dynamic PV-T collector model compatible with flow control studies and parameter estimation; the selection of differential temperature controller setpoints for PV-T systems, according to criteria of stability and cost-effective pump use; and, the comparison of supply-loop flow controls for use in SDHW PV-T systems.

6.1.1. Dynamic PV-T collector model

The modelling activities included the development of a dynamic single-node multi-segment PV-T collector model. The model developed extends the validated single-node Perers (1993) model for non-hybrid collectors to PV-T collectors but considers a different approach than the one used by Amrizal et al. (2013) for their validated model, instead adopting the standard Florschuetz (1979) modelling approach for consistency. The model was also able to overcome some of the limitations of the cell temperature model used by Amrizal et al. (2013) by adopting a zero-capacitance estimator compatible with a non-negligible heat loss coefficient temperature dependence, PV generation and based on the assumption the collector efficiency factor construct remains constant and valid during transients and stagnation. The model was validated according to a three-pronged approach. A study of the PV-T collector efficiency factor sensitivity to the mass flow rate, fluid temperature and irradiance was undertaken to confirm it to be a weak function of these variables, which proved to be the case. The second step focused on comparisons against published step responses of comparable models and an almost 30-minute test sequence, both for non-hybrid operation, which the model was generally able to reproduce. The third step focused on hybrid operation, namely the cell temperature model, which was compared with the validated HWB model for flow rate, fluid inlet temperature and irradiance steps, as well as in daily and annual SDHW system simulations, all of which revealed minimal yet coherent differences in terms of electrical efficiency.

6.1.2. Differential temperature controller setpoints for PV-T systems

Analytical and numerical design methods for the selection of differential temperature controller setpoints in PV-T systems were developed based on previous efforts for non-hybrid systems and compared. It was determined that the turn-on (ΔT_{on}) and turn-off (ΔT_{off}) setpoints for stable and cost-effective operation of PV-T systems generating electricity should ideally be higher and lower, respectively, than those for non-hybrid operation or equivalent non-hybrid systems, and more so at higher irradiances, due to the temperature dependence of photovoltaic conversion process and the reduced absorption. However, the magnitude of these changes due to PV conversion were reasoned to be negligible and of limited practical relevance for representative PV-T systems and conditions. Finally, the effect of measurement errors on the conditions for stable and cost-effective operation in PV-T systems was predicted and translated into analytical relations in what amounts to a revision and extension of the work of Alcone and Herman (1981) to PV-T systems.

6.1.3. Comparison of DTSSHPC and DTSTLHC supply-loop pump controllers for SDHW PV-T systems

A comparison between DTSSHPC and DTSTLHC supply-flow controllers for use in SDHW PV-T systems was conducted. These two prominent controllers were compared by way of an extensive set of dynamic simulations for Central and Western European locations and using optimisation to minimise controller configuration-induced bias. The simulations revealed DTSSHPC-operated PV-T systems configured for maximum auxiliary energy savings can consistently outperform DTSTLHC-operated ones in this regard by at least 0.2-0.7% of the reference end use thermal energy demand, but in turn, can also underperform electrical efficiency-wise, by roughly up to 0.4% of the same measure, if DTSTLHC is configured for the maximum electrical energy efficiency. Thus, the main advantage of DTSSHPC for use in PV-T systems is its ability to reduce the auxiliary energy consumption.

Moreover, a negative correlation was found between the auxiliary energy savings gain enabled by DTSSHPC and the auxiliary energy savings level, essentially showing that oversized systems benefit less from this control. Furthermore, an analysis of the seasonal variation of the auxiliary energy savings difference revealed DTSSHPC enabling low and high gains during the Summer for over- and undersized systems, respectively, meaning undersized systems can take advantage of DTSSHPC all year round while oversized systems will tend to do so mostly during the Winter, and are for this reason bound to benefit less annually from DTSSHPC.

The same proved to be true in terms of primary energy savings and financial savings, with undersized systems benefiting the most from DTSSHPC though not consistently and by lower yet comparable margins due to the parasitic energy and the generally negative effect on PV conversion. Also, low parasitic to auxiliary energy price ratios in gas-assisted systems were found to favour DTSSHPC, with a twofold

increase relative to reference prices shown to be sufficient to make all gas-assisted systems simulated viable, albeit marginally, whereas those using electrical heaters proved consistently viable at reference prices. However, DTSSHPC does not appear to be a conservative control choice for SDHW PV-T systems, on account of the marginal performance gains, the conditions to realise them and the risks entailed.

6.2. Future work

During the course of the research activities pursued, some unexplored ideas sprang to mind, among which the following can be highlighted:

- Configuration-scheduled DTSSHPC for ST systems – One of the problems of DTSSHPC is the difficulty in selecting the appropriate ramp for a whole year, which generally leads to subnominal flow rates during many high insolation days or excessively high flow rates during low insolation days. Instead, it would be interesting to investigate the ability to alternate between controller configurations seamlessly (e.g., between DTSSHPC and DTSTLHC) and in a way responsive to the weather and system states;
- Validation of the dynamic PV-T collector model for improved parameter estimation – The dynamic PV-T collector model proposed introduces one additional term relative to the ISO 9806:2013 standard's quasi-dynamic test method equation, and its aim is to independently account for the effect of electricity generation on thermal performance and not to predict electricity generation. Thus, its inclusion may improve the quality of parameter fits for standardised thermal performance tests of PV-T collectors.

6.3. Contributions

The main contributions of the activities conducted can be summarised as follows:

- Development and analysis of analytical and numerical steady-state design methods for the selection of differential temperature controller setpoints in PV-T systems, based on stable and cost-effective operation;
- Development of a dynamic single-node PV-T collector model based on the Perers model, using a zero-capacitance cell temperature estimator responsive to electricity generation, the heat loss coefficient temperature dependence and premised on a constant collector efficiency factor for all flow regimes;
- Comparative analysis of DTSSHPC and DTSTLHC supply-loop flow controllers for SDHW PV-T systems in Central and Western European locations.

The contributions and research activities developed during the course of this program led to several papers published in peer-reviewed scientific journals and conference proceedings as author and co-author, namely:

1. Magalhães, P., Martins, J., Joyce, A., Performance Assessment of Tank Fluid Purging and Night Cooling as Overheating Prevention Techniques for Photovoltaic-Thermal (PV-T) Solar Water Heating Systems. In: Camarinha-Matos, L., Parreira-Rocha, M., Ramezani, J. (Eds.) Technological Innovation for Smart Systems. DoCEIS 2017. IFIP Advances in Information and Communication Technology, 2017, 499, pp. 337-347. https://doi.org/10.1007/978-3-319-56077-9_33

2. Magalhães, P., Martins, J., Joyce, A. Comparative Analysis of Overheating Prevention and Stagnation Handling Measures for Photovoltaic-thermal (PV-T) Systems, Energy Procedia, Volume 91, 2016, pp. 346-355, ISSN 1876-6102, http://dx.doi.org/10.1016/j.egypro.2016.06.282.

3. Magalhães, P., Lopes, R. A., Martins, J., Joyce, A. Grid interaction analysis of solar water heating photovoltaic-thermal (PV-T) systems with thermal storage tanks and electrical auxiliary heaters. In: 2015 9th International Conference on Compatibility and Power Electronics (CPE), Costa da Caparica, 2015, pp. 76-81. doi: 10.1109/CPE.2015.7231052

4. Magalhães, P., Martins, J., Joyce, A., Coelho, L., Tavares, N., Pereira, R. Solar Trigeneration System Model for Off-Grid Residential Applications. In: Technological Innovation for Value Creation - IFIP Advances in Information and Communication Technology, 2012, 372, pp. 375-384. https://doi.org/10.1007/978-3-642-28255-3_41

5. Joyce, A., Coelho, L., Martins, J.F., Tavares, N., Pereira, R., Magalhães, P. A PV/T and Heat Pump based Trigeneration System Model for Residential Applications. In: ISES Solar World Congress, Kassel, Germany, 28 August - 2 September, 2011. doi:10.18086/swc.2011.19.19

The contents of these papers were all presented publicly by the candidate and all focus on PV-T technology. More precisely, the common theme among them is the development of a core PV-T system model – which went on to become the model described in Appendix D – to address research questions concerning: autonomous and grid-connected PV-T trigeneration systems (papers #4 and #5); analysis of PV-T system performance (paper #3); and analysis of overheating prevention methods applied to PV-T systems[44] (papers #1 and #2). Among these, the first two papers listed use the PV-T collector model described in Chapter 3, the second of which is a journal paper initially submitted for the 2015 Solar Heating and Cooling for Buildings and Industry conference (IEA SHC 2015). In addition to these, two additional papers are expected to be submitted for publication based on the work on setpoint selection and the controller comparison detailed in Chapters 4 and 5, respectively.

[44]The work conducted on this topic was originally planned for inclusion in this document but was ultimately not included for reasons of succinctness and theme.

Bibliography

Adams, A. S., Keith, D. W., 2013. Are global wind power resource estimates overstated? Environmental Research Letters 8, 1–9.

Affolter, P., Eisenmann, W., Fechner, H., Rommel, M., Schaap, A., Sorensen, H., Tripanagnostopoulos, Y., Zondag, H., 2005. PVT roadmap: A European guide for the development and market introduction of PV-Thermal technology. Tech. rep., PV-Catapult.

Affolter, P., Ruoss, D., Toggweiler, P., Haller, A., November 1997. New generation of hybrid solar collectors / phase 1. Tech. Rep. 56360/1686, EPFL.

Affolter, P., Ruoss, D., Toggweiler, P., Haller, A., 2000. New generation of hybrid solar PV/T collectors. Report DIS 56360/16868, EPFL.

Alcone, J. M., Herman, R. W., 1981. Simplified methodology for choosing controller set-points. In: Proceedings of the ASME Solar Energy Division Third Annual Conference on Systems Simulation, Economic Analysis/Solar Heating and Cooling Operational Results. pp. 345–347.

Amrizal, N., Chemisana, D., Rosell, J. I., 2013. Hybrid photovoltaic-thermal solar collectors dynamic modeling. Applied Energy 101, 797–807.

Amrizal, N., Chemisana, D., Rosell, J. I., Barrau, J., 2012. A dynamic model based on the piston flow concept for the thermal characterization of solar collectors. Applied Energy 94, 244–250.

Andersson, B. A., 2000. Materials availability for large-scale thin-film photovoltaics. Progress in Photovoltaics: Research and applications 8 (1), 61–76.

Andrews, J. W., June 1981. Evaluation of flat-plate photovoltaic/thermal hybrid systems for solar energy utilization. Tech. rep., United States Department of Energy, Contract No. DE-AC02-76CH00016.

Arto, I., Capellan-Perez, I., Lago, R., Bueno, G., Bermejo, R., 2016. The energy requirements of a developed world. Energy for Sustainable Development 33, 1–13.

Asghar, M. S. J., 1999. Smooth speed control of single-phase induction motors by integral-cycle switching. IEEE Transactions on Energy Conversion 14 (4), 1094–1099.

Aydin, D., Casey, S. P., Riffat, S., 2015. The latest advancements on thermochemical heat storage systems. Renewable and Sustainable Energy Reviews 41, 356–367.

Badescu, V., 2008. Optimal control of flow in solar collector systems with fully mixed water storage tanks. Energy Conversion and Management 49, 169–184.

Barthel, F., Cabrera, M., Faaij, A., Giroux, M., Hall, D., Kagramanian, V., Kononov, S., Lefevre, T., Moreira, R., Nötstaller, R., Odell, P., Taylor, M., 2000. Energy and the Challenge of Sustainability: World Energy Assessment. United Nations Development Programme, Ch. Energy Resources, pp. 135–171.

Beckman, W. A., Thornton, J., Long, S., Wood, B. D., 1994. Control problems in domestic hot water systems. Solar Energy 53, 233–236.

Bendib, B., Belmili, H., Krim, F., 2015. A survey of the most used MPPT methods: Conventional and advanced algorithms applied for photovoltaic systems. Renewable and Sustainable Energy Reviews 45, 637–648.

Bliss, R. W., December 1959. The derivations of several "plate-efficiency factors" useful in the design of flat-plate solar heat collectors. Solar Energy 3 (4), 55–64.

BLS, 2017. CPI Inflation Calculator. Last access: March 20th 2017.
URL `https://data.bls.gov/cgi-bin/cpicalc.pl`

Bollen, M. H., Hassan, F., 2011. Integration of Distributed Generation in the Power System. Wiley-IEEE Press.

Brazeau, R. H., Edwards, M. A., 2011. A review of the sustainability of residential hot water infrastructure: public health, environmental impacts, and consumer drivers. Journal of Green Building 6 (4), 77–95.

Burt, S., December 9 2015. Ships, Planes and Climate Change. EarthJustice. Last access: December 21st 2017.
URL `http://earthjustice.org/blog/2015-december/ships-planes-and-climate-change`

Buxton, N., 2016. COP 21 Charades: Spin, Lies and Real Hope in Paris. Globalizations, 1–4.

Byrne, J., Kurdgelashvili, L., 2011. Handbook of Photovoltaic Science and Engineering, 2nd Edition. Wiley, Ch. The Role of Policy in PV Industry Growth: Past, Present and Future, pp. 39–81.

Campoccia, A., Dusonchet, L., Telaretti, E., Zizzo, G., 2014. An analysis of feed-in tariffs for solar PV in six representative countries of the European. Solar Energy 107, 530–542.

Candelise, C., Winskel, M., Gross, R., 2012. Implications for CdTe and CIGS technologies production costs of indium and tellurium scarcity. Progress in Photovoltaics: Research and applications 20 (6), 816–831.

CEN, 2006. EN 12975-2:2006. Thermal solar systems and components. Solar collectors. Test methods.

Cengel, Y. A., 2003. Heat Transfer: A Practical Approach. McGraw-Hill.

Chapin, D. M., Fuller, C. S., Pearson, G. L., 1954. A new silicon p-n junction photocell for converting solar radiation into electrical power. Journal Of Applied Physics 25 (5), 676.

Chen, Z., Dragsted, J., Furbo, S., Perers, B., 2010. Theoretical study on a solar collector loop during stagnation. In: Proceedings of the EuroSun 2010 Conference. Graz, Austria.

Chen, Z., Dragsted, J., Furbo, S., Perers, B., Fan, J., 2015. Behavior of a solar collector loop during stagnation. Journal of Solar Energy Engineering 137 (3), 1–10.

Chow, T., 2003. Performance analysis of photovoltaic-thermal collector by explicit dynamic model. Solar Energy 75, 143–152.

Chow, T., Bai, Y., Fong, K., Lin, Z., 2012. Analysis of a solar assisted heat pump system for indoor swimming pool water and space heating. Applied Energy 100, 309–317.

Chow, T., Chan, A., Fong, K., Lin, Z., He, W., Ji, J., 2009. Annual performance of building-integrated photovoltaic/water-heating system for warm climate application. Applied Energy 86, 689–696.

Close, D. J., April-June 1967. A design approach for solar processes. Solar Energy 11 (2), 112–122.

Conway, T. M., 1977. Fluid flow control strategies in flat-plate and evacuated tube collectors. In: International Solar Energy Society, Annual Meeting. Vol. 1. pp. 9–11.

Cristofari, C., Notton, G., Canaletti, J. L., 2009. Thermal behavior of a copolymer PV/Th solar system in low flow rate conditions. Solar Energy 83, 1123–1138.

Cruickshank, C. A., Baldwin, C., 2016. Storing Energy, With Special Reference to Renewable Energy Sources. Elsevier, Ch. Sensible Thermal Energy Storage: Diurnal and Seasonal, pp. 291–309.

Crutzen, P. J., Stoermer, E. F., May 2000. The "anthropocene". International Geosphere-Biosphere Programme (IGBP) Newsletter (41), 17–18.

Davis, E. S., January 1975. Stability of Differential Thermostats for Solar Collection Systems, Jet Propulsion Laboratory Internal Memo: 393-10.

Davis, P. R., 2015. Advances in Thermal Energy Storage Systems. Elsevier, Ch. Monitoring and control of thermal energy storage systems, pp. 411–432.

de Brito, M. A. G., Galotto, L., Sampaio, L. P., de Azevedo e Melo, G., Canesin, C. A., 2013. Evaluation of the Main MPPT Techniques for Photovoltaic Applications. IEEE Transactions on Industrial Electronics 60 (3), 1156–1167.

de Castro, C., Mediavilla, M., Miguel, L. J., Frechoso, F., 2011. Global wind power potential: Physical and technological limits. Energy Policy 39, 6677–6682.

de Castro, C., Mediavilla, M., Miguel, L. J., Frechoso, F., December 2013. Global solar electric potential: A review of their technical and sustainable limits. Renewable and Sustainable Energy Reviews 28, 824–835.

de Castro, C., Óscar Carpintero, Frechoso, F., Mediavilla, M., de Miguel, L. J., 2014. A top-down approach to assess physical and ecological limits of biofuels. Energy 64, 506–512.

de Vos, A., 1980. Detailed balance limit of the efficiency of tandem solar cells. Journal of Physics D: Applied Physics 13 (5), 839–846.

Dikkers, R. D., Kennish, W. J., Winn, C. B., Huston, W., 1984. Research priorities for improving the effectiveness of active solar hot water and space conditioning systems. Tech. Rep. NBSIR 84-2980, U.S. Department of Energy.

DIN, December 2011. DIN V 18599-1:2011-12.

DIN, May 2013. DIN V 18599-1 Berichtigung 1. Ber 1:2013-05.

Dlugokencky, E., Tans, P., September 2017. Trends in Atmospheric Carbon Dioxide. Last access: December 21st 2017.
URL `https://www.esrl.noaa.gov/gmd/ccgg/trends/`

Drück, H., 2011. Solar thermal technology - threats and options. In: ISES Solar World Congress 2011. Kassel, Germany, 28 August - 2 September 2011.

Drück, H., Sommer, K., 2013. Pv-wärme - zukunftstechnologie oder unsinn? In: OTTI - 23. Symposium Thermische Solarenergie 24.04.-26.04.2013; Kloster Banz, Bad Staffelstein.

Duffie, J. A., Beckman, W., 2013. Solar Engineering of Thermal Processes, 4th Edition. Wiley.

Duffie, J. A., Beckman, W. A., 1980. Solar Engineering of Thermal Processes. Wiley.

Dupeyrat, P., Kwiatkowski, G., Ménézo, C., Rommel, M., Stryi-Hipp, G., 2011a. Experimental and numerical assessment of PV-T collector for combined production of electricity and domestic hot water in the frame of project "PVTCOL". In: International Solar Energy Society SWC 2011 Conference Proceedings. Kassel, Germany, 28 August - 2 September 2011.

Dupeyrat, P., Menezo, C., Fortuin, S., 2014. Study of the thermal and electrical performances of PVT solar hot water system. Energy and Buildings 68, 751–755.

Dupeyrat, P., Menezo, C., Rommel, M., Henning, H.-M., 2011b. Efficient single glazed flat plate photovoltaic-thermal hybrid collector for domestic hot water system. Solar Energy 85, 1457–1468.

Dupeyrat, P., Ménézo, C., Wirth, H., Hofmann, P., Kwiatkowski, G., Rommel, M., Stryi-Hipp, G., 2010. Design of a flat-plate Photovoltaic-Thermal (PV-T) hybrid collector: modelling and experimental investigations. In: International Solar Energy Society EuroSun 2010 Conference Proceedings. Graz, Austria, 28 September - 01 October 2010.

Dusonchet, L., Telaretti, E., 2015. Comparative economic analysis of support policies for solar PV in the most representative EU countries. Renewable and Sustainable Energy Reviews 42, 986–998.

EC, July 2009. Commission Regulation (EC) No 641/2009 of 22 July 2009. Official Journal of the European Union L191, 35–41.

EC, July 2012. Commission Regulation (EU) No 622/2012 of 11 July 2012. Official Journal of the European Union L180, 4–8.

Eckert, V., March 20 2015. European power grids keep lights on through solar eclipse. Reuters.

ECOHEATCOOL, 2006. Ecoheatcool work package 1: The european heat market. Tech. rep., Euroheat and Power.

EIA, 2016. International Energy Outlook 2016. U.S. Energy Information Administration.

Eicker, U., 2003. Solar Technologies for Buildings. Wiley.

Eicker, U., 2009. Low Energy Cooling for Sustainable Buildings. Wiley.

Eicker, U., Dalibard, A., 2011. Photovoltaic-thermal collectors for night radiative cooling of buildings. Solar Energy 85 (7), 1322–1335.

Eisentraut, A., Brown, A., 2014. Heating without global warming: Market developments and policy considerations for renewable heat. Tech. rep., International Energy Agency.

Ellabban, O., Abu-Rub, H., Blaabjerg, F., 2014. Renewable energy resources: Current status, future prospects and their enabling technology. Renewable and Sustainable Energy Reviews 39, 748–764.

Emery, K., 2011. Handbook of Photovoltaic Science and Engineering, 2nd Edition. Wiley, Ch. Measurement and Characterization of Solar Cells and Modules, pp. 797–840.

ENTSOE, February 2015 2015. Solar Eclipse 2015 - Impact Analysis - Report prepared by Regional Group Continental Europe and Synchronous Area Great Britain. Tech. rep., European Network of Transmission System Operators for Electricity.

Epp, B., Banse, S., 2015. Success and crisis close together. Sun & Wind Energy 6, 22–35.

Eurostat, 2017a. Energy Database of the Statistical Office of the European Union (Eurostat). Last access: December 21st 2017.
URL http://ec.europa.eu/eurostat/web/energy/data/database

Eurostat, 2017b. Labour costs in the EU. 58/2017. Last access: December 21st 2017.
URL http://ec.europa.eu/eurostat/en/web/products-press-releases/-/3-06042017-AP

Evans, D. L., 1981. Simplified method for predicting photovoltaic array output. Solar Energy 27 (6), 555–560.

EWGLI, EWGLINET, 2005. European guidelines for control and prevention of travel associated legionnaires' disease. Tech. rep., EWGLI and EWGLINET.

Falvo, M., Capparella, S., 2015. Safety issues in PV systems: Design choices for a secure fault detection and for preventing fire risk. Case Studies in Fire Safety 3, 1–16.

Feltrin, A., Freundlich, A., 2008. Material considerations for terawatt level deployment of photovoltaics. Renewable Energy 33, 180–185.

Field, C. B., Campbell, J. E., Lobell, D. B., 2008. Biomass energy: the scale of the potential resource. Trends in Ecology and Evolution 23 (2), 65–72.

Fischer, S., Heidemann, W., Müller-Steinhagen, H., Perers, B., Bergquist, P., Hellström, B., 2004. Collector test method under quasi-dynamic conditions according to the European Standard EN 12975-2. Solar Energy 76 (1-3), 117–123.

FISE, June 6th 2016. Photovoltaics report. Tech. rep., Fraunhofer Institute for Solar Energy Systems, ISE, Freiburg.

Florschuetz, L. W., 1979. Extension of the Hottel-Whillier model to the analysis of combined photovoltaic/thermal flat plate collectors. Solar Energy 22, 361–366.

Fortuin, S., Hermann, M., Stryi-Hipp, G., Nitz, P., Platzer, W., 2014. Hybrid PV-Thermal collector development: concepts, experiences, results and research needs. Energy Procedia 48, 37–47.

Frank, E., Hess, S., Zahler, C., November 9th 2012. General requirements and relevant parameters for process heat collectors and specific collector loop components: Deliverable A 1.1. Tech. rep., IEA SHC Task 49, SolarPACES Annex IV, Solar Process Heat for Production and Advanced Applications.

Frank, E., Mauthner, F., Fischer, S., 2015. Overheating prevention and stagnation handling in solar process heat applications - Task 49 Technical Report A.1.2. Tech. rep., International Energy Agency Solar Heating and Cooling Programme.

Fridleifsson, I., Bertani, R., Huenges, E., Lund, J. W., Ragnarsson, A., Rybach, L., January 2008. The possible role and contribution of geothermal energy to the mitigation of climate change. In: Hohmeyer, O., Trittin, T. (Eds.), Proceedings of the IPCC Scoping Meeting on Renewable Energy Sources. pp. 59–80.

Furbo, S., Shah, L. J., 1996. Optimum solar collector fluid flow rates. In: Goetzberger, A., Luther, J. (Eds.), Proceedings of Eurosun 96 Conference. Vol. 1. German Solar Energy Society, German Solar Energy Society, pp. 189–193.

García-Olivares, A., 2015. Substituting silver in solar photovoltaics is feasible and allows for decentralization in smart regional grids. Environmental Innovation and Societal Transitions 17, 15–21.

García-Olivares, A., 2016. Energy for a sustainable post-carbon society. Scientia Marina 80.S1, 257–268.

GES, 2010. Planning and Installing Solar Thermal Systems: a guide for installers, architects and engineers. Earthscan.

Ghani, F., Duke, M., 2011. Numerical determination of parasitic resistances of a solar cell using the Lambert W-function. Solar Energy 85, 2386–2394.

Gicquel, R., 1979. Behavior of plane solar collectors under transient conditions. International Chemical Engineering 19.1, 51–65, translated from Revue Generale de Thermique by G.D. Fulford.

Goswami, D. Y., 2015. Principles of solar engineering. CRC Press.

Gray, J. L., 2011. Handbook of Photovoltaic Science and Engineering, 2nd Edition. Wiley, Ch. The Physics of Solar Cells, pp. 82–129.

Green, M. A., 2009. Estimates of Te and In Prices from Direct Mining of Known Ores. Progress in Photovoltaics: Research and applications 17, 347–359.

Green, M. A., 2011. Learning experience for thin-film solar modules: First Solar, Inc. case study. Progress in Photovoltaics: Research and applications 19, 498–500.

Green, M. A., Hishikawa, Y., Warta, W., Dunlop, E. D., Levi, D. H., Hohl-Ebinger, J., Ho-Baillie, A. W., 2017. Solar cell efficiency tables (version 50). Progress in Photovoltaics Research and Applications 25, 668–676.

Grundfos, 2012. PWM interface in UP pumps. Hvac oem rev 9, Grundfos.

Grundfos, 2016. Grundfos Data Booklet: ALPHA2/ALPHA3 Circulator pumps 50/60 Hz.

Gunn, K., Stock-Williams, C., 2012. Quantifying the global wave power resource. Renewable Energy 44, 296–304.

Gustavson, M. R., April 1979. Limits to wind power utilization. Science 204 (4388), 13–17.

Haller, M., Perers, B., Bales, C., Paavilainen, J., Dalibard, A., Fischer, S., Bertram, E., 2014. TRNSYS Type 832 v5.10 "Dynamic Collector Model by Bengt Perers" Updated Input-Output Reference. Tech. rep.

Hamududu, B., Killingtveit, A., 2012. Assessing climate change impacts on global hydropower. Energies 5, 305–322.

Han, Y., Wang, R., Dai, Y., 2009. Thermal stratification within the water tank. Renewable and Sustainable Energy Reviews 13, 1014–1026.

Hansen, J., Sato, M., Kharecha, P., Beerling, D., Berner, R., Masson-Delmotte, V., Pagani, M., Raymo, M., Royer, D. L., Zachos, J. C., 2008. Target Atmospheric CO2: Where Should Humanity Aim? The Open Atmospheric Science Journal 2, 217–231.

Harrison, S., Cruickshank, C. A., 2012. A review of strategies for the control of high temperature stagnation in solar collectors and systems. Energy Procedia 30, 793–804.

Haurant, P., Ménézo, C., Dupeyrat, P., 2014. The PHOTOTHERM project: full scale experimentation and modelling of a photovoltaic-thermal (PV-T) hybrid system for domestic hot water applications. Energy Procedia 48, 581–587.

Haurant, P., Ménézo, C., Gaillard, L., Dupeyrat, P., 2015a. A Numerical Model of a Solar Domestic Hot Water System Integrating Hybrid Photovoltaic/Thermal Collectors. Energy Procedia - 6th International Building Physics Conference, IBPC 2015 78, 1991–1997.

Haurant, P., Ménézo, C., Gaillard, L., Dupeyrat, P., 2015b. Dynamic numerical model of a high efficiency PV-T collector integrated into a domestic hot water system. Solar Energy 111, 68–81.

Hegedus, S., Luque, A., 2011. Handbook of Photovoltaic Science and Engineering, Second Edition. Wiley, Ch. Achievements and Challenges of Solar Electricity from Photovoltaics, pp. 1–38.

Herczfeld, P. R., Fischl, R., Jr., S. K., 1980. Solar flat plate collector control system sensitivity analysis. In: Proceedings of the Systems Simulation and Economic Analysis Conference. pp. 23–25.

Herczfeld, P. R., Fischl, R., Orbach, A., 1978a. Optimizing solar energy systems using continuous flow control. In: Sun: Mankind's future source of energy; Proceedings of the International Solar Energy Congress, New Delhi, India, January 16-21, 1978. Vol. 3. Pergamon Press, pp. 1523–1530.

Herczfeld, P. R., Klafter, R. D., Fischl, R., Orbach, A., 1978b. Study of pump cycling in the control of solar heating and cooling systems. In: Proceedings of the First Workshop on the Control of Solar Energy Systems for Heating and Cooling. May 23-25, 1978. Hyannis, Massachussetts.

Hermann, M., 2011. Development of a bionic solar collector with aluminum roll-bond absorber. Tech. rep., Bionicol Project, 7th Framework Programme/Theme 5/Energy, Grant Agreement number 219036.

Hermann, M., February 2013. Fractherm - bionic channel structures for energy-efficient heat transport. Slide presentation at the "3.8 billion years of free energy research" Symposium. Bad Nieuweschans, Netherlands. 26 February 2013.

Hermann, W. A., 2006. Quantifying global exergy resources. Energy 31, 1685–1702.

Hertwich, E. G., Gibon, T., Bouman, E. A., Arvesen, A., Suh, S., Heath, G. A., Bergesen, J. D., Ramirez, A., Vega, M. I., Shi, L., 2015. Integrated life-cycle assessment of electricity-supply scenarios confirms global environmental benefit of low-carbon technologies. Proceedings of the National Academy of Sciences of the United States of America 112 (20), 6277–6282.

Hess, S., 2016. Renewable Heating and Cooling: Technologies and Applications. Elsevier, Ch. Solar thermal process heat (SPH) generation, pp. 41–65.

Hirsch, U. T., 1985. Control strategies for solar water heating systems. Master's thesis, University of Wisconsin-Madison.

Hofmann, P., Dupeyrat, P., Kramer, K., M.Hermann, Stryi-Hipp, G., 2010. Measurements and benchmark of PV-T collectors according to EN12975 and development of a standardized measurement procedure. In: Proceedings of EuroSun 2010.

Hohm, D. P., Ropp, M. E., 2000. Comparative study of maximum power point tracking algorithms using an experimental, programmable, maximum power point tracking test bed. In: Conference Record of the Twenty-Eighth IEEE Photovoltaic Specialists Conference.

Hohm, D. P., Ropp, M. E., 2003. Comparative study of maximum power point tracking algorithms. Progress in Photovoltaics: Research and Applications 11, 47–62.

Hoogwijk, M., de Vries, B., Turkenburg, W., 2004. Assessment of the global and regional geographical, technical and economic potential of onshore wind energy. Energy Economics 26, 889–919.

Hottel, H. C., Whillier, A., 1955. Evaluation of flat-plate solar collector performance. In: Transactions of the Conference on the Use of Solar Energy.

Huang, B. J., 1994. Transient performance of solar systems with a bang-bang controller. Journal of the Chinese Society of Mechanical Engineering 15 (5), 409–417.

Huang, B. J., Lin, T. H., Hung, W. C., Sun, F. S., 1999. Solar photo-voltaic/thermal co-generation collector. In: Proceedings of the ISES 1999 Solar World Congress.

Huang, B. J., Lin, T. H., Hung, W. C., Sun, F. S., 2001. Performance evaluation of solar photovoltaic/thermal systems. Solar Energy 70, 443–448.

Huang, B. J., Lu, J. H., 1982. Performance test of solar collector with intermittent output. Solar Energy 28 (5), 413–420.

Huber, M., Dimkova, D., Hamacher, T., 2014. Integration of wind and solar power in Europe: Assessment of flexibility requirements. Energy 69, 236–246.

Hudon, K., 2014. Future energy: Improved, Sustainable and Clean Options for Our Planet. Elsevier, Ch. Solar Energy - Water Heating, pp. 433–451.

IEA, 2008. Empowering Variable Renewables Options for Flexible Electricity Systems. International Energy Agency Publications, International Energy Agency.

IEA, 2010. World Energy Outlook 2010. International Energy Agency Publications, International Energy Agency.

IEA, 2011. Harnessing Variable Renewables: A Guide to the Balancing Challenge. International Energy Agency Publications, International Energy Agency.

IEA, 2013. Resources to Reserves 2013: Oil, Gas and Coal Technologies for the Energy Markets of the Future. International Energy Agency Publications, International Energy Agency.

IEA, 2014. The Power of Transformation - Wind, Sun and the Economics of Flexible Power Systems. International Energy Agency Publications.

IEA, 2015a. CO2 emissions from fuel combustion: highlights. Tech. rep., International Energy Agency.

IEA, 2015b. Energy and Climate Change: World Energy Outlook Special Report. International Energy Agency Publications, International Energy Agency.

IEA, 2015c. Key world energy statistics. Tech. rep., International Energy Agency, International Energy Agency.

IEA, 2015d. World Energy Outlook 2015. International Energy Agency Publications.

IEA-PVPS, 2010. Trends in Photovoltaic Applications: Survey report of selected IEA countries between 1992 and 2010. Tech. rep., International Energy Agency, Photovoltaic Power Systems Programme, report IEA-PVPS T1-20:2011.

IEA-PVPS, 2014a. PVPS Report: Snapshot of global PV 1992-2013, Preliminary Trends Information from the IEA PVPS Programme. Tech. rep., International Energy Agency, Photovoltaic Power Systems Programme.

IEA-PVPS, March 2014b. Review of failures of photovoltaic modules. Tech. rep., IEA-PVPS.

IEA-PVPS, 2016a. 2015 snapshot of global photovoltaic markets. Tech. rep., International Energy Agency, Photovoltaic Power Systems Programme.

IEA-PVPS, 2016b. Annual report 2015. Tech. rep., International Energy Agency, Photovoltaic Power Systems Programme.

IEA-PVPS, 2016c. Trends 2016 in Photovoltaic Applications: Survey Report of Selected IEA Countries between 1992 and 2015. Tech. rep., International Energy Agency, Photovoltaic Power Systems Programme.

IEC, April 2005. IEC 61215:2005. Crystalline silicon terrestrial photovoltaic (PV) modules - Design qualification and type approval.

Isaacs, J. D., Seymour, R. J., 1973. The ocean as a power resource. International Journal of Environmental Studies 4, 201–205.

Ishaque, K., Salam, Z., Syafaruddin, 2011. A comprehensive MATLAB Simulink PV system simulator with partial shading capability based on two-diode model. Solar Energy 85, 2217–2227.

ISO, 2013. ISO 9806:2013. Solar energy - Solar thermal collectors - Test methods.

IVPH, 2017. World Maps of Köppen-Geiger climate classification. Last access: December 21st 2017.
URL `http://koeppen-geiger.vu-wien.ac.at/`

Jacobson, M. Z., Archer, C. L., 2012. Saturation wind power potential and its implications for wind energy. Proceedings of the National Academy of Sciences of the United States of America 109 (39), 15679–15684.

Jeffries, E., 2015. Coming clean. Nature Climate Change 5, 93–95.

Kahwaji, G., Winn, C. B., August 1986. Effect of the cycling rate on energy collection for bang-bang controllers. Journal of Solar Energy Engineering 108 (3), 206–213.

Kalogirou, S., 2003. The potential of solar industrial process heat applications. Applied Energy 76, 337–361.

Kalogirou, S., Tripanagnostopoulos, Y., 2007. Industrial application of PV/T solar energy systems. Applied Thermal Engineering 27, 1259–1270.

Kalogirou, S. A., 2009. Solar Energy Engineering: Processes and Systems. Elsevier.

Kaltschmitt, M., 2007. Renewable Energy: Technology, Economics and Environment. Springer, Ch. Energy system, pp. 1–7.

Kaltschmitt, M., Streicher, W., Wiese, A., 2007. Renewable Energy: Technology, Economics and Environment. Springer.

Kamminga, W., 1985. Experiences of a solar collector test method using fourier transfer functions. International Journal of Heat Mass Transfer 28 (7), 1393–1404.

Kamminga, W., 1986. The testing of an evacuated tubular collector with a heat pipe using the fourier frequency domain. International Journal of Heat Mass Transfer 29 (1), 83–90.

Karimi, M., Mokhlis, H., Naidu, K., Uddin, S., Bakar, A., 2016. Photovoltaic penetration issues and impacts in distribution network - A review. Renewable and Sustainable Energy Reviews 53, 594–605.

Kato, K., 2012. PV module failures observed in the field: solder bond and bypass diode failures. Presented at IEA-PVPS Workshop.

Kent, T. B., McGavin, M. J., 1978. Development of a novel controller. In: Proceedings of the First Workshop on the Control of Solar Energy Systems for Heating and Cooling. May 23-25, 1978. Hyannis, Massachussetts.

Klein, S. A., Duffie, J. A., Beckman, W. A., 1974. Transient considerations of flat-plate solar collectors. Journal of Engineering for Power 96 (2), 109–113.

Knudsen, S., 2002. Consumers' influence on the thermal performance of small SDHW systems - theoretical investigations. Solar Energy 73 (1), 33–42.

Kottek, M., Griser, J., Beck, C., Rudolf, B., Rubel, F., June 2006. World Map of the Köppen-Geiger climate classification updated. Meteorologische Zeitschrift 15, 259–263.

Kramer, K., Helmers, H., December 2013. The interaction of standards and innovation: Hybrid photovoltaic-thermal collectors. Solar Energy 98, 434–439.

Kutscher, C. F., Davenport, R. L., Dougherty, D. A., Gee, R. C., Masterson, P. M., May, E. K., August 1982. Design approaches for solar industrial process heat systems: Nontracking and line-focus collector technologies. Tech. Rep. SERI/TR-253-1356, UC Category 62, Prepared Under Task No. 1007.99, WPA NO. 279-81. Prepared for the U.S. Department of Energy, Contract No. EG-77-C-01-4042, Solar Energy Research Institute.

Lako, P., de Noord, M., Eder, H., Reisinger, H., 2003. Hydropower development with a focus on Asia and Western Europe. Overview in the framework of VLEEM 2. Tech. rep., ECN Policy Studies.

Lämmle, M., 2016. Personal communication.

Lämmle, M., Fortuin, S., Hermann, M., 2015. Thermisches Management von PVT-Kollektoren - Ergebnisse aus Systemsimulationen.

Lämmle, M., Kroyer, T., Fortuin, S., Wiese, M., Hermann, M., 2016a. Development and modelling of highly-efficient PVT collectors with low-emissivity coatings. Solar Energy 130, 161–173.

Lämmle, M., Thoma, C., Hermann, M., June 2016b. A PVT Collector Concept with Variable Film Insulation and Low-Emissivity Coating. Energy Procedia 91, 72–77, Proceedings of the 4th International Conference on Solar Heating and Cooling for Buildings and Industry (SHC 2015).

Lauterbach, C., Schmitt, B., Jordan, U., Vajen, K., 2012. The potential of solar heat for industrial processes in Germany. Renewable and Sustainable Energy Reviews 16, 5121–5130.

Leenders, F., Schaap, A. B., van der Ree, B. G. C., van der Helden, W. G. J., 2000. Technology review on PV/thermal concepts. In: Proceedings of Eurosun 2000.

Lewis, R., 1977. Proportional versus on/off differential temperature controls. Solar Heating and Cooling 2 (4).

Lewis, R., Carr, J. B., 1978a. An advanced freeze protection control logic for direct circulation (draindown) systems. In: Proceedings of the First Workshop on the Control of Solar Energy Systems for Heating and Cooling. May 23-25, 1978. Hyannis, Massachussetts.

Lewis, R., Carr, J. B., 1978b. Comparative study of on/off and proportionally controlled systems. In: Proceedings of the First Workshop on the Control of Solar Energy Systems for Heating and Cooling. May 23-25, 1978. Hyannis, Massachussetts.

Lienhard IV, J. H., Lienhard V, J. H., 2008. A Heat Transfer Textbook. Phlogiston Press.

Lu, X., McElroy, M. B., Kiviluoma, J., 2009. Global potential for wind-generated electricity. Proceedings of the National Academy of Sciences of the United States of America 106 (27), 10933–10938.

Luo, W., Khoo, Y. S., Hacke, P., Naumann, V., Lausch, D., Harvey, S. P., Singh, J. P., Chai, J., Wang, Y., Aberle, A. G., Ramakrishna, S., 2017. Potential-induced degradation in photovoltaic modules: a critical review. Energy & Environmental Science 10, 43–68.

Luque, A., Hegedus, S., 2011. Handbook of Photovoltaic Science and Engineering. Wiley.

Manzini, G., Gramazio, P., Guastella, S., Liciotti, C., Baffoni, G. L., 2015. The fire risk in photovoltaic installations - Checking the PV modules safety in case of fire. Energy Procedia 81, 665–672.

Martinelli, F., Caruso, A., Moschini, L., Turano, A., Scarcella, C., Speziani, F., 2000. A comparison of legionella pneumophila occurrence in hot water tanks and instantaneous devices in domestic, nosocomial, and community environments. Current Microbiology 41, 374–376.

Martinez, D. M., Ebenhack, B. W., 2008. Understanding the role of energy consumption in human development through the use of saturation phenomena. Energy Policy 36, 1430–1435.

Mathys, W., Stanke, J., Harmuth, M., Junge-Mathys, E., 2008. Occurrence of legionella in hot water systems of single-family residences in suburbs of two german cities with special reference to solar and district heating. International Journal of Hygiene and Environmental Health 211 (1-2), 179–185.

Mauthner, F., Weiss, W., Spür-Dür, M., 2016. Solar heat worldwide: Markets and contribution to the energy supply 2014. Tech. rep., International Energy Agency, Solar Heating and Cooling Program.

Messenger, R. A., Ventre, J., 2005. Photovoltaic Systems Engineering, 2nd Edition. CRC Press.

Meyers, S., Schmitt, B., Vajen, K., 2015. Techno-economic comparison of solar thermal and PV for heat generation in industrial processes. In: Proceedings of

the ISES Solar World Congress 2015. Daegu, Republic of Korea, 08 - 12 November 2015.

Miller, L. M., Gans, F., Kleidon, A., 2011. Estimating maximum global land surface wind power extractability and associated climatic consequences. Earth System Dynamics 2 (1), 1–12.

Milman, O., 2015a. James Hansen, father of climate change awareness, calls Paris talks 'a fraud'. The Guardian. Last access: December 21st 2017.
URL https://www.theguardian.com/environment/2015/dec/12/james-hansen-climate-change-paris-talks-fraud

Milman, O., 2015b. John Kerry rejects leading climate scientist's claim Paris talks were 'fraud'. The Guardian. Last access: December 21st 2017.
URL https://www.theguardian.com/environment/2015/dec/13/john-kerry-james-hansen-climate-change-paris-talks-fraud

Mittelman, G., Kribus, A., Dayan, A., 2007. Solar cooling with concentrating photovoltaic/thermal (CPVT) systems. Energy Conversion and Management 48, 2481–2490.

Montzka, S. A., Dlugokencky, E. J., Butler, J. H., 2011. Non-CO2 greenhouse gases and climate change. Nature 476, 43–50.

Moriarty, P., Honnery, D., 2016. Can renewable energy power the future? Energy Policy 93, 3–7.

Mork, G., Barstow, S., Kabuth, A., Pontes, M. T., 2010. Assessing the global wave energy potential. In: Proceedings of the ASME 2010 29th International Conference on Ocean, Offshore and Arctic Engineering (OMAE2010), June 6-11, 2010, Shanghai, China.

Muralidhar, G. K., Nagaraju, J., Mohan, S., 1989. Effectiveness of a differential temperature controller on a solar water heating system: An experimental study. Journal of Solar Energy Engineering 111 (1), 97–99.

Muschaweck, J., Spirkl, W., 1993. Dynamic solar collector performance testing. Solar Energy Materials & Solar Cells 30 (2), 95–105.

Naked Energy, 2012. Company brochure. Tech. rep., Naked Energy.

NASA/GISS, 2017. Global land-ocean temperature index. Last access: December 21st 2017.
URL http://climate.nasa.gov/vital-signs/global-temperature/

Naumann, P., Wolfson, R., 1984. Proportional versus on/off control: A detailed comparison. Journal of Solar Energy Engineering 106 (4), 423–427.

Nayak, J., Amer, E., Deshpande, S., 2000. Comparison of three transient methods for testing solar flat-plate collectors. Energy Conversion and Management 41, 677–700.

Newton, B. J., 1995. Modeling of solar storage tanks. Master's thesis, University of Wisconsin-Madison.

Nhut, L. M., Park, Y. C., 2013. A study on automatic optimal operation of a pump for solar domestic hot water system. Solar Energy 98, 448–457.

Norton, B., 2014. Harnessing Solar Heat. Springer.

NREL, 2014. National Solar Radiation Data Base Viewer. Last access: March 17th 2017.
URL https://maps.nrel.gov/nsrdb-viewer/

Ntsaluba, S., Zhu, B., Xia, X., 2016. Optimal flow control of a forced circulation solar water heating system with energy storage units and connecting pipes. Renewable Energy 89, 108–124.

OECD, 2015. Climate Finance in 2013-14 and the USD 100 billion goal: A report by the OECD in collaboration with Climate Policy Initiative. Tech. rep., Organisation for Economic Co-operation and Development.

Orbach, A., Rorres, C., Fischl, R., May 1981. Optimal control of a solar collector loop using a distributed-lumped model. Automatica 17 (3), 535–539.

Orenstein, K., December 1 2015. COP Blog: Paris's $100bn question. Environmental Finance. Last access: December 21st 2017.
URL https://www.environmental-finance.com/content/analysis/cop-blog-pariss-100bn-question.html

Pasternak, A. D., 2000. Global energy futures and human development: A framework for analysis. Tech. rep., U.S. Department of Energy.

Pejsa, J. H., 1978. Cost effective control systems for solar heating and cooling applications. In: Proceedings of the First Workshop on the Control of Solar Energy Systems for Heating and Cooling. May 23-25, 1978. Hyannis, Massachussetts.

Pejsa, J. H., Bassett, W. W., Wenzler, S. A., Nguyen, K. H., Olson, T. J., September 1978. Cost-effective control systems for solar heating and cooling applications. Tech. rep., Honeywell, Inc., work Performed Under Contract No. EG-77-C-03-1592.

Perers, B., 1993. Dynamic method for solar collector array testing and evaluation with standard database and simulation programs. Solar Energy 50, 517–526.

Perers, B., 1997. An improved dynamic solar collector test method for determination of non-linear optical and thermal characteristics with multiple regression. Solar Energy 59 (4-6), 163–178.

Perers, B., 2010. An improved dynamic solar collector model including condensation and asymmetric incidence angle modifiers. In: Proceedings of the EuroSun 2010 Conference. Graz, Austria.

Pern, F. J., 1996. Factors that affect the EVA encapsulant discoloration rate upon accelerated exposure. Solar Energy Materials and Solar Cells 41-42, 587–615.

Peters, G. P., Andrew, R. M., Solomon, S., Friedlingstein, P., 2015. Measuring a fair and ambitious climate agreement using cumulative emissions. Environmental Research Letters 10, 1–9.

Peuser, F. A., Remmers, K.-H., Schnauss, M., 2002. Solar thermal systems: successful planning and construction. Solarpraxis.

Pillai, U., 2015. Drivers of cost reduction in solar photovoltaics. Energy Economics 50, 286–293.

POSHIP, 2001. The potential of solar heat for industrial processes, project No. NNE5-1999-0308.

Prapas, D. E., Veliannis, I., Evangelopoulos, A., Sotiropoulos, B. A., 1995. Large DHW solar systems with distributed storage tanks. Solar Energy 55 (3), 175–184.

Rabl, A., 1985. Active Solar Collectors and Their Applications. Oxford University Press.

Rashid, M. H., 2010. Power Electronics Handbook: Devices, Circuits and Applications. Academic Press.

RESOL, 2015. DeltaSol BS/2 Solar Controller Manual. RESOL.

RESOL, 2016. DeltaSol AL EHE Solar Controller Manual.

Reuss, M., Melzer, J., January 2013. Vacuum Super-Insulated Heat Storage for High Solar Fraction. Presentation at SMEThermal 2013. January 29th 2013. Berlin, Germany. Last access: January 9th 2018.
URL http://www.solarthermalworld.org/sites/gstec/files/news/file/2013-02-03/presentation_vsi_insulation_reuss_and_melzer.pdf

Reyes, O., December 14 2015. Seven Wrinkles in the Paris Climate Deal. Foreign Policy in Focus. Last access: December 21st 2017.
URL http://fpif.org/seven-wrinkles-paris-climate-deal/

Rezk, H., Eltamaly, A. M., 2015. A comprehensive comparison of different MPPT techniques for photovoltaic systems. Solar Energy 112, 1–11.

Rockendorf, G., Sillmann, R., Podlowski, L., Litzenburger, B., 1999. PV-Hybrid and thermoelectric collectors. Solar Energy 67 (4-6), 227–237.

Rogelj, J., den Elzen, M., Hohne, N., Fransen, T., Fekete, H., Winkler, H., Schaeffer, R., Sha, F., Riahi, K., Meinshausen, M., June 2016. Paris Agreement climate proposals need a boost to keep warming well below 2 degree Celsius. Nature 534, 631–639.

Saltiel, C., Sokolov, M., 1985. Optimal control of a multicomponent solar collector system. Solar Energy 34, 463–473.

Santbergen, R., Rindt, C., Zondag, H., van Zolingen, R., 2010. Detailed analysis of the energy yield of systems with covered sheet-and-tube PVT collectors. Solar Energy 84, 867–878.

Schaber, K., Steinke, F., Muhlich, P., Hamacher, T., 2012. Parametric study of variable renewable energy integration in Europe: Advantages and costs of transmission grid extensions. Energy Policy 42, 498–508.

Schiff, E. A., Hegedus, S., Deng, X., 2011. Handbook of Photovoltaic Science and Engineering, 2nd Edition. Wiley, Ch. Amorphous Silicon-based Solar Cells, pp. 487–545.

Schiller, S. R., Warren, M. L., Auslander, D. M., December 1979. Comparison of proportional and on/off solar collector loop control strategies using a dynamic collector model. Tech. rep., Lawrence Berkeley Laboratory, University of California, prepared for the U.S. Department of Energy under Contract W-7405-ENG-48. Submitted to the Journal of Solar Energy.

Schiller, S. R., Warren, M. L., Auslander, D. M., 1980. Comparison of proportional and on/off solar collector loop control strategy using a dynamic collector model. Journal of Solar Energy Engineering 102 (4), 257–262.

Schlesinger, R. J., 1976. Operating cycle for a typical solar heating system. Solar Engineering 1:2, 26–28.

Schlesinger, R. J., 1977. Preliminary comparison of proportional and full on-off control systems for solar energy applications. In: Proceedings of the International Solar Energy Society, Annual Meeting, Orlando, Florida, June 6-10, 1977. pp. 9–15 to 9–18, sections 1-13. (A78-11212 01-44) Cape Canaveral, Fla., International Solar Energy Society, 1977, p. 9-15 to 9-18.

Schlesinger, R. J., 1978. Field test data on a comparison between proportional and on/off differential thermostats. In: Proceedings of the First Workshop on the Control of Solar Energy Systems for Heating and Cooling. May 23-25, 1978. Hyannis, Massachussetts.

Schmidt, T., Mangold, D., Müller-Steinhagen, H., 2003. Seasonal thermal energy storage in Germany. In: Proceedings of the ISES Solar World Congress 2003. Göteborg, Sweden, 14.-19.06.2003.

Schnieders, J., 1997. Comparison of the energy yield predictions of stationary and dynamic solar collector models and the models' accuracy in the description of a vacuum tube collector. Solar Energy 61 (3), 179–190.

Schramski, J. R., Gattie, D. K., Brown, J. H., 2015. Human domination of the biosphere: Rapid discharge of the earth-space battery foretells the future of humankind. Proceedings of the National Academy of Sciences of the United States of America 112, 9511–9517.

Schröder, K. P., Smith, R. C., 2008. Distant future of the sun and earth revisited. Monthly Notices of the Royal Astronomical Society 306, 155–163.

SEECI, October 1981. Controllers for solar domestic hot water systems: A subcontract report. Tech. Rep. SERI/TR-98189-1A, SERI, 1617 Cole Boulevard, Golden, Colorado 80401, prepared under subcontract No. AH-9-8189-1.

Shioda, T., February 26th 2013. Delamination failures in long-term field-aged PV modules from point of view of encapsulant. 2013 NREL PV Module Reliability Workshop.

Shockley, W., Queisser, H. J., 1961. Detailed balance limit of efficiency of p-n junction solar cells. Journal of Applied Physics 32 (3), 510–519.

Siddiqui, M. U., Arif, A. F. M., Kelley, L., Dubowsky, S., 2012. Three-dimensional thermal modeling of a photovoltaic module under varying conditions. Solar Energy 86 (9), 2620–2631.

Skoplaki, E., Palyvos, J. A., 2009. On the temperature dependence of photovoltaic module electrical performance: A review of efficiency/power correlations. Solar Energy 83, 614–624.

Smil, V., 1999. Energies: An Illustrated Guide to the Biosphere and Civilization. MIT Press.

Smil, V., 2003. Energy at the Crossroads: Global Perspectives and Uncertainties. MIT Press.

Smil, V., 2004. Encyclopedia of Energy. Vol. 6. Elsevier, Ch. World History and Energy, pp. 549–561.

Smil, V., 2008. Energy in Nature and Society: General Energetics of Complex Systems. MIT Press.

Smith, G., A.Onions, P., Infield, D. G., 2000. Predicting islanding operation of grid connected PV inverters. IEE Proceedings - Electric Power Applications 147 (1), 1–6.

Solar Keymark, 2017. The Solar Keymark Database. Last access: 21st December 2017.
URL http://www.solarkeymark.dk/

Solargis, 2017. Solargis report: Solar resource overview. Tech. rep., Solargis.

Sonnenkraft, 2009. Sonnenkraft SKSC2 controller manual.

Sorensen, B., 2004. Renewable Energy: Its physics, engineering, use, environmental impacts, economy and planning aspects, 3rd Edition. Elsevier Science.

Soto, W. D., Klein, S., Beckman, W., 2006. Improvement and validation of a model for photovoltaic array performance. Solar Energy 80, 77–88.

SPE, 2016. Global Market Outlook For Solar Power / 2016 - 2020. Tech. rep., SolarPower Europe (SPE).

STECA, 2014. Steca TR A301 PWM: Installation and operating instructions.

Steinke, F., Wolfrum, P., Hoffmann, C., 2013. Grid vs. storage in a 100% renewable Europe. Renewable Energy 50, 826–832.

Stoffel, B., 2015. Assessing the Energy Efficiency of Pumps and Pump Units: Background and Methodology. Elsevier.

Streicher, W., June 2012. Solar Thermal Heating Systems: Lecture book, SOLNET Summer course at the University of Innsbruck. Innsbruck, Austria. July 16-20 2012.

Streicher, W., 2016. Renewable Heating and Cooling: Technologies and Applications. Elsevier, Ch. Solar thermal technologies for domestic hot water preparation and space heating, pp. 9–39.

Streicher, W., Bales, C., June 2005. Thermal energy storage for solar and low energy buildings - State of the art by the IEA Solar Heating and Cooling Task 32. Lleida University, Ch. Combistores.

Swanson, T. D., Ollendorf, S., June 4-6 1979. Orlando, Florida. 1979. Study on the application of NASA Energy Management Techniques for Control of a Terrestrial Solar Water Heating System. In: AIAA Terrestrial Energy Systems Conference.

Tobías, I., del Canizo, C., Alonso, J., 2011. Handbook of Photovoltaic Science and Engineering, 2nd Edition. Wiley, Ch. Crystalline Silicon Solar Cells and Modules, pp. 265–313.

Trieb, F., Schillings, C., O'Sullivan, M., Pregger, T., Hoyer-Klick, C., 2009. Global potential of concentrating solar power. In: Proceedings of the SolarPACES 2009 Conference, 15-18 September 2009, Berlin, Germany.

Tripanagnostopoulos, Y., 2007. Aspects and improvements of hybrid photovoltaic/thermal solar energy systems. Solar Energy 81, 1117–1131.

Tripanagnostopoulos, Y., Nousia, T., Souliotis, M., Yianoulis, P., 2002. Hybrid photovoltaic / thermal solar systems. Solar Energy 72 (3), 217–234.

TRNSYS, 2009. TRNSYS 17: a TRaNsient SYstem Simulation program. Volume 4: Mathematical Reference. Tech. rep., TRNSYS.

UNDP, 2011. Human Development Report 2011. Palgrave Macmillan, United Nations Development Programme.

UNDP, December 2015. Human Development Report 2015. United Nations Development Programme, United Nations Development Programme.

UNFCCC, December 2015. Adoption of the Paris Agreement, FCCC/CP/2015/L.9/Rev.1. United Nations Framework Convention on Climate Change.

Vázquez, M., Rey-Stolle, I., 2008. Photovoltaic module reliability model based on field degradation studies. Progress in Photovoltaics: Research and Applications 16, 419–433.

Vidal, O., Goffé, B., Arndt, N., 2013. Metals for a low-carbon society. Nature Geoscience 6, 894–896.

Villalva, M. G., Gazoli, J. R., Filho, E. R., 2009. Comprehensive approach to modeling and simulation of photovoltaic arrays. IEEE Transactions on Power Electronics 24 (5), 1198–1208.

Volk, M., 2005. Pump Characteristics and Applications, 2nd Edition. Taylor & Francis Group, LLC.

Vries, D., 1998. Design of a photovoltaic/thermal combi-panel. Ph.D. thesis, Technische Universiteit Eindhoven.

WBGU, 2009. Welt im Wandel: Zukunftsfähige Bioenergie und nachhaltige Landnutzung. Wissenschaftlicher Beirat der Bundesregierung Globale Umweltveränderungen.

Weiss, W., Mauthner, F., 2012. Solar heat worldwide: Markets and contribution to the energy supply 2010. Tech. rep., IEA-SHC.

Weiss, W., Streicher, W., Suter, J.-M., Letz, T., Kovacs, P., Jordan, U., Jaehnig, R. H. D., Visser, H., Druck, H., Bales, C., Perers, B., Peter, M., Vajen, K., Bergmann, I., Meir, M., Rekstad, J., 2003. Solar Heating Systems for Houses: A design handbook for solar combisystems. James & James.

Wilo, 2016. Datasheet for Wilo-Yonos PICO-STG 15/1-13.

Wilson, J., Ball, S., Huddleston, C., Ramsden, E., Ibrahim, D., 2008. Test and Measurement: Know It All. Newnes.

Winn, C. B., 1983. Advances in Solar Energy: An Annual Review of Research and Development, Volume 1. Vol. 1. Springer, New York, USA, Ch. Controls in Solar Energy Systems, pp. 209–240.

Winn, C. B., 1993. Active Solar Energy Systems. MIT Press, Ch. Controls in Active Solar Energy Systems, pp. 81–150.

Wirth, H., 2016. Recent Facts about Photovoltaics in Germany. Tech. rep., Fraunhofer ISE, Last access: October 10th 2016.

Wolf, M., 1976. Performance analysis of combined heating and photovoltaic power systems for residences. Energy Conversion 16, 79–90.

World Bank, July 2016. World development indicators database. Last access: September 7th 2016.
URL http://databank.worldbank.org/data/download/GDP.pdf

WRI, June 2015. CAIT Climate Data Explorer. Last access: September 13th 2016.
URL http://cait.wri.org

Wuestling, M. D., Klein, S. A., Duffie, J. A., 1985. Promising control alternatives for solar water heating systems. Journal of Solar Energy Engineering 107, 215–221.

Xu, L., December 1992. Dynamic model of an integral-cycle controlled single-phase induction machine. IEEE Transactions on Energy Conversion 7 (4), 761–767.

Zondag, H., 2008. Flat-plate PV-Thermal collectors and systems: A review. Renewable and Sustainable Energy Reviews 12, 891–959.

Zondag, H., de Vries, D., van Helden, W., van Zolingen, R., van Steenhoven, A., 2002. The thermal and electrical yield of a PV-Thermal collector. Solar Energy 72, 113–128.

Zondag, H., de Vries, D., van Helden, W., van Zolingen, R., van Steenhoven, A., 2003. The yield of different combined PV-thermal collector designs. Solar Energy 74, 253–269.

Zondag, H., van Helden, W., 2002. Stagnation temperature in PVT collectors. In: PV in Europe Conference. Rome.

Appendices

A. PV-T collector's PV power variation due to pump control

Transitions from fluid circulation to stagnation and vice-versa are implicit in the thermal energy collection process of active ST systems, including SDHW systems. For those using PV-T collectors, however, these transitions also have repercussions on electricity generation, since the PV conversion is temperature sensitive, which can be quantified using the Florschuetz (1979) steady-state PV-T collector model. Consider a transition from stagnation ($\dot{m}_c = 0$) to fluid circulation ($\dot{m}_c \neq 0$):

$$\Delta P_{pv} = P_{pv}\left(\dot{m}_c \neq 0\right) - P_{pv}\left(\dot{m}_c = 0\right) \tag{A.1}$$

Replacing (2.45) in (A.1), yields:

$$\Delta P_{pv} = A_c \tau \eta_{pv,r} \rho_{pv} G_T \beta_{pv,r} \left[T_{pv,m}\left(\dot{m}_c \neq 0\right) - T_{pv,m}\left(\dot{m}_c = 0\right)\right] \tag{A.2}$$

Substituting $T_{pv,m}\left(\dot{m} \neq 0\right)$ and $T_{pv,m}\left(\dot{m} = 0\right)$ from (2.46) in (A.2) leads to:

$$\Delta P_{pv} = A_c \tau \eta_{pv,r} \rho_{pv} \beta_{pv,r} G_T \tilde{F}_R \left[\left(T_{f,in} - T_a\right) - \frac{\tilde{S}}{\tilde{U}_L}\right] \tag{A.3}$$

A similarity can be easily detected between (2.38) and (A.3), and replacing the former in the latter reveals a relationship between ΔP_{pv} and $\dot{Q}$:

$$\Delta P_{pv} = \frac{\tau \eta_{pv,r} \rho_{pv} \beta_{pv} G_T}{\tilde{U}_L} \dot{Q} \tag{A.4}$$

Another similarity can be identified between (2.40) and (A.4), which can be used to simplify the latter into a more straightforward function of $\dot{Q}$:

$$\Delta P_{pv} = \frac{U_L - \tilde{U}_L}{\tilde{U}_L} \dot{Q} \tag{A.5}$$

B. Study of collector efficiency factor sensitivity for PV-T collectors

The collector efficiency factor is generally regarded as a weak function of the mass flow rate and temperature in typical collector designs (Kalogirou, 2009; Duffie and Beckman, 2013; Goswami, 2015). These influences can nevertheless be quantified using Nusselt number correlations for internal forced convection. Consider a harp-type collector with uniform flow distribution among its round riser tubes and a convective heat transfer coefficient given by (B.1), where Nu_D is the Nusselt number, k is the heat carrier thermal conductivity and d is the tube internal diameter.

$$h_{f,riser} = Nu_D \cdot \frac{k}{d} \tag{B.1}$$

The flow regime in the tubes is typically laminar but may not be fully developed, meaning thermal entrance region effects should be considered (Wuestling et al., 1985; Duffie and Beckman, 2013). Assuming the tube surface temperature is uniform – a conservative assumption according to Duffie and Beckman (2013) – the average Nusselt number can be given by (B.2), where Gz is the Graetz number expressed as (B.3), in turn where Pr is the Prandtl number, Re_D is the Reynolds number, both with fluid properties evaluated at bulk temperature, and L/d is the normalised tube length with respect to the tube diameter (Lienhard IV and Lienhard V, 2008).

$$\bar{Nu}_D = 3.657 + \frac{0.0668 \cdot Gz^{1/3}}{0.04 + Gz^{-2/3}} \tag{B.2}$$

$$Gz = Re_D Pr \cdot \frac{d}{L} \tag{B.3}$$

Alternatively, if the flow is turbulent or transitional ($2300 \leq Re_D \leq 5 \cdot 10^6$) the Nusselt number can be given by the Gnielinski correlation, (B.4), where f_D is the Darcy friction factor, which can be determined by solving the implicit Colebrook equation or the approximate solution proposed by S. E. Haaland, (B.5), where ε/d is the relative surface roughness (Cengel, 2003; Lienhard IV and Lienhard V, 2008).

$$Nu_D = \frac{(f_D/8)\,(Re_D - 1000)\,Pr}{1 + 12.7\sqrt{f_D/8}\,(Pr^{2/3} - 1)} \tag{B.4}$$

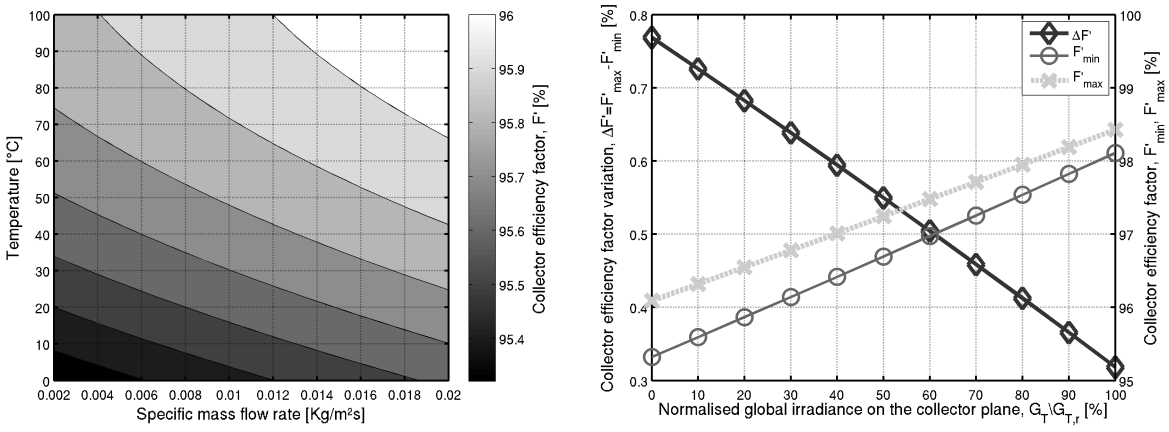

Figure B.1.: Collector efficiency factor as a function of the fluid temperature and specific mass flow rate, for the reference PV-T collector with PV generation disabled (left-hand side plot), and collector efficiency factor range of variation due to the same factors while the PV-T collector is generating electricity, as a function of the normalised irradiance on the collector plane (right-hand side plot).

$$\frac{1}{\sqrt{f_D}} = -1.8 \cdot \log\left[\frac{6.9}{Re_D} + \left(\frac{\varepsilon/d}{3.7}\right)\right] \tag{B.5}$$

The thermal conductance between the absorber and the collector fluid ($U_{f,p}$) can then be computed according to (B.6), where C_b is the bond conductance and $h_{pv,p}$ is the heat transfer coefficient between the PV cells and the absorber plate.

$$U_{f,p} = \left[\frac{W}{d_{riser} h_{f,riser} \pi} + \frac{W}{C_b} + \frac{1}{h_{pv,p}}\right]^{-1} \tag{B.6}$$

The collector efficiency factor can then be determined according to (2.42). Temperatures found in SDHW systems are typically between 0 and 100°C and specific mass flow rates range from 0.002 Kg/m²s for low flow systems to 0.02 Kg/m²s for high flow systems. Within these ranges, the collector efficiency factor for the reference PV-T collector described in Table 4.1 varied by less than 0.8% (absolute) with PV generation disabled, and little more than 0.3% otherwise, as documented in Figure B.1, while the convective heat transfer coefficient varied by 22.2% (relative).

C. Mean plate temperature equations for PV-T collectors

As with the HWB model, several expressions can be derived for the mean plate temperature using the Florschuetz PV-T collector model. In order to do so, one can start by recalling the various equations for the useful heat generated by PV-T collectors, (C.1), (C.2) and (C.3):

$$\dot{Q} = A_c \left[\tilde{S} - \tilde{U}_L \left(T_{pv,m} - T_a\right)\right] \tag{C.1}$$

$$\dot{Q} = A_c \tilde{F}_R \left[\tilde{S} - \tilde{U}_L \left(T_{f,in} - T_a\right)\right] \tag{C.2}$$

$$\dot{Q} = A_c \tilde{F}' \left[\tilde{S} - \tilde{U}_L \left(T_{f,m} - T_a\right)\right] \tag{C.3}$$

By solving (C.1) and (C.2) for $T_a + \tilde{S}/\tilde{U}_L$, equating them and solving for $T_{pv,m}$, the following equation results:

$$T_{pv,m} = T_{f,in} + \frac{\dot{Q}}{A_c \tilde{F}_R \tilde{U}_L} \left(1 - \tilde{F}_R\right) \tag{C.4}$$

Alternatively, the same process repeated using (C.1) and (C.3) leads to:

$$T_{pv,m} = T_{f,m} + \frac{\dot{Q}}{A_c \tilde{F}' \tilde{U}_L} \left(1 - \tilde{F}'\right) \tag{C.5}$$

Another option is to replace (C.2) and (C.3) in (C.4) and (C.5), respectively, to yield equations sensitive to the weather conditions (G_T through $\tilde{S}$, and T_a):

$$T_{pv,m} = \tilde{F}_R T_{f,in} + \left(T_a + \frac{\tilde{S}}{\tilde{U}_L}\right) \left(1 - \tilde{F}_R\right) \tag{C.6}$$

$$T_{pv,m} = \tilde{F}' T_{f,m} + \left(T_a + \frac{\tilde{S}}{\tilde{U}_L}\right) \left(1 - \tilde{F}'\right) \tag{C.7}$$

D. Dynamic PV-T system model

D.1. Description

The system model comprises several submodels interacting with each other in accordance with the diagram of Figure 5.1. The submodels concern system components namely the PV-T collectors, the thermal storage tank, the DTSTLH and DTSSHP controllers, the pipe segments, the supply-loop pipeline, the circulation pump and the demand-loop mixing circuit, which are briefly described next.

D.1.1. PV-T collector

The PV-T collectors were modelled via the dynamic single-node multi-segment model described in Chapter 3. In essence, the model is based on the ISO 9806:2013 standard's quasi-dynamic test method equation and as such, models the collector heat capacity, convective heat losses and their wind and temperature dependences, longwave radiative heat losses (though neglected in this study), beam and diffuse components of solar irradiance and respective incidence angle effects, but is also compatible with discretisation along the flow path and responsive to electricity generation. Electricity generation is assumed to take place according to a linear cell efficiency temperature dependence and the cell temperature is estimated using a zero-capacitance model sensitive to the dynamic mean fluid temperatures, electricity generation and the temperature dependence of the collector heat losses.

D.1.2. Thermal storage tank

The thermal storage tank model reproduced the one-dimensional storage model proposed by Newton (1995). The model accounts for stratification along the vertical direction through multiple uniform nodes, de-stratification through thermal conduction between fluid layers and along the tank wall, heat losses to the surroundings according to a constant heat loss coefficient, simultaneous fluid withdrawal and replenishment via double ports, charging via internal coiled heat exchangers using an iterative method and consistent with a Nusselt number correlation of the type $Nu = C_{t,he} \cdot Ra_D^{n_{t,he}}$ (where Ra_D is the Rayleigh number, while $C_{t,he}$ and $n_{t,he}$ are determined empirically), charging via immersed electrical heating elements (e.g., auxiliary system), and prevents thermal inversions by mixing fluid layers. The model was validated against TRNSYS type 60 – an implementation of the same model available for a reputable though different simulation environment widely used in solar thermal system studies – for accuracy in idle, charging and discharging modes.

D.1.3. Auxiliary system

Both electrical and boiler-type auxiliary systems were modelled as electrical heating elements. In other words, both systems were modelled as constant heat gains to the storage tank controlled by a thermostat. While simplistic, this approach relies on a differentiated treatment in terms of system efficiency, energy prices and primary energy factors *post-simulation*, and is for that reason convenient to reduce the number of simulations necessary to consider both systems.

D.1.4. Pipe segments

The pipe segments were modelled using the plug-flow approach previously followed for TRNSYS type 31 (TRNSYS, 2009). According to this model, isothermal fluid segments of variable size travel from inlet to outlet according to the prevailing mass flow rate, and the outlet temperature for a given time frame is determined by the weighted average of the outgoing fluid segments and new segments formed assume the inlet temperature. The difference between this implementation and the one known as TRNSYS type 31 is the heat loss coefficient to the surroundings, which in this case depends on the material thermal resistances across the pipe and insulation, the Churchill and Chu Nusselt number correlation for external free convection in horizontal isothermal pipes, (D.1), and those for internal convection in smooth tubes, namely the Dittus-Boelter for turbulent flow (D.2) and the constant surface temperature one ($Nu = 3.66$) for laminar flow (Cengel, 2003). The model was validated against TRNSYS type 31 by forcing the same heat loss coefficient.

$$Nu = \left\{0.6 + 0.387 \cdot Ra_D^{1/6} \cdot \left[1 + (0.599/Pr)^{9/16}\right]^{-8/27}\right\}^2 \tag{D.1}$$

$$Nu = 0.023 \cdot Re^{0.8} \cdot Pr^n \tag{D.2}$$

D.1.5. Demand-loop water mixing circuit

The demand-loop water mixing circuit model ensures the right amount of tank and mains water are withdrawn and mixed to satisfy the load flow rate and temperature specifications. The model assumes the flow reaching the loads is well mixed at a temperature corresponding to the mass-weighted average temperature of the two originals streams and at a flow rate equivalent to the sum of both original flow rates, as in TRNSYS type 11, and reverse engineers the tank and mains flow rates from these assumptions (TRNSYS, 2009). In addition to this idealised mixing behaviour, no piping heat losses were modelled for the demand loop.

D.1.6. Supply-loop hydraulic circuit

The supply-loop hydraulic circuit model consists of a pipeline pressure loss model, and is only used to determine the pump power consumption in conjunction with the circulation model. The model is based on the assumption the power delivered to the fluid by the pump is given by (D.3), a cubic function of the supply-loop mass flow rate ($\dot{m}$) – previously used in numerous studies though in some cases assumed to represent the electrical pump power instead – and proportional to a coefficient (K_p) dependent on the pipeline's characteristics (Winn, 1983; Saltiel and Sokolov, 1985; Badescu, 2008; Nhut and Park, 2013; Ntsaluba et al., 2016). The equation generally corresponds to turbulent flow and leads to a pipeline pressure drop (Δp) proportional to square of the supply-loop mass flow rate in accordance with (D.4).

$$P_{fluid} = K_p \cdot \dot{m}^3 \tag{D.3}$$

$$\Delta p = K_p \cdot \rho \cdot \dot{m}^2 \tag{D.4}$$

D.1.7. Circulation pump

The circulation pump model consists of an electrical power model based on interpolation of manufacturer-supplied data for speed-controlled pumps. Concretely, the model relies on at least two pressure difference versus volumetric flow rate (Δp-Q) and electrical power versus volumetric flow rate ($P_{pump,el}$-Q) constant speed curves. From this data, a polynomial approximation of the resulting electrical power consumption for circulation, (D.5), is used to make calculations simpler and quicker.

$$P_{pump,el} = o_3 \cdot \dot{m}^3 + o_2 \cdot \dot{m}^2 + o_1 \cdot \dot{m}^1 + o_0 \tag{D.5}$$

D.2. Setup

The dynamic PV-T system model was set up in accordance with the details already provided in Section 5.3.2. The configuration also uses the parameter values listed in Tables D.2 and D.3. In turn, Figure D.2 shows the monthly average mains water temperature and wind speed, by location. Finally, the selected pump's Δp-Q and $P_{pump,el}$-Q curves (corresponding to a pump from a well-known pump manufacturer and obtained from publicly available resources) are given in Figure D.1. The pump power polynomials for each of the six pipelines are provided in Table D.1.

Table D.1.: Parameter values used to configure the hydraulic submodel (the polynomial returns W when the independent variable is in Kg/s).

Pipeline	$\dot{m}_{c,min}/A_c$	$\dot{m}_{c,nom}/A_c$	K_p	Pump power polynomial			
#	[Kg/m²s]	[Kg/m²s]	[W/Kg³/s³]	o_3	o_2	o_1	o_0
1	0.0050	0.02	3625	28031	-3079.3	245.6	-3.2
2	0.0075	0.02	1604	6548.1	-693.3	99.5	-1.2
3	0.0100	0.02	1000	5881.1	-855.7	96.7	-1.2
4	0.0125	0.02	1000	2416.8	6.5	26.0	0.7
5	0.0150	0.02	1000	-1303.6	982.0	-58.7	3.1
6	-	0.02	1000	0	0	0	5.9

Table D.2.: Parameter values used to configure the PV-T collector, thermal storage tank and insulated pipe segment models

Parameter	Value	Unit
A_c	1.27	m²
$(\tau\alpha)_n$	92.63	%
$U_{L,1}$	4.8972	W/m²K
$U_{L,2}$	0.0274	W/m²K²
U_W	0.7009	J/m³K
C_A	20	kJ/m²K
F'	95	%
τ	94	%
b_0	0.1	-
K_d	1	-
$T_{pv,r}$	25	°C
$G_{T,r}$	1000	W/m²
β_{pv}	-0.45	%/°C
$\eta_{pv,r}$	14.54	%
ρ_{pv}	67	%
N_{seg}	40	-
$N_{c,sh}$	4	-
$N_{c,s}$	1	-

Parameter	Value	Unit
V_t	0.3	m³
H_t	1.6	m
U_t	0.15	W/m²K
$k_{t,w}$	16	W/mK
$\delta_{t,w}$	5	mm
$D_{t,he}$	0.028	m
$d_{t,he}$	0.025	m
$L_{t,he}$	17	m
$k_{t,he}$	400	W/mK
$C_{t,he}$	0.5	-
$n_{t,he}$	0.25	-
$k_{pipe,ins}$	0.04	W/mK
$\delta_{pipe,ins}$	0.02	m
d_{pipe}	0.018	m
k_{pipe}	400	W/mK
δ_{pipe}	1	mm
$L_{pipe,int}$	3	m
$L_{pipe,ext}$	2	m

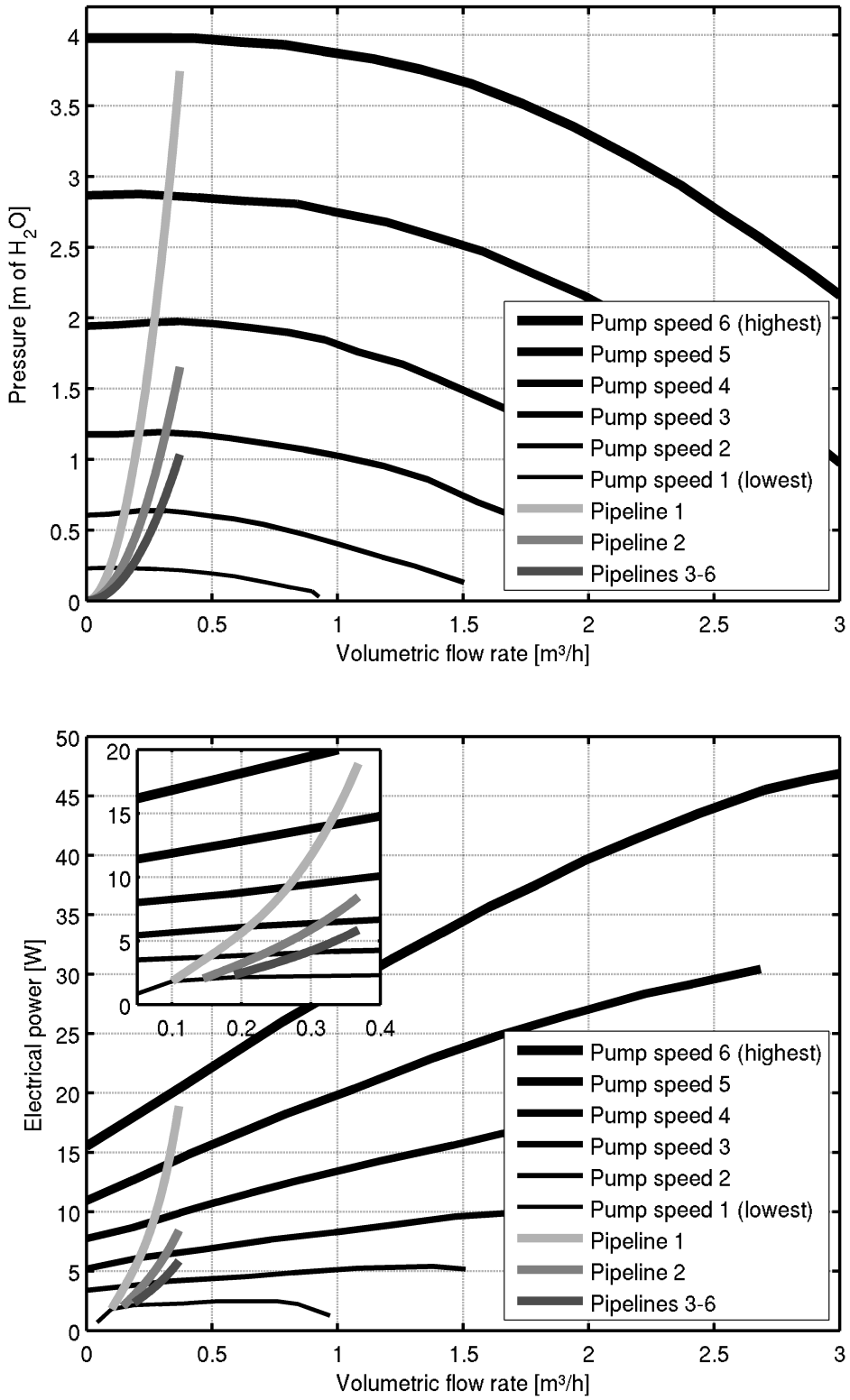

Figure D.1.: Pressure lift/drop versus flow rate curves (Δp-Q; above) and electrical power versus flow rate ($P_{pump,el}$-Q; below) curves, for the reference high-efficiency variable-speed circulation pump and the various system pipelines (1-6).

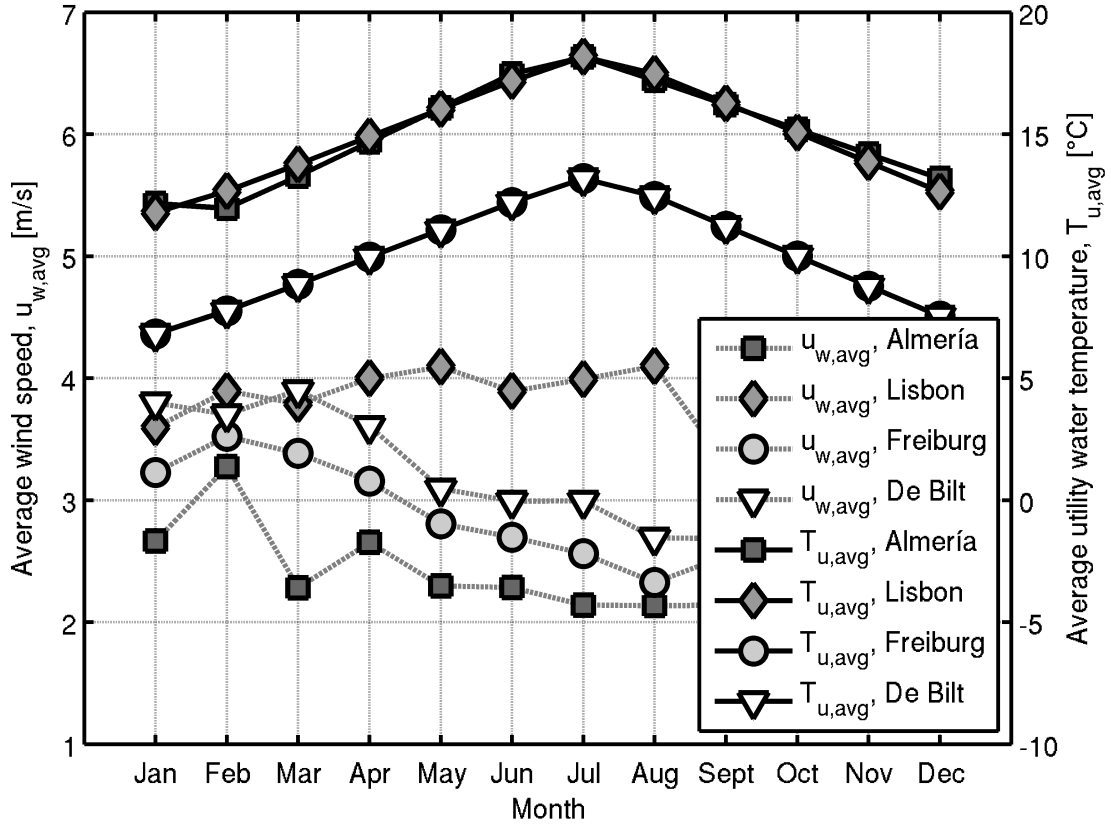

Figure D.2.: Average monthly wind speed and mains water temperature.

Table D.3.: Parameter values used to configure the dynamic PV-T system

Parameter	Value	Unit	Description
T_{room}	22	°C	Room temperature
$T_{c,max}$	95	°C	Maximum collector temperature
$\Delta T_{c,max}$	10	°C	Collector loop cool-off deadband
Δt_{delay}	4	min	Minimum pump running time
V_{load}	0.2	m^3	Daily load volume
T_{load}	45	°C	Load temperature
$T_{t,aux}*$	60	°C	Backup system reference temperature
$\Delta T_{t,aux}$	5	°C	Backup system temperature deadband
P_{aux}	2500	W	Backup system power rating
$\eta_{el,pec}$	90	%	Power converter electrical efficiency
T_f	60	°C	Fluid temperature for property evaluation

E. Estimating c_1 and c_3 from EN 12975:2006 performance test data

The EN 12975:2006 and ISO 9806:2013 standardised thermal collector performance test reports don't always provide values for the zero-reduced temperature heat loss coefficient ($F'U_{L,1}$, or c_1) and the wind-dependence of the heat loss coefficient ($F'U_W$, or c_3), but instead often provide a single nominal value ($F'U_L = F'U_{L,1} + F'U_W u_W$, or c_{13}) for a predetermined range of wind speeds and the stagnation temperature. Such was the case for the PV-T collector reproduced in this study, as originally published by Dupeyrat et al. (2011b), whose stagnation temperatures and performance estimation parameters were determined in accordance with the EN 12975:2006 standard's high temperature resistance and static test methods using an indoor simulator, whose specifications stipulate that wind speeds (u_W) parallel to the collector plane should be under 1 m/s and in the range of 3±1 m/s, respectively. Consequently, the stagnation temperatures calculated using the published parameter values originally provided are about 20°C lower than the measured temperatures presented in the same publication for the same collector[45]. Therefore, the parameter values published (η_0, c_{13} and c_2) should not be used for different wind conditions than those used in the original tests or unacceptable errors will result.

$$\eta = \eta_0 - c_{13} \cdot \left(\frac{T_{f,m} - T_a}{G_T}\right) - c_2 \cdot G_T \cdot \left(\frac{T_{f,m} - T_a}{G_T}\right)^2 \tag{E.1}$$

$$c_{13} = c_1 + c_3 u_w \tag{E.2}$$

The ability to reproduce the collector performance and stagnation temperatures under different wind conditions is important for representative simulations and as such, a method to determine the zero-reduced temperature heat loss coefficient (c_1) and the wind dependence of the heat loss coefficient (c_3) was developed. The method proposed for this purpose relied on (E.1) and (E.2) in addition to the stagnation temperature and the open-circuit mode thermal performance parameter values originally published, in a bid to simplify the analysis (i.e., by focusing on open-circuit mode

[45] As a side note, the ISO 9806:2013 standard provides an additional method for the calculation of the stagnation temperature compared to the EN 12975-2:2006 standard, which adds exactly 20°C to the stagnation temperature determined by solving the quadratic equation (E.1), precisely due to the convective losses caused by the higher wind speeds.

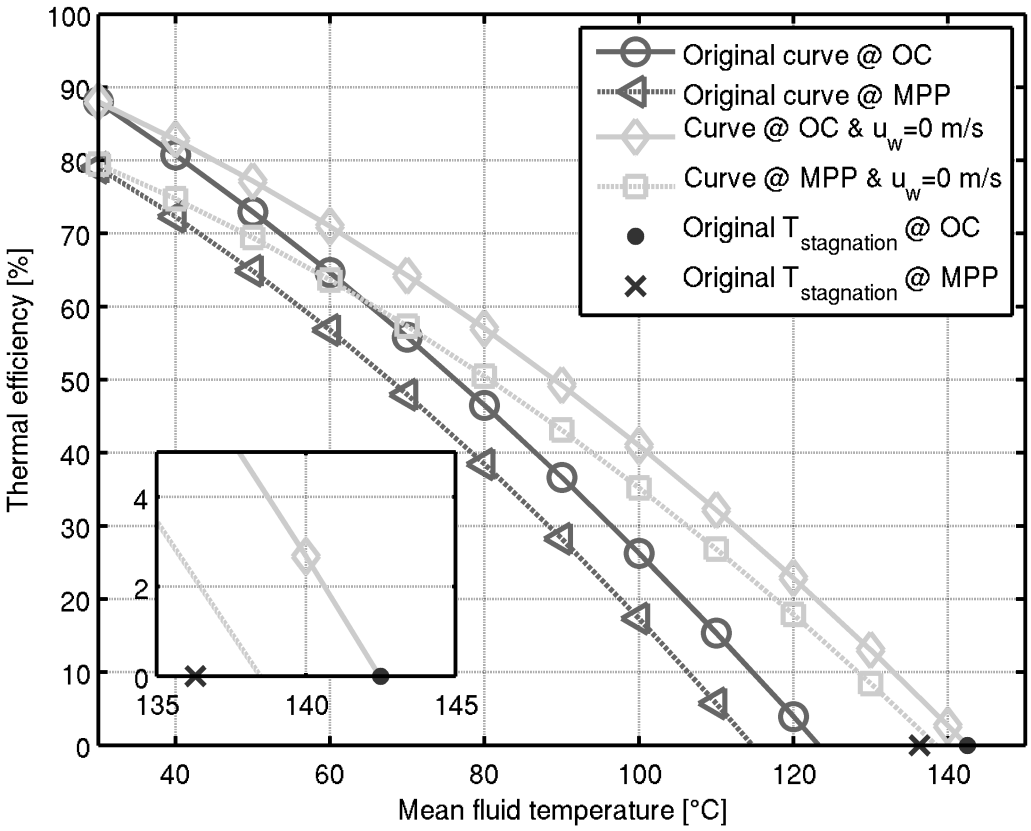

Figure E.1.: Steady-state thermal efficiency curves using originally published data and those estimated using the method proposed, and comparison against the stagnation temperatures ($T_{stagnation}$) reported in Dupeyrat et al. (2011b).

and accounting for PV conversion separately) while complying with the reference stagnation temperature. This method implies the static test and the high temperature resistance test are assumed to have taken place at wind speeds of exactly 3 m/s and 0 m/s, respectively, while any potential effect on the zero loss efficiency (η_0) or the quadratic heat loss coefficient (c_2) is deemed negligible. The method allowed the stagnation temperature to be estimated without error during open-circuit mode and with a 2.2°C error during MPP operation, as shown in Figure E.1, which is a significant improvement over the approximately 20°C error determined previously.